Characterisation of mRNA binding proteins as potential therapeutic targets: models and tools

Dissertation

zur Erlangung des Grades

des Doktors der Naturwissenschaften

der Naturwissenschaftlich-Technischen Fakultät

der Universität des Saarlandes

von

Tarek Kröhler

Saarbrücken

2022

Tag des Kolloquiums:	14. Februar 2023
Dekan:	Prof. Dr. Ludger Santen
Berichterstatter:	Prof. Dr. Alexandra K. Kiemer
	Prof. Dr. Jörn E. Walter
Vorsitz:	Prof. Dr. Uli Müller
Akad. Beisitzer:	Dr. Agnes-Valencia Weiss

Contents

Abstract

Cancer is one of the most common three causes of premature death worldwide. In past years, colorectal cancer and primary liver cancer are among the malignancies with the highest incidence and mortality rates. This study focuses on two RNA-binding proteins (RBPs) that are aberrantly expressed in those cancer species and contribute to cancer initiation and progression.

The first chapter addresses the role of the RBP ZFP36 ring finger protein (TTP) in hepatocellular carcinoma. The effect of a liver-specific TTP-knockout on tumour initiation was investigated *in vivo* using the diethylnitrosamine hepatocarcinogenesis model in mice. Further, TTP was overexpressed in various hepatoma cells to study the impact on several hallmarks of cancer *in vitro*. It is shown that TTP exerts tumour-promoting actions during hepatocarcinogenesis and tumour-suppressive actions during hepatic tumour progression.

In the second chapter, the RNA-editing method TRIBE is combined with hydrodynamic gene delivery to transfect murine liver cells and enable the identification of new RNA targets of the RBP insulin-like growth factor 2 mRNA-binding protein 2 (IMP2) *in vivo*.

In the third chapter, IMP2 is validated as target for cancer therapy by employing 2D and 3D cell culture models of CRISPR/Cas9-mediated IMP2 knockout cells *in vitro* as well as zebrafish embryo xenografts *in vivo*. Based on these results, hit compounds of the screening for small molecule inhibitors of IMP2 could be tested.

Zusammenfassung

Krebs ist eine der drei häufigsten Todesursachen weltweit, wobei Darmkrebs und primärer Leberkrebs mit die höchsten Inzidenz- und Sterberaten in den vergangenen Jahren aufwiesen. Diese Studie konzentriert sich auf zwei RNA-bindende Proteine (RBPs), deren abnormales Vorkommen in diesen Krebsarten zur Krebsentstehung und -fortschreitung beiträgt.

Das erste Kapitel adressiert die Rolle des RBPs Ringfingerprotein ZFP36 (TTP) beim hepatozellulären Karzinom. Anhand des Diethylnitrosamin-Hepatokarzinogenesemodells in Mäusen wurde der Effekt des leberspezifischen Ausschaltens von TTP auf die Tumorentstehung *in vivo* untersucht. Außerdem wurde TTP in Leberkrebszellen überexprimiert, um Auswirkungen auf Krebsmerkmale *in vitro* zu studieren. Es wird gezeigt, dass TTP während der Krebsentstehung fördernd und während Tumorprogression unterdrückend wirkt.

Im zweiten Kapitel wird die RNA-Editierungsmethode TRIBE mit dem hydrodynamischen Gentransfer kombiniert, um Leberzellen in Mäusen zu transfizieren und die Identifizierung neuer RNA-Ziele des RBPs Insulinähnlicher Wachstumsfaktor 2-mRNA-bindendes Protein 2 (IMP2) *in vivo* zu ermöglichen.

Im dritten Kapitel wird IMP2 als Ziel für die Krebstherapie validiert; i*n vitro* durch Verwendung von IMP2-K.o.-Zellen (generiert *via* CRISPR/Cas9) in 2D- und 3D-Zellkulturmodellen, sowie *in vivo* mittels Zebrafischembryo-Xenotransplantaten. Darauf basierend konnten Trefferverbindungen aus dem Screening nach niedermolekularen Hemmstoffen von IMP2 getestet werden.

1 Introduction

1.1 Cancer

According to most recent estimates of global mortality data (WHO, 2020), cancer is among the top three causes for premature deaths in 183 countries of the world, even leading in 57 countries including China (Figure 1). In 2020, the International Agency for Research on Cancer (IRAC) estimated the worldwide cancer incidence with 19.3 million new cases and cancer mortality with approximately 10.0 million cancer deaths (Figure 2A). Moreover, cancer is suggested to surpass cardiovascular disease as worldwide leading cause for premature deaths over the course of this century (Bray et al., 2021). In line, the global cancer burden is predicted to be 28.4 million new cases in 2040, representing a 47% increase of cancer incidence compared to the year 2020 (Sung et al., 2021).

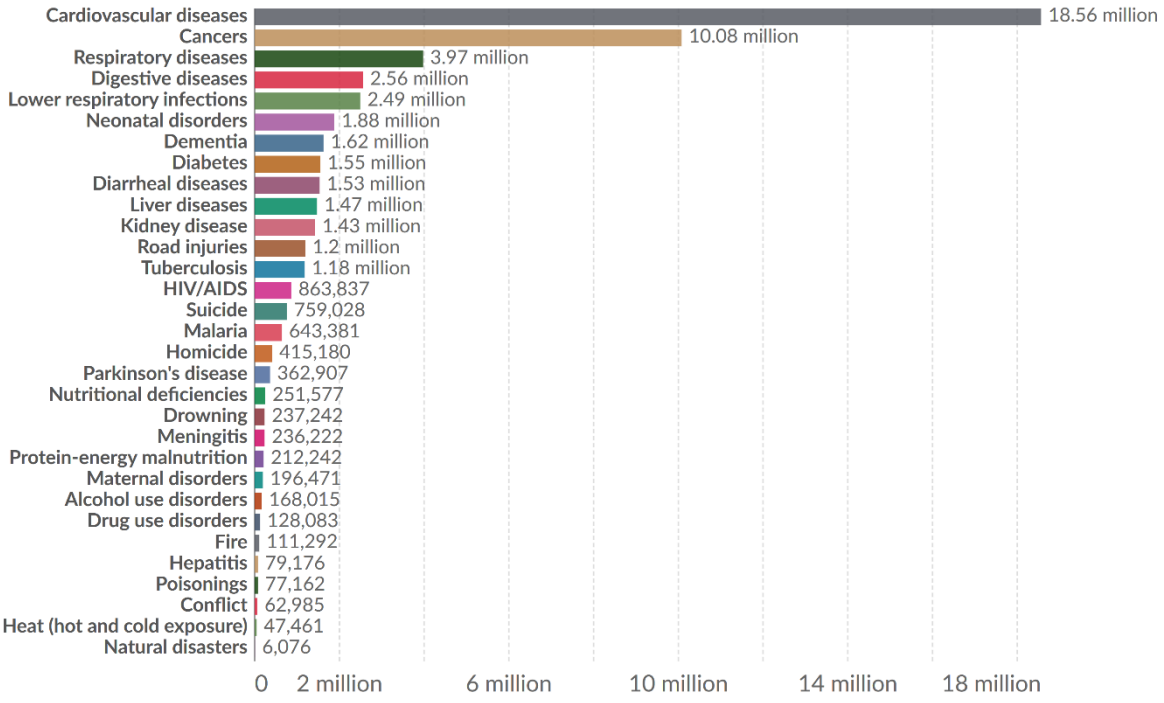

Figure 1| Global mortality by cause in 2019. Underlying data source is the Global Burden of Disease (GBD) 2019 study (GBD 2019 Diseases and Injuries Collaborators, 2020). Data were visualised by OurWorldinData.org (accessed on February 24, 2021). Licensed under CC BY 4.0.

However, the present work focuses on colorectal cancer (CRC) and the hepatocellular carcinoma (HCC), the most common type of primary liver cancer. Both cancer entities are among the top three malignancies in terms of mortality (Figure 2).

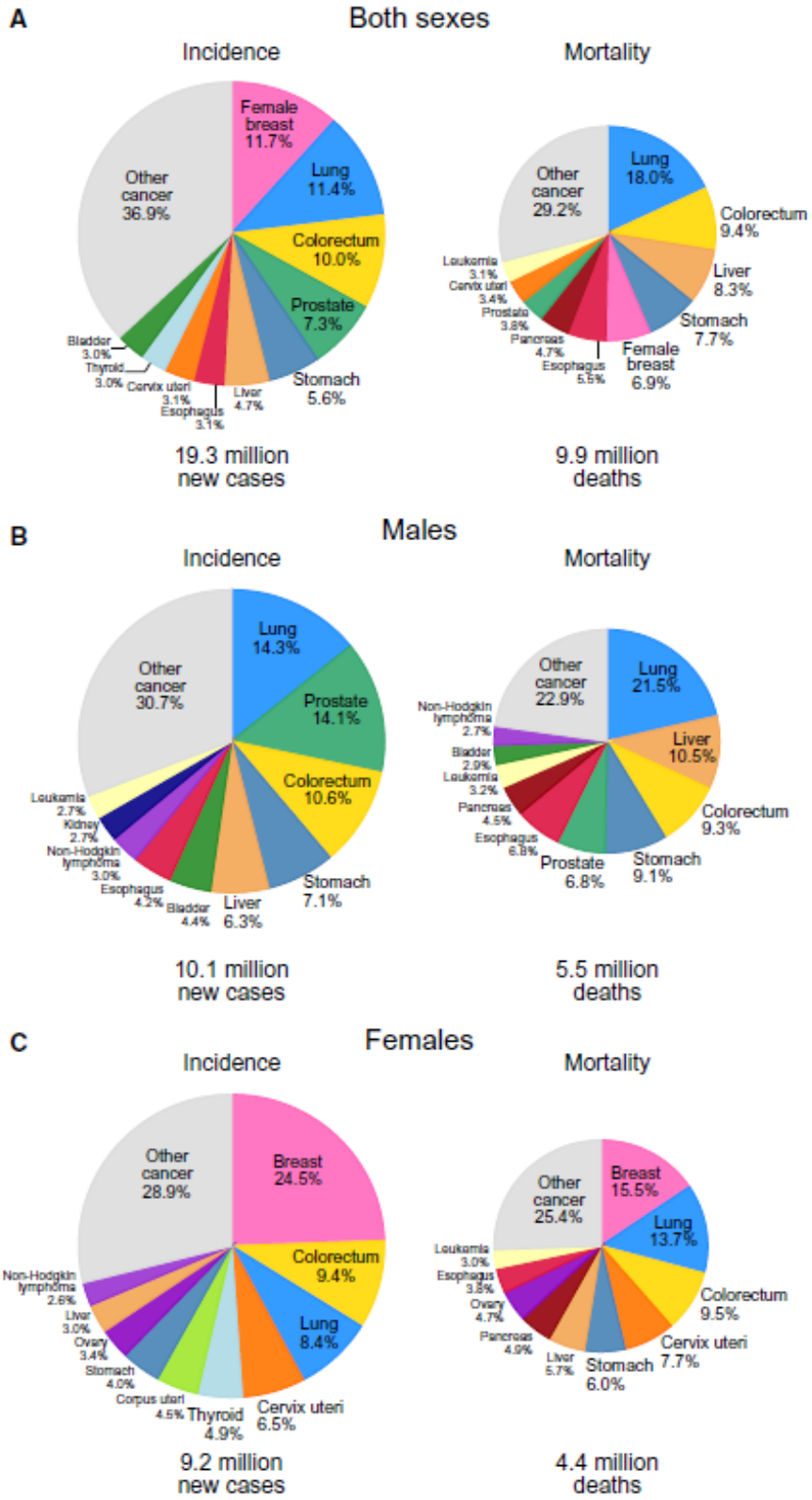

Figure 2| Tumour incidence and mortality of the top 10 most common cancers in 2020. The area of the pie charts is proportional to the total number of cases and deaths for (A) both sexes, (B) men, and (C) women. Slices indicating colorectal cancer are coloured yellow, slices accounting for liver cancer are light brown. From "Global Cancer Statistics 2020: GLOBOCAN Estimates of Incidence and Mortality Worldwide for 36 Cancers in 185 Countries" by Sung, H., Ferlay, J., Siegel, R. L., Laversanne, M., Soerjomataram, I., Jemal, A., & Bray, F. (2021), *CA: A Cancer Journal for Clinicians, 71*(3), 209–249 (https://doi.org/10.3322/caac.21660). With permission, copyright © 2021 American Cancer Society.

1.1.1 Colorectal cancer

Overall, CRC ranks third with approximately 1.9 million new cases in 2020 and second in terms of mortality, which is a share of 9.4% of the total number of deaths (Figure 2A). The incidence rate in females is 1.2% less than in males with comparable mortality rates (Figure 2B and Figure 2C). There is a high variation in CRC incidence rates by world regions, with the highest rates in European regions, Australia, and New Zealand and lowest rates in Africa (Figure 3). This fact is reflected by a positive dose-response relationship between the age-standardised incidence rates and the Human Development Index (HDI) for CRC (Fidler et al., 2016). Therefore, CRC can be considered a marker of socioeconomic development and, in countries undergoing major transition, incidence rates tend to rise uniformly with increasing HDI (Sung et al., 2021).

Besides hereditary forms (5-10%), most cases of CRC are sporadic (88-94%) and accompanied with environmental factors such as a sedentary lifestyle combined with a diet rich in meat and fat, and poor in fibre, folate, and calcium. Obesity and diabetes mellitus can be seen both, as a result, but also as independent risk factors additional to high alcohol intake and smoking (Weitz et al., 2005).

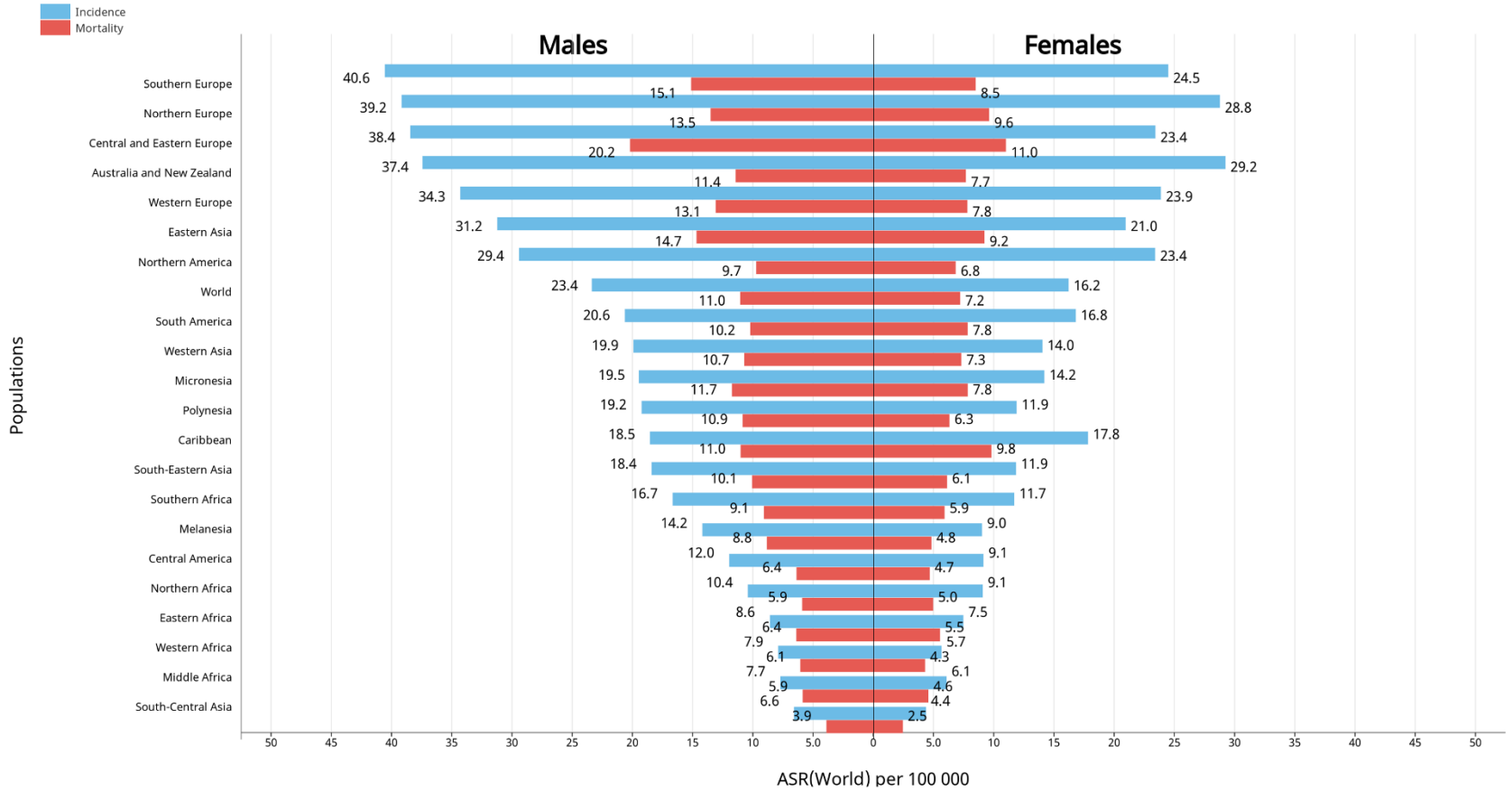

Figure 3| Estimated age-standardised incidence rates by world regions and sex for colorectal cancer (including cancer of colon, rectum and anus) in 2020. Incidence rates (blue) and mortality rates (red) are shown in descending order of the world (W) age-standardised rate. Underlying data source is GLOBOCAN 2020. Data were visualised by the Global Cancer Observatory (https://gco.iarc.fr, accessed on October 26, 2021) of the International Agency for Research on Cancer.

1.1.2 Hepatocellular carcinoma

In 2020, primary liver cancer is estimated to be the sixth most diagnosed cancer and the third leading cause of cancer-related death worldwide, with approximately 900,000 new cases and 830,000 deaths, respectively (Figure 2A). Incidence and mortality rates are at least two times higher among men than among women in all regions of the world (Figure 4). There are to hypothesis for this gender-specific effect. On the one hand, this may be related to sex-specific differences in exposure to risk factors such as a higher probability of hepatitis B virus (HBV) or hepatitis C virus (HCV) infections and higher consume of alcohol and cigarettes in men (El-Serag & Rudolph, 2007). On the other hand, the effect can be explained by sexual hormones. Estrogens are supposed to be protective, and androgens are believed to promote HCC (Mucci et al., 2001; Yu et al., 2000). The highest incidence rates are observed in transitioning countries in Eastern Asia (Mongolia), Micronesia, South-Eastern Asia (Thailand, Cambodia, and Viet Nam), and North Africa (Egypt and Niger) (Sung et al., 2021). In men, liver cancer ranks fifth in terms of incidence and second in terms of mortality (Figure 2B).

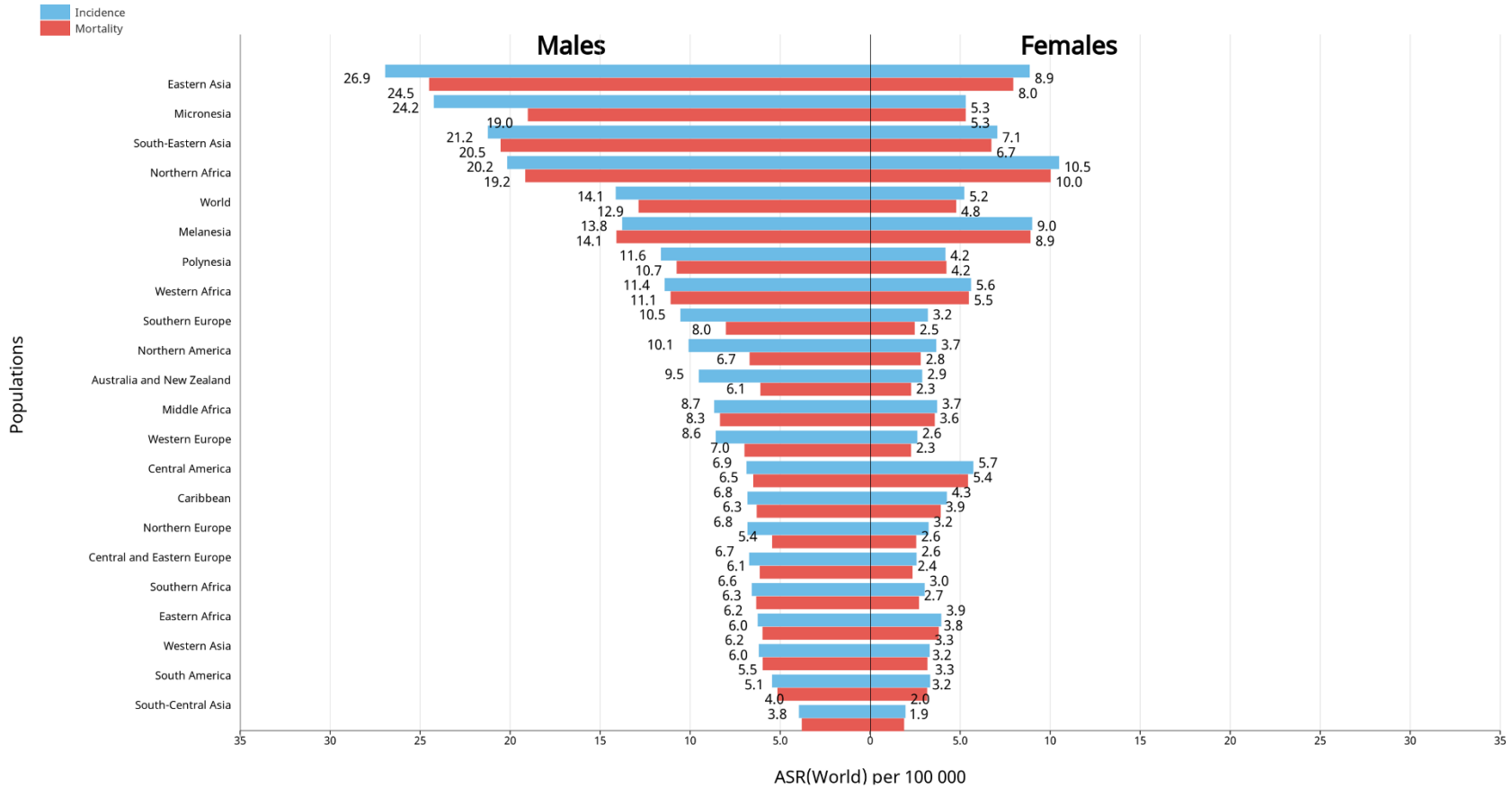

Figure 4| Estimated age-standardised incidence rates by world regions and sex for liver cancer in 2020. Incidence rates (blue) and mortality rates (red) are shown in descending order of the world (W) age-standardised rate. Underlying data source is GLOBOCAN 2020. Data were visualised by the Global Cancer Observatory (https://gco.iarc.fr, accessed on October 26, 2021) of the International Agency for Research on Cancer.

Additional to HBV or HCV infections, heavy alcohol intake and smoking, other risk factors for HCC, the predominant form of primary liver cancer with up to 90% of all liver cancer cases, include aflatoxin-contaminated foods, excess body weight ,obesity, and diabetes mellitus type 2 (T2DM) (Sung et al., 2021). These risk factors vary in the different geographically regions of the world. Particularly, the latter factors, which are associated with the metabolic syndrome (Figure 5), have become more relevant in the recent past due to the unhealthy western lifestyle growing in industrialised societies. They contribute to a wide spectrum of liver pathologies, ranging from hepatic steatosis to non-alcoholic steatohepatitis (NASH), and favour HCC development (Fujiwara et al., 2017). NASH, the progressive form of non-alcoholic fatty liver disease (NAFLD), is characterised by the presence of inflammation and hepatocyte ballooning, occurs in 25-40% of NAFLD patients, and lead in 2.8% of the cases to HCC (Kucukoglu et al., (2021). Nowadays, the described pathologies are compromised under the umbrella term MAFLD (metabolic-associated fatty liver disease), indicating the great impact of metabolic syndrome-associated risk factors for liver pathogenesis and HCC (Eslam et al., 2020).

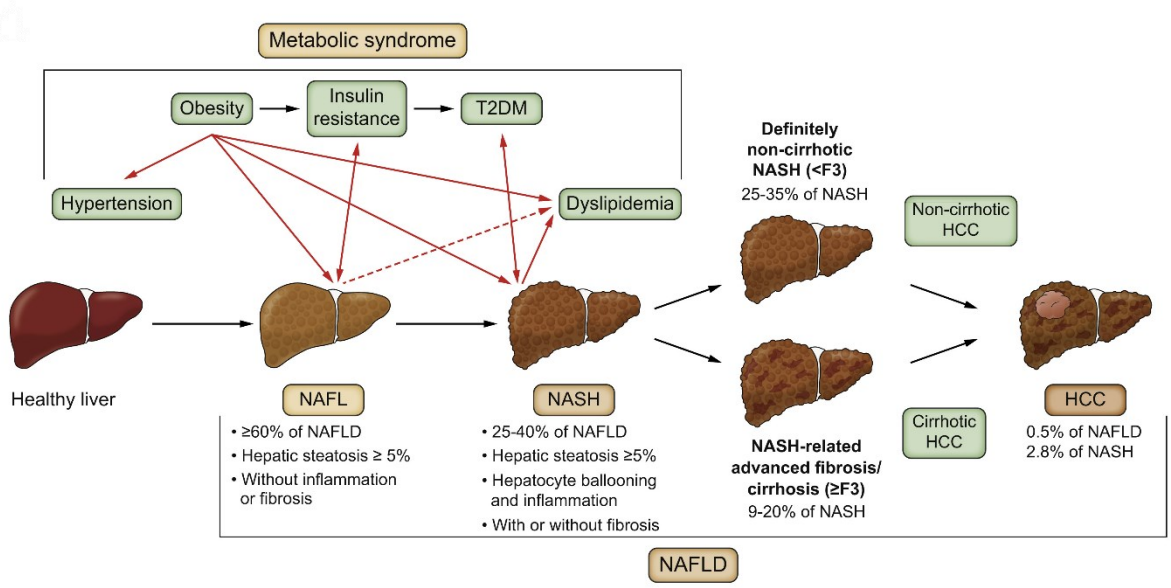

Figure 5| Natural history of NAFLD and its metabolic syndrome-associated risk factors. Non-alcoholic fatty liver disease (NAFLD) comprises a spectrum of liver pathologies ranging from simple hepatic steatosis (non-alcoholic fatty-liver, NAFL) to non-alcoholic steatohepatitis (NASH), which is characterised by the presence of inflammation and hepatocyte ballooning, with or without fibrosis. Obesity, insulin resistance, T2DM, dyslipidaemia, and hypertension are components of the metabolic syndrome and constitute risk factors for development of NAFLD, its hepatic manifestation. Red arrows indicate a risk for the target condition, whereas black arrows indicate a possible development/progression of the target condition. This figure and parts of the legend were adapted from "Hepatokines and adipokines in NASH-related hepatocellular carcinoma" by Kucukoglu, O., Sowa, J. P., Mazzolini, G. D., Syn, W. K., & Canbay, A. (2021) *Journal of Hepatology, 74*(2), 442–457 (https://doi.org/10.1016/j.jhep.2020.10.030). Copyright © 2020 European Association for the Study of the Liver. Licensed under CC BY-NC-ND 4.0.

1.2 RNA binding proteins

RNA-binding proteins (RBPs) are central players in post-transcriptional gene regulation. They can interact with coding and various kinds of non-coding RNAs to form functional ribonucleoprotein (RNP) complexes. The assembly of these RNP particles is dynamic as the composition changes depending on stage of life of the RNA and its cellular context (Singh et al., 2015). Thereby, a whole network of RBPs determine the fate of RNA molecules being involved in all processes throughout RNA life: transcription, splicing, 5'-capping, polyadenylation, transport, localisation, translation, and stability (Dreyfuss et al., 2002; Mitchell & Parker, 2014)(Figure 6).

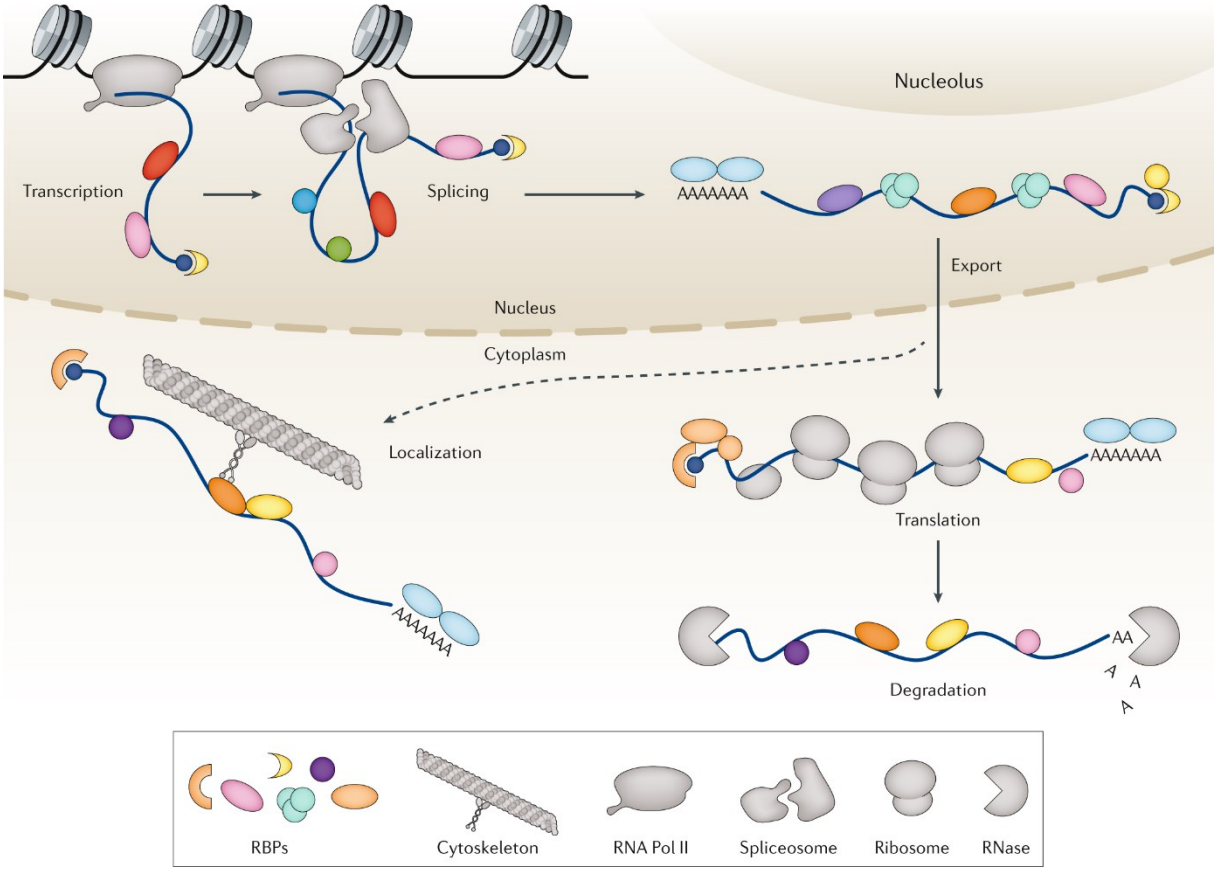

Figure 6| Impact of RBPs on the life cycle of RNA. Regulation of nuclear processes (e.g. transcription, splicing, 5'-capping, polyadenylation) and cytoplasmatic processes (e.g. localisation, translation, degradation) throughout RNA life by different RBPs. RNA Pol II, RNA polymerase II; RBP, RNA-binding protein. From "RNA-binding proteins in human genetic disease" by Gebauer, F., Schwarzl, T., Valcárcel, J., & Hentze, M. W. (2021), *Nature Reviews. Genetics, 22*(3), 185–198 (https://doi.org/10.1038/s41576-020-00302-y). With permission, copyright © 2020, Springer Nature Limited.

RNA-binding proteins harbour a modular structure of well-defined RNA-binding domains (RBDs) which facilitate the interaction with RNAs by binding to sequence-specific motifs and/or RNA secondary structures (Lunde et al., 2007). Most frequent RBDs include the RNA

recognition motif (RRM), the DEAD motif, the zinc-finger domain, and the heterogeneous nuclear ribonucleoprotein (hnRNP)-K homology (KH) domain. Additionally, Gerstberger et al. (2014) describe approximately 30 other canonical RBDs of lesser abundance, all being summarized in Figure 7.

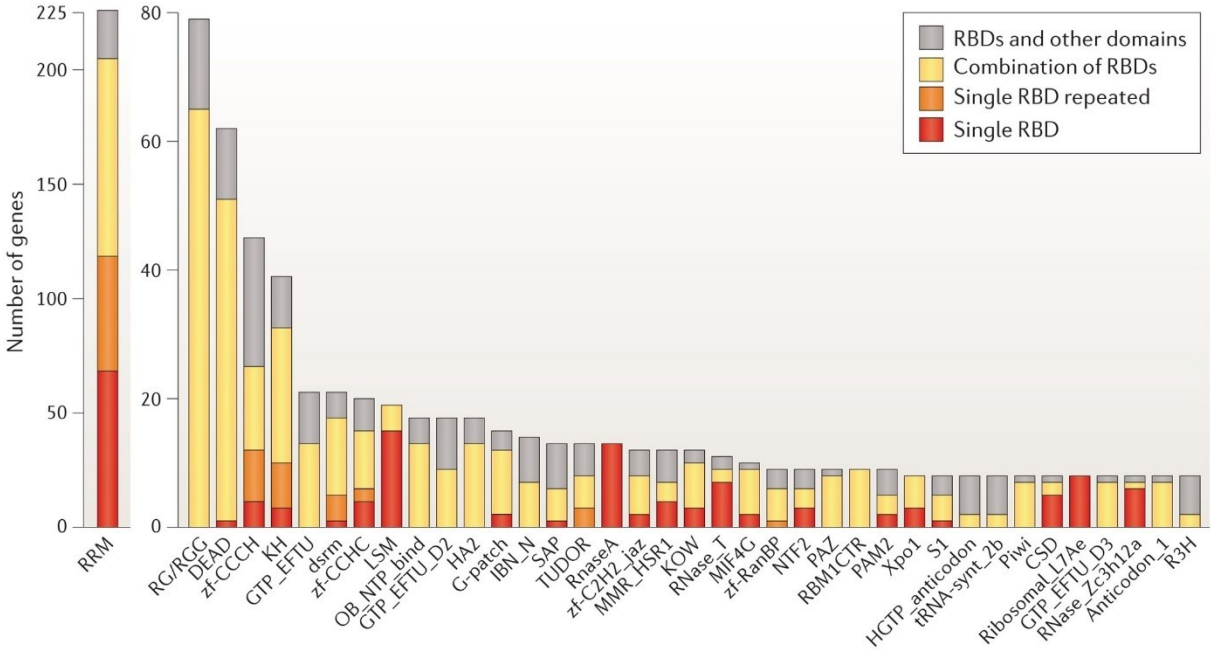

Figure 7| Analysis of RBDs in human genes. Counts of proteins with RNA-binding domains (RBDs) from the Protein families (Pfam) database with eight or more members in humans. Domain names are listed according to Pfam nomenclature. Counts are subdivided to indicate the number of genes containing one RBD as the only structural domain in the encoded protein (red); repeats of the same class of RBD (orange); one or more RBDs in combination with RBDs of different classes (yellow); or combinations of the RBD with one or more domains unrelated to RNA metabolic function (grey). From "A census of human RNA-binding proteins" by Gerstberger, S., Hafner, M., & Tuschl, T. (2014), *Nature Reviews. Genetics, 15*(12), 829–845 (https://doi.org/10.1038/nrg3813).

The combination of multiple RBDs within one protein offers synergistic effects for the RBP. It provides the protein with higher binding specificity and affinity than it would be possible with single domains that often bind short RNA stretches with weak affinity (Lunde et al., 2007). By contrast, various studies using RNA interactome capture to identify new RBPs throughout the genome, have revealed 1,218 RNA-binding proteins in different human cell lines (Baltz et al., 2012; Beckmann et al., 2015; Castello et al., 2012) of which 55% lack canonical RBDs (Beckmann et al., 2016). Further, Castello et al. (2016) indicate that half of the RNA-binding sites in RBPs map to intrinsically disordered regions, that is functional protein domains without defined three-dimensional structure (Calabretta & Richard, 2015) that can interact with RNA in a non-

canonical manner (Järvelin et al., 2016). These intrinsically disordered regions are subject to intense posttranscriptional modifications altering the functional state of RBPs suggesting a metabolic and signal-dependent regulation of RBPs (Castello et al., 2016). Other possible regulatory mechanisms are cofactor-binding (Clingman et al., 2014) or protein-protein interactions (Haghighat & Sonenberg, 1997).

Vice versa, RNA is able to control the activity of RBPs, a feature Hentze et al. (2018) named "riboregulation". For example, the RBPs protein kinase R (PKR) and retinoic acid-inducible gene I protein (RIGI) are involved in the host defence against viral infections. They act as cytoplasmatic sensors for virus-derived RNA products and can be activated due to binding of double-stranded RNA or 5' triphosphate RNA (Bou-Nader et al., 2019; Habjan & Pichlmair, 2015; Rehwinkel, 2013).

1.2.1 Role of RBPs in cancer

As mentioned above, RBPs are pivotal for controlling post-transcriptional gene regulation — from pre-messenger-RNA (pre-mRNA) splicing to protein translation (Figure 6). Due to the great number of possible interaction partners and their impact on RNA metabolism, it is no surprise that small alterations in expression and/or activity of RBPs have a great effect on the fine-tuned network of downstream signalling pathways. Therefore, a deregulation of RBP expression or functions underlie a broad spectrum of human disorders including genetic diseases and cancer (Gebauer et al., 2021; Lukong et al., 2008; Mohibi et al., 2019). Aberrant RBP expression and/or activity in cancer depends on various mechanisms including genomic alterations, transcriptional and post-transcriptional control, and posttranscriptional modifications.

According to the definition of Hanahan and Weinberg (2011), genome instability and mutations are major aspects underlying a multitude of the hallmarks of cancer (Figure 8).

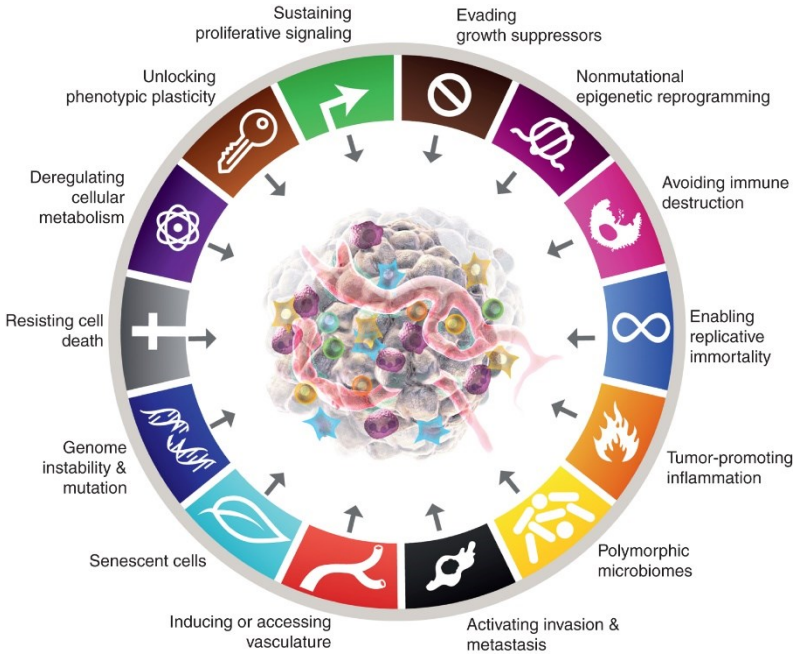

Figure 8| Hallmarks of cancer. Latest update of the original "Hallmarks of Cancer" graphic by Hanahan & Weinberg (2011). From "Hallmarks of Cancer: New Dimensions" by Hanahan D. (2022), *Cancer Discovery, 12*(1), 31–46 (https://doi.org/10.1158/2159-8290.CD-21-1059). With permission, copyright © 2022 American Association for Cancer Research.

A systematic analysis of RBPs in 11 solid tumours revealed genomic alterations, such as copy number variations and protein-affecting mutations, in 15% of the investigated RBPs (Sebestyén et al., 2016). In line, Neelamraju et al. (2018) identified 281 out of 1298 RBP-encoding genes (~22%) being significantly enriched for mutations in at least one cancer type, including most, frequently, frameshift and in-frame deletions as well as missense, nonsense, and silent mutations. The average mutation frequency was ~3 mutations per Mb across 26 cancer types (Neelamraju et al., 2018). Additionally, RBPs, such as CUGBP Elav-like family member 2 (CELF2), can be epigenetically regulated. Hypermethylation of CELF2's promoter site results in transcriptional silencing in human breast cancer (Pique et al., 2019).

Further, RBPs are post-transcriptionally controlled due to interactions with non-coding RNAs or other RBPs. On the one hand, the translation of ELAV-like RNA-binding protein 1 (ELAVL1, HUR) can be repressed by the micro-RNAs (miRNAs) miR-125a and miR-519 resulting in reduced proliferation of breast, cervical, colon, and ovarian cancer cells *in vitro* (Abdelmohsen et al., 2008; X. Guo et al., 2009). On the other hand, ELAVL1 can increase the translation rate of musashi RNA binding protein 1 (MSI1), an important RBP for stem cell maintenance and tumourigenesis, by stabilising its mRNA (Vo et al., 2012).

Among all mechanisms, PTMs, such as acetylation, methylation, phosphorylation, and ubiquitination, take the leading role in influencing RBP activity as IDRs are "hotspots" for PTMs (Castello et al., 2016). For instance, Src-associated protein in mitosis of 68 kDa (Sam68, Khdrbs1), a KH domain-containing RBP involved in cell-cycle control, is acetylated by the acetyltransferase cAMP responsive element binding- binding protein (CREB-binding protein) enhancing the ability of Sam68 to bind poly(U) RNA (Babic et al., 2004). Conversely, the RNA-binding ability of Sam68 is negatively regulated by phosphorylation of its Src-homology (SH) 2 and SH3 domains or methylation of arginine residues (Derry et al., 2000; Rho et al., 2007).

On the molecular level alternative splicing is one major aspect, which is affected by dysregulated RBPs in cancer (S. C. Lee & Abdel-Wahab, 2016; E. Wang & Aifantis, 2020). Constitutive splicing and alternative splicing (Figure 9) are performed by the spliceosome, a multimeric protein complex (Jurica & Moore, 2003; Rino & Carmo-Fonseca, 2009). Thereby cis-regulatory splicing elements, such as exonic or intronic splicing enhancers or silencers, are targeted by serine/arginine-rich proteins and heterogeneous nuclear ribonucleoproteins (hnRNPs), which represent subfamilies of RBPs. These RBPs act as key regulators of the splice-site selection and recognition by the spliceosome resulting in alternative isoforms that potentially encode non-functional proteins (Coltri et al., 2019).

Like alternative splicing, alternative polyadenylation (APA), that is the addition of a poly(A) tail to different loci at the 3' end of mRNA transcripts to prevent their decay, results in various mRNA isoforms that are discriminated by their coding sequence or 3'-untranslated region (3'-UTR). Therefore, on the one hand APA can affect the function of encoded proteins. On the other hand, APA has an impact on the stability, localisation, and translational efficiency of the target mRNA due to the variations in the 3'-UTRs, which represent important docking platforms for regulatory factors, particularly for repressive miRNAs. This is one reason, why in cancer cells mRNA isoforms with shorter 3'-UTRs exhibit an increased stability and up to 10-fold more protein production (Mayr & Bartel, 2009).

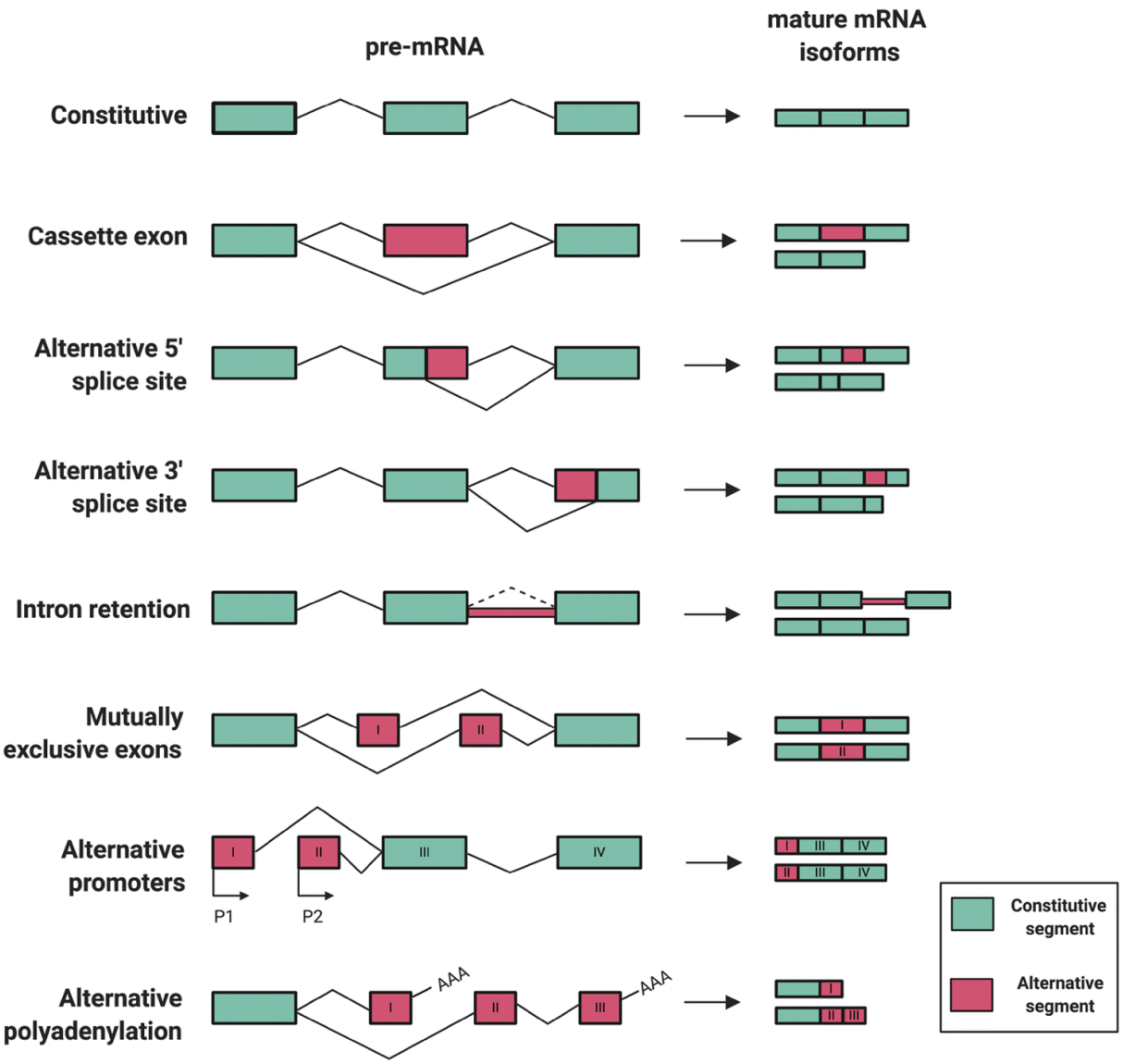

Figure 9| Constitutive and alternative splicing events. Depicted are seven types of alternative splicing events (alternative polyadenylation included). Compared to constitutive splicing, exons can be skipped completely (cassette exon) or only a part of an exon can be included into the mature mRNA isoform (alternative 5' or 3' splice site). Additionally, there is the possibility that an intron is not spliced out (intron retention). Mutually exclusive exons are characterised by skipping and retention of at least one exon each. The use of alternative promoters results in different mRNA transcripts as well as alternative polyadenylation. Boxes represent exons and lines represent introns. From "Alternative splicing in aging and longevity" by Bhadra, M., Howell, P., Dutta, S., Heintz, C., & Mair, W. B. (2020), *Human Genetics, 139*(3), 357–369 (https://doi.org/10.1007/s00439-019-02094-6). With permission, copyright © 2019, Springer-Verlag GmbH Germany, part of Springer Nature.

Contrary, 3'-UTRs can harbour *cis*-destabilising elements such as adenylate/uridylate (AU)–rich elements (AREs), which are present in 16% of all protein coding transcripts (Gruber et al., 2011). These short sequence motifs include an AUUUA pentamer core in additional AU context, for example UAUUUAU, UUAUUUAU or overlapping repeats of the pentamer (Khabar, 2017). There are two classification systems for AREs: the class classification (class I-

class III), which is based on the context of the pentamer, and the cluster classification (cluster 1-cluster 5) based on the number of repeats of the pentamer core (Khabar, 2017). However, ARE sequences are targeted by ARE-binding proteins (ARE-BPs), another subfamily of RBPs, predominantly leading to the decay of the mRNA transcript initiated by the removal of the protective 7-methylguanylate (m^7G) cap at the 5′ end or deadenylation of the 3′ poly(A) tail (Lykke-Andersen & Wagner, 2005). Frequently, transcripts of oncogenes, growth factors, and inflammatory cytokines contain AREs and altered stability of those contribute to carcinogenesis (Hitti et al., 2016; Otsuka et al., 2019).

As mentioned, RBPs are central players in the regulation of the intracellular localisation of mRNAs. They can bind to specific sequences, "zipcodes", in the regulatory 3′-UTR of target transcripts to induce the assembly of multimeric complexes linking mRNAs to motor proteins that facilitate the transport along the cytoskeleton to a subcellular destination. One prominent example is the insulin-like growth factor (IGF) 2 mRNA binding protein 1 (IGF2BP1, IMP1, ZBP1, VICKZ1) that associates with the actin beta (*ACTB*) transcript in the cell's nucleus to promote its translocation to actin-rich protrusions in primary fibroblasts and neurons. Thereby, translation initiation in the cytoplasm is blocked until the RNP reaches the destination in the cell periphery, where IMP1 is phosphorylated by the spatially restricted tyrosine kinase SRC to initiate translation (Hüttelmaier et al., 2005). Primarily, IMP1 interacts with mRNA targets encoding important mediators for cell adhesion and motility, such as E-cadherin, β-actin, α-actinin and the actin-related protein 2/3 (Arp2/3) complex. Therefore, downregulation of IMP1 is associated with increased cell migration and metastasis in breast cancer cell lines and tumours (Gu et al., 2012; Gu et al., 2009).

At last, RBPs are key actors in one of the most important and complex processes inside the cell: mRNA translation. RBPs like the eukaryotic translation initiation factor (eIF) 4F, an important conglomerate of eIF4E, eIF4G, and RNA helicase eIF4A, and the poly(A)-binding protein exert translational control as they facilitate binding to the 5′-m^7G cap of mRNA initiating mRNA translation. In cancer, many translation initiation factors are dysregulated and show an altered expression and/or activity (Ruggero, 2013). Additionally, mutations of oncogenes, such as *MYC*, *RAS*, phosphatidylinositol-4,5-bisphosphate 3-kinase catalytic subunit-α (*PIK3CA*), and tumour suppressors like phosphatase and tensin homologue (*PTEN*) and tumour protein p53

(*TP53*), frequently occur in signalling pathways that are tightly connected to the translation machinery (Bhat et al., 2015; Ruggero, 2013).

Moreover, cells have the possibility to circumvent cap-mediated mRNA translation under tumour-associated stress conditions. One example are internal ribosome entry sites (IRES) located in the regulatory 5′-untranslated region (5′-UTR) of the mRNA that facilitate direct recruitment of the ribosome mediated by IRES *trans*-acting factors, another subfamily of RBPs potentially misregulated in carcinogenesis (Faye & Holcik, 2015).

All these molecular mechanisms contribute to the transformation into malignant cells and shape the phenotype of cancer cells characterised by the hallmarks of cancer (Figure 8).

1.2.2 ZFP36 ring finger protein

ZFP36 ring finger protein, also known as Tristetraprolin (TTP), G0/G1 switch regulatory protein 24 (GOS24) or growth factor-inducible nuclear protein 475 (NUP475), is a RBP with a size of 326 amino acids (aa) (~34 kDa). The protein is encoded by the *ZFP36* gene, which contains two exons and is located on chromosome 19q13.2 (GRCh38.p13). TTP is the founding member of a small superfamily of RBPs named TPA-inducible sequence 11 (TIS11) family that consist of four mammalian paralogues: TTP (TIS11), TIS11B (ZFP36L1, ERF-1, BRF-1), TIS11D (ZFP36L2, ERF-2, BRF-2), and Zfp36l3, which was only detected in the placenta and extraembryonic tissues in rodents (Blackshear et al., 2005). All family members share the same protein-binding domains, that is the highly conserved tandem CCCH (cysteine-cysteine-cysteine-histidine) zinc finger motif (Brooks & Blackshear, 2013). Generally, zinc fingers are composed of 25-30 aa forming a $\alpha\beta\beta\alpha$ secondary structure that coordinate a central Zn^{2+} ion and are classified based on the amino acid residues interacting with this zinc ion (Hudson et al., 2004). In addition, TTP possesses an amino-terminal nuclear export sequence, a carboxy-terminal NOT1-binding domain and, of note, in between three proline-rich domains consisting of four consecutive prolines, being responsible for the protein's name (not shown in Figure 10).

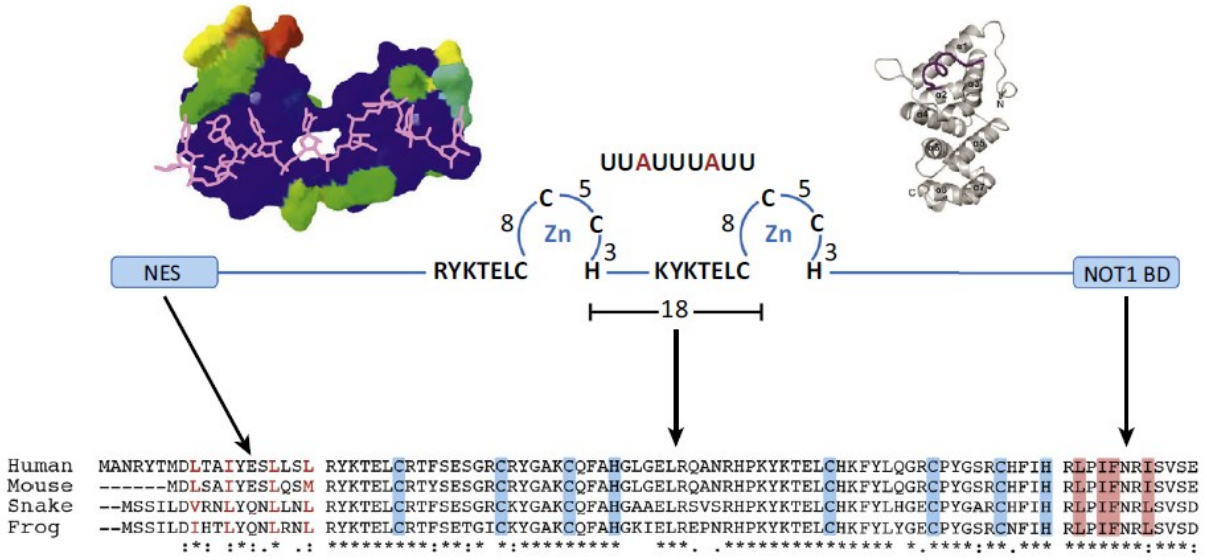

Figure 10| Critical domains of Tristetraprolin. In the centre of the figure is a schematic diagram of three critical domains of Tristetraprolin (TTP): the N terminal nuclear export sequence (NES), the central tandem CCCH zinc finger (TZF) domain, and the C-terminal NOT1-binding domain (NOT1 BD). The key cysteines and histidines in each finger, as well as the conserved lead-in sequences, are indicated for the TZF domain, as is the ideal 9-base RNA-binding site that is a component of many adenosine-uridine-rich regions in TTP target mRNAs. The first proline-rich domain between NES and TZF as well as the two others between TZF and NOT1BD are not depicted. At the upper left is shown a structural model of the human TTP TZF domain bound to the same 9-base RNA sequence as shown at the top; RNA is in magenta in this figure. This structural model is reproduced from Carrick et al. (2004), with permission, and is based on the original structure of the ZFP36L2 (TIS11D) TZF domain (Hudson et al., 2014). At the upper right is a diagram of the crystal structure of the C terminal NOT1-binding domain peptide of TTP (maroon), binding to the three internal helices from the human NOT1 protein (grey); this structure is reproduced from Fabian et al. (2013), with permission. At the bottom are shown parts of an amino acid sequence alignment done with Clustal Omega of human TTP with its orthologs from mouse, snake, and frog. According to Clustal conventions, asterisks at the bottom indicate sequence identity at that site; a colon indicates a conserved residue; and a period indicates a less well-conserved residue. Shown are the N termini of the proteins, with their conserved NESs; in this case, the branched chain amino acids are coloured red. The TZF domain alignment is shown in the middle, with the critical cysteines and histidines shaded in blue. The NOT1-binding domains are shown on the right, with the sequences representing the extreme C termini of the proteins. Highlighted in pink are the amino acid residues that are inserted into the hydrophobic groove of the NOT1 protein central domain (upper right) (Fabian et al., 2013). The spaces in the sequence alignments represent gaps of various sizes. The sequences are from the following Gen Bank accession numbers: human (*Homo sapiens*), NP_003398.2; mouse (*Mus musculus*), NP_035886.1; snake [*Protobothrops mucrosquamatus* (Taiwanhabu)], XP_015676155.1; and frog (*Xenopus tropicalis*), NP_001106542.1. This figure and caption were adapted from "Tristetraprolin as a Therapeutic Target in Inflammatory Disease" by Patial, S., & Blackshear, P. J. (2016), *Trends in Pharmacological Sciences, 37*(10), 811–8210 (https://doi.org/10.1016/j.tips.2016.07.002P). With permission, copyright © 2016 Elsevier Ltd.

Initially, TTP was identified in murine fibroblasts as gene that could be rapidly induced in response to insulin and other mitogens (Lai et al., 1990). It belongs to the introduced subclass of ARE-BPs dooming their mRNA targets to decay. A requirement for that is the interaction between the tandem zinc finger domain of the protein and consensus motifs in the 3′-UTR of

mRNA targets containing at least an AUUUA pentamer core in additional AU context (Khabar, 2017). As a result, TTP mediates either the 5′ to 3′ decay by recruitment of a decapping enzyme complex including 5′-3′ exoribonuclease 1 (XRN1) (Fenger-Gron et al., 2005) or the 3′ to 5′ shortening of the poly(A) tail by the CCR4-CF1-NOT1 deadenylation complex (Lai et al., 1999).

Approximately 16% of human protein-coding genes harbour at least one occurrence of the ARE consensus motif WUAUUUAUW (W referring to IUPAC nucleotide code, i.e. A or T) in their 3′-UTR (Gruber et al., 2011) and many of these genes participate in inflammation, immune response, and carcinogenesis (Khabar, 2017; Lourou et al., 2019). For instance, TTP is one element of a negative feedback loop controlling the production of the important inflammatory cytokine tumour necrosis factor (TNF). On the one hand, TTP expression can be triggered by the same agents that stimulate TNF production, including TNF itself (Hahn et al., 2014). On the other hand, TTP inhibits TNF production by destabilizing its mRNA (Carballo et al., 1998). The physiological role of TTP has been shown in TTP-deficient mice. They appear normal at birth but develop a complex syndrome of inflammatory arthritis, dermatitis, cachexia, autoimmunity and myeloid hyperplasia within the first eight weeks of their lifetime (Taylor et al., 1996). This phenotype is comparable with that investigated in *Tnf*-transgenic mice (Probert et al., 1996) and their development can be abrogated by the injection of TNF antibodies (Taylor et al., 1996). Not only numerous pro-inflammatory molecules are targeted by TTP due to AREs in their 3′-UTR (Brooks & Blackshear, 2013), but also anti-inflammatory cytokines such as interleukin (IL)-10. As part of a negative feedback loop, TTP is induced by IL-10, but also controls the production of IL-10, indicating that TTP can influence both, initiation and resolution of inflammatory processes (Gaba et al., 2012). Moreover, TTP is implicated in the regulation of the glucocorticoid-induced leucine zipper (GILZ), a molecule that mediates the anti-inflammatory effects of glucocorticoids by nuclear factor kappa B (NF-κB) inhibition (Bereshchenko et al., 2019). Hoppstädter et. al. (2012) found a TTP-mediated GILZ downregulation on mRNA and protein level in TTP-overexpressing THP-1 cells.

Several studies have demonstrated downregulated TTP expression in human malignancies, such as breast, cervical, colorectal, gastric, liver, lung, pancreatic, and prostate cancer, suggesting tumour suppressive actions of TTP (Al-Souhibani et al., 2010; Berglund et al., 2016;

Coelho et al., 2017; Goddio et al., 2012; Montorsi et al., 2016; Sanduja et al., 2009; Sohn et al., 2010; Wei et al., 2016). A list of oncogenes and tumour suppressors that are involved in tumourigenesis, harbour AREs, and are subject to TTP-mediated mRNA decay are reviewed by J. M. Park et al. (2018) (Figure 11). Noteworthy, only three genes out of 24 are regarded as tumour suppressors, for instance cyclin-dependant kinase inhibitor 1A (p21, *CDKN1A*), large tumour suppressor kinase 2 (*LATS2*), and aryl-hydrocarbon receptor repressor (*AHRR*) (Al-Haj et al., 2012; H. H. Lee et al., 2013; H. H. Lee et al., 2010).

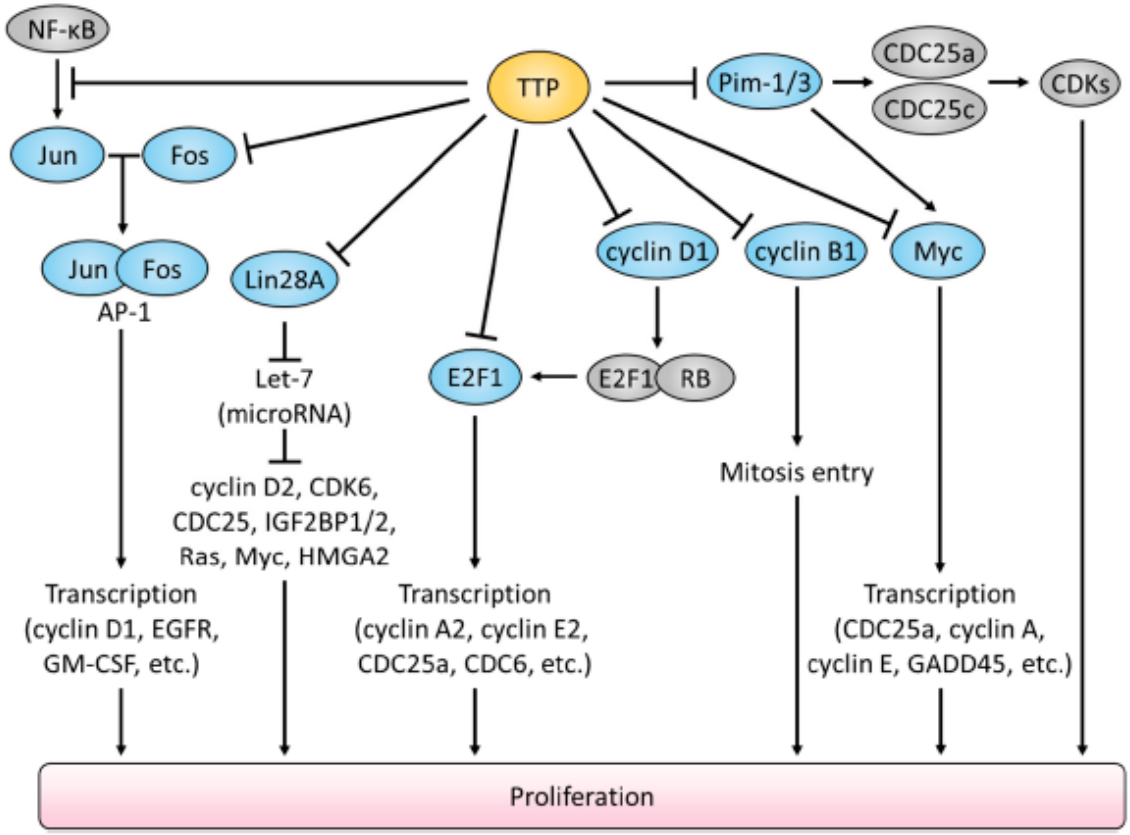

Figure 11| TTP-mediated inhibition of oncogenic signal pathways attenuating cell proliferation. From "Roles of tristetraprolin in tumorigenesis" by Park, J. M., Lee, T. H., & Kang, T. H. (2018), *International journal of molecular sciences*, *19*(11), 3384 (https://doi.org/10.3390/ijms19113384). Licensed under CC BY 4.0.

The majority of these genes are involved in cellular proliferation due to their direct or indirect impact on cyclin-dependant cell-cycle progression. Another mechanism is the TTP-mediated suppression of lin-28-homolog A (Lin28A), which further downstream leads to an increase of the let-7 family of tumour suppressor miRNAs (J. Y. Lee et al., 2013). Consecutively, the expression of high mobility group AT-hook 2 (HMGA2) can be suppressed, an oncogene that is upregulated in nearly all human malignancies (Mansoori et al., 2021).

Aside from its regulatory role in mRNA stability, TTP participates in NF-κB-mediated gene transcription. It inhibits the expression of the oncogenic transcription factor c-Jun by selectively blocking the nuclear translocation of NF-κB subunit p65 (L. Xu et al., 2015).

TTP is also involved in the regulation of key processes during tumour progression, such as epithelial-mesenchymal-transition (EMT), angiogenesis, migration, and metastasis. Recent studies indicate the interaction between TTP and EMT marker genes, including zinc finger protein snail 1 (*Snail1*), twist-related protein 1 (*Twist1*), zinc finger E-box binding homeobox 1 (*ZEB1*), SRY-box transcription factor 9 (*SOX9*), and MET transcriptional regulator MACC1 (*MACC1*) (Montorsi et al., 2016; Yoon et al., 2016). In an oral mucosa invasion model TTP promoted cancer cell invasion *via* matrix metalloproteinase (MMP) 9, MMP2, and IL-6 (Van Tubergen et al., 2013). Vascular endothelial growth factor (VEGF), a highly specific mitogen and mediator of pathophysiological angiogenesis, is induced in response to hypoxia or cytokines by tumour cells. TTP binding to the 3'-UTR of *VEGF* mRNA leads to its destabilisation and facilitate maintenance of basal VEGF levels (Essafi-Benkhadir et al., 2007).

1.2.3 Insulin-like growth factor 2 mRNA-binding protein 2

The IGF2 mRNA-binding protein 2 (IGF2BP2/IMP2/VICKZ2) has a size of 599 aa (~66 kDa) and is encoded by the *IGF2BP2* gene, which contains 16 exons and is located on chromosome 3q27.2 (GRCh38.p13). Among seven splice variants (Figure 12), p62 (IGF2BP2-2) is the most common one, lacking exon 10 of the *IGF2BP2* transcript, and is translated into a 62 kDa protein with 556 aa (J.-Y. Zhang et al., 1999). IMP2 and its transcript variants belong to a family of highly conserved RBPs with two mammalian paralogues (IMP1 and IMP3) sharing the same structure of RBDs: two N-terminal RRMs are followed by four KH domains at the C-terminus (Nielsen et al., 1999). These six canonical RBDs are arranged into three pairs (RRM12, KH12, KH34) (Biswas et al., 2019).

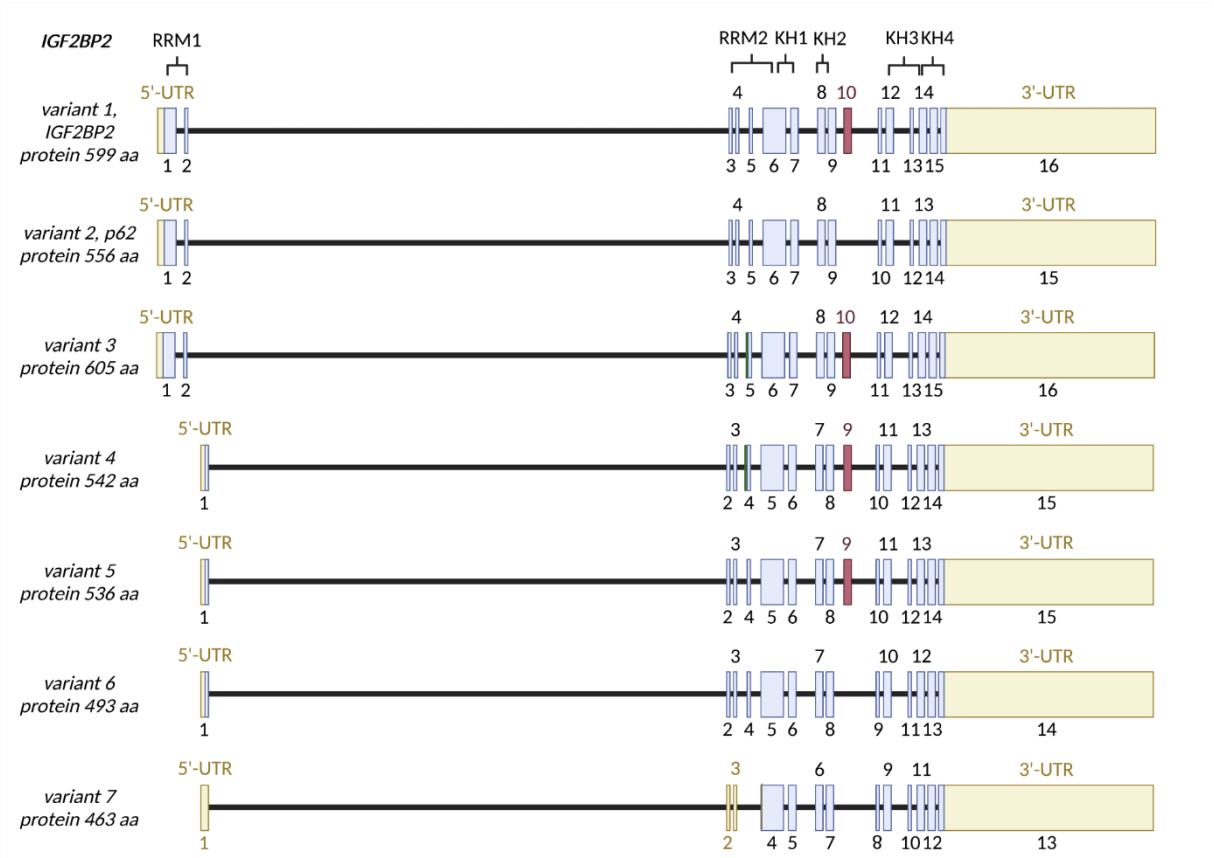

Figure 12| *IGF2BP2* transcript variants. Comparison of the exons of the *IGF2BP2* gene that are contained in different transcript variants (1-7) are shown (predicted transcript variants are not depicted). Respectively, the size of the encoded protein is written below the name of the transcript variant. On top, the location of the encoded RBDs RRM1-2 and KH1-4 is marked. Numbers of the exons are written above or below each exon (blue rectangles). The part of the exons containing the 5' UTR and 3'-UTR is coloured yellowish. Exon 10, referred to transcript variant 1, is labelled red and spliced out in the transcripts 2, 6, and 7. Transcript 4-6 sharing the same first exon that is different to those of the other variants. Transcription start site of variant 7 is encoded in exon 4 or exon 6, when referring to transcript variant 1. Additionally, variants 3 and 4 share the same 18 bp extension in the beginning of exon 5 or 4, which is labelled green. Transcript variant 1 (NM_006548.6), variant 2 (NM_001007225.3), variant 3 (NM_001291869.3), variant 4 (NM_001291872.3), variant 5 (NM_001291873.2), variant 6 (NM_001291874.3), and variant 7 (NM_001291875.3) according to GRCh38.p13. Created with BioRender.com.

Each RRM of IMP2 contains approximately 75 aa and structurally follows a $\beta_1\alpha_2\beta_2\beta_3\alpha_2\beta_4$ topology comprising four anti-parallel β-sheets stacked against two α helices (Figure 13). Moreover, RRM1 contains in their β_1- and β_3-sheets two conserved sub-motifs consisting of six or eight aa with the consensus sequences (L/I)-(F/Y)-(V/I)-X-(N/G)-L or (R/K)-G-(F/Y)-(G/A)-(F/Y)-V-X-(F/Y) (Mohibi et al., 2019). The KH domains are typically around 70 aa long and composed of three α-helices and three-stranded anti-parallel β-sheets forming a conserved $\beta\alpha\alpha\beta$ core (Grishin, 2001). Additionally, KH domains share a conserved GXXG loop motif and a variable loop, which are involved in nucleotide binding (Biswas et al., 2019). Furthermore, KH2 and KH4 domains of IMP2 harbour nuclear export signals (Conway et al., 2016; Nielsen et al., 2003), enabling the predominantly cytoplasmatic protein to transport target transcripts out of the nucleus, protecting them from degradation, and regulating their translation spatially and temporally (Cao et al., 2018). The human IMP-family members possess an overall sequence identity of 56% (Bell et al., 2013), when focussing only on individual RBDs the identity even reaches 70% (Biswas et al., 2019).

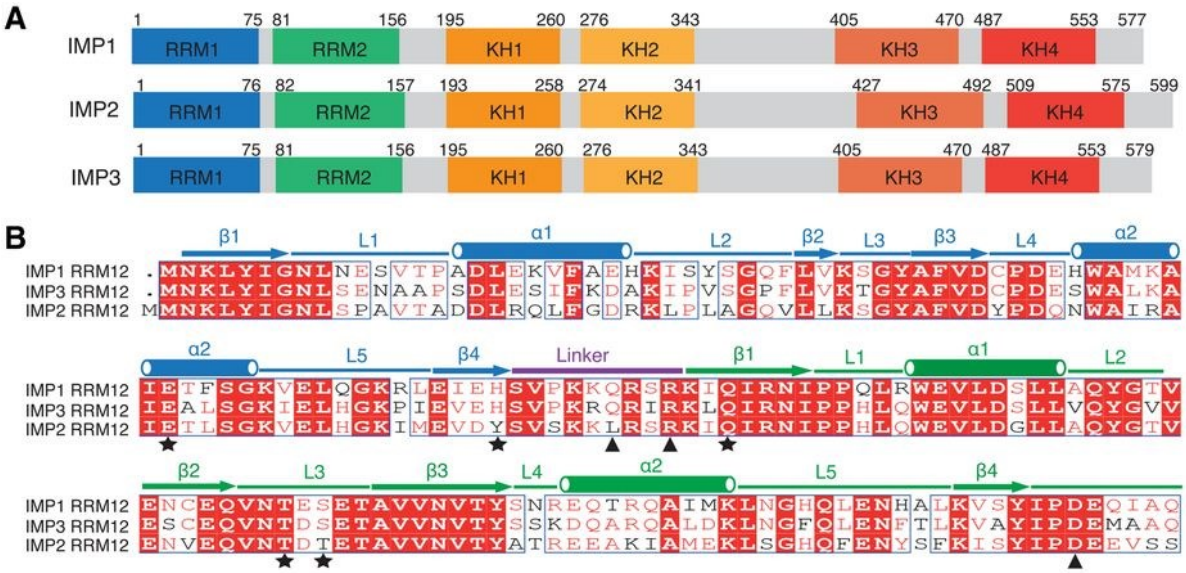

Figure 13| RNA-binding domains of the IMP-family members and structure of RRM1 and RRM2. (A) Schematic diagram showing conserved domain arrangement of IMP-family members. (B) Sequence alignment of RRM12 domains of IMP1-3. Identical residues (white), highly conserved (red), and not conserved (black) are depicted. Residues involved in the RRM1-RRM2 interface (star) and the linker-RRM2 (C-terminus) interactions (triangle) are shown. Figure and caption from "Structural basis of IMP3 RRM12 recognition of RNA" by Jia, M., Gut, H., & Chao, J. A. (2018), *RNA*, 24(12), 1659–1666 (https://doi.org/10.1261/rna.065649.118). Licensed under CC BY-NC 4.0.

IMP2 and its paralogues are oncofetal proteins that control RNA processing of their target mRNAs at multiple steps including stabilisation, localisation, and translation. Their physiological expression primarily takes place during embryogenesis and tissue maturation,

where they are believed to be important for cell migration, metabolism, and stem cell renewal (Degrauwe et al., 2016). After birth, the expression of IMP1 and IMP3 is either completely absent or heavily downregulated, whereas IMP2 expression persists in several adult organs. However, re-expression is accompanied with malignant transformation in several aggressive cancer types (Bell et al., 2013; Czepukojc et al., 2019; Degrauwe et al., 2016). Initially, at the same time p62 was identified as an autoantigen in HCC (J.-Y. Zhang et al., 1999), and Nielsen et al. (1999) reported a cDNA called IMP2 that was completely identical to p62 except for an insertion of 43 aa between the KH2 and KH3 domains, corresponding to exon 10. Overexpression of IMP2 promotes hepatocarcinogenesis, is associated with elevated levels of the fetal markers AFP (alpha fetoprotein) and DLK1/Pref-1/FA-1 (delta like non-canonical Notch ligand 1), aggressive tumour phenotypes and poor outcome for patients (Kessler et al., 2013, 2015, M. Lu et al., 2001). Furthermore, IMP2 levels correlate with IGF2 expression in HCC (Kessler et al., 2013). IGF2, in turn, can bind as ligand to various receptors, including the IGF receptors and insulin receptors, and activate downstream signal pathways leading to inhibition of apoptosis, increased proliferation, and metastasis in tumours, especially in CRC (Kasprzak & Adamek, 2019). Moreover, other target transcripts of IMP2 encoding mitochondrial components and thousands of putative binding sequences were identified using immunoprecipitation approaches (Conway et al., 2016; Dai et al., 2015; Hafner et al., 2010), but still only a few client mRNAs are confirmed targets of IMP2 (Cao et al., 2018).

Recently, IGF2BPs have been reported to belong to a distinct family of N^6-methyladenosine (m6A) readers that interact with client mRNAs through binding of the consensus GG(m6A)C sequence, thereby stabilising target transcripts (H. Huang et al., 2018). m6A is the most abundant internal transcriptional modification of eukaryotic mRNA and is implicated in the regulation of gene expression by affecting mRNA metabolism (S. Wang et al., 2022). Due to its multiple potential interaction partners, IMP2 is involved in a wide spectrum of physiological functions including embryonic development (Liu et al., 2019; Nielsen et al., 1999), particularly the regulation of the differentiation of neural precursor cells (Fujii et al., 2013), muscle cell motility (Boudoukha et al., 2010), and energy metabolism (Janiszewska et al., 2012; Laggai et al., 2014). Strikingly, these physiological consequences can be observed in mice with homozygous *Imp2* deletion. They are phenotypically smaller in size than their normal littermates, which is a result of the reduced lean mass gain and fat deposition after weaning,

leading also to an increased lifespan (Dai et al., 2015). In addition, *Imp2* null mice are resistant to diet-induced obesity and fatty liver and exhibit improved glucose tolerance and insulin sensitivity, increased energy expenditure, and elevated levels of the polypeptide UCP1 (uncoupling protein 1, thermogenin) in brown adipocytes, which is accompanied by an increase of uncoupled oxygen consumption (Dai et al., 2015). *Vice versa*, liver-specific overexpression of p62 in transgenic mice displayed steatosis and an induction of fatty liver associated with an increase of fatty acid elongation due to elevated levels of the underlying enzyme elongation of very long chain fatty acids protein 6 (ELOVL6) (Laggai et al., 2014; Tybl et al., 2011). ELOVL6 catalyses the elongation of C12-C16 saturated and monounsaturated fatty acids and promotes hepatosteatosis (Matzuka et al., 2012). Moreover, p62 transgenics, fed a methionine-choline-deficient diet to mimic non-alcoholic fatty liver disease as one main risk factor for HCC, indicated an earlier onset and a more pronounced manifestation of fibrosis (Simon et al., 2014).

Further, in 2007 three independent studies demonstrated that the genetic variance within the *IGF2BP2* gene, that is single nucleotide polymorphisms (SNPs) in intron 2, is strongly associated with T2DM, a widespread disease in humans (Saxena et al., 2007; Scott et al., 2007; Zeggini et al., 2007). Recently, Greenwald and colleagues (2019) revealed IMP2 T2DM-associated SNPs (rs7646518) that reduce islet enhancer activity and IGF2BP2 expression. Additionally, conditional inactivation of IGF2BP2 in mouse islets led to impaired glucose-mediated insulin secretion (Greenwald et al., 2019). IMP2 stabilises the mRNA of the glucose transporter GLUT1 and thereby supports aerobic glycolysis and tumour cell proliferation in pancreatic ductal adenocarcinoma (S. Huang et al., 2019). Another study, investigating IMP2 implications in the respiratory chain in more detail, found that IMP2 regulates oxidative phosphorylation in gliomaspheres, stabilises mRNA coding for mitochondrial respiratory chain complex subunits, and finally is also able to directly interact with complex I (NADH:ubiquinone oxidoreductase) proteins (Janiszewska et al., 2012).

As part of a feedback loop, IMP2 is regulated by a complex network including let-7 family members and HMGA2 (Figure 11) (Cleynen et al., 2007; Schaeffer et al., 2012). In the context of cancer, overexpression of the oncofetal IMP2 correlates with a poor prognosis for patients suffering from HCC, esophageal adenocarcinoma, head and neck squamous cell carcinoma, breast, gallbladder, colorectal, and pancreatic cancer (A. Barghash et al., 2016; A. Barghash et

al., 2015; Deng et al., 2020; Kessler et al., 2013, 2015, 2017; W. Liu et al., 2013; X. Xu et al., 2019; Ye et al., 2016). In line with these findings, IMP2 promotes several hallmarks of cancer, such as genomic instability, stem cell maintenance, and cancer cell migration and invasion (Degrauwe et al., 2016; Kessler et al., 2015; Y. Li et al., 2015; Xing et al., 2019). The regulatory role of IMP2 and its interaction partners in various cancer entities is summarised in Figure 14.

.

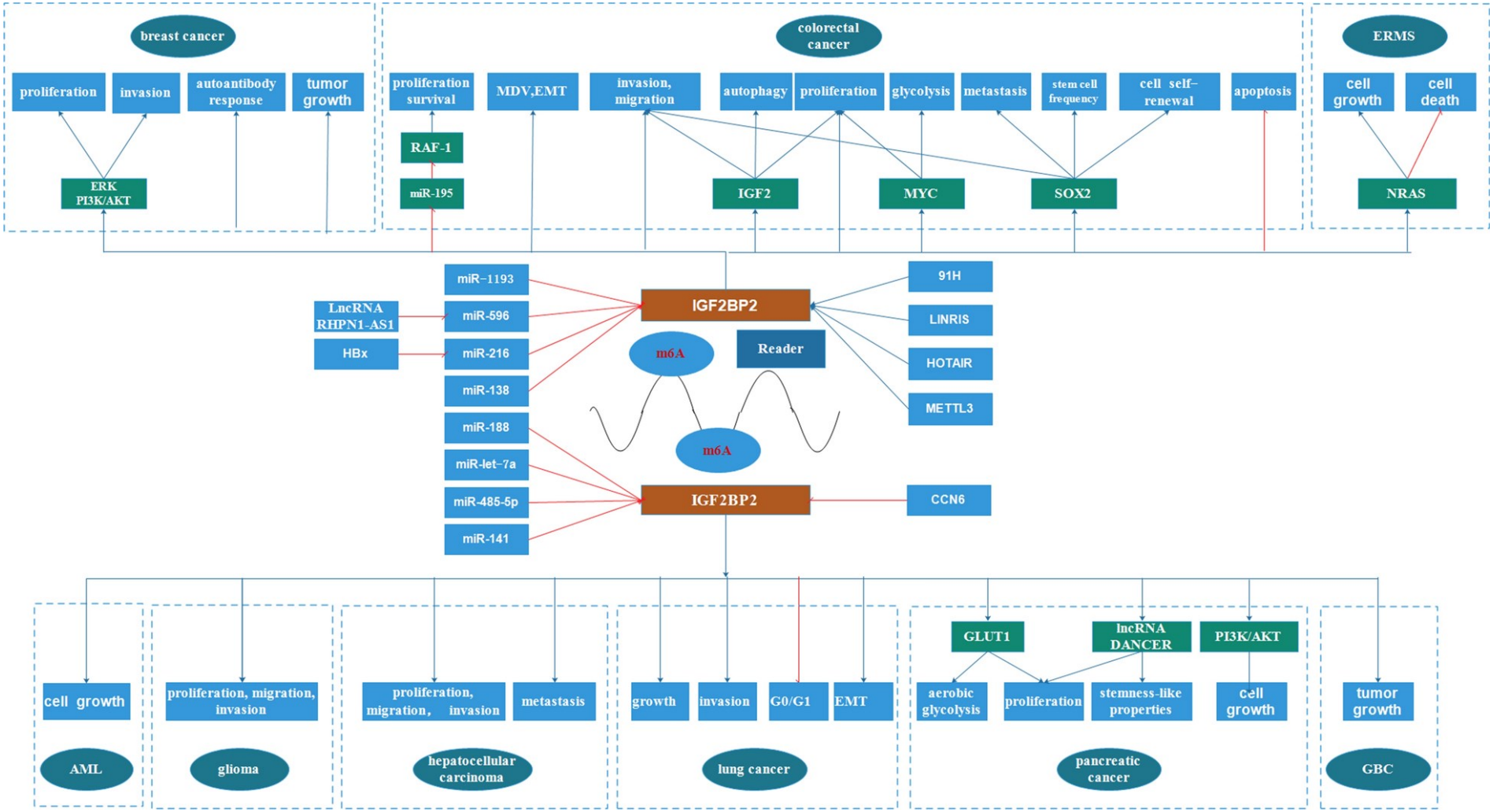

Figure 14| Regulatory network of IMP2 and its interaction partners in different cancer entities. IMP2/IGF2BP2 performs its multiple modulatory functions by interacting with miRNAs, long non-coding RNAs (lncRNAs), mRNAs and other m6A-related genes. Blue lines: activation; red lines: inhibition. AML: acute myelocytic leukaemia; EMT: epithelial-mesenchymal-transition; ERMS: embryonal rhabdomyosarcoma; GBC: gallbladder carcinoma; MDV: microvessel density value, surrogate marker for angiogenesis. From "The role of IGF2BP2, an m6A reader gene, in human metabolic diseases and cancers" by Wang, J., Chen, L., & Qiang, P. (2021), *Cancer Cell International, 21*(1), 99 (https://doi.org/10.1186/s12935-021-01799-x). Licensed under CC BY 4.0.

1.2.4 Target identification mediated by RNA-protein interactions

In recent years much effort has been devoted to the studies of RNA-protein interaction (Ramanathan et al., 2019) expanding the human RBPome from 1,542 experimentally validated RBPs in 2014 (Gerstberger et al., 2014) up to 2,986 representatives in 2021 (Z. Zhang et al., 2021), accounting for approximately 15% of all protein-coding genes in humans. Thereby a great variety of strategies has been employed including various variants of UV irradiation-induced cross-linking and immunoprecipitation (CLIP) to capture ribonucleoprotein complexes in intact cells (F. Lee & Ule, 2018). Further applied methods were mass spectrometry analysis of proteins using enrichment strategies that take advantage of eukaryotic poly(A) tails of mRNA (Baltz et al., 2012; Castello et al., 2012), psoralen probe-based RNA tagging (Z. Zhang et al., 2021), 5-ethynyluridine labelling (Bao et al., 2018; R. Huang et al., 2018), solubility of RNPs in organic solvents (Queiroz et al., 2019; Trendel et al., 2019; Urdaneta et al., 2019), and silica affinity (Asencio et al., 2018; Shchepachev et al., 2019). Each method has its own limitations such as retrieving nonphysiologically relevant RNA-protein interactions, biased analysis towards poly-adenylated or non-poly(A) RNA and/or uridine-rich protein binding sites, possible interference during RNP complex formation or glycoprotein contamination due to similar physicochemical properties like RNA adducts (Perez-Perri et al., 2021; Smith et al., 2020). Particularly the CLIP approaches strongly rely on the experimental conditions. For instance, the number of overlapping hits of three different studies investigating potential mRNA targets of the RBP TAR DNA binding protein (TDP-43, TARDBP) by RNA sequencing of immunoprecipitated TDP-43-RNA-complexes in HeLa cells, HEK293E cells, and rat neurons was less than 5% (Buratti et al., 2013). In addition, poor cross-linking efficiency between RNA and RBP (in general only 1-5%), bypassing cross-linked nucleotides by a reverse transcriptase, cellular toxicity of photoactivatable ribonucleosides such as 4-thiouridine, and the need for highly specific antibodies are experimental challenges to overcome (Burger et al., 2013; Darnell, 2010; Ramanathan et al., 2019).

Lately, McMahon and colleagues published a genetic tool enabling the identification of *in vivo* targets of RBPs called TRIBE (targets of RNA-binding proteins identified by editing) (McMahon et al., 2016). This method is based on a fusion protein composed of the RBP of interest and the catalytic domain of an ADAR (adenosine deaminases acting on RNA) enzyme (Figure 15). Thereby the RBP replaces the double-stranded RBD of ADAR and determines

RNA recognition of the fusion protein. As a result, target transcripts of the RBP undergo an adenosine-to-inosine conversion by the catalytic ADAR domain, which allows to identify RNA targets by sequence comparison of edited and native RNAs.

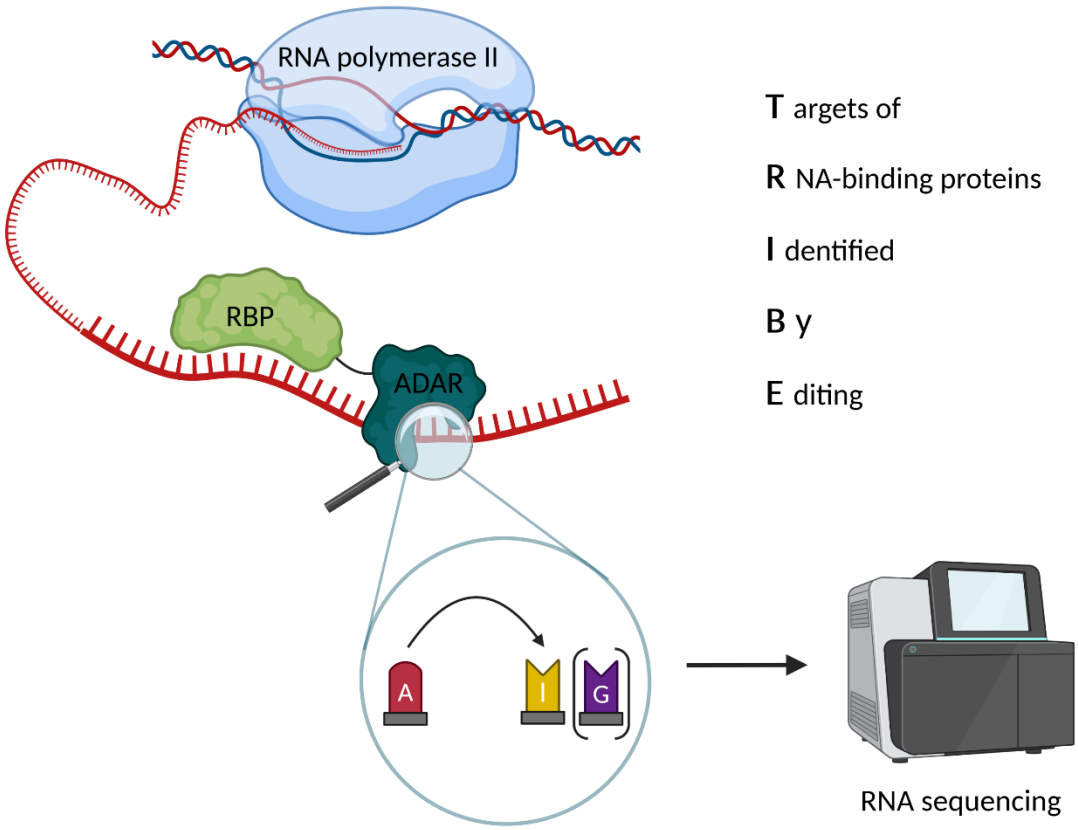

Figure 15| Principle of the TRIBE method. The RBP is fused to the catalytical domain of an ADAR enzyme. Editing events in RNA targets leading to an adenosine (A)-to-inosine (I) conversion and inosines are read as guanosines (G) during RNA sequencing. Due to that, sequence comparisons between native and edited RNAs are possible and enable the identification of new target transcripts of the RBP. Created with BioRender.com

So far, the TRIBE approach has not been used extensively, but the method allows to determine RNA-protein interactions with minimal false positives (Biswas et al., 2021) and there is neither a need for purification of the protein of interest, nor a dependence on RNA-protein cross-linking (Ramanathan et al., 2019).

1.3 Clustered regularly interspaced short palindromic repeats/CRISPR-associated

Nowadays the clustered regularly interspaced short palindromic repeats/CRISPR-associated (CRISPR/Cas) technology is the most promising and versatile tool in genome editing and has revolutionised various fields of life science including medicine, biotechnology, and agriculture. CRISPR/Cas and previous representatives of genome editing tools such as meganucleases, zinc finger nucleases (ZFNs), and transcription activator-like effector nucleases (TALENs) have the same basic principle in common (Figure 16).

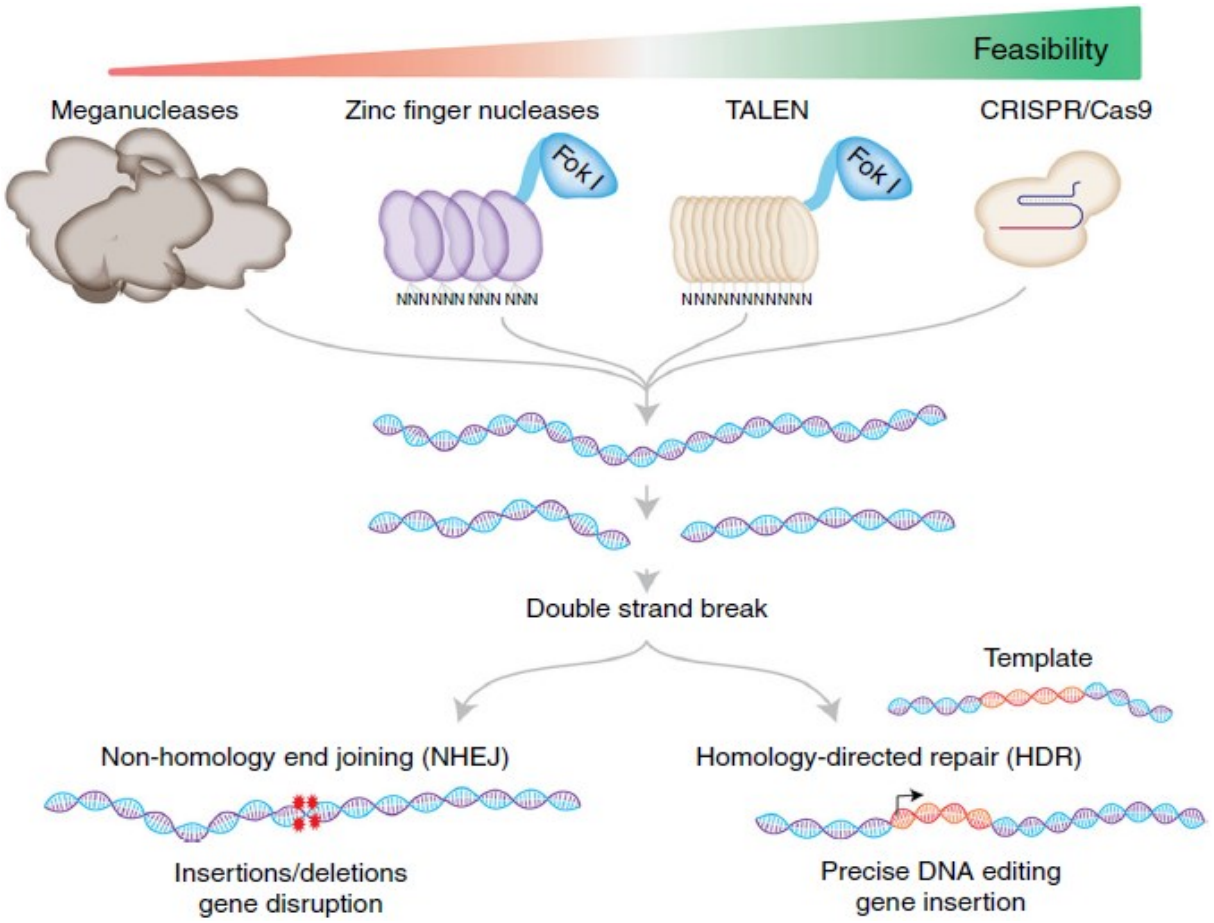

Figure 16| Genome editing technologies and its basic principle. Meganucleases represent engineered restriction enzymes characterised by a 14–40 bp long DNA recognition site. Zinc finger nucleases (ZFNs) are composed of 6-7 small zinc ion-regulated protein motifs, each recognising a nucleotide triplet, whereas transcription activator-like effector nucleases (TALENs) can recognise individual nucleotides. The latter two are fusion proteins harbouring the cleavage domain of the endonuclease Fok I that requires homodimerization for DNA cleavage. Thus, it is mandatory to design two ZFN or TALEN proteins. Unlike protein–DNA recognition, the clustered regularly interspaced short palindromic repeats/CRISPR-associated (CRISPR/Cas) system uses specific guide RNAs that guide the Cas endonucleases to the target sites by Watson-Crick base pairing. Thereby, target specificity is controlled by protospacer adjacent motifs (PAMs) in the DNA. All these tools result in DNA double-strand breaks and are repaired either by error-prone non-homologous end joining (NHEJ) or homology-directed repair (HDR). While NHEJ results in random indels (=insertions or deletions) and gene disruption at the target site, HDR can be harnessed to insert a specific DNA template (single stranded or double stranded) at the target site for precise gene editing. From "The CRISPR tool kit for genome editing and beyond" by Adli M. (2018), *Nature communications, 9*(1), 1911 (https://doi.org/10.1038/s41467-018-04252-2). Copyright © 2018, The Author(s). Licensed under CC BY 4.0.

The overall goal is to introduce a double-strand break into DNA that needs to be repaired by the cell's own repair mechanisms. Two major pathways are classical nonhomologous end joining (c-NHEJ) and homology directed repair (HDR) (Adli, 2018). Typically, c-NHEJ is an error-prone mechanism resulting in uncontrollable, but predictable, insertions and deletions (indels) to disrupt a genomic sequence by frameshift mutations. Contrary, the competing HDR pathway is particularly active in dividing cells, but less efficient. It can be utilised to precisely install targeted mutations or to knock in larger DNA when a single stranded or double-stranded DNA template is offered (Anzalone et al., 2020). One big advantage is the feasibility of the CRISPR/Cas systems, particularly CRISPR/Cas9, because it is simpler and more flexible to use than the other presented tools, and in terms of editing efficiency at least equivalent (Adli, 2018).

1.3.1 History of CRISPR/Cas

Originally, CRISPR/Cas was discovered in 1987 during studies on a gene (*iap*) responsible for the isozyme conversion of alkaline phosphatase in *E. coli* (Ishino et al., 1987). They identified five highly homologues sequences of 29 nt arranged as direct repeats with 32 nt as spacing at the 3' end flanking region of *iap* (Ishino et al., 1987) (Figure 17). A decade later, Jansen and Mojica coined the acronym CRISPR to unify the description of these repetitive DNA elements, which were found to be present throughout procaryotes, and to reflect their features (Jansen et al., 2002; Mojica et al., 2000). Simultaneously, CRISPR-associated genes and their relationship to adjacent CRISPR loci were revealed (Jansen et al., 2002). In 2005, the origin of the intervening DNA sequences of CRISPR loci was deciphered, giving the first hint that these extrachromosomal, phage-associated elements are implicated in bacterial immunity (Mojica et al., 2005). Two years later the experimental proof was delivered by Horvath and colleagues while trying to achieve phage resistance for the dairy bacterial strain *Streptococcus thermophilus* (Barrangou et al., 2007). They characterised the CRISPR/Cas system as an adaptive nucleic acid-based immunity system of prokaryotes (Figure 18), whereby the specificity is dictated by the spacer sequences (CRISPR RNA, crNRA) and spacer acquisition and phage defence is mediated by Cas enzymes (Barrangou et al., 2007). Following this breakthrough, different classes of CRISPR/Cas systems and its components were identified. For instance, Jörg Vogel and Emmanuelle Charpentier uncovered the small non-coding trans-activating crRNA (tracrRNA) in the type II system of *S. pyogenes* (Figure 19). This tracrRNA is complementary

to the repeat regions of crRNA precursor transcripts and, in complex with RNase III and Cas9, is involved in their maturation (Deltcheva et al., 2011). In the same year, Siksnys and colleagues transferred an active CRISPR/Cas type II system from *S. thermophilus* into *E. coli* and demonstrated that these systems can be transplanted across different genera providing heterologous interference against invasive nucleic acids (Sapranauskas et al., 2011). In 2012, different scientists, including the later Nobel prize winners Jennifer A. Doudna and Emmanuelle Charpentier, published that the RNA duplex, composed of mature crRNA base-paired to tracrRNA, guides Cas9 to target DNA complementary to the crRNA, which results in a double-strand break performed by the two cleavage domains HNH and RuvC-like domain of the endonuclease (Gasiunas et al., 2012; Jinek et al., 2012). Moreover, the tracrRNA:crRNA duplex can be condensed to one single guide RNA (sgRNA or gRNA) to achieve Cas9-mediated DNA cleavage *in vitro* (Jinek et al., 2012). Thereafter, Feng Zhang and George M. Church were the first, who achieved genome editing in mammalian cells using engineered CRISPR/Cas type II systems demonstrating the easy feasibility of the technology (Cong et al., 2013; Mali et al., 2013). Not much later, the Chinese scientist He Jiankui shocked the scientific community with a questionable report about HIV resistant twin baby girls resulting from germline editing using the gene scissors CRISPR/Cas. Nowadays, the first clinical trials with CRISPR-based gene therapies against HIV-1 (ClinicalTrials.gov: trials NCT03399448 and NCT03164135) cancer (ClinicalTrials.gov: trial NCT02793856), and Leber congenital amaurosis (ClinicalTrials.gov: trial NCT03872479) are completed or ongoing (Y. Lu et al., 2020; Maeder et al., 2019; Stadtmauer et al., 2020).

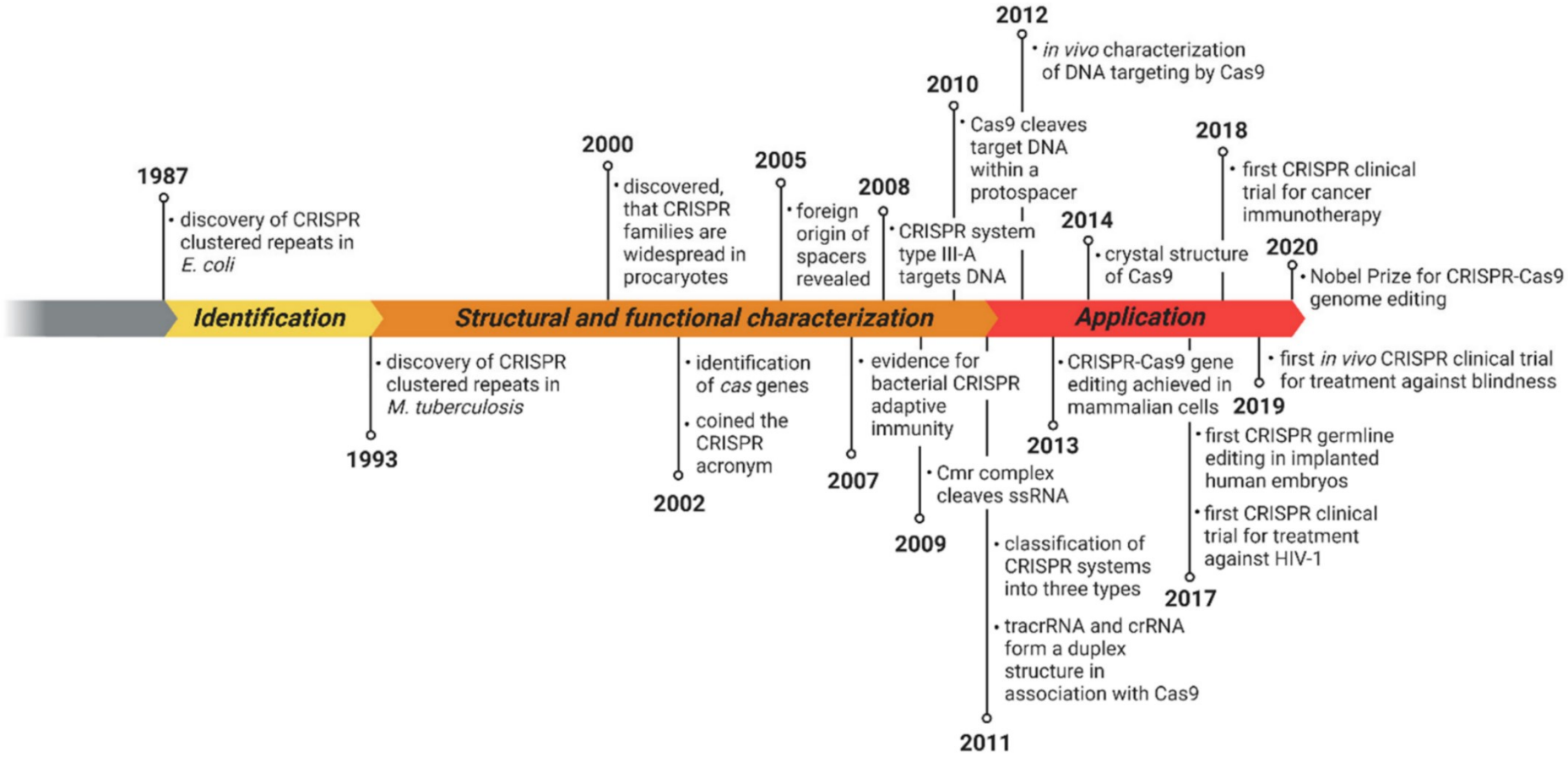

Figure 17| Milestones in the evolution of CRISPR/Cas systems. CRISPR: clustered regularly interspaced short palindromic repeats; Cas: CRISPR-associated; crRNA: CRISPR RNA; tracrRNA: trans-activating CRISPR RNA. From "Novel CRISPR-Cas systems: an updated review of the current achievements, applications, and future research perspectives" by Nidhi, S., Anand, U., Oleksak, P., Tripathi, P., Lal, J. A., Thomas, G., Kuca, K., & Tripathi, V. (2021), *International Journal of Molecular Sciences, 22*(7), 3327 (https://doi.org/10.3390/ijms22073327). Licensed under CC BY 4.0.

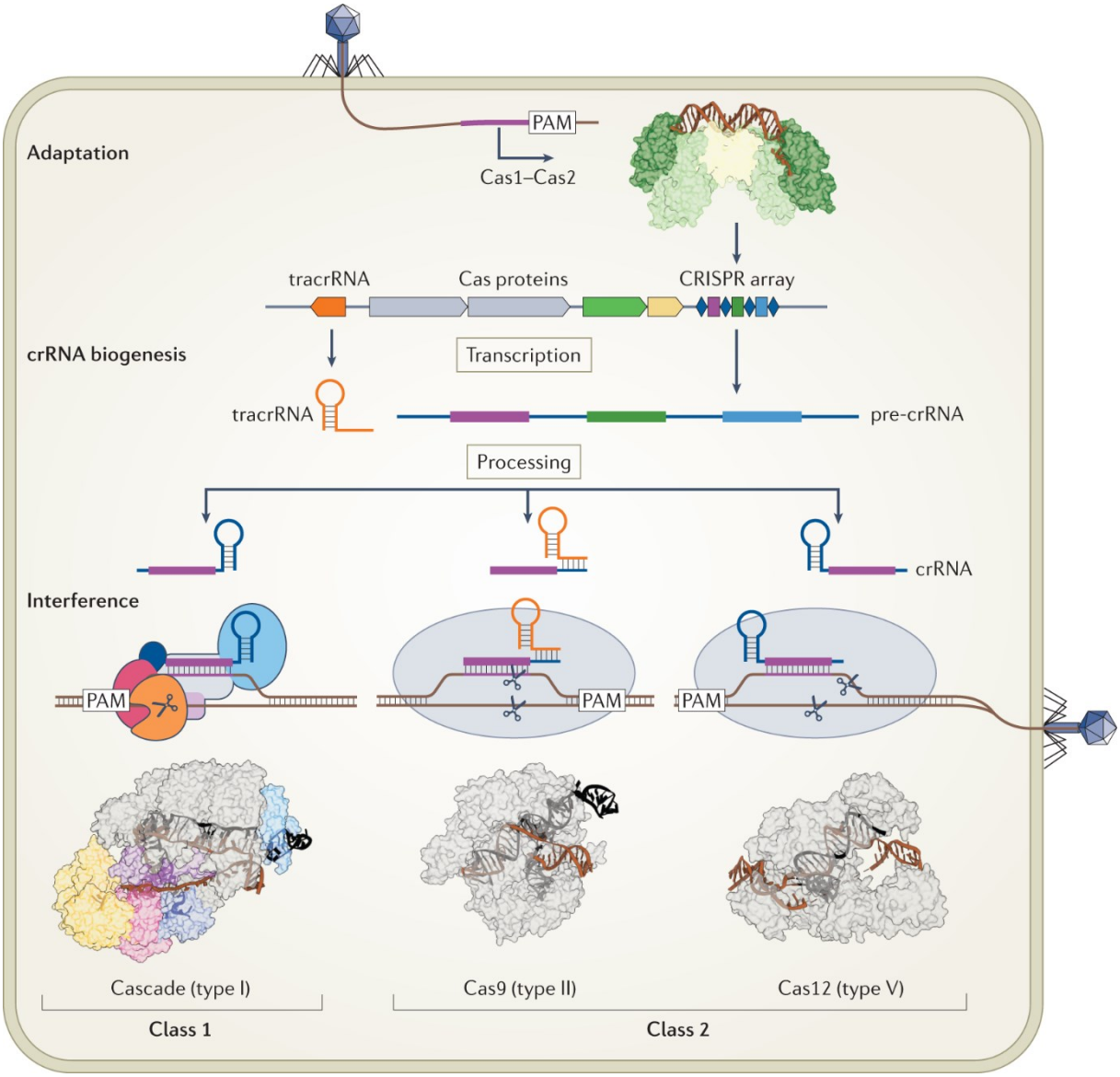

Figure 18| CRISPR–Cas systems provide bacteria and archaea with adaptive immunity. The three stages of CRISPR immunity: adaptation, CRISPR RNA (crRNA) biogenesis and interference. In adaptation, Cas1–Cas2 (Protein Data Bank [PDB] ID 5DS4) (Nuñez et al., 2015) inserts protospacers, derived from foreign genetic elements, into the CRISPR array as new spacers (represented as differently coloured rectangles) that are separated by CRISPR repeats (represented as blue diamonds). During crRNA biogenesis, the CRISPR array is transcribed into pre-crRNA, which is processed into mature crRNAs that each have a single spacer. The crRNA (or in some cases, the dual crRNA–trans-activating crRNA (tracrRNA)) assembles with the effector protein or complex to form a surveillance complex that recognizes and degrades foreign genetic elements complementary to the crRNA spacer during interference. Class 1 systems have multisubunit effector complexes, whereas class 2 systems have single-subunit effector proteins. Target cleavage by the class 1 type I Cascade–Cas3 effector complex (left), the class 2 type II Cas9 effector (centre) and the class 2 type V Cas12a effector (right) is depicted schematically, and representative structures of the effector complexes are shown beneath: Cascade–Cas3 bound to crRNA and target DNA (PDB ID 6C66) (Xiao et al., 2018); Cas9 bound to guide RNA (composed of crRNA and tracrRNA) and target DNA (PDB ID 4UN3) (Anders et al, 2014); and Cas12a bound to crRNA and target DNA (PDB ID 5NFV) (Swarts et al, 2017). Nucleic acids in the structures are colour-coded: DNA, brown; RNA, black. PAM, protospacer adjacent motif. Figure and caption from "Structural biology of CRISPR-Cas immunity and genome editing enzymes" by Wang, J. Y., Pausch, P., & Doudna, J. A. (2022), Nature reviews. Microbiology. (https://doi.org/10.1038/s41579-022-00739-4). With permission, copyright © 2022, Springer Nature Limited.

1.3.2 CRISPR/Cas systems

Although the classification of CRISPR/Cas systems is constantly updated, there are generally two classes of CRISPR/Cas systems including six different types plus diverse subtypes so far (Figure 19) (Makarova et al., 2020). The main difference between the two classes are the effector modules that are responsible for the interference against foreign nucleic acids in bacterial immunity (Figure 18). Class 1 CRISPR/Cas systems share an effector complex build of multiple Cas proteins that together bind crRNA and process target DNA, whereas the functional analogue in class 2 systems is only a single multidomain crRNA-binding protein (Makarova et al., 2020). Due to less mandatory components, class 2 systems are easier to handle and therefore more attractive tools for genome editing. That is why the class 2 type II CRISPR/Cas9 system was chosen in the present work as one approach to knockout *IGF2BP2 in vitro* as it requires only a designable sgRNA and the Cas9 enzyme.

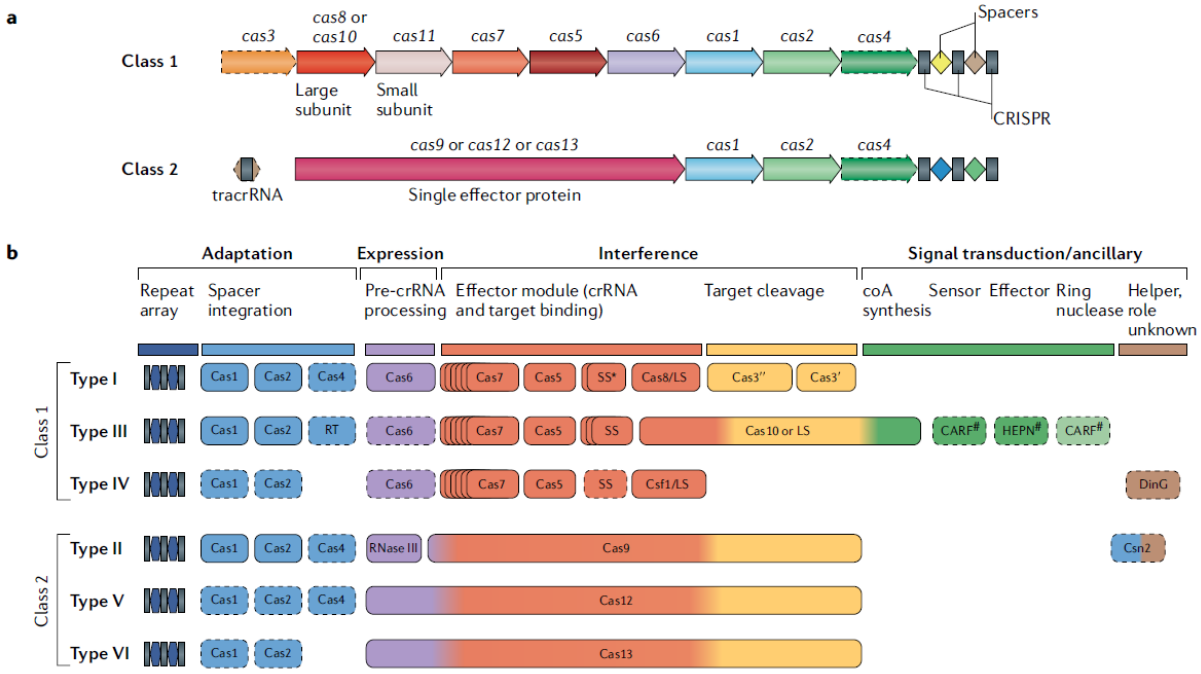

Figure 19| Classification of CRISPR/Cas systems and their modular organisation. Structural organisation of the CRISPR/Cas array in class 1 and class 2 systems (a) and their functional modules (b). The colour scheme indicates the typical relationships between the structural and functional organisation of the six types of CRISPR/Cas systems. Protein names follow the current nomenclature. Dispensable (and/or missing, in some subtypes and variants) components are indicated by dashed outlines. The three colours for Cas9, Cas10, Cas12 and Cas13 reflect the fact that these proteins contribute to different stages of the CRISPR/Cas response. LS: large subunit; SS: small subunit; tracrRNA: trans-activating CRISPR RNA; CARF: CRISPR associated Rossmann fold; HEPN: higher eukaryotes and prokaryotes nucleotide binding domain proteins. Figure modified from Makarova et al. (2015). From "Evolutionary classification of CRISPR-Cas systems: a burst of class 2 and derived variants" by Makarova, K. S., Wolf, Y. I., Iranzo, J., Shmakov, S. A., Alkhnbashi, O. S., Brouns, S., Charpentier, E., Cheng, D., Haft, D. H., Horvath, P., Moineau, S., Mojica, F., Scott, D., Shah, S. A., Siksnys, V., Terns, M. P., Venclovas, Č., White, M. F., Yakunin, A. F., Yan, W., … Koonin, E. V. (2020), *Nature reviews. Microbiology, 18*(2), 67–83 (https://doi.org/10.1038/s41579-019-0299-x). With permission, copyright © 2019 Springer Nature Limited.

1.3.3 Prime editing

Liu and colleagues were the first to describe prime editing utilising a modified gRNA, named prime editing gRNA (pegRNA), and a Cas9 nickase fused to a reverse transcriptase (prime editor) as effector molecule for precise genome editing. This method can mediate all kinds of insertions, deletions, and base-to-base conversions with lower off-target activity at known Cas9 off-target sites and fewer by-products, while showing equal or higher activity compared to Cas9-mediated HDR (Anzalone et al., 2019). There are different prime editor systems and with increasing number of the system editing efficiency was optimised, but also more complexity was added. In this thesis, the prime editor 2 system was chosen as second approach to disrupt the gene sequence of the RBP IMP2 as this system represents a good compromise of editing efficiency and practical feasibility. The mode of action is illustrated in Figure 20 and summarised in five steps by Scholefield and Harrison (2021).

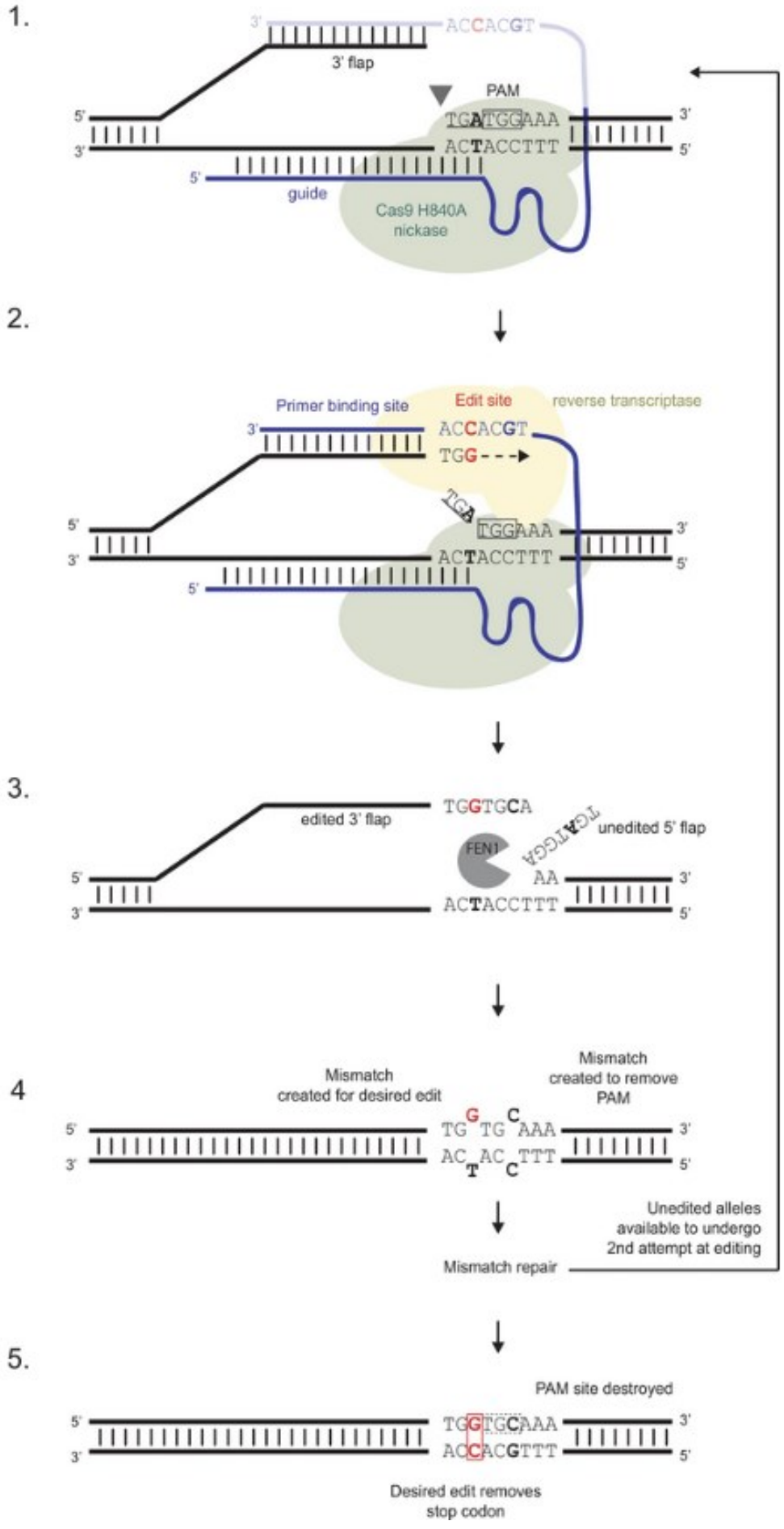
1.
3'
ACCACGT
3' flap
PAM
5'
3'
TGATGGAAA
ACTACCTTT
3'
5'
5'
guide
Cas9 H840A
nickase
2.
Primer binding site
Edit site
reverse transcriptase
3'
ACCACGT
TGG
TGA
5'
3'
TGGAAA
ACTACCTTT
3'
5'
5'
3.
edited 3' flap
TGGTGCA
TGATGGA
unedited 5' flap
FEN1
5'
3'
AA
ACTACCTTT
3'
5'
4
Mismatch
created for desired edit
Mismatch
created to remove
PAM
5'
3'
TG G TG C AAA
AC T AC C TTT
3'
5'
Unedited alleles
available to undergo
2nd attempt at editing
Mismatch repair
5.
PAM site destroyed
5'
3'
TGGTGCAAA
ACCACGTTT
3'
5'
Desired edit removes
stop codon

Figure 20| Mode of action of prime editor systems in five steps. Prime editing, in particular the prime editor 2 system, has two components: a Cas9 nickase fused to a modified reverse-transcriptase (referred to as PE2=Prime editor 2) and a multifunctional prime editing guide RNA (pegRNA). The Cas9 nickase is a mutant Cas9 protein that harbours the H840A mutation in the HNH nuclease domain of Cas9. As a result, Cas9 nickase is only capable of introducing single-strand breaks into DNA instead of double-strand breaks like the wild-type variant. The pegRNA is a sgRNA extended at the 3' end with a reverse transcriptase template including the edit (edit site) and a primer-binding site (PBS): 1. The Cas9-H840A/pegRNA complex binds to the desired target region and creates a nick 3 bp upstream of the PAM site. The nick must be upsteam of the first variant site (in this case a TGA stop codon) and occurs on the same strand as the PAM liberating a 3' flap. 2. This 3' flap forms a sequence-specific interaction with the approximately 10-16 nt PBS located at the 3' end of the pegRNA. This RNA/DNA hybrid serves as the starting point for new DNA synthesis using the edit site as a template; the modified RT polymerase copies the template thereby extending the 3' flap. 3. The edited 3' flap displaces the variant unedited 5' flap, which is removed by flap structure-specific endonuclease 1 (FEN1). 4. In this example, this leaves two mismatches to be resolved, one in the edited codon (G ≠ T), and one in the modified PAM (C ≠ C) which can be introduced as an option to prevent further editing to the corrected sequence. 5. Mismatch Repair resolves the DNA resulting in either precisely edited DNA (with no indels), or the original variant sequence. In the latter case where the PAM sequence has not been modified, the Cas9-H840A/pegRNA complex can bind to the variant sequence again and have another attempt at prime editing. Green: Cas9-H40A nickase; yellow: reverse transcriptase; grey box: PAM site; blue: pegRNA; red: edit site. From "Prime editing - an update on the field" by Scholefield, J., & Harrison, P. T. (2021), *Gene therapy, 28*(7-8), 396–401 (https://doi.org/10.1038/s41434-021-00263-9). Licensed under CC BY 4.0.

1.4 Objectives

RBPs fulfil their role as central players in post-transcriptional gene regulation due to their impact on RNA metabolism. Aberrant RBP expression affects an abundance of downstream RNA targets and can lead, depending on the signalling pathway in which they are involved, to the onset of a disease such as cancer development. The different chapters within this thesis address the following issues:

(I) TTP and its role in HCC tumour initiation and progression.

(II) Employing TRIBE for IMP2 target identification.

(III) Validation of IMP2 as new target for cancer therapy

2 Materials and methods

2.1 Cell culture

2.1.1 Cultivation of cell lines

Tumour cell lines were cultured in RPMI-1640 (#R0883, Merck, Darmstadt, Germany) (HepG2, Huh7, PLC/PRF/5) or high glucose DMEM (#D6546, Merck) (HCT116, SW480) medium, supplemented with 10% FCS (#F7524, Merck), 100 U/ml penicillin, 100 mg/ml streptomycin (#P4333, Merck), and 2 mM glutamine (#G7513, Merck) (RPMI-1640) or 4 mM glutamine (DMEM), unless stated otherwise. Cells were maintained at 37 °C in a humidified atmosphere of 5% CO_2. Subculturing of the cells was performed at the latest at 90% confluency of the cell layer. Therefore, cells were washed with PBS (1×) buffer (2.7 mM KCl, 1.8 mM KH_2PO_4, 137 mM NaCl, and 10 mM Na_2HPO_4 dissolved in distilled water, pH adjusted to 7.4, autoclaved for sterilisation) and detached with trypsin-EDTA (#T3924, Merck). The reaction was stopped with complete supplemented culture medium and cell suspensions were centrifuged for 5 min at 250×*g* prior to resuspension in the culture media. The resuspended cells were either used for further passaging and/or for seeding cells for experiments.

2.1.2 Freezing and thawing of cells

Cells were detached as described above and counted using LUNA-FL™ Dual Fluorescence Cell Counter (Logos Biosystems, Dongan-gu Anyang-si, South Korea). After centrifugation (250×*g*, 5 min), cells were resuspended in FCS containing 10% DMSO (#D8418, Merck), which was pre-cooled on ice. Aliquots of at least one million cells were pipetted into cryovials and immediately frozen at -80 °C overnight using Mr. Frosty® (#5100-0001, Thermo Fisher Scientific, Waltham, MA, USA) to ensure a cooling rate of -1 °C/min. The next morning, the cryovials were transferred into a liquid nitrogen tank for long term storage.

To thaw cells from the liquid nitrogen tank, cryovials were warmed up in a water bath at 37 °C and the thawed cell suspension was transferred immediately into prewarmed complete growth medium. Following a centrifugation for 5 min at 250×*g* the cells were resuspended in prewarmed complete growth medium and cultured as described in 2.1.1.

2.1.3 Transient TTP overexpression

For overexpression experiments, a vector (pZeoSV2(–)) containing the human TTP coding sequence tagged with the human influenza hemagglutinin tag or the vector with the antisense sequence as a control (#V855-01, Thermo Fisher Scientific) was used (Hoppstädter et al., 2012). The vectors were kindly provided by Prof. Dr. Hartmut Kleinert (Fechir et al., 2005), and the sequence was verified by Sanger sequencing. Transient TTP overexpression in hepatoma cells was established by transfection with the vector using jetPEI®-Hepatocyte reagent (#102-05N, Polyplus transfection, Illkirch, France) as recommended by the manufacturer. Successful TTP overexpression was confirmed *via* Western blot for each experiment. These experiments were performed by Kevan Hosseini (Pharmaceutical Biology, Saarland University, Saarbrücken, Germany).

2.1.4 MTT assay

Hepatoma cells (HepG2, Huh7, and PLC/PRF/5) were seeded into 96-well plates, transfected with TTP or a control vector, and treated with different concentrations of doxorubicin (#D1515, Merck) or sorafenib (#LKT-S5868, Biomol GmbH, Hamburg, Germany) and the respective solvent control. 24 h after the treatment, the cytostatic substances were removed and 5 mg/ml MTT (3-[4,5-dimethylthiazol-2-yl]-2,5-diphenyltetrazolium bromide, #M5655, Merck) in medium was added. After 2 h incubation, the formazan crystals were solved in DMSO, and the absorbance was measured at 550 nm with 690 nm as reference wavelength in a microplate reader (Tecan Sunrise™, Tecan Group Ltd., Männedorf, Switzerland). These experiments were performed by Kevan Hosseini (Pharmaceutical Biology, Saarland University, Saarbrücken, Germany).

2.1.5 Scratch assay

Cells were seeded into 12-well plates, transfected with TTP or a control vector, and scratched 48 h after transfection with a pipet tip. The first image was taken immediately after the scratch; the second image was taken 24 h after the scratch using a 5× objective. Images were obtained and analysed with an Axio Observer Z1 epifluorescence microscope equipped with an AxioCam Mrm (Zeiss, Oberkochen, Germany). Data were analysed with the TScratch software (version 1.0, CSElab, Zürich, Switzerland). These experiments were performed by Kevan Hosseini (Pharmaceutical Biology, Saarland University, Saarbrücken, Germany).

2.1.6 Incucyte® 2D and 3D proliferation, migration, and chemosensitivity

2D proliferation/chemosensitivity

Ten thousand HCT116 cells per well were seeded into 96-well plates and incubated for 24 h (37 °C, 5% CO_2) prior to 48 h of treatment with the chemotherapeutic drugs oxaliplatin (Y0000271, European Pharmacopoeia Reference Standard, EDQM Council of Europe, Strasbourg, France dissolved in PBS (1×)), 5-fluoruracil (F6627, Merck), and regorafenib (R-8024, LC Laboratories, Woburn, MA, USA) (both dissolved in DMSO). The drugs were diluted to the following concentrations using a 50 mM stock solution (µM): 0.1, 0.2, 0.5, 0.75, 1, 2, 5, 7.5, 10, 15, 20, 50, 75, 100. Medium was discarded and 180 µl of the treatment solution was added. 20 µl of resazurin (R7017; Merck, 0.15 mg/ml in PBS (1x)) was added and fluorescence was measured after 4 h of incubation at λ=590 nm with a POLARstar Omega (BMG LABTECH GmbH, Ortenberg, Germany) microplate reader. IC_{50} and IC_{20} values were determined by using sigmoidal dose-response fit in the software OriginPro® 2020 (Table 1). These experiments were performed by Sandra Kendzia (Institute of Pharmacy, Experimental Pharmacology for Natural Sciences, Martin Luther University Halle-Wittenberg, Halle, Germany).

Table 1| Drugs and concentrations used for chemosensitivity testing. The IC_{50}, IC_{20} values (50% and 20% inhibitory concentrations) and means of both values are displayed.

Drug	Abbreviation	IC_{50} (µM)	Mean IC_{50}, IC_{20} (µM)	IC_{20} (µM)
Oxaliplatin	OHP	2.57	1.42	0.26
5-Fluoruracil	5FU	22.20	13.02	3.84
Regorafenib	REGO	8.08	5.66	3.24

HCT116 wild-type and IMP2 knockout cells (clone 47-1) were seeded into 96-well plates (2,500 cells and 100 µl medium/well) overnight. After incubation for 24 h, the cells were treated with the chemotherapeutics oxaliplatin, 5-fluoruracil, and regorafenib by adding 100 µl of a 2-fold concentrated solution of the drug in medium. The final concentrations in the wells corresponded to the IC_{50} and IC_{20} values and means of both values (Table 1). Cell confluency was monitored in an Incucyte® S3 system for 96 h by taking pictures every 8 h. Cell confluency was determined using the IncuCyte® ZOOM Basic Analyzer Software Module and was normalised to the starting point, that is the first time point after treatment (t=0 h).

3D proliferation

For spheroid formation, HCT116 wild-type and IMP2 knockout cells (3,000/well) were seeded into low attachment U-bottom plates (#781900, Brand, Wertheim, Germany) and were centrifuged for 3 min at 200×*g*. After spheroid formation for three days, spheroid area was monitored in an Incucyte® S3 system and analysed using Incucyte® Spheroid Analysis Software Module, if not indicated otherwise. The spheroid area was normalised to 3-day-old spheroids (t=0 h). These experiments were performed by Charlotte Dahlem (Pharmaceutical Biology, Saarland University, Saarbrücken, Germany).

Migration

HCT116 wild-type and IMP2 knockout cells (100,000/well) were seeded into Incucyte® ImageLock 96-well plates. The next day, when the cells were close to 100% confluency, scratches were performed using the Incucyte® 96-well WoundMaker Tool (Incucyte® Migration Kit). Subsequently, the cells were washed twice with 2% FCS-containing high glucose DMEM medium, which was also used for further cultivation. Cell migration was monitored for 48 h in an Incucyte® S3 system and the cell-covered wound area was analysed and quantified using the Incucyte® Scratch Wound Analysis Software Module.

2.1.7 Electrical Cell–substrate Impedance Sensing

Seven thousand HCT116 wild-type or IMP2 knockout cells (clone 47-1) per well were seeded into 96-well plates (96W10E+) coated with rat tail collagen (#C766160, Merck, 30 µg/ml in 0.2% acetic acid). Cell impedance was assessed in an Electrical Cell−substrate Impedance Sensing Zθ (theta) instrument (Applied BioPhysics Inc., NY, USA). Measurements were started immediately after cell seeding and were taken every 450−900 s for each well These experiments were performed by Charlotte Dahlem (Pharmaceutical Biology, Saarland University, Saarbrücken, Germany).

2.2 Bacterial culture

The following *E. coli* strains served as host organisms for transformation and amplification of exogenous plasmid DNA:

TOP10 (Thermo Fisher Scientific). Genotype: *F- mcrA Δ(mrr-hsdRMS-mcrBC) φ80lacZΔM15 ΔlacX74 nupG recA1 araD139 Δ(ara-leu)7697 galE15 galK16 rpsL(StrR) endA1 λ-*.

GT116 (Invivogen, San Diego, CA, USA). Genotype: *F- mcrA Δ(mrr-hsdRMS-mcrBC) Φ80lacZΔM15 ΔlacX74 recA1 endA1 Δdcm ΔsbcC-sbcD*.

DH5α (Addgene, Cambridge, MA, USA). Genotype: *F- Φ80lacZΔM15 Δ(lacZYA-argF) U169 recA1 endA1 hsdR17 (rk-, mk+) phoA supE44 thi-1 gyrA96 relA1 λ-*.

2.2.1 Liquid cultures

Liquid cultures of bacteria were prepared in aqueous lysogeny broth medium pH 7±0.2 (LB medium Luria/Miller, #X968.1, Carl Roth, Karlsruhe, Germany) composed of 10% (m/v) tryptone, 5% (m/v) yeast extract, and 10% (m/v) NaCl. If needed, 100 µg/ml ampicillin (#A9518, Merck) or 50 µg/ml kanamycin (#K0254, Merck) was added to the LB medium as selection marker. Single colonies were picked from freshly streaked agar plates (37.5% (m/v) agar in culture medium, autoclaved prior to pouring) to inoculate the growth medium. Incubation was performed at 37 °C and 250 rpm in an incubator shaker or as described in the protocols of the plasmid isolation kits (cf. 2.2.4).

2.2.2 Generation of competent E. coli

The calcium chloride method was used to generate competent *E. coli* for incorporation of exogenous plasmid DNA. A liquid culture of bacteria was grown overnight in LB medium. The next morning, 5 ml of the suspension was diluted to 100 ml with LB medium and allowed to grow to an OD_{600} of 0.4. The culture was then cooled down on ice for 30 min, centrifuged at 2,000×*g* and 4 °C, and resuspended in 10 ml ice cold aqueous $CaCl_2$ solution (75 mM $CaCl_2$, 15% glycerol). After 30 minutes of incubation on ice, cells were centrifuged at 2,000×*g* and 4 °C, resuspended in 2.5 ml ice cold $CaCl_2$ solution, aliquoted, and stored at -80 °C.

2.2.3 Transformation

Fifty ng of plasmid DNA were pipetted to 50 µl of competent *E. coli* freshly thawed on ice. After 20 min of incubation on ice, heat shock was performed at 42 °C for 2 min in a heating block prior to another 2 min incubationeunhunderfünzign on ice. Nine hundred and fifty microlitres of pre-warmed LB medium or SOC medium (2% (m/v) tryptone, 0.5% (m/v) yeast extract, 10 mM NaCl, 2.5 mM KCl, 10 mM MgCl, 10 mM $MgSO_4$, 20 mM glucose in water, sterile filtered) was added, and the bacterial suspension was incubated for 60 min at 37 °C and 250 rpm using an incubator shaker. One hundred microlitres and 200 µl of the suspension

were plated on agar plates containing the respective selection antibiotic and incubated overnight at 37 °C.

2.2.4 Plasmid isolation

Isolation of bacterial plasmids were performed according to the manufacturer's instructions using either the High Pure Plasmid Isolation Kit (#11754777001, Roche, Basel, Switzerland), the QIAprep Spin Miniprep Kit, the QIAGEN Plasmid Midi Kit or the EndoFree Plasmid Giga Kit (#27106, #12143, #12391 Qiagen, Hilden, Germany). The latter kit was used to obtain endotoxin-free plasmid DNA for *in vivo* experiments. The concentration of the isolated plasmid DNA was determined by measuring the absorbance at λ=260 nm and quality was checked by measuring/calculating the purity ratio absorbance at λ=260 nm/absorbance at λ=280 nm with a NanoDrop Lite Spectrophotometer (#ND-LITE, Thermo Fisher Scientific). Plasmid DNA with a purity ratio greater than 1.8 was considered pure and accepted.

2.3 Mice

2.3.1 Animal welfare

Animal handling was conducted in accordance with the guidelines of the local animal welfare committee (permission numbers: 37/2014, 04/2020). Mice were housed in groups of five under controlled conditions: 12 h light/12 h dark cycle, 22 °C ±2 °C temperature, 55% ±10% relative humidity, and access to food and water *ad libitum*.

2.3.2 Generation of liver-specific Ttp-knockout mice

C57BL/6 $Ttp^{fl/fl}$ mice carrying flox sites flanking exon 2 of TTP were crossed with albumin-Cre transgenic mice in order to generate liver-specific *Ttp*-KO (ls*Ttp*-KO) mice (Sawicki et al., 2018). Ls*Ttp*-KO was confirmed measuring *Zfp36* (gene name for TTP) expression by quantitative polymerase chain reaction (qPCR) (Supplementary Figure 4). TTP expression was almost absent in ls*Ttp*-KO, suggesting that the predominant TTP expression in the liver is found in hepatocytes. The animals were kindly provided by Perry J. Blackshear (Signal Transduction Laboratory, Research Triangle Park, NC, USA).

2.3.3 Diethylnitrosamine injections

For the short-term experiment mimicking acute hepatic inflammation, wild-type and 9-week-old male ls*Ttp*-KO mice were intraperitoneally injected with either a 100 mg/kg body weight diethylnitrosamine (DEN) solution or with a 0.9% NaCl solution as a sham-control (Kessler et

al., 2014, 2015; Naugler et al., 2007). Forty-eight hours after the injection, the mice were sacrificed.

For the long-term experiment, which mimics hepatocarcinogenesis (Schultheiss et al., 2017; Vesselinovitch, 1990), wild-type and 2-week-old male ls*Ttp*-KO mice were intraperitoneally injected with either a 5 mg/kg body weight DEN solution or a 0.9% NaCl solution as a sham-control to determine the effects of TTP on hepatic tumour initiation. Twenty-two weeks after the injection, the mice were sacrificed.

Injections were performed by Kevan Hosseini (Department of Pharmacy, Pharmaceutical Biology, Saarland University, Saarbrücken, Germany).

2.3.4 Histology

For histological analysis, paraffin-embedded liver tissue specimens were cut into 5 µm sections and stained with hematoxylin and eosin (HE) (Kessler et al., 2015; Schultheiss et al., 2017; Tybl et al., 2011). Based on histological analysis by Johannes Haybaeck (Department of Pathology, Neuropathology and Molecular Pathology, Medical University of Innsbruck, Innsbruck, Austria), macroscopic tumours were confirmed as tumours.

2.3.5 Gas chromatography-mass spectrometry analysis of hepatic fatty acids

The fatty acid profile was measured by gas chromatography-mass spectrometry (GC-MS) as previously described (Fengler et al., 2016; Kessler et al., 2014; Laggai et al., 2014; Simon et al. 2014) by Katja Gemperlein (Department of Microbial Natural Products, Helmholtz Institute for Pharmaceutical Research Saarland, Saarbrücken, Germany). In short, snap-frozen liver tissue samples were pestled in liquid nitrogen and freeze-dried overnight using a Beta 2-8 LSCbasic freeze-dryer (Martin Christ Gefriertrocknungsanlagen GmbH, Osterode am Harz, Germany). Aliquots of 2-5 mg of tissue dry weight were hydrolysed using the fatty acid methyl ester method according to Bode et al. (2006). GC-MS was carried out on an Agilent 6890N gas chromatograph (Agilent Technologies, Waldbronn, Germany) equipped with a 7683B split/splitless injector with autosampler (Agilent Technologies) and coupled to a 5973 electron impact mass selective detector (Agilent Technologies) as previously described (Kessler et al., 2014). Absolute amounts of fatty acids were quantified by integration of the peaks in relation to the integral of methyl-nonadecanoate (#74208, Merck) as an internal standard and to liver tissue dry weight.

2.3.6 Hydrodynamic gene delivery and liver preparation for downstream analysis

For hydrodynamic gene delivery (HGD) experiments, 12-14-week-old C57BL/6J mice were fixed in a restrainer and rapidly injected (within 5 s) into the lateral tail vein with 2.5 ml of 12.5 µg/ml sterile, endotoxin-free solution of plasmid DNA (Supplementary Figure 8 and Supplementary Figure 9) in PBS (1×) (#TMS-012-A, Merck). Before the injections, blood circulation of the mice was stimulated by using an infrared lamp. In accordance with the local animal welfare officer the originally planned injection volumes of 2.6 -3.2 ml, corresponding to 10% of the body weight of the mice, were reduced to 2.5 ml due to the bad health status of the first injected mouse after administration of 3 ml of sterile, endotoxin-free PBS (1×). This mouse showed no spontaneous mouse behaviour until euthanasia 1 h post injection. Thus, an injection volume of 2.5 ml represented a compromise between the health of the mice and an injection volume to create a sufficient venous pressure for the uptake of foreign plasmid DNA. The mice were observed for one hour after injection and their health status was checked again 6 h and 24 h post injection, which represented the time point of sacrifice. Hydrodynamic injections were performed by Elien Van Wonterghem (VIB Center for Inflammation Research, Ghent, Belgium).

Directly after removing the liver, one sixth of the left lateral lobe was embedded in Tissue-Tek® O.C.T. Compound (#4583, Sakura Finetek Europe B.V., The Netherlands) and slowly, air bubble-free frozen in liquid nitrogen. From these samples cryo-sections were prepared and analysed *via* fluorescence microscopy by Marion Schwarz (Institute of Neurobiology (Zoology/Physiology), Saarland University, Saarbrücken, Germany).

One third of each liver lobe (left and right lateral lobe, left and right medial lobe, and caudate lobe) was transferred to neutral buffered paraformaldehyde (4% w/v in 10 mM PBS (1x)) for downstream tertiary butyl alcohol dehydration and paraffin embedding according to Zhanmu et al. (2019). Subsequently, these samples were subjected to immunohistochemical analyses, that is tissue sectioning and antibody staining using EnVision®+ Dual Link System-HRP (DAB+) (#K406511-2, Agilent Technologies, CA, USA) for green fluorescent protein (GFP) (recombinant anti-GFP antibody, #ab183734, [EPR14104], Abcam, Cambridge, United Kingdom), mCherry (Anti-mCherry antibody, #ab125096, [1C5], Abcam), and IMP2 (anti-p62C antibody from M. Lu et al. (2001) by Johannes Haybaeck (Department of Pathology,

Neuropathology and Molecular Pathology, Medical University of Innsbruck, Innsbruck, Austria). The number of positive hepatocytes were histologically scored (in a blinded fashion).

Another third of each lobe was frozen in liquid nitrogen for RNA isolation and qPCR. Remaining liver slices were shortly stored in cold RPMI-1640 prior to hepatocyte isolation. Therefore, livers were digested using the Liver Dissociation Kit mouse (#130-105-807, Miltenyi Biotec B.V. & Co. KG, Bergisch Gladbach, Germany), resuspended in PBS (1×) and subjected to fluorescence-activated cell sorting (FACS) analysis using GFP and phycoerythrin (PE)-CF594 channel.

2.4 Zebrafish studies

AB wild-type zebrafish embryos were used for xenograft models. Zebrafish husbandry was conducted as described previously (Dahlem et al., 2020). Zebrafish husbandry and all experiments were performed in accordance with the European Union Directive on the protection of animals used for scientific purpose (Directive 2010/63/EU) and the German Animal Welfare Act (§11 Abs. 1 TierSchG). Embryos were euthanised not later than 5 days post fertilisation (dpf).

Parental and IMP2 knockout HCT116 cells (clone 47-1) were used for proliferation studies in a zebrafish embryo xenograft model. 2 ×10^6 cells were suspended in 1 µl of 0.1% BSA/PBS (1×). At 2 dpf, 2 nl of the cell suspension was injected into the yolk sac by a FemtoJet® microinjector (Eppendorf, Hamburg, Germany). Before injection, the tumour cells were stained with the cell tracker orange dye (#C34551, Thermo Fisher Scientific) according to the manufacturer's protocol. Single embryos were placed into 96-well plates and imaged the next day with a Leica M205 FCA fluorescence stereomicroscope (1 day post injection, dpi). Tumour growth was determined at 3 dpi by analysis of the fluorescent tumour area and quantification by ImageJ. The growth rate was calculated as follows: (tumour area 3 dpi − tumour area 1 dpi)/tumour area 1 dpi. The effects of compound injection on the zebrafish embryo development and viability were assessed by microscopic observation of the eye, heart, and body axis formation, heartbeat, and pigmentation. All zebrafish experiments were performed by Charlotte Dahlem (Department of Pharmacy, Pharmaceutical Biology, Saarland University, Saarbrücken, Germany).

2.5 Development of IMP2 knockout tumour cell lines *via* CRISPR/Cas9

CRISPR/Cas9 was chosen as tool to generate mammalian *IGF2BP2* knockout cell lines. Two different strategies were followed to disrupt the coding sequence of the gene at different genomic loci. The first approach utilized the cells error-prone repair mechanism c-NHEJ to randomly create small indels after a double-strand break at a target site in exon 4. Prime editing as second approach is based on the concepts of Anzalone et. al. (2019) and focus on precise editing of protospacer adjacent motifs (PAMs) in exon 6 of *IGF2BP2*. Both processes aimed to erase important protein domains downstream of RRM2 of *IGF2BP2* (Figure 12 and Figure 13A). Exon 4 (cf. 2.5.1) and exon 6 (cf. 2.5.2) were chosen as target sites due to following reasons: (i) close distance to the start site of the *IGF2BP2* gene, (ii) both exons encode a part of RRM2 as an important protein domain, (iii) both exons are shared by all major transcript variants of *IGF2BP2* according to the University of California Santa Cruz (UCSC) genome browser (https://genome.ucsc.edu). Ribonucleoprotein delivery of Cas9:sgRNA complex was chosen due to less off-target activity compared to Cas9 plasmid DNA transfection (Liang et al., 2015). In line, prime editing was chosen because of the great versatility for the introduction of precise DNA mutations, higher editing efficiencies and fewer by-products than other homology-directed repair-utilising methods with simultaneous lower off-target editing of Cas9 nickase compared to wild-type Cas9 (Anzalone et. al., 2019).

2.5.1 Approach 1: RNP delivery of Cas9:sgRNA

The CRISPR/Cas9 system was delivered as RNP into two human colorectal (HCT116, SW480) and two hepatocellular carcinoma (Huh7, HepG2) cell lines. Therefore, a validated sgRNA (TrueGuide™ synthetic guid RNA, Thermo Fisher Scientific, Waltham, MA, USA) targeting *IGF2BP2* 5'-GATGGACTTTTGGCTCAATA-3' and a recombinant Cas9 protein (TrueCut™ Cas9 Protein v2, #A36496, Thermo Fisher Scientific) were transferred in 1:1 molar ratio into the cells by using Lipofectamine™ CRISPRMAX™ Cas9 transfection reagent (#CMAX00001, Thermo Fisher Scientific) according to the manufacturer's instructions. Cell number and volumes of transfection reagents were adjusted to 12-well format by doubling the recommendations for 24-well plates. In brief, 80,000 cells were seeded into a 12-well plate using antibiotics-free medium, incubated overnight (12-16 h), and transfected the next morning at a confluency of 30-70%. After 48 h incubation time, the cells were detached, counted, and seeded into 96-well plates at a concentration of 0.8 cells/well for limiting dilution

cloning. The remaining cells were used for gDNA extraction and verification of editing efficiency *via* T7E1 mismatch assay (cf. 2.5.3).

Clones were cultured for downstream experiments until knockout of IGF2BP2 or at least reduced expression could be confirmed by Western blot. Reduced IMP2 expression resulted from monoallelic editing of the target region as assessed by Sanger sequencing. Thus, these clones underwent the whole procedure again until knockout was achieved. At least two rounds of CRISPR/Cas9 editing did not induce a biallelic knockout in Huh7 cells.

2.5.2 Approach 2: prime editing

Design of prime editor 2 system

The prime editor 2 system was used to achieve *IGF2BP2* knockout in HCT116 cells. pCMV-PE2-P2A-GFP (plasmid #132776, Addgene) and pU6-pegRNA-GG-acceptor (plasmid #132777, Addgene) were a gift from David R. Liu (Anzalone et al., 2019). Vectors were chosen to deliver the prime editor (Supplementary Figure 10) and pegRNA component (Supplementary Figure 11) of system 2. Golden Gate cloning was used to insert designed pegRNAs (Table 2) into the latter construct according to the protocol provided by Anzalone et al. (2019). The cloning strategy is summarised in Figure 21.Three different spacers targeting different loci of exon 6 served as a basis for the pegRNA assembly. For the design of the spacer sequences tools like CHOPCHOP (https://chopchop.cbu.uib.no/) and CRISPOR (http://crispor.tefor.net/) were used to crosscheck on-target activity and off-targets. Following design criteria were taken into consideration: (i) the pU6-pegRNA-GG-acceptor vector for delivery of the pegRNA contains a U6 promoter. For efficient and precise transcription of the U6 promoter by human RNA polymerase III an adenine or guanine as first base at the 5′ end of the spacer is mandatory (Gao et al., 2017; Ma et al., 2014). (ii) According to Graf et al. (2019) TT- and GCC-motifs within the last four bases of the targeting sequence drastically decrease CRISPR/Cas9-mediated gene editing efficiency and should be avoided. In contrast, purines proximal to the PAM slightly increase knockout efficiency. (iii) In accordance with Wong et al. (2015) stretches of at least four contiguous RNA bases and UUU-motif within the last six bases of the targeting sequence (seed region) were avoided due to correlation with poor CRISPR activity. Desired mutations were planned to disrupt the PAM of the spacer sequences to prevent further editing to the mutated sequence. The length of the primer-binding site (PBS) was kept equal with 13 nt, but the size of the reverse transcriptase (RT) template varied between 10-16 nt (Table 2).

Table 2| Assembly of pegRNAs. Sequences of the single components, including a spacer, linked to the common sgRNA scaffold (5'-AGAGCTAGAAATAGCAAGTTAAAATAAGGCTAGTCCGTTATCAACTTGAAAAAGTGGCACCGAGTCG-3'), and the 3'extension. PBS: primer-binding site, RT: reverse transcriptase, nt: nucleotides.

pegRNA	abbreviation	spacer sequence (5'→3')	3'extension (5'→3')	PBS length (nt)	RT template length (nt)
pegRNA1_GGtoT_11ntRT	pegRNA1_11	GACCACTCTTCCCGGGAGCA	GCGTGGATTGCTCCCGGGAAGAGT	13	11
pegRNA1_GGtoT_15ntRT	pegRNA1_15	GACCACTCTTCCCGGGAGCA	AGGGGCGTGGATTGCTCCCGGGAAGAGT	13	15
pegRNA4_-GG_10ntRT	pegRNA4_10	AGAGCCATGGAGAAGCTAAG	TGATGCGCTTAGCTTCTCCATGG	13	10
pegRNA4_-GG_16ntRT	pegRNA4_16	AGAGCCATGGAGAAGCTAAG	TCAAACTGATGCGCTTAGCTTCTCCATGG	13	16
pegRNA6_+TA_10ntRT	pegRNA6_10	ATGCCCGCTTAGCTTCTCCA	AGCCTAATGGAGAAGCTAAGCGG	13	10
pegRNA6_+TA_16ntRT	pegRNA6_16	ATGCCCGCTTAGCTTCTCCA	TTTCAGAGCCTAATGGAGAAGCTAAGCGG	13	16

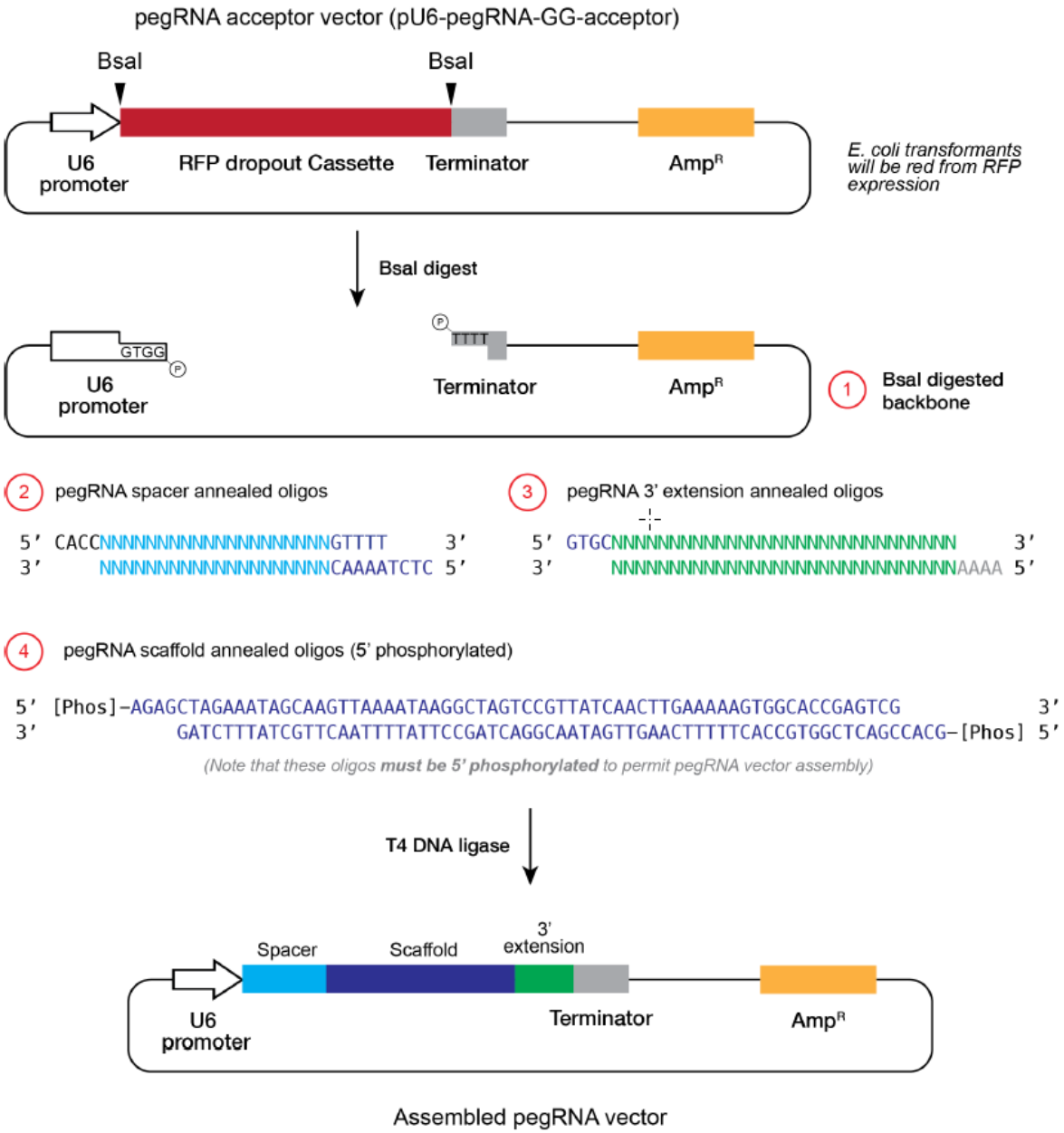

Figure 21| Overview of the pegRNA cloning by Golden Gate assembly. In brief, pU6-pegRNA-GG-acceptor was digested using high fidelity BsaI restriction enzyme to remove the RFP dropout cassette as placeholder for the pegRNA sequence. Subsequently, annealed spacer and 3' extension oligonucleotides (oligos) as well as annealed and 5' phosphorylated (by T4 polynucleotide kinase) scaffold oligos were ligated into the gel-purified backbone of the vector using T4 DNA ligase to assemble the pegRNA. Supplementary Note 3 from "Search-and-replace genome editing without double-strand breaks or donor DNA" by Anzalone, A. V., Randolph, P. B., Davis, J. R., Sousa, A. A., Koblan, L. W., Levy, J. M., Chen, P. J., Wilson, C., Newby, G. A., Raguram, A., & Liu, D. R. (2019), *Nature, 576*(7785), 149–157 (https://doi.org/10.1038/s41586-019-1711-4). With permission, copyright © 2019, the author(s), under exclusive licence to Springer Nature Limited.

100,000 cells/well were seeded into 24-well plates overnight and transfected the next morning (after 16-24 h) at a confluency of approximately 60% with an equimolar ratio of the two vectors (2 µg total DNA content). 2 µl lipofectamine 3000 (Thermo Fisher Scientific) was used according to the manufacturer's instructions. 48-72 h post transfection, transfection efficiency

was checked by measuring the green-fluorescent area of the cells using the Incucyte® S3 system (Sartorius, Göttingen, Germany). Subsequently, the cells were washed with PBS (1×)

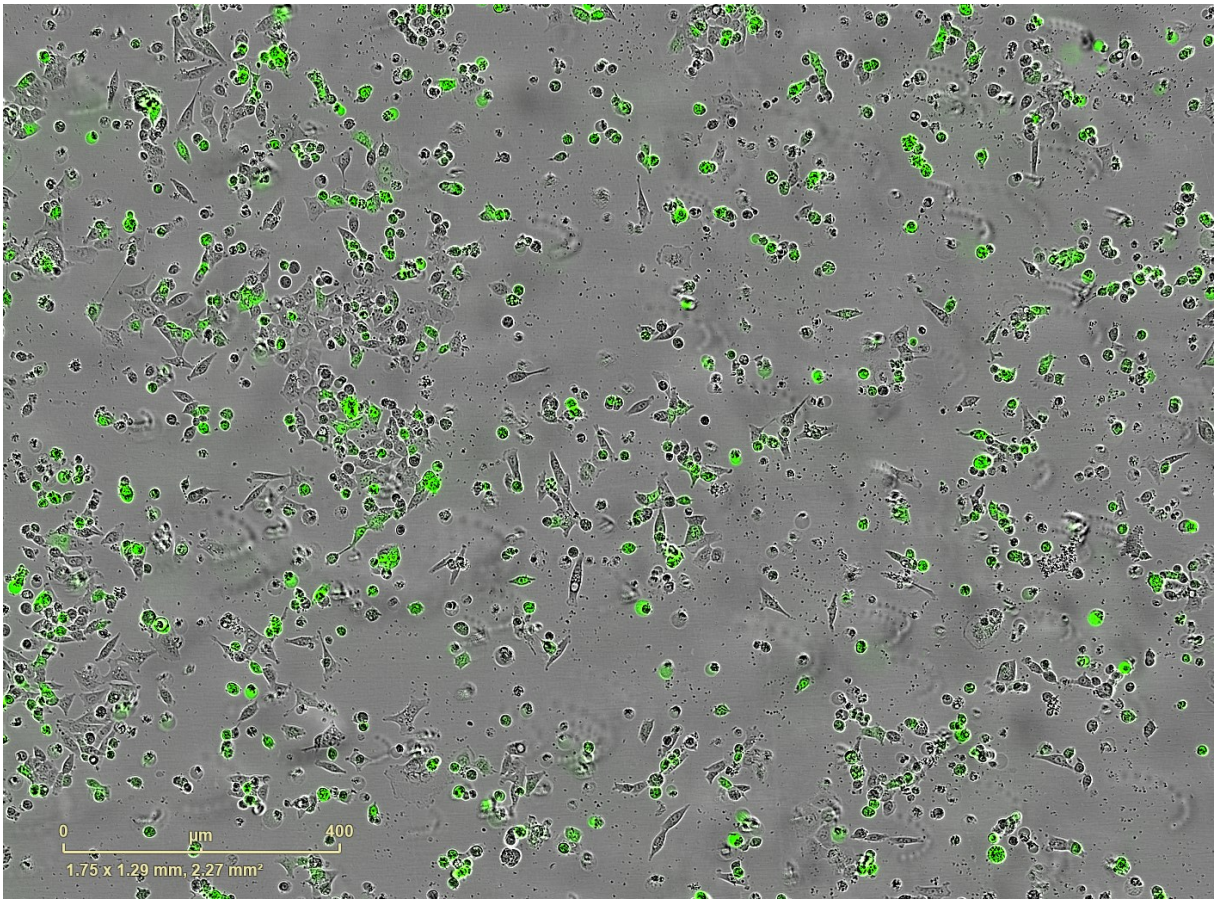

Figure 22| Proof of transfection using Incucyte® S3. Representative picture of HCT116 cells cotransfected with both prime editing components (pCMV-PE2-P2A-GFP and pegRNA4_16 included in pU6-pegRNA-GG-acceptor). Green appearing cells indicate GFP expression and therefore successful transfection of HCT116 cells with at least pCMV-PE2-P2A-GFP vector. Scale bar is shown in lower left corner.

(cf. 2.1.1), detached with trypsin-EDTA and resuspended in medium to gain a single cell suspension. Single GFP-positive cells were picked manually with a micro needle under a microscope (by Konstantin Lepikhov, Institute of Genetics/Epigenetics, Saarland University, Saarbrücken, Germany) and were transferred into collagen-coated 60 mm dishes into the squares of a grid (0.5 cm distance of the lines to each other) that had been drawn on the bottom of the dishes. The dishes were prepared using 2 ml of 30 µg/ml collagen stock in 0.2% acetic acid (collagen from rat tail, #C766160, Merck) and were dried under sterile air flow. After washing with 2 ml PBS (1×) and a second round of drying the collagen-coated dishes were stored overnight at 4 °C until usage the next day. Sterile-filtered 24 h conditioned DMEM cell culture medium from parental wild-type cells supplemented with 20% FCS was used to grow the cell clones. Periodically, colony formation of the single clones was surveyed until stable

colonies were established that did not get in touch with each other. To ensure clonality, cells of the colonies were also separated into 96-well plates using the cell printer C.SIGHT™ (CYTENA, Freiburg, Germany).

2.5.3 Verification of genome editing

The T7E1 endonuclease assay was conducted by using the Alt-R™ Genome Editing Detection Kit (#1075931, Integrated DNA Technologies, Skokie, IL, USA) in order to confirm and quantify genomic alterations at the target locus mediated by CRISPR/Cas9:sgRNA RNP complexes (cf. 2.5.1). The underlying principle of the assay is the ability of T7E1 to cleave DNA heteroduplexes, which harbour mismatches bigger than 1 bp between wild-type and CRISPR-edited DNA strands. As described in the manufacturer's instructions, genomic DNA of control and transfected tumour cells, representing a mixed population of wild-type and CRISPR-edited cells, was extracted by using QuickExtract™ DNA Extraction Solution (#101094, Biozym, Hessisch Oldendorf, Germany) and PCR amplified with minor adjustments: 4 µl of the DNA extract was added to a master mix composed of 5 µl HOT FIREPol® EvaGreen® qPCR Mix Plus (#08-25-00020, Solis BioDyne, Tartu, Estonia), 14.5 µl H_2O (molecular biology grade #A7398,0500, AppliChem, Darmstadt, Germany) and 0.75 µl of 10 µM forward (5'-GGGAAAGGAAAGTAGCAACCG -3') and reverse primer (5'-TGGGAGCCAATAAGCCAATGT -3'), respectively. The PCR conditions are summarised in Table 3.

Table 3| PCR conditions for verification experiments.

Denaturation	95 °C	15 min	
Denaturation	95 °C	20 s	40 cycles
Annealing	64 °C	20 s	
Elongation	72 °C	45 s	
Plate read			
Final elongation	72 °C	5 min	
Melting curve	65 °C – 95 °C	Increment 0.5 °C/5 s	

T7E1-digested PCR products were mixed with a suitable volume of 10× loading buffer (40 mM EDTA disodium, 0.05% bromophenol blue, 0.05% xylene cyanol, 70% glycerol, H_2O ad 50 ml),

loaded onto 2% agarose gels with 0.5 µg/ml ethidium bromide (#E1510, Merck), and separated in TBE buffer (90 mM Tris, 90 mM H_3BO_3, 2 mM EDTA disodium, in H_2O) at 100 V (Figure 23). A 50 bp DNA ladder (#SM0372, Thermo Fisher Scientific) was used to estimate the sizes of the digested fragments. The DNA bands were visualised using a UV transilluminator in a light-protected cabinet and the photo software ArgusX1 (Biostep, Stollberg, Germany).

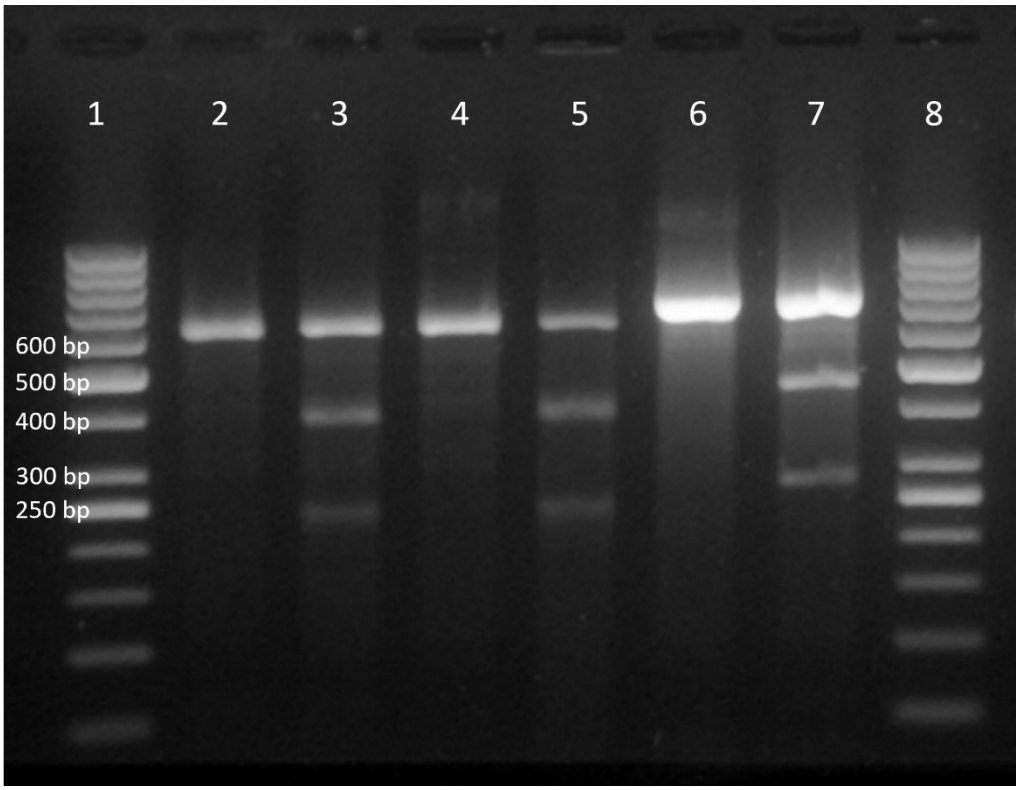

Figure 23| T7E1 mismatch assay. Representative 2% agarose gel of T7E1-digested PCR products of HepG2 wild-type (2), HepG2 wild-type and edited (3), SW480 wild-type (4), and SW480 wild-type and edited (5) cells, as well as the Alt-R homoduplex negative control (6) and heteroduplex positive control (7). 50 kb DNA ladder (1 and 8). Respectively, two mismatch fragments of the mixed HepG2 (3) and SW480 (5) cells and the Alt-R heteroduplex (7) indicate a successful genome editing in a certain share of the cells. Two mismatch fragments (375 bp and 256 bp) together have the same size as the PCR products of the respective wild-type cells (601 bp).

2.5.4 Identification of genome-edited clones by real-time PCR

Cell clones, generated by limiting dilution cloning or separated by cell printing, were investigated by PCR using allele-specific primer pairs to discriminate wild-type colonies from genome-edited clones. Only the 3' end of the forward primers were altered, depending on the targeted genomic locus of *IGF2BP2* and its mutations. Primer sequences and PCR conditions are listed in Table 4 and were used in a 25 µl PCR setup as described above (cf. 2.5.3). Presence of mutant and the absence of wild-type PCR amplicons of genome-edited clones were confirmed by agarose gel electrophoresis.

Table 4| Primer sequences and PCR conditions to discriminate wild-type cells from genome-edited clones. Differences at the 3' end between the forward primers of each pair of the respective target locus are labelled in red. wt: wild-type; mu: mutant; +: insertion; -: deletion; N/A: not available.

Genotype	Mutation at target locus	Forward primer sequence (5'→3')	Reverse primer sequence (5'→3')	Annealing temperature (°C)	Primer concentration (µM)
Exon 4					
wt	N/A	GGATGGACTTTTGGCTCAAT	TTTCTCCCTGGAGTTGACC	66	0.3
mu	+A	GGATGGACTTTTGGCTCAAA	TTTCTCCCTGGAGTTGACC	66	0.3
Exon 6					
wt_1	N/A	CATGGAGAAGCTAAGCGGG	CCGATGATGGCACCAACAAAC	66	0.3
mu_1	-GG	GCCATGGAGAAGCTAAGCGC	CCGATGATGGCACCAACAAAC	66	0.3
wt_2	N/A	AGAGCCATGGAGAAGCTAAGCGG	TGTCTGGCCTGAGAAGTGCC	66	0.3
mu_2	-GG	AGAGCCATGGAGAAGCTAAGCGC	TGTCTGGCCTGAGAAGTGCC	66	0.3

2.5.5 Sanger sequencing analysis

Genomic DNA was extracted using QuickExtract™ DNA Extraction Solution (#101094, Biozym) prior to PCR amplification of the edited region as described above (cf. 2.5.3). The resulting PCR amplicons were purified with the NucleoSpin™ Gel and PCR Clean-up Kit (#740609, Macherey-Nagel, Düren, Germany), premixed with the sequencing primer 5'-TGGGAGCCAATAAGCCAATGTAG-3' and sent for analysis *via* Sanger sequencing by Macrogen Europe B.V. (Amsterdam, the Netherlands). The web-based analysis tool CRISP-ID , was used to detect indel formation by aligning the *IGF2BP2* wild-type sequence to those of the edited clones. The predicted functional consequences of the resulting mutations in the *IGF2BP2* gene on the protein were analysed by the web application MutationTaster (Schwarz et al., 2014).

2.5.6 Single nucleotide primer extension and ion-pair reversed-phase high-performance liquid chromatography separation

Single nucleotide primer extension (SNuPE) and ion-pair reversed-phase high-performance liquid chromatography (IP/RP-HPLC) separation experiments were performed by Sascha Tierling (Institute of Genetics/Epigenetics (Saarland University, Saarbrücken, Germany). Five microlitres of gel-purified PCR product was added to a master mix containing 3 µl of 30 µM primer with the sequence 5'-CTGTCCCATATT-3', 2.5 µl of 10×TERMIPol® reaction buffer c (contained in #01-03-00500, Solis BioDyne), 2 µl of 25 mM $MgCl_2$, 1.25 µl of 1 mM ddGTP and ddTTP each, 1 µl of 5U/µl TERMIPol® DNA Polymerase (#01-03-00500, Solis BioDyne), and 9 µl H_2O. Primer extension reactions were performed at 96 °C for 2 min followed by 50 cycles 96 °C/30 s, 50 °C/30 s, 60 °C/1 min. IP/RP-HPLC was conducted to separate the SNuPE products at 50 °C using a WAVE® 3500 system (Transgenomic, Omaha, NE, USA) combined with a XBridge OST C_{18}, 2.5 µm (4.6 x 50 mm) column (Waters Milford, MA, USA). A gradient of acetonitrile from 7.25%-8.5% was generated by continuously mixing buffer B (0.1 M TEAA, 25% acetonitrile) to buffer A (0.1 M TEAA) over 8 min with a flow rate of 0.9 ml/min (corresponding to a share of 29–34% buffer B).

2.6 RNA isolation and reverse transcription

Total RNA from cultured cells was isolated using the High Pure RNA Isolation Kit (#11828665001, Roche) following the instructions of the manufacturer. RNA isolation from murine liver tissue was performed by first homogenizing snap-frozen liver tissue in QIAzol™

lysis reagent (#79306, Qiagen) using a high-performance disperser (T 25 digital ULTRA-TURRAX®, IKA®, Staufen, Germany) prior to total RNA extraction with the Direct-zol™ RNA Miniprep Plus Kit (#R2071, Zymo Research Europe, Freiburg, Germany), according to the manufacturer's protocol. Contamination of the RNA by residual genomic DNA was removed by DNase I treatment using the DNA-free™ DNA Removal Kit (#AM1906, Thermo Fisher Scientific). RNA concentration was determined by measuring the absorption at λ=280 nm using a NanoDrop™ Lite spectrophotometer (Thermo Fisher Scientific). RNA quality was checked by the absorption ratio A_{260}/A_{280}. Samples with ratios higher than 1.9 were accepted for downstream analyses. RNA content of all samples was adjusted to the same level prior to reverse transcription *via* the High Capacity cDNA Reverse Transcription Kit (#4368813, Thermo Fisher Scientific), following the manufacturer's instructions. The RNase inhibitor RNaseOUT™ (#10777019, Thermo Fisher Scientific) was used for all reactions.

2.7 Quantitative polymerase chain reaction

qPCR analysis of cDNA was conducted in 20 µl format using the ready-to-use HOT FIREPol® EvaGreen® qPCR Mix Plus (#08-25-00020, Solis BioDyne) mixed with respective primers for the target transcript. The qPCR setup including primer sequences and concentrations as well as the analysis conditions are listed in Table 5 and Table 6. Samples were analysed in triplicate. The reaction was performed in a CFX96 touch™ Real-Time PCR detection system (Bio-Rad Laboratories, Hercules, CA, USA), and data were recorded with the CFX Manager™ software (version 3.1):

Table 5| Conditions for qPCR analyses.

Denaturation	95 °C	15 min	
Denaturation	95 °C	15 s	40 cycles
Annealing	See Table 6	20 s	
Elongation	72 °C	20 s	
Plate read			
Melting curve	65 °C – 95 °C	Increment 0.5 °C/5 s	

For human samples, absolute gene expression was normalized to the housekeeping gene *ACTB* (actin beta) or *RNA18SN5* (RNA, 18S ribosomal N5). Murine data were normalized to

Ppia (peptidylprolyl isomerase A) or *Csnk2a2* (casein kinase 2 alpha 2) mRNA values. Standard plasmids were generated by ligation of gel-purified PCR amplicons of the gene transcripts of interest into the pGEM-T® Easy vector (#A137A, Promega, Madison, WI, USA) according to the manufacturer's instructions.

Table 6| Primer sequences and qPCR conditions.

Gene	NCBI accession number	Forward primer sequence (5′→3′)	Reverse primer sequence (5′→3′)	Annealing temperature (°C)	Primer concentration (µM)
			Homo sapiens		
ACTB	NM_001101.3	TGCGTGACATTAAGGAGAAG	GTCAGGCAGCTCGTAGCTCT	60	0.2
BCL2	NM_000633.2; NM_000657.2	ACAACATCGCCCTGTGGATGAC	ACTTGTGGCTCAGATAGGCACC	64	0.25
DANCR	NR_024031.2	GCTCCAGGAGTTCGTCTCTTAC	TGCGCTAAGAACTGAGGCAG	60	0.25
E2F1	NM_005225.2	AGTTCATCAGCCTTTCCCCACC	CTCCAAGCCCTGTCAGAAATCC	59	0.25
ELAVL1	NM_001419.2	GGTGACATCGGGAGAACGAA	CCAAGCTGTGTCCTGCTACT	60	0.25
HMGA1	NR_024031.2	CTAATTGGGACTCCGAGCCG	GTAGCAAATGCGGATGCCTT	60	0.25
IGF2BP1	NM_006546.3; NM_001160423.1	GCCTCCATCAAGATTGCACCAC	AGCTTCACTTCCTCCTTGGGAC	62	0.2
IGF2BP2	NM_006548.4	CAATCTGATCCCAGGGTTG	GCCCTGCTGGTGGAGATAG	60	0.2
***IGF2BP2* (TRIBE)**	NM_006548.6	GTTCCCGCATCATCACTCTTAT	GAATCTCGCCAGCTGTTTGA	62	0.2
IGF2BP3	NM_006547.2	TCCCACCCAATTTGTTGGAGCC	GCAGCCCCCGCATTTTCTTTAC	62	0.2
MYC	NM_002467.5; NM_001354870.1	AGCCACAGCATACATCCTGTCC	CTCGTCGTTTCCGCAACAAGTC	56	0.2
NEAT1_v1/v2	NR_131012.1; NR_028272.1	TGCTACAAGGTGGGGAAGACTG	CCCACACCCCAAACAAAACAA	60	0.25
NEAT1_v2	NR_131012.1	TTTCAAAGGGAGCAGCAAGGG	ACGGCACAGGCAAATAAGACAC	64	0.25
RNA18SN5	NR_003286.4	AGGTCTGTGATGCCCTTAGA	GAATGGGGTTCAACGGGTTA	61	0.25
VEGFA	NM_001171623.1	CGCTTACTCTCACCTGCTTCTG	GGTCAACCACTCACACACACAC	60	0.25
XIAP	NM_001167.3; NM_001204401.1	AATAGTGCCACGCAGTCTACA	CAGATGGCCTGTCTAAGGCAA	64	0.25
ZFP36	NM_003407.3	TCGCCACCCCAAATACAA	TTCGCTAGGGTTGTGGAT	60	0.25
			Mus musculus		
Csnk2a2	NM_009974.3	GTAAAGGACCCTGTGTCAAAGA	GTCAGGATCTGGTAGAGTTGCT	60	0.4
***Igf2bp2* (TRIBE)**	NM_183029.2	TTGGATGGGCTGTTGGCTGA	GTGACGTTGACAACGGCAGTT	60	0.2
Ppia	NM_008907.1	GCGTCTCCTTCGAGCTGTTT	CACCCTGGCACATGAATCCT	59	0.5
***Rn18s* (TRIBE)**	NR_003278.3	AGGTCTGTGATGCCCTTAGA	GAATGGGGTTCAACGGGTTA	61	0.25
Zfp36	NM_011756.4	CTTCATCCACAACCCCACC	CAGGGAAGGGCCAGAAAAG	60	0.25

2.8 Sodium dodecyl sulfate–polyacrylamide gel electrophoresis and Western blot

Protein lysates originating from cell clones in the course of IMP2 knockout cell line development were prepared from pelleted cells that were washed with PBS (1×) twice prior to treatment with either an aqueous lysis buffer composed of 50 mM Tris-HCl, 1% sodium dodecyl sulfate (SDS), 10% glycerol, 5% β-mercaptoethanol, 0.004% bromophenol blue, or RIPA buffer (50 mM Tris-HCl, 1% triton X-100, 0.1% SDS, 0.5% sodium deoxycholate, 150 mM NaCl, in H_2O), supplemented with the protease inhibitor cocktail cOmplete® Mini (#04693124001, Roche). If samples were not directly used for analysis, they were stored at -80 °C. Otherwise, the protein lysates were incubated on ice for 30 min and vortexed in between, sonicated for 10 s, and in the case of RIPA lysates, the protein concentration was determined using the Pierce™ BCA Protein Assay Kit (#23225, Thermo Fisher Scientific). Subsequently, the protein samples were denatured at 95 °C for 5 minutes and cooled down on ice prior to loading onto 1.5 mm thick polyacrylamide gels (4% stacking gel and 12% resolving gel). Before denaturation of RIPA lysates, an appropriate volume of the loading buffer concentrate Roti®-Load 1 (#K929, Carl-Roth) was added to the samples. Sodium dodecyl sulfate–polyacrylamide gel electrophoresis (SDS-PAGE) was performed using the Mini-PROTEAN® systems (Bio-Rad Laboratories). A voltage of 80 V was applied, which was increased to 120 V after the samples entered the resolving gel. The protein size was estimated by using a prestained protein ladder (PageRuler™, #26616, Thermo Fisher Scientific) that ran in parallel to the samples. Electrophoretic transfer of the proteins onto an Immobilon®-FL PVDF membrane (#IPFL00010, Merck) was conducted using a Mini Trans-Blot® cell (Bio-Rad Laboratories). After blotting overnight (12-16 h), the membrane was allowed to air-dry before it was soaked in methanol and rinsed with distilled water. Hereafter, the membrane was incubated for 1.5 h in blocking buffer for fluorescent western blotting (RBB, #MB-070, Rockland Immunochemicals, Limerick, PA, USA) prior to immunodetection of the proteins. For this, the membrane was incubated for 1.5 h with a mixture of two primary antibodies (anti-p62C, and anti-α-tubulin or anti-GAPDH as housekeeping proteins) diluted in RBB (Table 7) at room temperature. Subsequently, the membrane was washed three times for five minutes with PBST (phosphate buffered saline containing 1% Tween® 20) and once for five minutes with PBS (1×) before 1.5 h incubation with an IRDye-conjugated secondary antibody protected from light at room temperature. After repeating the washing procedure (see above), the signal was detected using an Odyssey® CLx

Imaging System (LI-COR Biosciences, Lincoln, NE, USA) running its software Image Studio (version 5.2.5).

Table 7| Antibodies used for immunodetection of proteins.

Antibody	Dilution	Catalogue number	Supplier
Mouse anti-α-tubulin [DM1A] mAb	1:1,000 in RBB	T9026	Merck, Darmstadt, Germany
Mouse anti-GADPH [OTI2D9]	1:2,000 in RBB	TA802519	OriGene Technologies, Rockville, MD, USA
Rabbit anti-p62C (anti-IGF2BP2)	1:1,000 in RBB		M. Lu et al., (2001)
Rabbit anti-TTP polyclonal antibody	1:2,000 in 5% milk powder-PBST	ab36558	Abcam, Cambridge, United Kingdom
IRDye® 680RD goat anti-rabbit IgG	1:10,000 in RBB	926-68071	LI-COR Biosciences, Lincoln, NE, USA
IRDye® 800CW goat anti-mouse IgG	1:10,000 in RBB	926-32210	

2.9 Flow cytometry

Flow cytometric analysis of murine liver leukocyte composition was performed as described previously (Kessler et al., 2019; N. Wang et al., 2011). To determine the number of leukocytes, 1 µg of the fluorescein isothiocyanate (FITC) mouse anti-mouse cluster of differentiation (CD) 45.2 antibody (#561874 [104], BD Biosciences, Heidelberg, Germany) in 100 µl was used. To detect the composition of leukocytes, 0.5 µg of each antibody were added: allophycocyanin (APC) rat anti-mouse Ly6G (#560599 [1A8], BD Biosciences), APC-R700 rat anti-mouse CD11b (#564985 [M1/70], BD Biosciences), BV421 rat anti-mouse Ly6C (#562727 [AL-21], BD Biosciences), BV510 mouse anti-mouse NK 1.1 (#563096 [PK136], BD Biosciences), PE hamster anti-mouse CD11c (#55740 [HL3], BD Biosciences), and FITC human anti-mouse F4/80 (#130-102-327 [REA126], Miltenyi Biotec, Bergisch Gladbach, Germany). To determine the composition of the leukocytes, the following gating strategy was applied: forward scatter (FSC)low debris and erythrocytes, and multiplets with a non-linear side scatter (SSC)-A/SSC-H ratio were excluded. Viability was determined by 7-amino-actinomycin D (7-AAD) staining.

Viable cells (7-AAD$^-$) were analysed for CD11b and Cd11c expression. Myeloid dendritic cells were defined as CD11b$^+$ CD11c^{hi} cells, and neutrophils were identified as Ly6G$^+$ cells within the CD11b$^+$ CD11c$^-$ population. CD11b$^+$ CD11c$^-$ Ly6G$^-$ NK1.1$^-$ cells were further divided into subpopulations according to their Ly6C and F4/80 expression, that is macrophages (Ly6C^{lo} F4/80^{hi}) and monocytes (Ly6C^{hi} F4/80^{lo}), following Blériot et al. (2015) and Ramachandran et al. (2012). All gates were defined by using fluorescence minus one control. Flow cytometric analysis of human hepatoma cell proliferation was performed as described previously (Schultheiss et al., 2017) using the PE Mouse Anti-Human Ki-67 Set (#5113743, BD Biosciences). Graphical illustrations were performed with BD FACSuite™ (BD Biosciences). Flow cytometry was performed by Kevan Hosseini (Department of Pharmacy, Pharmaceutical Biology, Saarland University, Saarbrücken, Germany).

2.10 Human HCC

Paraffin-embedded liver samples (n=31) from randomly selected pseudonymised HCC patients who underwent liver resection at the Saarland University Medical Center between 2005 and 2010 were obtained as described previously (Kessler et al., 2013). The study protocol was approved by the local Ethics Committee (47/07). Samples had a mixed etiology, including NASH, alcoholic liver disease, viral hepatitis, hemochromatosis, porphyria, and cryptogenic cirrhosis (Kessler et al., 2013). For differential *ZFP36* expression between tumour (n=247) and non-tumour (n=239) samples, the log2 of an RMA-normalised data set (GSE14520, Roessler et al., 2010) of an AffymetrixGeneChip HG-U133A 2.0 was analysed. Similarly, differential gene expression was analysed in data set GSE25097 (Tung et al., 2011) between healthy (n=6), cirrhotic (n=40), adjacent non-tumour (n=243), and tumour tissue (n =268), and in data set GSE20238 (Minguez et al., 2011) between vascular invasive (n=45) and non-invasive (n=34) HCC samples. Differential expression analysis was based on the Kolmogorov–Smirnov test. Pearson correlation was applied to detect correlations between genes of interest. RNA sequencing expression data from The Cancer Genome Atlas (TCGA) pan cancer dataset, comparing ZFP36 expression in tumour and non-tumour liver tissue, was produced *via* Toil (Vivian et al., 2017). RSEM (B. Li & Dewey, 2011) reported transcripts per million values were downloaded *via* the UCSC Xena Browser (https://xenabrowser.net) and comprised 373 primary solid tumours as well as 50 matched non-tumour tissue samples. Correlation analysis

was performed by Ahmad Barghash (School of Electrical Engineering and Information Technology, German Jordanian University, Jordan).

2.11 Statistics

Data analysis and statistics of experimental data were performed using the OriginPro® 2020 software (OriginLabs, Northampton, MA, USA). All data are displayed either as columns with mean values ±SD or as individual values and boxplots (interquartile) range with mean (square) and median (line), if not stated otherwise. Normality was tested with the Shapiro–Wilk algorithm. Grubbs test was performed to identify possible outliers. Depending on normality, one-way analysis of variance (ANOVA) followed by Scheffe post-hoc test or Kruskal–Wallis–ANOVA followed by Mann–Whitney test was performed. Two-way ANOVA followed by Scheffe post-hoc test was performed on data belonging to four different comparison groups. Two-sample *t*-test was used to calculate statistical differences between two groups and Fisher's-exact test was used for categorical data. Differences were considered statistically significant with $p \leq 0.05$.

3 Chapter I: the mRNA-binding protein TTP/*ZFP36* in hepatocarcinogenesis and hepatocellular carcinoma

This chapter have been published in:

Kröhler, Tarek, Kessler, S. M., Hosseini, K., List, M., Barghash, A., Patial, S., Laggai, S., Gemperlein, K., Haybaeck, J., Müller, R., Helms, V., Schulz, M. H., Hoppstädter, J., Blackshear, P. J., & Kiemer, A. K. (2019). The mRNA-binding protein TTP/ZFP36 in hepatocarcinogenesis and hepatocellular carcinoma. *Cancers*, *11*(11), 1754. https://doi.org/10.3390/cancers11111754

3.1 Introduction

HCC, the predominant form of liver cancer, is the second most common cause of cancer-related death worldwide (Bruix et al., 2015; Tang et al., 2018). Besides viral hepatitis in North Africa and East Asia (Farazi & DePinho., 2006), alcohol abuse, obesity, type 2 diabetes, and metabolic disorders represent the major risk factors for the development of HCC in Northern Europe, the USA, and Canada (El-Serag, 2012; Reeves et al., 2016). The initiation and progression of cancer are provoked by a dysregulated expression of proteins controlling diverse cellular phenotypes: cell cycle, differentiation, apoptosis, angiogenesis, and cell invasiveness (Hanahan & Weinberg, 2011). Biosynthesis of these proteins is strongly regulated by the concentrations of their respective mRNAs in the cytoplasm, which depend on both mRNA synthesis and degradation. The cytoplasmic stability of many mRNAs is controlled by RBPs, some of which have been shown to be deregulated in HCC. However, most of the studies focus on upregulated RBPs (Dang et al., 2017; Gutschner et al., 2014; Kessler et al., 2015; T. Li et al., 2017). ARE-BPs, a subgroup of RBPs control the stability of mRNAs by binding to ARE located within their 3'-UTR (Guhaniyogi & Brewer, 2001). A prominent member of these ARE-BPs, TTP, accelerates the decay of transcripts (Blackshear, 2002). TTP expression is repressed in several human cancers (Hitti et al., 2016; Sanduja et al., 2012) and a loss of functional TTP can impact patient prognosis (Brennan et al., 2009). HCC usually develops in the course of metabolic changes. Recent evidence showed that hepatocytic TTP seems to rather amplify metabolic disorders by promoting insulin resistance, quite in contrast to its tumour

suppressor role (Sawicki et al., 2018). Since, to the best of our knowledge, nothing is known about a potential role of TTP in tumour initiation, we conducted this study to address the potential role of TTP in hepatocarcinogenesis. We analysed the effect of a ls*Ttp*-KO in mice treated with the tumour-inducing agent DEN. In addition, we investigated the impact of TTP overexpression in a set of hallmarks of cancer in order to study cancer progression. Our findings revealed tumour-promoting actions of TTP in tumour initiation, due to metabolic and inflammatory action, but tumour-suppressive actions in HCC progression.

3.2 Results

3.2.1 TTP and tumour initiation

In order to study the role of TTP in liver tumour initiation, we employed ls*Ttp*-KO mice (Sawicki et al., 2018) in the DEN hepatocarcinogenesis mouse model. Wild-type and ls*Ttp*-KO mice were treated with DEN at the age of two weeks to induce tumours, and were sacrificed at the age of six months, representing an early time point and therefore rather modelling tumour initiation (Kessler et al., 2014). The tumour incidence was significantly lower in DEN-treated ls*Ttp*-KO animals compared to DEN-treated wild-type animals (Figure 24A), while there was no statistical difference regarding tumour incidence between the genotypes in the sham-treated groups. The number of tumours per animal was significantly lower in the DEN-treated ls*Ttp*-KO animals compared to DEN-treated wild-type mice (Figure 24B). While tumours of DEN-treated ls*Ttp*-KO mice showed a solid growth pattern, tumours of wild-type animals were of trabecular, solid, or mixed pattern (Figure 24C).

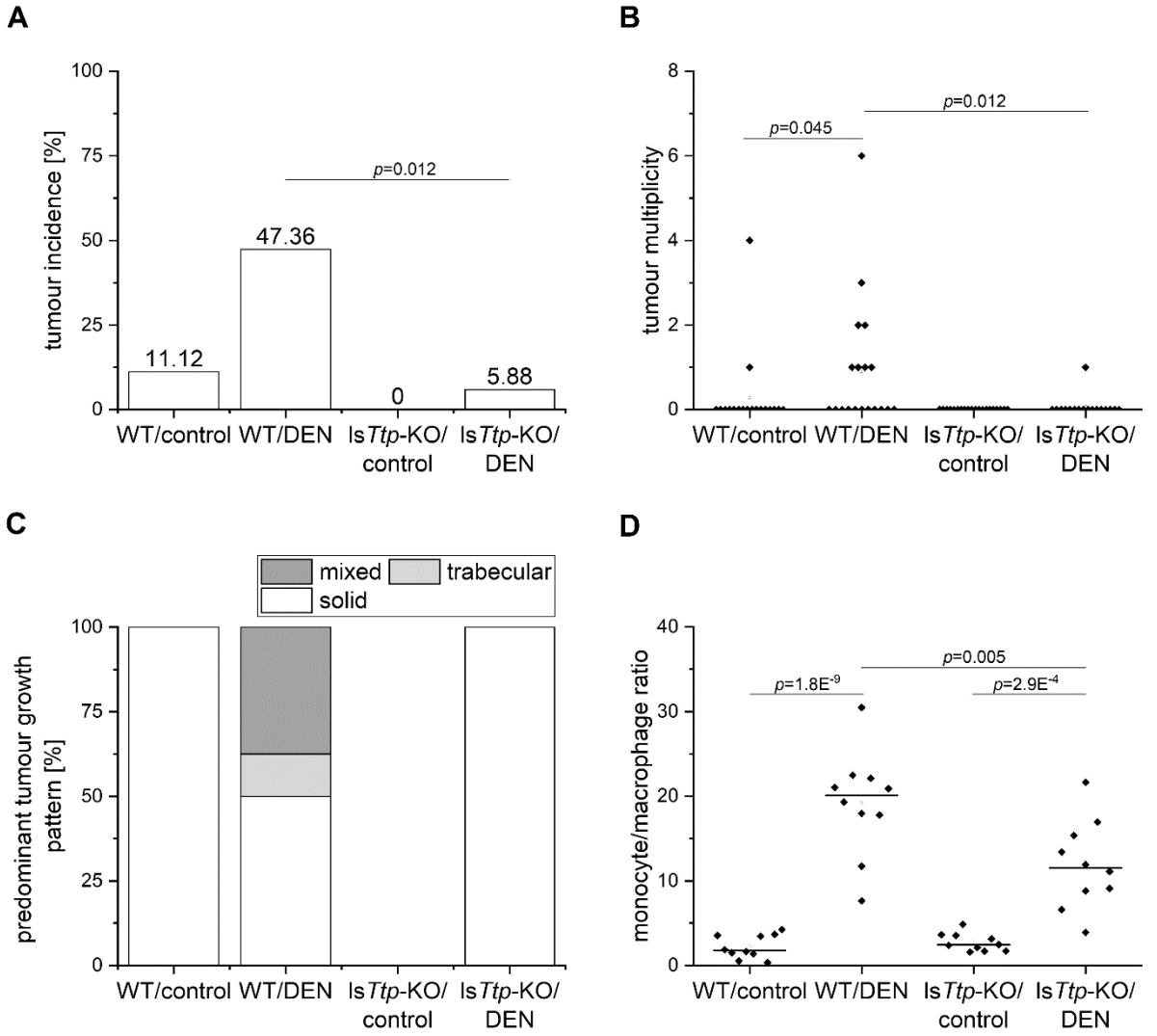

Figure 24| Amount and pattern of tumours and hepatic monocyte to macrophage ratio in DEN- or sham-treated wild-type (WT) and ls*Ttp*-KO mice. (A): tumour incidence. (B): tumour multiplicity. (C): predominant tumour growth pattern. (D): monocyte/macrophage ratio analysed by multi-colour flow cytometry (short-term experiment). n=10, each. From "The mRNA-binding protein TTP/ZFP36 in hepatocarcinogenesis and hepatocellular carcinoma" by Kröhler, T., Kessler, S. M., Hosseini, K., List, M., Barghash, A., Patial, S., Laggai, S., Gemperlein, K., Haybaeck, J., Müller, R., Helms, V., Schulz, M. H., Hoppstädter, J., Blackshear, P. J., & Kiemer, A. K. (2019), *Cancers, 11*(11), 1754 (https://doi.org/10.3390/cancers11111754). Licensed under CC BY 4.0. Also published in similar way in "Pathomechanisms in hepatocellular carcinoma: characterisation of leukocyte recruitment, the role of the mRNA-binding protein tristetraprolin and nuclear paraspeckles" (Doctoral thesis, Saarland University, Saarbrücken, Germany) by Hosseini, K. (2017) (https://doi.org/10.22028/D291-27154).

3.2.2 DEN-induced leukocyte recruitment and hepatic lipids

Short-term (48 h) DEN treatment represents a well-established approach to modeling metabolic and inflammatory events in early hepatocarcinogenesis (Kessler, et al., 2014; Naugler et al., 2007). We hypothesised that protection from DEN-induced liver cancer in ls*Ttp*-KO mice is a consequence of attenuated leukocyte recruitment and lipogenesis. Short-term DEN treatment is characterised by a highly increased monocyte/macrophage ratio (Kessler et al., 2019). While both genotypes exhibited such an increased monocyte/macrophage ratio as

assessed by flow cytometric analysis, the ratio was significantly lower in ls*Ttp*-KO mice compared to wild-types (Figure 24D). No difference could be observed between the genotypes in the sham-treated group (Figure 24D). In the long-term model, there is only a very mild inflammation, which was somewhat lower in ls*Ttp*-KO mice.

The amount and pattern of hepatic lipids are altered during inflammatory conditions and contribute to hepatocarcinogenesis (Dembek et al., 2017; Horie et al., 2004; Kessler et al., 2014). Accordingly, short-term DEN treatment also induces lipogenesis (Kessler et al., 2014). Fatty acid profiling revealed a significant increase in the sum of both saturated fatty acids and poly-unsaturated fatty acids in DEN-treated wild-type livers (Figure 25A–C). However, this increase was less pronounced in ls*Ttp*-KO livers (Figure 25A–C).

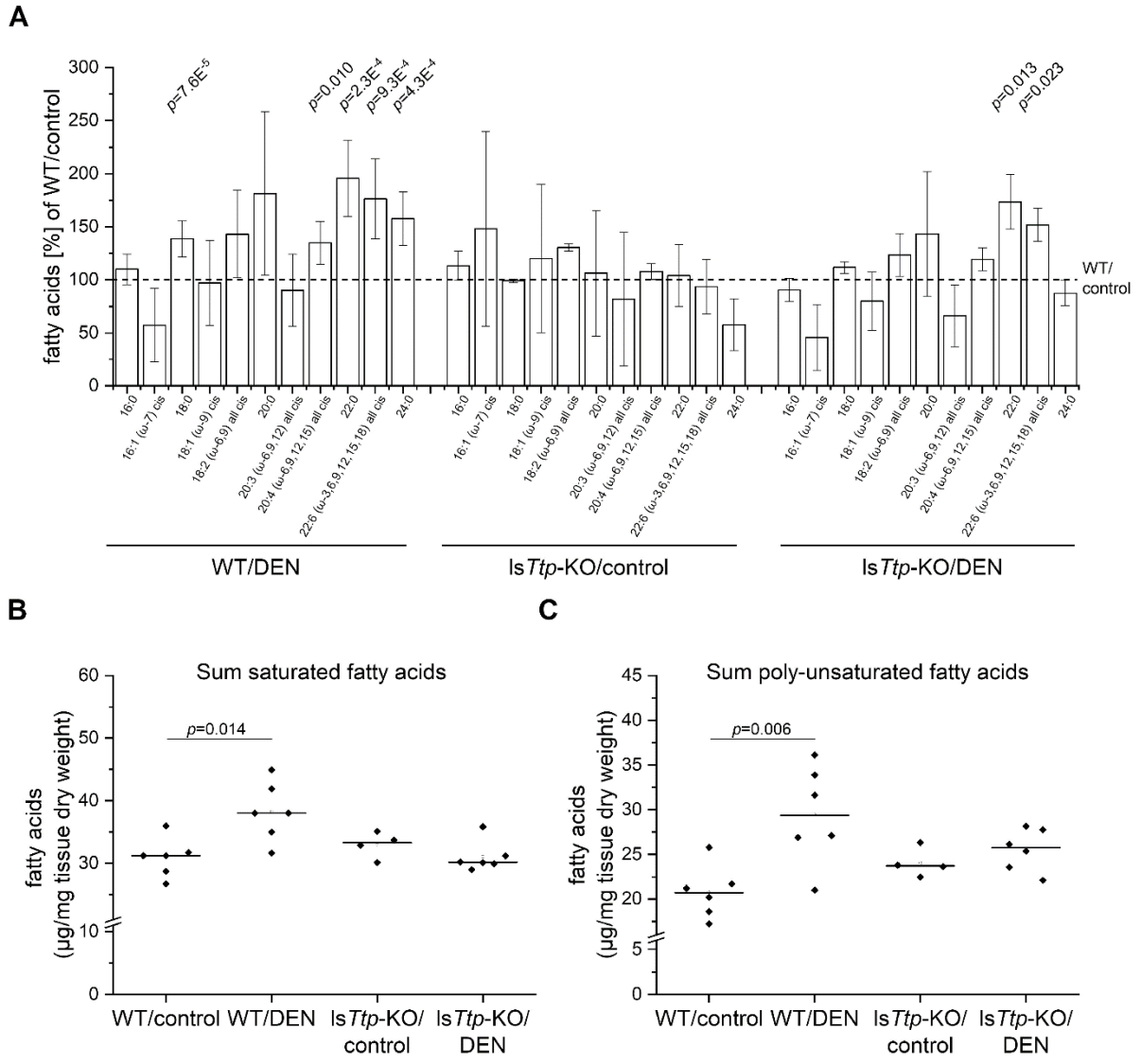

Figure 25| Hepatic fatty acid profile in short-term DEN-treated ls*Ttp*-KO mice. (A): Overview of hepatic fatty acids (FAs) in the four comparison groups. The values for the represented FAs are normalised to the corresponding FA in WT/control, which is set to 100 % and is illustrated by the dashed line. Statistical differences refer to the respective control, which means that WT/DEN is compared with WT/control and ls*Ttp*-KO/DEN is compared with ls*Ttp*-KO/control. Error bars indicate SD. Graphs for single FAs are shown in Supplementary Figure 1. (B): Sum saturated FAs (14:0, 16:0, 17:0, 18:0, 20:0, 22:0, 24:0). (C): Sum poly-unsaturated FAs (18:2 (ω-6,9) all cis, 20:2 (ω-6,9) all cis, 20:3 (ω-6,9,12) all cis, 20:4 (ω-6,9,12,15) all cis, 22:5 (ω-3,6,9,12,15) all cis, 22:6 (ω-3,6,9,12,15,18) all cis). n=6 (WT/control), n=6 (WT/DEN), n=4 (ls*Ttp*-KO/control), n=6 (ls*Ttp*-KO/DEN). Rhombi illustrate single data points, horizontal black lines illustrate median, and white rectangles illustrate means. Significant *p* values (α<0.05) are shown. (14:0=myristic acid, 16:0=palmitic acid, 16:1 (ω-7) cis=palmitoleic acid, 17:0=margaric acid, 18:0=stearic acid, 18:1 (ω-9) cis=oleic acid, 18:2 (ω-6,9) all cis=linoleic acid, 20:0=arachidic acid, 20:2 (ω-6,9) all cis=eicosadienoic acid, 20:3 (ω-6,9,12) all cis=eicosatrienoic acid, 20:4 (ω-6,9,12,15) all cis=arachidonic acid , 22:0=behenic acid, 22:5 (ω-3,6,9,12,15) all cis=docasapentaenoic acid, 22:6 (ω-3,6,9,12,15,18) all cis=docosahexaenoic acid, 24:0=lignoceric acid). From "The mRNA-binding protein TTP/ZFP36 in hepatocarcinogenesis and hepatocellular carcinoma" by Kröhler, T., Kessler, S. M., Hosseini, K., List, M., Barghash, A., Patial, S., Laggai, S., Gemperlein, K., Haybaeck, J., Müller, R., Helms, V., Schulz, M. H., Hoppstädter, J., Blackshear, P. J., & Kiemer, A. K. (2019), *Cancers, 11*(11), 1754 (https://doi.org/10.3390/cancers11111754). Licensed under CC BY 4.0.

Profiling of individual fatty acids revealed an increase of individual, but not all, fatty acids, which was almost abrogated in the DEN-treated ls*Ttp*-KO mice (Figure 25A, Supplementary Figure 1). Since reprogramming of energy metabolism has been described as a hallmark of cancer (Hanahan & Weinberg, 2011), we also assessed fatty acid profiles in livers after long-term (six months) DEN treatment. However, no significant difference in the amount of fatty acids upon DEN treatment was observed in either genotype (Figure 25A–C, Supplementary Figure 2). Interestingly, though, sham-treated ls*Ttp*-KO mice showed distinctly increased levels of saturated and mono-unsaturated fatty acids compared to wild-types (Figure 26A–C, Supplementary Figure 2), suggesting that ls*Ttp*-KO mice change their phenotype over time.

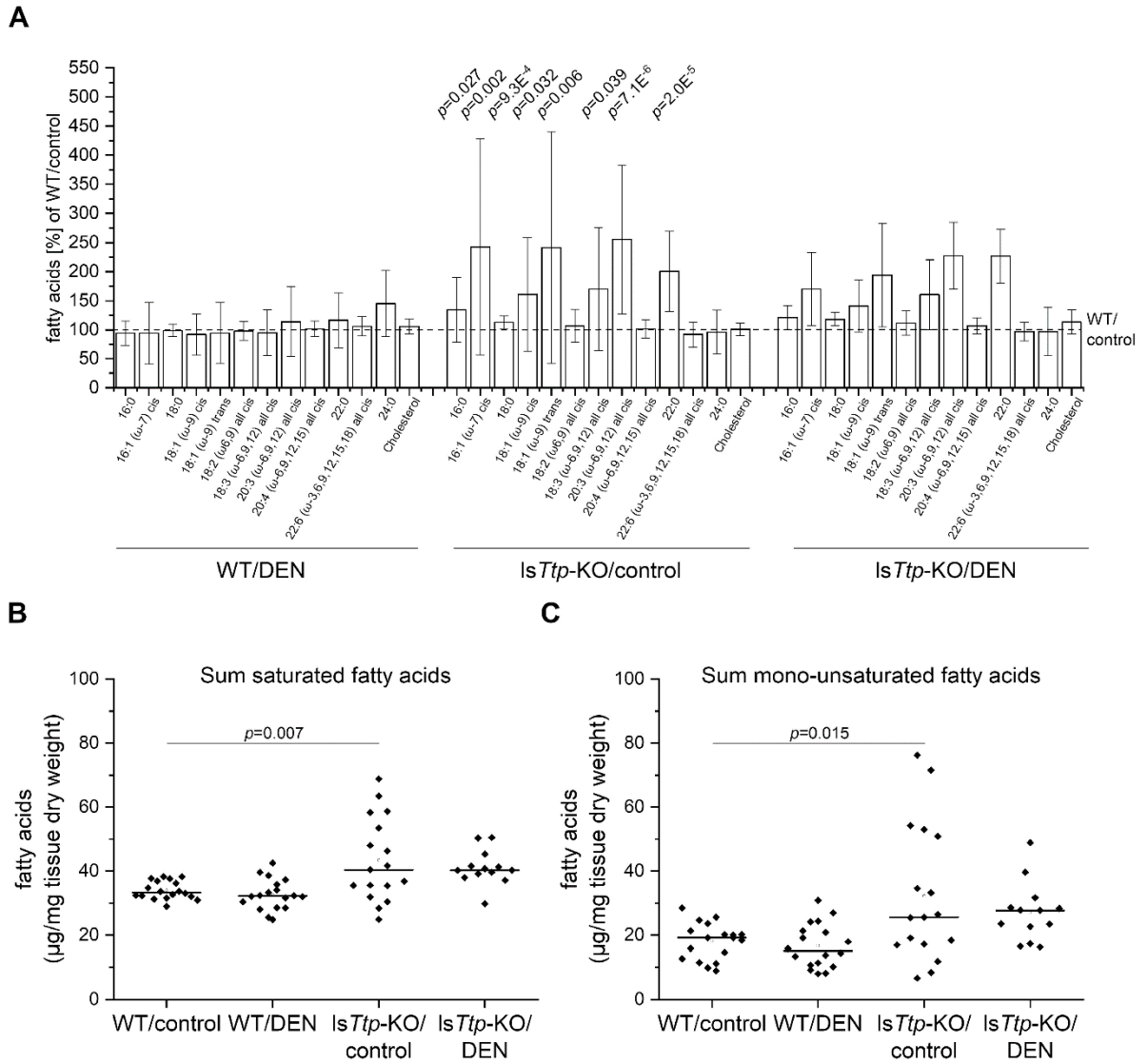

Figure 26| Hepatic fatty acid profile in long-term DEN-treated ls*Ttp*-KO mice. (A): Overview of hepatic fatty acids (FAs) in the four comparison groups. The values for the represented FAs are normalised to the corresponding FA in WT/control, which is set to 100 % and is illustrated by the dashed line. Statistical differences refer to the respective partner undergoing same treatment but different genotype, which means that WT/control is compared with ls*Ttp*-KO/control and WT/DEN is compared with ls*Ttp*-KO/DEN. Error bars indicate SD. Graphs for single FAs are shown in Supplementary Figure 2. (B): Sum saturated FAs (14:0, 16:0, 17:0, 18:0, 20:0, 22:0, 24:0). (C): Sum-polyunsaturated FAs (18:2 (ω-6,9) all cis, 20:2 (ω-6,9) all cis, 20:3 (ω-6,9,12) all cis, 20:4 (ω-6,9,12,15) all cis, 22:5 (ω-3,6,9,12,15) all cis, 22:6 (ω-3,6,9,12,15,18) all cis). (B)+(C): n=6 (WT/control), n=6 (WT/DEN), n=4 (lsTtp-KO/control), n=6 (lsTtp-KO/DEN). Rhombi illustrate single data points, horizontal black lines illustrate median, and white rectangles illustrate means. Significant *p* values (α<0.05) are shown. (14:0=myristic acid, 16:0=palmitic acid, 16:1 (ω-7) cis=palmitoleic acid, 17:0=margaric acid, 18:0=stearic acid, 18:1 (ω-9) cis=oleic acid, 18:2 (ω-6,9) all cis=linoleic acid, 20:0=arachidic acid, 20:2 (ω-6,9) all cis=eicosadienoic acid, 20:3 (ω-6,9,12) all cis=eicosatrienoic acid, 20:4 (ω-6,9,12,15) all cis=arachidonic acid , 22:0=behenic acid, 22:5 (ω-3,6,9,12,15) all cis=docasapentaenoic acid, 22:6 (ω-3,6,9,12,15,18) all cis=docosahexaenoic acid, 24:0=lignoceric acid). From "The mRNA-binding protein TTP/ZFP36 in hepatocarcinogenesis and hepatocellular carcinoma" by Kröhler, T., Kessler, S. M., Hosseini, K., List, M., Barghash, A., Patial, S., Laggai, S., Gemperlein, K., Haybaeck, J., Müller, R., Helms, V., Schulz, M. H., Hoppstädter, J., Blackshear, P. J., & Kiemer, A. K. (2019), *Cancers, 11*(11), 1754 (https://doi.org/10.3390/cancers11111754). Licensed under CC BY 4.0.

3.2.3 Effects of TTP on hallmarks of cancer

Our data suggested tumour-promoting actions of TTP by supporting tumour initiation. In order to clarify the role of TTP during tumour progression, TTP expression was investigated with respect to several hallmarks of cancer, among which sustaining proliferation might be the most important one. We therefore aimed to investigate a potential action of TTP on cell proliferation by MKI67 staining and flow cytometry in stably overexpressing cell lines. However, cells stably transfected with the overexpressing plasmid did not grow at all. Thus, the proliferation ability of transiently TTP-overexpressing cells was investigated. The proliferation in three different human hepatoma cell lines (HepG2, PLC/PRF/5, and Huh7) was dramatically decreased after TTP overexpression (Figure 27A-B), rather suggesting tumour-suppressing actions of TTP. In line with these findings, we observed that baseline expression of TTP was almost absent in all three cancer cell lines. Migration as another hallmark of cancer represents a prerequisite of tumour cells to metastasis (Hanahan & Weinberg, 2011). We determined the migratory potential of the cells by a scratch assay in TTP-overexpressing or vector control cells. The migratory ability of PLC/PRF/5 and HepG2 cells, but not of Huh7 cells, was inhibited by TTP (Figure 27C), further supporting the tumour-suppressing actions of TTP.

A

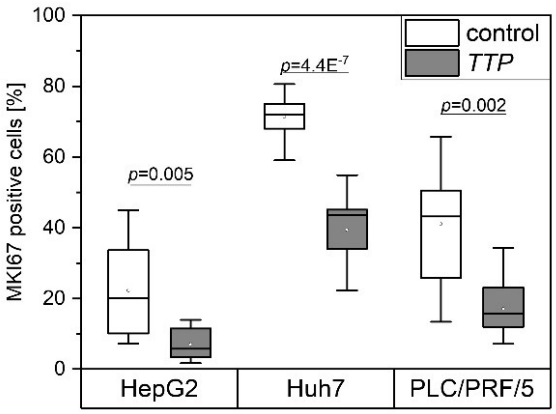
MKI67 positive cells [%]
100
80
60
40
20
0
control
TTP
p=0.005
p=4.4E-7
p=0.002
HepG2
Huh7
PLC/PRF/5

B

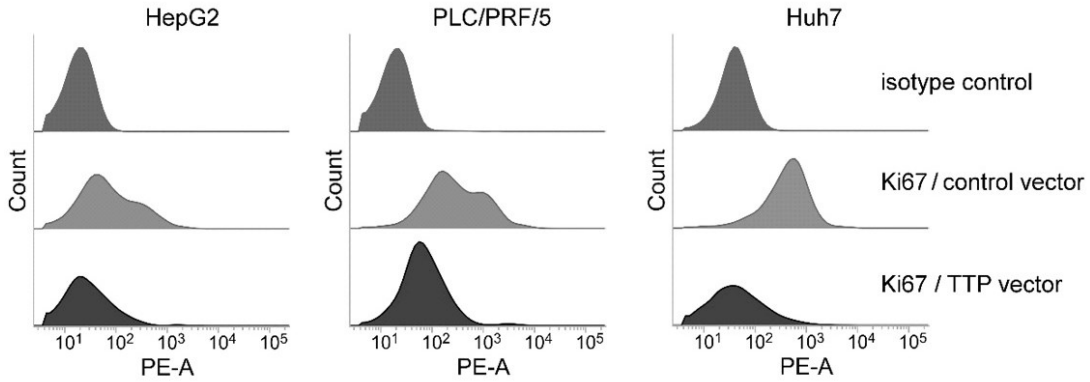
HepG2
PLC/PRF/5
Huh7
Count
PE-A
isotype control
Ki67 / control vector
Ki67 / TTP vector

C

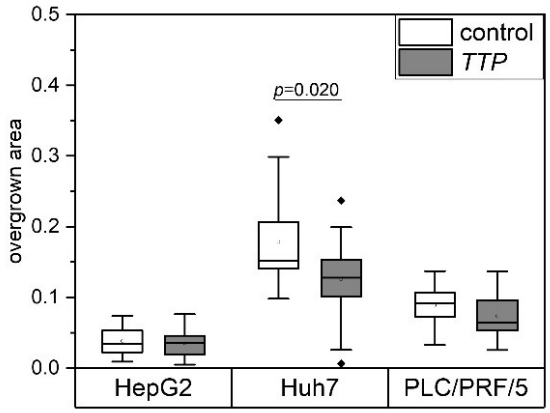
overgrown area
0.5
0.4
0.3
0.2
0.1
0.0
control
TTP
p=0.020
HepG2
Huh7
PLC/PRF/5

Figure 27| Proliferation and migration of TTP-overexpressing hepatoma cells. (A): Proliferation of cells transfected with either TTP or a control vector. (B): Flow cytometric analysis of the proliferation marker MKI67 in TTP-overexpressing (TTP vector) and control cells (control vector). The isotype controls represent the control cells. Representative histograms of MKI67 flow cytometric analyses are shown. n=3 (triplicates). (C): Migration of HepG2, Huh7, and PLC/PRF/5 cells transfected with either a TTP or a control vector. The difference between the open image area t(0) and t(24) was considered as overgrown area. n=5-6 (quadruplicates). From "The mRNA-binding protein TTP/ZFP36 in hepatocarcinogenesis and hepatocellular carcinoma" by Kröhler, T., Kessler, S. M., Hosseini, K., List, M., Barghash, A., Patial, S., Laggai, S., Gemperlein, K., Haybaeck, J., Müller, R., Helms, V., Schulz, M. H., Hoppstädter, J., Blackshear, P. J., & Kiemer, A. K. (2019), *Cancers, 11*(11), 1754 (https://doi.org/10.3390/cancers11111754). Licensed under CC BY 4.0. Also published in similar way in "Pathomechanisms in hepatocellular carcinoma: characterisation of leukocyte recruitment, the role of the mRNA-binding protein tristetraprolin and nuclear paraspeckles" (Doctoral thesis, Saarland University, Saarbrücken, Germany) by Hosseini, K. (2017) (https://doi.org/10.22028/D291-27154).

As a parameter of chemosensitivity, TTP-overexpressing cells, as well as control HepG2, PLC/PRF/5, and Huh7 cells, were treated with either sorafenib or doxorubicin. The results suggested an impact of TTP overexpression on chemosensitivity in all three cell lines (Figure 28A-F). However, the viability of untreated TTP-overexpressing cells was significantly lower than the number of untreated control cells in all three cell lines (Figure 28A-F). Therefore, the evaluation was adjusted in a way that TTP-overexpressing and control cells were normalised to the control cells. This revealed a less dramatically decreased, but still significantly different chemosensitivity (Supplementary Figure 3).

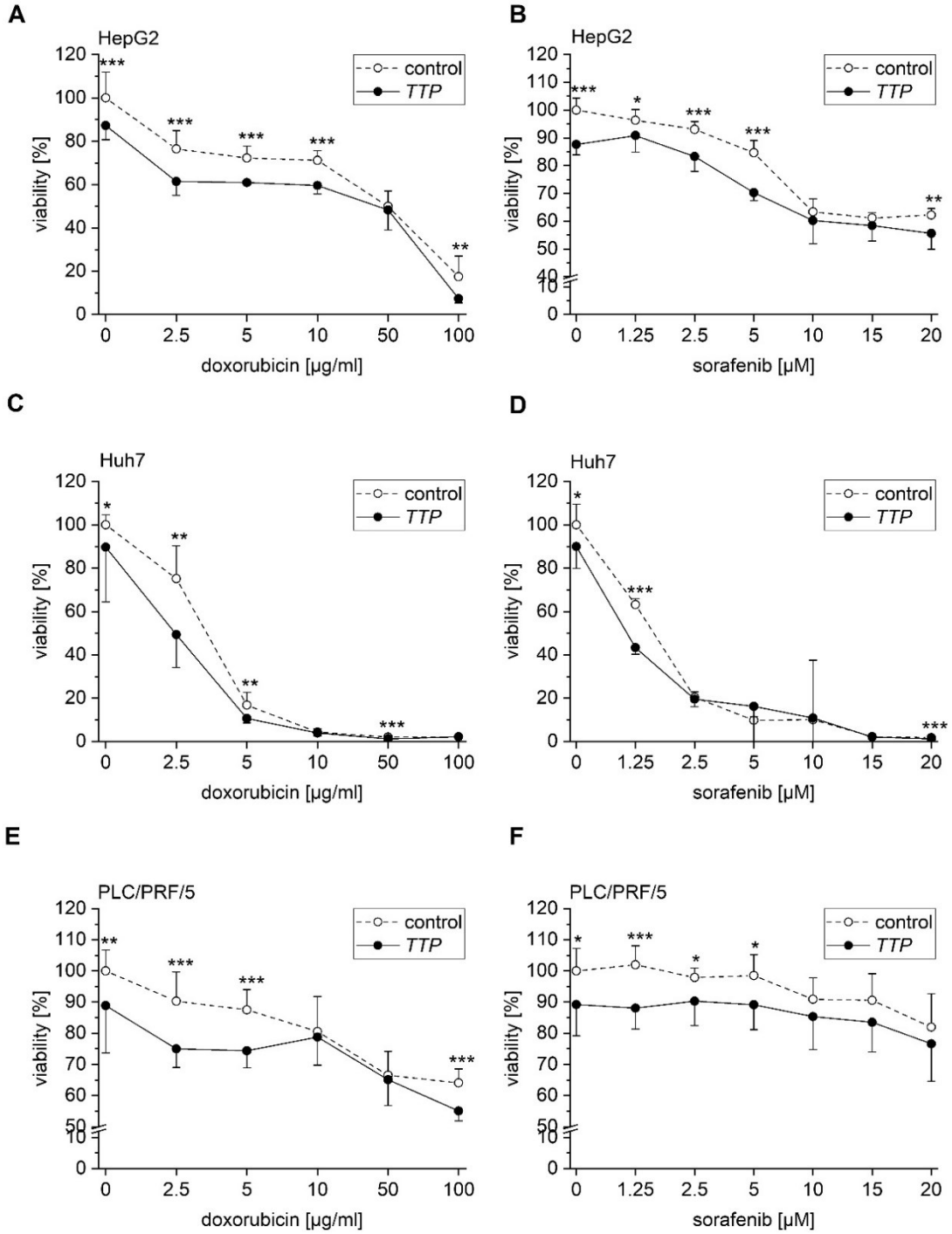

Figure 28| Effects of TTP overexpression on chemoresistance in hepatoma cells. Cells were transfected with either TTP or a control vector. 24 h after transfection, cells were treated with different concentrations of doxorubicin or sorafenib. Cell viability was determined *via* MTT assay. (A, B): HepG2 cells treated with doxorubicin (A) or sorafenib (B). (C, D): Huh7 cells treated with doxorubicin (C) or sorafenib (D). (E, F): PLC/PRF/5 cells treated with doxorubicin (E) or sorafenib (F). n=3 (for untreated controls n=6, quadruplicates). Statistical difference: *: $p<0.05$; **: $p<0.01$; ***: $p<0.001$. From "The mRNA-binding protein TTP/ZFP36 in hepatocarcinogenesis and hepatocellular carcinoma" by Kröhler, T., Kessler, S. M., Hosseini, K., List, M., Barghash, A., Patial, S., Laggai, S., Gemperlein, K., Haybaeck, J., Müller, R., Helms, V., Schulz, M. H., Hoppstädter, J., Blackshear, P. J., & Kiemer, A. K. (2019), *Cancers, 11*(11), 1754 (https://doi.org/10.3390/cancers11111754). Licensed under CC BY 4.0. Also published in similar way in "Pathomechanisms in hepatocellular carcinoma: characterisation of leukocyte recruitment, the role of the mRNA-binding protein tristetraprolin and nuclear paraspeckles" (Doctoral thesis, Saarland University, Saarbrücken, Germany) by Hosseini, K. (2017) (https://doi.org/10.22028/D291-27154).

3.2.4 Expression changes of potential TTP targets

Since TTP represents an mRNA destabilising factor, we hypothesised that TTP's tumour-suppressing actions were caused by an altered expression of its target genes, that is that TTP overexpression resulted in a downregulation of oncogenes, some of which are able to induce angiogenesis as a hallmark of cancer (Hanahan & Weinberg, 2011). Therefore, the expression of the oncogenes B-cell lymphoma 2 (*BCL2*), c-Myc (*MYC*), E2F1 transcription factor 1(*E2F1*), vascular endothelial growth factor A (*VEGFA*), and X-linked inhibitor of apoptosis (*XIAP*), which have been shown to be TTP targets in non-liver tissues (Selmi et al., 2015; H. Wang et al., 2016), was checked. To confirm the validity of these targets, we analysed the sequences of their 3'-UTRs and found TTP binding-motifs (Mukherjee et al., 2014) in abundance. Interestingly, AREs were also predicted in several yet unknown TTP targets, which had been suggested as tumour promoting genes and were therefore also analysed in TTP-overexpressing cells. One of them is the long transcript variant of nuclear enriched abundant transcript 1 (*NEAT1_v1*/*v2*), *NEAT1_v2*. Two other ARE containing genes represent RBPs themselves: *IGF2BP1* and *IGF2BP3*, which both promote hepatic tumour progression (Gutschner et al., 2014; Jeng et al., 2008). In HepG2 and Huh7 cells, all analysed genes tended to be less expressed after TTP overexpression (Figure 29A). *MYC*, *IGF2BP3*, and *VEGFA* were significantly lowered in TTP-overexpressing HepG2 cells (Figure 29A). In TTP-overexpressing Huh7 cells, *IGF2BP1* was the only gene that was significantly decreased (Figure 29A). *BCL2*, I*GF2BP1*, *NEAT1_v2*, and *VEGFA* were significantly lowered in PLC/PRF/5 cells (Figure 29A). Since *VEGFA*, a promoter of invasion in HCC (X. M. Li et al., 1998), was less expressed in HepG2 and PLC/PRF/5 cells, we hypothesised that TTP might play a role in HCC vascular invasion. Therefore, TTP (*ZFP36*) expression was evaluated in gene expression data from human HCC samples showing vascular invasion compared to samples without vascular invasion. In fact, TTP expression was slightly but significantly decreased in cancer tissues showing vascular invasion (Figure 29B).

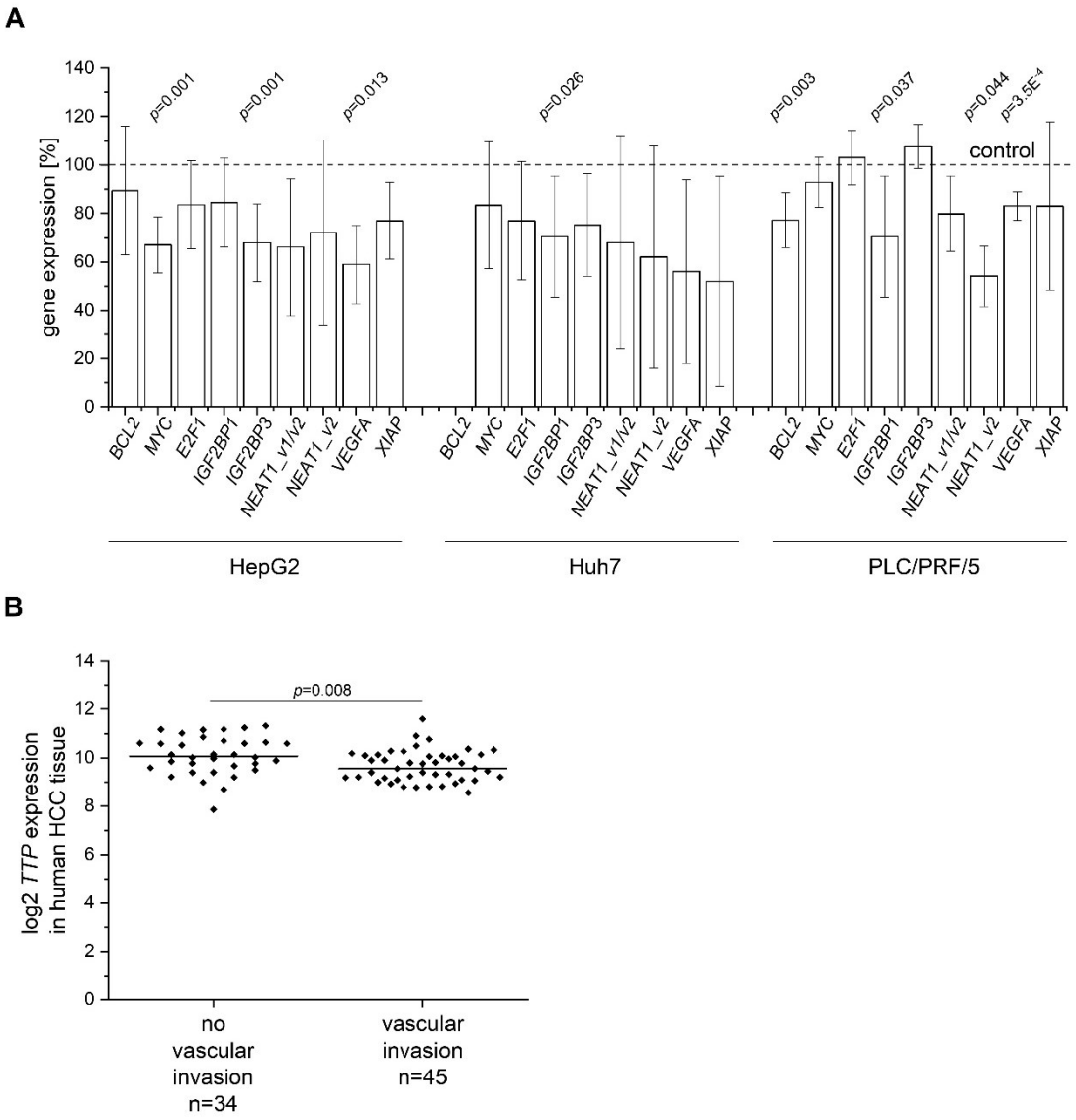

Figure 29| Oncogene expression in TTP-overexpressing hepatoma cells. (A) Expression levels normalised to cells treated with a control vector were determined in HepG2, Huh7, and PLC/PRF/5 cells by qPCR. *BCL2* was not determined in Huh7 cells since mRNA expression was below the detection limit. n=2 (triplicates). (B): TTP (*ZFP36*) expression in human HCCs grouped into tumours positive (n=45) or negative (n=34) regarding vascular invasion (GSE20238). From "The mRNA-binding protein TTP/ZFP36 in hepatocarcinogenesis and hepatocellular carcinoma" by Kröhler, T., Kessler, S. M., Hosseini, K., List, M., Barghash, A., Patial, S., Laggai, S., Gemperlein, K., Haybaeck, J., Müller, R., Helms, V., Schulz, M. H., Hoppstädter, J., Blackshear, P. J., & Kiemer, A. K. (2019), *Cancers, 11*(11), 1754 (https://doi.org/10.3390/cancers11111754). Licensed under CC BY 4.0. Also published in similar way in "Pathomechanisms in hepatocellular carcinoma: characterisation of leukocyte recruitment, the role of the mRNA-binding protein tristetraprolin and nuclear paraspeckles" (Doctoral thesis, Saarland University, Saarbrücken, Germany) by Hosseini, K. (2017) (https://doi.org/10.22028/D291-27154).

3.2.5 ZFP36 expression in human HCC tissue

Since TTP (*ZFP36*) has been shown to be downregulated in different human cancer types, including HCC (Sanduja et al., 2012), an extensive expression analysis of TTP mRNA in publicly available HCC data sets was performed: in a microarray data set comprising almost 250 HBV-derived HCC samples, in The Cancer Genome Atlas (TCGA) data comparing 373 HCCs with 50 non-tumour liver tissue samples, and in a data set comparing HCC tissue with healthy, cirrhotic, and non-tumour tissue of HCC patients. In all data sets, TTP mRNA levels were significantly lower in HCC than in non-tumour tissue (Figure 30A–C). No differential expression was observed for cirrhotic tissue, but the number of normal liver tissue samples was very low (Figure 30C). qPCR analysis of TTP mRNA expression in a set of human liver tumour samples from mixed etiologies and matched normal samples confirmed downregulation of TTP in tumour tissue (Figure 30D).

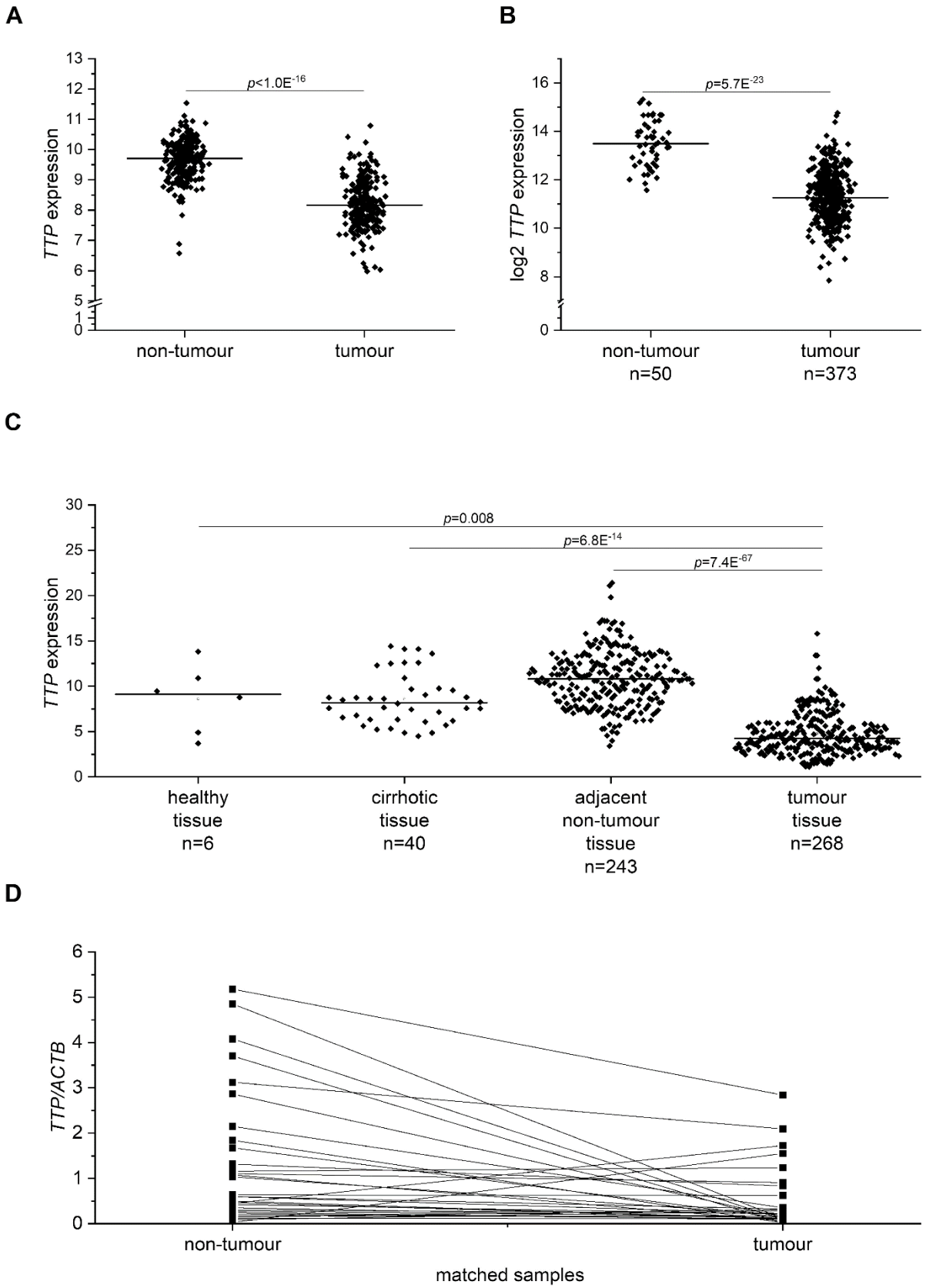
A
TTP expression
p<1.0E-16
non-tumour
tumour
B
log2 TTP expression
p=5.7E-23
non-tumour
n=50
tumour
n=373
C
TTP expression
p=0.008
p=6.8E-14
p=7.4E-67
healthy tissue n=6
cirrhotic tissue n=40
adjacent non-tumour tissue n=243
tumour tissue n=268
D
TTP/ACTB
non-tumour
tumour
matched samples

Figure 30| TTP (*ZFP36*) mRNA expression in human tumour and non-tumour liver tissue. (A): TTP mRNA expression in 247 human HCC samples relative to the mean of 239 non-tumour liver tissue samples (μ normal) (GSE14520). (B): TTP mRNA expression in tumour (n=373) and non-tumour (n=50) tissue (TCGA). (C): TTP mRNA expression in healthy, cirrhotic, adjacent non-tumour, and tumour liver tissues (500 samples; GSE25097). (D): TTP mRNA levels isolated of tumour and matched adjacent non-tumour tissues (n=31). From "The mRNA-binding protein TTP/ZFP36 in hepatocarcinogenesis and hepatocellular carcinoma" by Kröhler, T., Kessler, S. M., Hosseini, K., List, M., Barghash, A., Patial, S., Laggai, S., Gemperlein, K., Haybaeck, J., Müller, R., Helms, V., Schulz, M. H., Hoppstädter, J., Blackshear, P. J., & Kiemer, A. K. (2019), *Cancers, 11*(11), 1754 (https://doi.org/10.3390/cancers11111754). Licensed under CC BY 4.0. Also published in similar way in "Pathomechanisms in hepatocellular carcinoma: characterisation of leukocyte recruitment, the role of the mRNA-binding protein tristetraprolin and nuclear paraspeckles" (Doctoral thesis, Saarland University, Saarbrücken, Germany) by Hosseini, K. (2017) (https://doi.org/10.22028/D291-27154).

3.3 Discussion

TTP repression has been described in different human cancers (Hitti et al., 2016; Sanduja et al., 2012), and a loss of functional TTP can modulate diverse tumourigenic phenotypes (Brennan et al., 2009). In this study, we were able to confirm a downregulation of TTP (*ZFP36*) in HCC tissues and tumour suppressor functions of TTP in a set of hallmarks of cancer employing three different hepatoma cell lines (Hitti et al., 2016).

Employing an *in vivo* hepatocarcinogenesis model, our findings are the first to report a role of TTP in carcinogenesis. Since HCC develops based on chronic inflammation and metabolic alterations, a lower number of tumours in ls*Ttp*-KO animals might be connected to the recently described promotion of metabolic liver disease by TTP (Sawicki et al., 2018).

Although total ls*Ttp*-KO mice show a severe inflammatory phenotype (Carballo et al., 1998) and myeloid-specific ls*Ttp*-KO mice are highly susceptible to lipopolysaccharide treatment (Qiu et al., 2012), a hepatocyte-specific knockout of TTP seemed to have a rather inhibitory effect on inflammation as observed in the short-term mouse experiment: the monocyte to macrophage ratio of DEN-treated knockout mice was decreased compared to the DEN-treated wild-type mice. This increase in the monocyte to macrophage ratio has been reported before in DEN-treated animals (Kessler et al., 2019).

Although TTP knockdown has been shown to induce monocyte infiltration into three-dimensional tumour spheroids and macrophage infiltration into murine breast cancer xenografts (Milke et al., 2013), our data rather suggest that hepatocytic TTP promotes tumourigenesis by driving monocyte infiltration and thus tumour-promoting inflammation. This is further strengthened by TTP-dependent alterations in the hepatic fatty acid profile, which might promote tumourigenesis. During hepatocarcinogenesis in obesity-associated chronic liver disease, lipid accumulation can promote inflammation and *vice versa*

(Karagozian et al., 2014). Feeding ls*Ttp*-KO mice a high-fat diet to model steatohepatitis was described to improve insulin resistance (Sawicki et al., 2018). Thus, hepatocytic TTP, which accounts for more than 95% of the hepatic TTP levels (Sawicki et al., 2018 and Supplementary Figure 4), seems to rather facilitate metabolic liver disease. For tumour progression, however, lipid alterations in normal adjacent tissue might be less important than elevated lipids in tumour tissue and tumour stroma (Beloribi-Djefaflia et al., 2016).

In contrast to tumour initiation, our study suggests an inhibitory role of TTP in a set of hallmarks of cancer as characteristics of tumour progression. In fact, other factors promoting lipid deposition and inflammation can be beneficial for cancer progression. One example represents the fatty acid elongase ELOVL6, which contributes to the progression of pre-tumourous conditions, such as steatosis and steatohepatitis (Matsuzaka et al., 2012). However, it is downregulated in human liver cancer and its downregulation represents a negative clinical predictor (Kessler et al., 2014; Y. Li et al., 2019).

So far, downregulation of TTP in HCC has only been shown in one study using a very small patient cohort with n=24 samples (Sohn et al., 2010). We herewith were able to confirm the results from the latter study in several large HCC patient cohorts.

It is well known that cell migration is a critical factor for cancer metastasis (Vicente-Manzanares & Horwitz, 2011), which can occur already in the early stages of tumour progression (Balic et al., 2006; F. Li et al., 2007). TTP has been shown to inhibit the migration ability in prostate cancer, ovarian cancer, gastric cancer, and head and neck squamous cell carcinoma cells (H. H. Lee et al., 2014; Van Tubergen et al., 2011; H. Wang et al., 2016; Yoon et al., 2016). Additionally, TTP was suggested to decrease the metastatic potential in breast cancer (Al-Souhibani et al., 2010). To the best of our knowledge, this study is the first to show a migration- and proliferation-inhibitory effect of TTP in hepatic cells. Others were able to show a TTP-induced decrease of metabolic activity in a methylthiazoletetrazolium assay and adherence in a crystal violet assay (Sohn et al., 2010). The observed inhibition of proliferation may be the major reason why we failed to establish a stable overexpression of the TTP-containing plasmid in HepG2, Huh7, and PLC/PRF/5 cells.

TTP has been shown to downregulate several well-established markers for tumour progression like *BCL2*, *VEGFA*, and *MYC* in non-liver tissue (H. H. Lee et al., 2010; S. B. Park

et al., 2015; H. Wang et al., 2016). In line with these findings, we observed a decreased expression of MYC, VEGFA, and BCL2 in liver cancer cells overexpressing TTP. The decreased TTP expression in vascularized HCC tissue further supports the hypothesis that TTP might play a role in angiogenesis, which is a hallmark of tumour progression (Hanahan & Weinberg et al., 2011).

The different expression levels of the analysed genes comparing the three cell lines might be explained by the distinct heterogeneity of liver cancer itself (L. Li & Wang, 2016). According to this, the three analysed cell lines also have rather different phenotypes (Ghasemi et al., 2013; Hsu et al., 1993; Kanno et al., 2015).

Several targets of TTP (e.g. *BCL2*, *VEGFA*, and *MYC*) are associated with a poor chemosensitivity (H. Wang et al., 2016). Chemoresistance is widespread in HCC and characterises tumour progression (Worns et al., 2009). Interestingly, TTP overexpression in PLC/PRF/5 cells decreased the expression of the long transcript variant of the long non-coding RNA *NEAT1*, *NEAT1_v2*, which has been reported to enhance chemoresistance in different cancer cell lines, including hepatoma cells (Adriaens et al., 2016; Kessler et al., 2019). *NEAT1* is one of the least stable long non-coding RNAs (Clark et al., 2012), a presumed tumour promoter, and associated with chemoresistance (Adriaens et al., 2016; S. Guo et al., 2015). TTP has been described to mediate chemosensitivity to cisplatin in head and neck cancer cells (S.B. Park et al., 2015). In line with these findings, TTP improved chemoresistance towards sorafenib, an approved drug for systemic liver cancer therapy, as well as towards doxorubicin, which is widely used in chemoembolisation (Dhanasekaran et al., 2010; Worns et al., 2009). A connection between chemoresistance and TTP has also previously been suggested for breast cancer (J. Y. Lee et al., 2013). However, the main effect could be explained by a reduced viability due to TTP overexpression.

In conclusion, our data suggest that hepatocytic TTP plays an inflammation- and lipid-dependent role in promoting hepatic tumour initiation. In liver cancer progression, TTP exerts a major inhibitory effect. The potential limit of translatability of rodent models in HCC research due to differences in anatomy, physiology, and mechanisms of carcinogenesis (Ramachandran et al., 2012) must be addressed in future studies.

4 Chapter II: employing TRIBE for IMP2 target identification

4.1 Introduction

IMP2 is overexpressed in several tumour entities and accompanied with a poor outcome for patients (cf. 1.2.3). Thereby, IMP2 exerts its functions by interacting with a broad spectrum of mRNA targets involved in various signalling networks. Besides a few confirmed client mRNAs (Cao et al., 2018), still, most interaction partners of the RBP remain unknown. For the development of new diagnostics and therapies for cancer treatment, it is mandatory to identify new target structures *in vivo*. So far, binding sequences of IMP2 were investigated using immunoprecipitation approaches like RNA immunoprecipitation, enhanced CLIP and photoactivatable-ribonucleoside-CLIP *in vitro* (Conway et al., 2016; Dai et al., 2015; Hafner et al., 2010). Disadvantages are the requirement of a stable (over)expression of the RBP of interest in model cell lines (often HEK293 cells) prior to analysis and, associated with that, non-physiological concentrations of the RBP as well as a different cellular environment. Moreover, model cell lines have a different spectrum of target structures and enzymes that is not representative for the *in vivo* situation (Gupta et al., 2021; Jaitin et al., 2014).

Goal of this chapter was to use the TRIBE method (cf. 1.2.4) in combination with HGD to identify new target transcripts of IMP2 in hepatocytes *in vivo*. HGD is a non-viral method for gene delivery and high hepatic transgene expression in rodents. Thereby, the nucleic acids that normally cannot pass cell membranes due to their polarity, are dissolved in a high volume of an isotonic solution and rapidly injected into the teil vein of rodents (Bonamassa et al., 2011). This results in an increased venous pressure, an enlargement of liver fenestrae, and enhancement of membrane permeability of the hepatocytes leading to the uptake of nucleic acids (G. Zhang et al., 2004).

4.2 Results and discussion

Three wild-type male C57BL/6J mice were hydrodynamically injected with either control (mCherry-ADAR) or experimental (IMP2-ADAR) plasmid DNA (Supplementary Figure 8 and Supplementary Figure 9) and livers were removed 24 h post injection (cf. 2.3.6). Different strategies were followed to ensure transfection and to determine the transfection efficiency of the murine hepatocytes.

Quantitative PCR analyses revealed a significantly increased level of human *IGF2BP2* in IMP2-ADAR transfected mice (Figure 31A), indicating a successful gene delivery in those mice. As expected, *IGF2BP2* expression was neither found in control injected nor in wild-type mice due to missing coding sequence of human IMP2. To figure out, whether there is a liver lobule favoured using HGD as transfection method, we investigated the lobule-specific expression of *IGF2BP2* (Figure 31B) There was no statistically significant difference of *IGF2BP2* expression between the single liver lobules in IMP2-ADAR transfected mice. Thus, downstream experiments like RNA sequencing will not be limited to a specific liver lobule of the mice.

Moreover, we stained various sections of paraffin-embedded liver lobes for GFP, mCherry or IMP2 and scored the samples in a blinded fashion for the number of positive hepatocytes (Figure 32 and Table 8). Unexpectedly, GFP staining resulted only in a few GFP-positive hepatocytes in the control group and none in the experimental group (Figure 32, upper panel), although qualitative analysis of GFP expression by PCR had revealed similar values for the cycle threshold in both test groups injected with a plasmid (data not shown). In contrast to the non-injected or IMP2-ADAR injected species, single mCherry-ADAR samples were scored up to 3 (Table 8).

In general agreement, detection of paraffin embedded GFP is best done by immunohistochemical staining due to significant fluorescence quenching of GFP during the paraffin embedding process (Zhanmu et al., 2019). For instance, ethyl alcohol used for dehydration of tissues can damage GFP, which is why we used a modified protocol employing tertiary butanol (Zhanmu et al., 2019). In another study confocal laser scanning microscopy images of murine liver tissues were obtained after immunohistochemical staining for GFP 24 h post HGD of naked plasmid DNA (Matsui et al., 2015), indicating that GFP detection could be

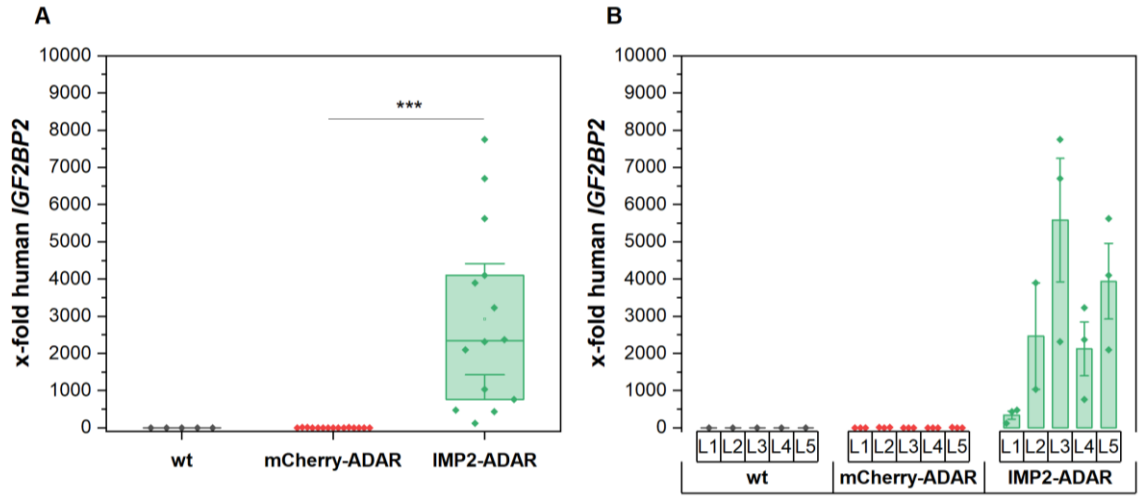

Figure 31| Control of experimental plasmid DNA transfection in murine livers by qPCR analysis. (A) Overall expression of human IMP2 (*IGF2BP2*) in mCherry-ADAR injected control (mCherry-ADAR) and IMP2-ADAR injected experimental mice compared to non-injected wild-type (wt) mice. Individual values (rhombi) are presented in a box blot with squares as mean values and whisker as ±SEM. ***: $p<0.001$ (one-way ANOVA). (B) Expression of *IGF2BP2* in the test groups individual liver lobules. L1: left lateral lobe; L2: left medial lobe; L3: right medial lobe; L4: right lateral lobe; L5: caudate lobe. Bars represent mean ±SEM and rhombi single liver lobules from each mouse. n=3 (triplicates of each of the five liver lobules) except wt (n=1). In both analyses *Rn18s* was used as housekeeping gene.

time critical. The paraffin embedding protocol used in this study took at least five days and samples needed to be shipped prior to immunohistochemical analysis, which may have impacted GFP stability. Further, in line with our expectations, the mCherry-staining indicated positive hepatocytes only in control-transfected mice. Those were scored 4 in average (Figure 32, middle panel and Table 8), which is the highest possible score for the number of positive hepatocytes in this setup. There was no difference in scoring between the individual liver lobules. Surprisingly, the staining for IMP2-positive hepatocytes revealed in both groups, control and experimental, elevated IMP2 levels with slightly higher scores in the mCherry-ADAR group (Figure 32, lower panel and Table 8). Due to no gene sequence of IMP2 incorporated into the mCherry plasmid, we assumed that the induction of IMP2 was caused by the hydrodynamic injections and its structural impact on the endothelium and hepatocytes leading to morphological changes (Suda et al., 2007). Hereby, laminins are maybe implicated in this process as they represent ubiquitous cell adhesion molecules, are major components of basement membranes, and underly both epithelial and endothelial cells (Durbeej, 2010). The translation of LAMB2 (laminin-β2), a subtype of the superfamily of laminins, is controlled by IMP2 (Schaeffer et al., 2012). Proliferative and anti-apoptotic effects of IMP2 are well known

(Figure 14, Huang et al., 2019; Kessler et al., 2013) and cell damage due to HGD may trigger endogenous *Igf2bp2* expression as one compensatory mechanism.

From our experience, the IMP2 antibody (M. Lu et al., 2001) used for the immunohistochemical stainings is not specific for human or murine IMP2 (Barghash et al., 2016; Kessler et al., 2013; Tybl et al., 2011), although one amino acid in the murine epitope is exchanged. In murine *Igf2bp2* (NCBI accession number NM_183029.2) the amino acid sequence PQGVASQRSK, against which the antibody is directed, is altered in that way that the serine (S) is replaced by a proline (P) (corresponding to P588 in NM_183029.2), which should theoretically impact antibody binding.

However, we subsequently analysed murine *Igf2bp2* expression in all three test groups using quantitative PCR (Figure 33). We found elevated, but not significantly increased, levels of *Igf2bp2* in mice that underwent hydrodynamic injections compared to non-injected wild-type controls (Figure 33A). Further, *Igf2bp2* induction was mainly restricted to the left lateral and medial liver lobe of the injected mice (Figure 33B). This trend is slightly reflected by the immunohistochemical scores for the IMP2-staining in mCherry-ADAR transfected mice. In average the scores for L1 and L2 were higher compared to L3-L5 in each mouse (Table 8).

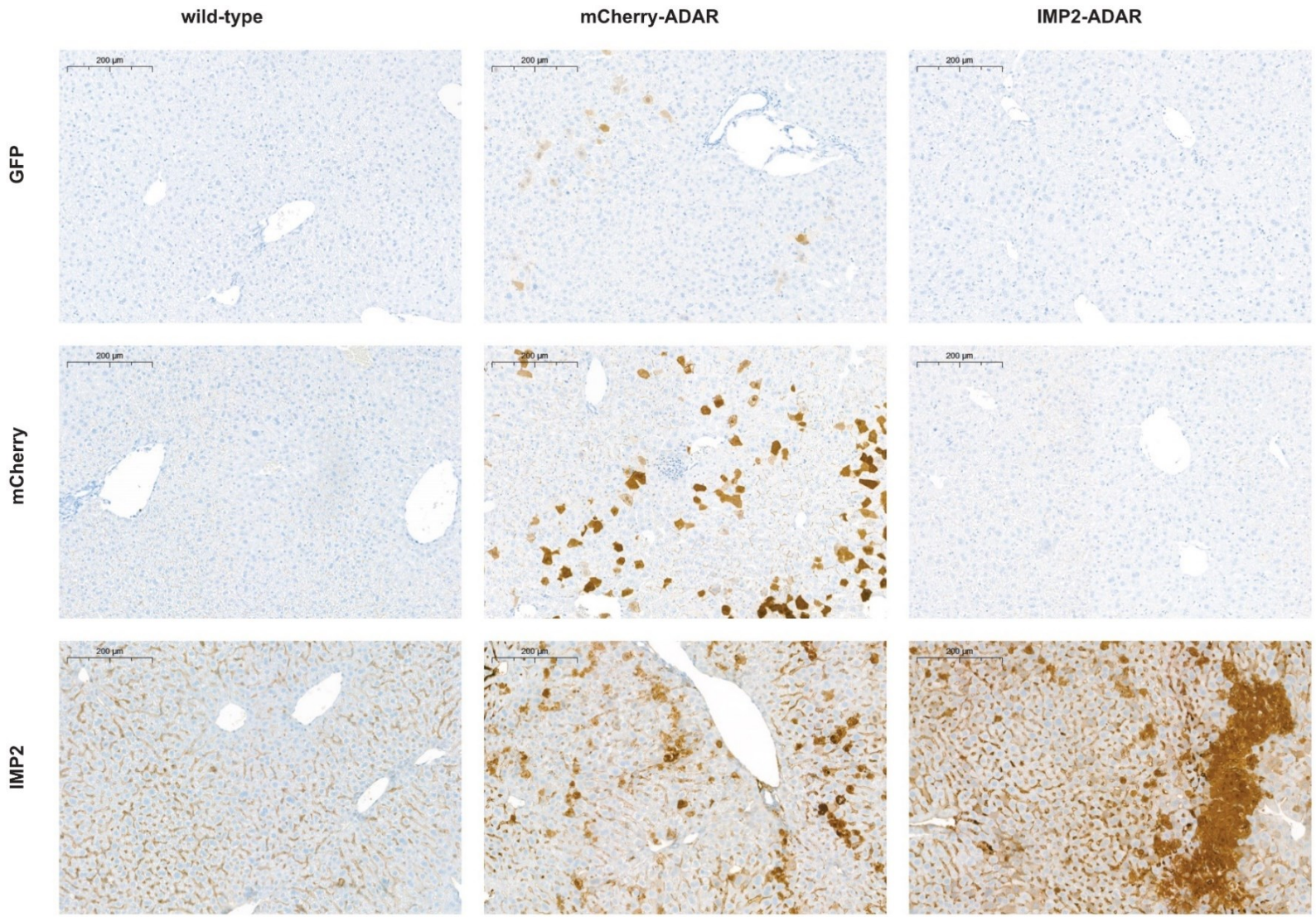

Figure 32| Immunohistochemical analysis of murine livers. Livers of non-injected wild-type, hydrodynamically transfected control (mCherry-ADAR) and experimental (IMP2-ADAR) mice stained for GFP, mCherry or IMP2. Cells appear brownish when they are positive for the respective staining. Representative pictures of each test group and staining were chosen. The scale is shown in the upper left corner.

Table 8| Score list for the immunohistochemical staining of all test groups. All five liver lobules of three mice per test group were histologically scored in a blinded fashion for the number of positive hepatocytes according to the following scoring scheme: 0: no positive hepatocytes; 1: almost no positive hepatocytes; 2: few positive hepatocytes; 3: moderately high number of positive hepatocytes; 4: many positive hepatocytes. L1: left lateral lobe; L2: left medial lobe; L3: right medial lobe; L4: right lateral lobe; L5: caudate lobe; N/A: not available.

GFP staining				
		Non-injected	**Control**	**Experimental**
		wild-type	**mCherry-ADAR**	**IMP2-ADAR**
Mouse	**Liver lobule**	**Score**	**Score**	**Score**
1	L1	0	2	0
	L2	0	2	0
	L3	0	2	1
	L4	0	3	0
	L5	0	0	0
2	L1	0	1	0
	L2	0	1	0
	L3	0	1	0
	L4	0	0	0
	L5	0	0	0
3	L1	0	1	0
	L2	0	1	0
	L3	0	1	0
	L4	0	1	0
	L5	0	0	0
mCherry staining				
1	L1	0	4	0
	L2	0	4	0
	L3	0	4	0
	L4	0	4	0
	L5	0	4	0
2	L1	0	4	0
	L2	0	3	0
	L3	0	4	0
	L4	0	4	0
	L5	0	3	0
3	L1	0	4	0
	L2	0	4	0
	L3	0	4	0
	L4	0	4	0
	L5	0	3	0

IMP2 staining				
		Non-injected	Control	Experimental
		wild-type	mCherry-ADAR	IMP2-ADAR
Mouse	Liver lobule	Score	Score	Score
1	L1	0	4	2
	L2	0	4	2
	L3	1	4	3
	L4	1	3	3
	L5	1	3	2
2	L1	0	3	3
	L2	0	3	N/A
	L3	1	2	3
	L4	0	3	4
	L5	0	2	2
3	L1	1	4	3
	L2	0	4	2
	L3	0	4	4
	L4	0	3	3
	L5	0	2	3

FACS analysis of isolated hepatocytes from fresh liver tissue revealed no significant differences in transfection efficiency between hepatocytes from wild-type livers and those of mCherry-ADAR and IMP2-ADAR transfected mice based on fluorescence signals in GFP and PE-CF594 channels (data not shown). In preliminary experiments, the intensity of the fluorescent signals of GFP (excitation: 395 nm, emission: 509 nm) and mCherry (excitation: 587 nm, emission: 610 nm) was examined against the autofluorescence of homogenised mouse liver tissue and its supernatant due to the known bio chromophores bilirubin and other bile components, having similar emission wavelengths and are metabolised in the liver (Croce et al., 2014). Only after addition of mCherry and not of GFP to either samples species, detection of a fluorescence signal above background level was possible (data not shown). Therefore, we expected at least a difference in the control transfected mice compared to the non-injected wild-type mice to derive a transfection efficiency for the experimental group. Moreover, there was also no fluorescence detectable in cryosections of the left lateral liver lobe by fluorescence microscopy.

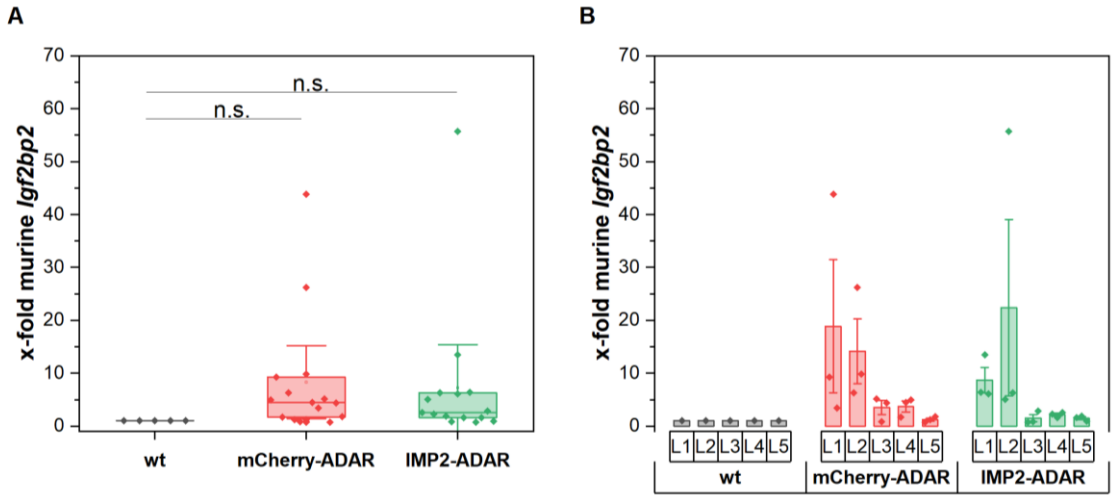

Figure 33| Analysis of *Igf2bp2* expression in murine livers by qPCR. (A) Overall expression of murine IMP2 (*Igf2bp2*) in mCherry-ADAR injected control (mCherry-ADAR) and IMP2-ADAR injected experimental mice compared to non-injected wild-type (wt) mice. Individual values (rhombi) are presented in a box blot with squares as mean values and whisker as ±SEM. n.s.: not significant ($\alpha \leq 0.05$, one-way ANOVA). (B) Expression of *Igf2bp2* in the test groups individual liver lobules. L1: left lateral lobe; L2: left medial lobe; L3: right medial lobe; L4: right lateral lobe; L5: caudate lobe. Bars represent mean ±SEM and rhombi single liver lobules from each mouse. n=3 (triplicates of each of the five liver lobules) except wt (n=1). In both analyses *Rn18s* was used as housekeeping gene.

Taken together, qPCR analysis and immunohistochemistry confirmed a successful transfection of murine hepatocytes with mCherry-ADAR control plasmid and IMP2-ADAR experimental plasmid, which is accompanied with an endogenous Igf2bp2 induction due to the hydrodynamic tail vein injections. Based on the immunohistochemical analysis, the transfection efficiency was estimated to be 40%.

In further experiments, samples need to be prepared for RNA sequencing (depletion of ribosomal RNA) and sequencing results must be bioinformatically analysed with respect to A-to-I editing events to identify new client mRNAs of IMP2. Thereby it also must be considered that IMP2 as a N^6-methyladenosine (m6A) reader (H. Huang et al., 2018) interact with client mRNAs harbouring m6A modifications in their sequences, which will most likely affect A-to-I editing (Xiang et al., 2018) efficiency.

5 Chapter III: validation of IMP2 as new target for cancer therapy

5.1 Introduction

IMP2 has diverse functions and plays an important role in cancer development and progression, especially in HCC and CRC (Kessler et al., 2015; T. Li et al., 2019; Wu et al., 2022). We hypothesised that IMP2 might be an attractive target to inhibit as a novel therapeutic approach for cancer therapy.

In this chapter, different CRISPR/Cas9 methods were applied to generate IMP2 knockout in mammalian tumour cell lines. First, IMP2 knockout was validated on gene and protein level. Subsequently, IMP2 knockout cells were used to validate IMP2 as a target for cancer therapy *in vitro* and *in vivo*, which paved the way for initial screenings of small molecule inhibitors of IMP2.

5.2 Results and discussion

5.2.1 Validation of IMP2 knockout on gene level

Cas9 protein and a validated sgRNA targeting exon 4 were delivered as RNP into human colorectal (HCT116, SW480) and hepatocellular carcinoma (Huh7, HepG2) cell lines (approach 1, cf. 2.5.1). Repeated runs of CRISPR/Cas9 editing resulted in clones showing preferably an insertion of adenine at the cut site either in both alleles of *IGF2BP2* (biallelic editing) or only in one allele (monoallelic editing) according to Sanger sequencing results (Table 9, Figure 34). Only two HCT116 clones indicated different mutations for each allele, that is monoallelic A insertion and 10 bp deletion (clone 47-2) or monoallelic G insertion combined with 10 bp deletion (clone 47-6). Nucleotide insertions (A or G) and/or deletions of 10 base pairs were predicted to create a frame shift with premature termination codon (PTC) at amino acid position 146 or 132 (instead of 600) resulting in nonsense-mediated mRNA decay (NMD) of *IGF2BP2* transcripts and thus in knockout of IMP2 protein. Contrary, biallelic 6 bp deletion in HepG2 clone 2 did not alter the reading frame leading to the loss of two aa at position 103 and 104 and was designated as polymorphism of the protein.

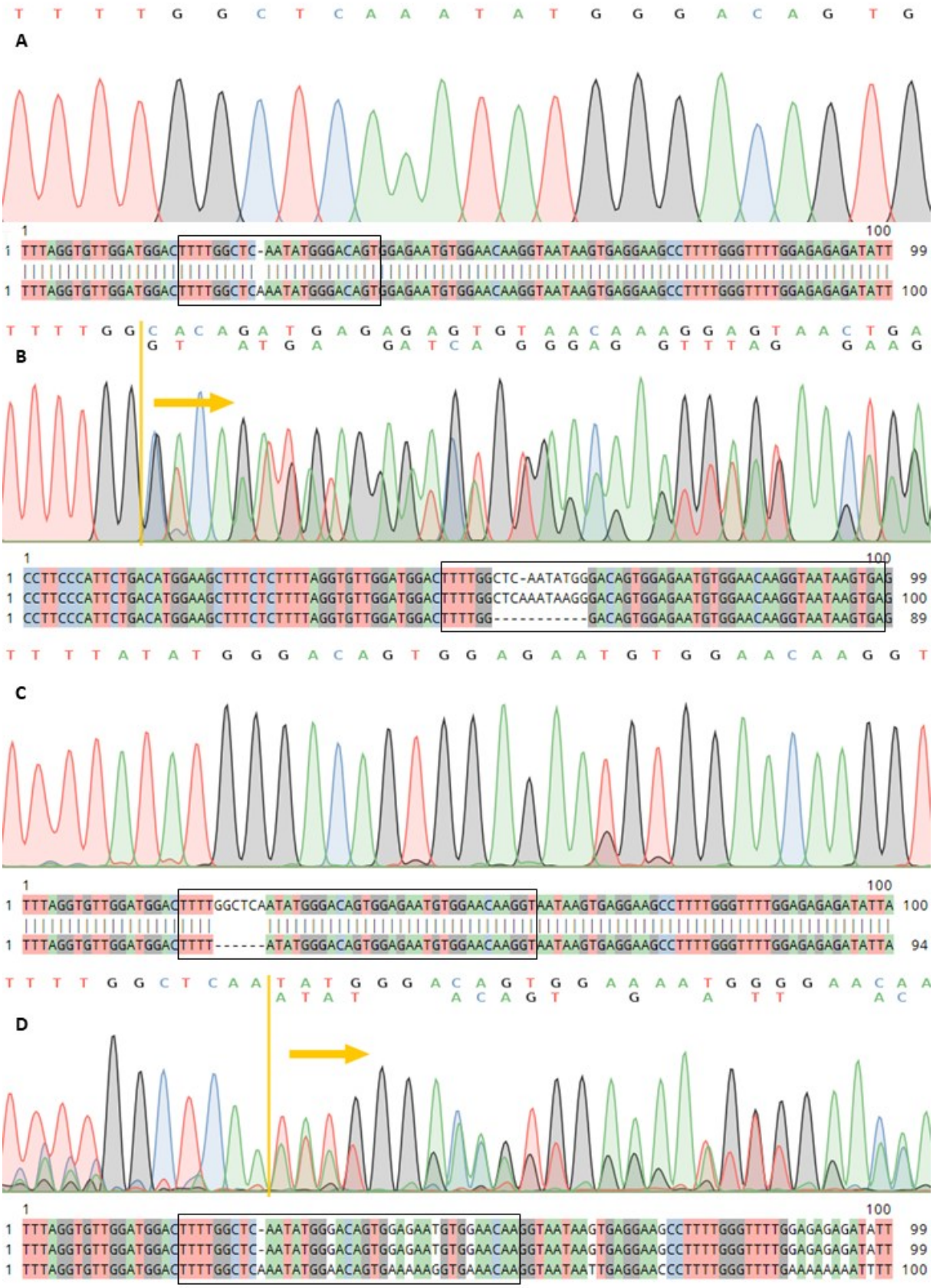
A
B
C
D

Figure 34| Most common indels in cell clones resulting from CRISPR/Cas9 approach 1 detected by Sanger sequencing. Respectively, sequencing chromatograms and below related sequence alignments with wild-type reference of different editing events in the *IGF2BP2* target locus are depicted. A) biallelic A insertion (e.g. HCT116 clone 47-1), B) biallelic editing with different mutations per allele (e.g., A insertion and 10 bp deletion in HCT116 clone 47-2), C) biallelic 6 bp deletion (e.g. HepG2 clone 2), and D) monoallelic A insertion (e.g. Huh7 clone 1). First line of the alignments represents the wild-type sequence. Only one line below the reference indicates the same sequence alteration in both alleles (biallelic editing) and two lines below the reference indicate difference sequences of each allele (monoallelic editing). Black frames in the sequence alignments demonstrate the section shown in the chromatograms above. Yellow arrows highlight the start site of at least two different sequences/alleles in cell clones. Colour code visualises matches in aligned sequences. A: adenine (green), C: cytosine (blue), G: guanine (black), T: thymine (red). -: missing DNA base.

To confirm monoallelic and biallelic adenine insertions in most of the mutated CRISPR/Cas9 cell clones, SNuPE analysis was performed on the complementary strand of the *IGF2BP2* target locus using a primer whose 3' end stops directly at the mutation site upstream of the PAM (Figure 35). Thus, extension of the primer with a thymine or guanine on the complementary strand indicates an adenine or cytosine on the target strand. The appearance of only thymine extended primers in HPLC chromatograms indicates biallelic adenine insertion and IMP2 knockout, whereas guanine elongated primers demonstrate wild-type sequences. A mixture of both primer extensions results from monoallelic editing, for instance Huh7 clone 1.

Table 9| Sanger sequencing and SNuPE results of clones resulting from *IGF2BP2* knockout trials in colorectal (HCT116, SW480) and hepatocellular carcinoma (HepG2, Huh7) cell lines using CRISPR/Cas9 approach 1. +: insertion, -: deletion, A: adenine, G: guanine, bp: base pairs, wt: wild-type, N/A: allele is edited, but exact mutation sequence is not available, /: not tested.

Cell line	Clone	Allele 1	Allele 2	SNuPE
HCT116	47	wt	N/A	/
	47-1	+A	+A	Biallelic +A
	47-2	+A	-10 bp	Monoallelic +A
	47-3	+A	+A	Biallelic +A
	47-4	+A	+A	Biallelic +A
	47-5	+A	+A	Biallelic +A
	47-6	+G	-10 bp	/
	47-7	+A	+A	Biallelic +A
	47-8	+A	+A	Biallelic +A
	47-9	+A	+A	Biallelic +A
	47-10	+A	N/A	Monoallelic +A
SW480	15	+A	+A	/
	17	wt	-5 bp	/
	23	+A	+A	/
HepG2	2	-6 bp	-6 bp	/
	4	+A	+A	Biallelic +A
	5	+A	+A	/
Huh7	1	wt	+A	Monoallelic +A

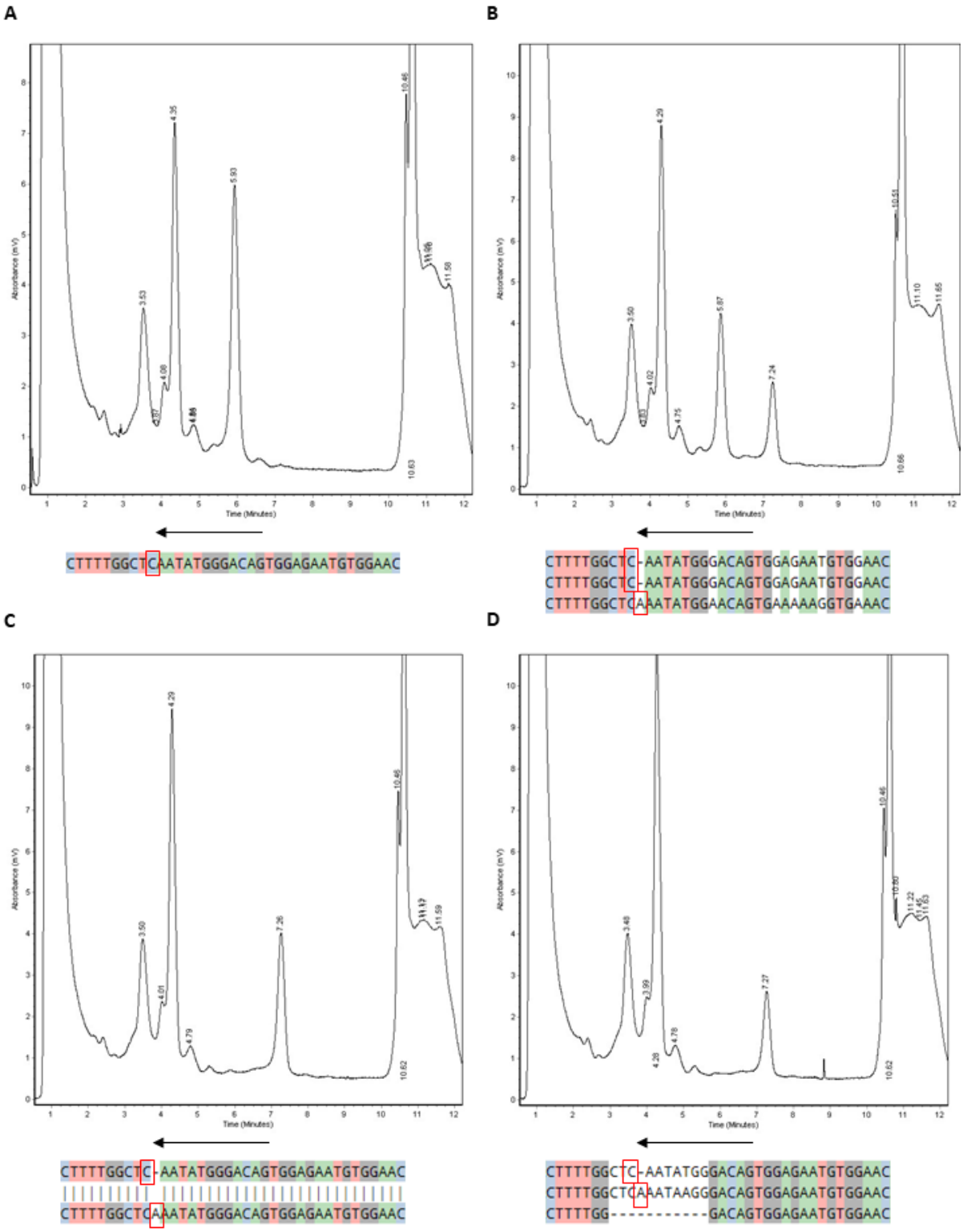
A
B
C
D
Absorbance (mV)
Time (Minutes)
CTTTTGGCTCAATATGGGACAGTGGAGAATGTGGAAC
CTTTTGGCTC-AATATGGGACAGTGGAGAATGTGGAAC
CTTTTGGCTCAAATATGGAACAGTGAAAAAGGTGAAAC
CTTTTGGCTC-AATATGGGACAGTGGAGAATGTGGAAC
CTTTTGGCTCAAATATGGGACAGTGGAGAATGTGGAAC
CTTTTGGCTC-AATATGGGACAGTGGAGAATGTGGAAC
CTTTTGGCTCAAATAAGGGACAGTGGAGAATGTGGAAC
CTTTTGG----------GACAGTGGAGAATGTGGAAC

Figure 35| SNuPE analysis of edited clones harbouring an adenine insertion at *IGF2BP2* target site in exon 4. HPLC chromatograms show the separation of SNuPE products (extended SNuPE primers) with retention times on x-axis (min) and absorbance on y-axis (mV). Peaks at approximately 4.30 min represent non-elongated SNuPE primer provided in excess. G- or T-extended primers are visualised by the peaks at approximately 5.90 min and 7.25 min respectively. Below the chromatograms sequence alignments of wild-type (first line) and mutated sequences harbouring at least a monoallelic adenine insertion are depicted. Red frames indicate the single position to be extended by the SNuPE primer (black arrow) in the target strand. Note, SNuPE analysis was performed on the complementary strand. Thus, G-extended primers indicate *IGF2BP2* wild-type sequence and T-extended primers represent the mutated sequence with A insertion. Colour code visualises matches in aligned sequences. A: adenine (green), C: cytosine (blue), G: guanine (black), T: thymine (red). -: missing DNA base. Chosen chromatograms are representative for monoallelic adenine insertions in clones from different cell lines. A) *IGF2BP2* wild-type, B) monoallelic A insertion (e.g. Huh7 clone 1), C) biallelic A insertion (e.g. HCT116 clone 47-1), D) monoallelic A insertion plus 10 bp deletion (e.g. HCT116 clone 47-2). The latter deletion cannot be detected with this method due to loss of the primer binding site, which is why only a small peak for T-extended primer is visible in the chromatogram.

Noteworthy, deletions at the target site could not be detected with this method due to loss of the primer binding site. However, edited sequences harbouring at least one additional adenine could be confirmed in all investigated cell clones as shown in the HPLC chromatograms. Furthermore, biallelic adenine insertion in representative clones (HCT116 clone 47-1, SW480 clone 15, HepG2 clone 4) was investigated by PCR using allele-specific primers for wild-type and genome-edited DNA sequence (Figure 36). As expected, PCR amplicons of wild-type sequence were only visible in wild-type cells, whereas PCR amplicons of the genome-edited sequence only showed up in IMP2 knockout clones.

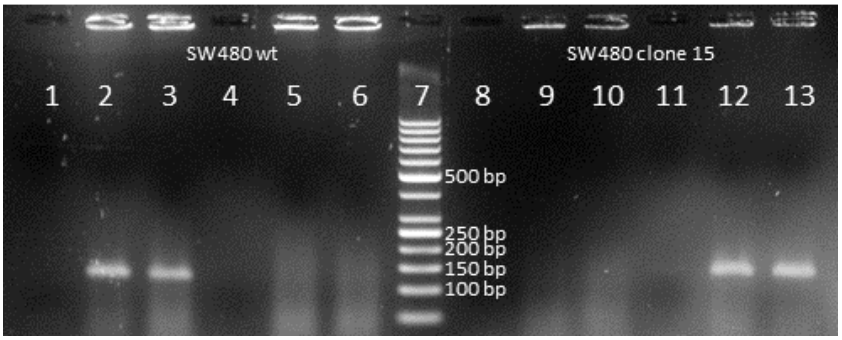

Figure 36| Discrimination of wild-type cells and genome-edited clones by PCR and gel electrophoresis. Representative 2% agarose gel of PCR products amplifying either wild-type (wt) sequence or genome-edited sequence (adenine insertion) at CRISPR/Cas9 target site in exon 4 of *IGF2BP2* using the example of SW480 wt cells and SW480 clone 15 (IMP2 knockout clone). Lane 1, 4, 8, 11: no template control; lane 2, 3, 9, 10: amplicon of wt sequence (130 bp); lane 5, 6, 12, 13: amplicon of adenine inserted sequence (131 bp). n=2.

In a second approach (cf. 2.5.2), the recent CRISPR/Cas method prime editing was used to disrupt the genetic sequence of *IGF2BP2* in exon 6 in HCT116 cells. For three different genomic loci pegRNAs were designed with the intention to introduce PTCs in PAM sequences by different kinds of mutations: transversion of two guanines into one thymine (GG→T, pegRNA1), deletion of two guanines (-GG, pegRNA4), and insertion of thymine and adenine

(+TA, pegRNA6) (Table 2). However, edited cell clones only survived from pegRNA4_16 cotransfected cells: two clones showing monoallelic editing (clone 9 and 10) and one clone showing biallelic GG deletion (clone 12). To exclude contamination of clone 12 with other possibly edited HCT116 cells during initial culturing of all transfected (GFP positive) cell clones in the 60 mm dishes, clone 12 were subjected to a cell printer to confirm clonality of all clones originating from clone 12. Indeed, Sanger sequencing of the resulting clones revealed mutants with both, monoallelic and biallelic GG deletion, five of them were kept (12-1 to 12-5, Table 10, Figure 37). Discrimination of wild-type cells and -GG mutants by PCR and gel

Table 10| Sanger sequencing results of clones resulting from *IGF2BP2* knockout trials in HCT116 cells using prime editing (CRISPR/Cas9 approach 2). Clones 12-1 to 12-5 originate from clone 12. wt: wild-type -: deletion, G: guanine.

Cell line	pegRNA	Clone	Allele 1	Allele 2
HCT116	4_16	9	wt	-GG
		10	wt	-GG
		12	-GG	-GG
		12-1	-GG	-GG
		12-2	-GG	-GG
		12-3	-GG	-GG
		12-4	wt	-GG
		12-5	wt	-GG

electrophoresis with two allele-specific primer pairs (cf. 2.5.4) failed. One possibility is that there is no destabilising interaction between the nucleotide at the 3' end of the wild-type forward primer (G in wt_2) and the complementary cytosine in the mutant sequence, which results in wild-type PCR amplicons in both, wild-type cells and knockout cells. An additional strong destabilising nucleotide at the penultimate site of the forward primer would have been necessary for discrimination (Bui & Liu, 2009). However, primer design is restricted to the mutation site at target locus.

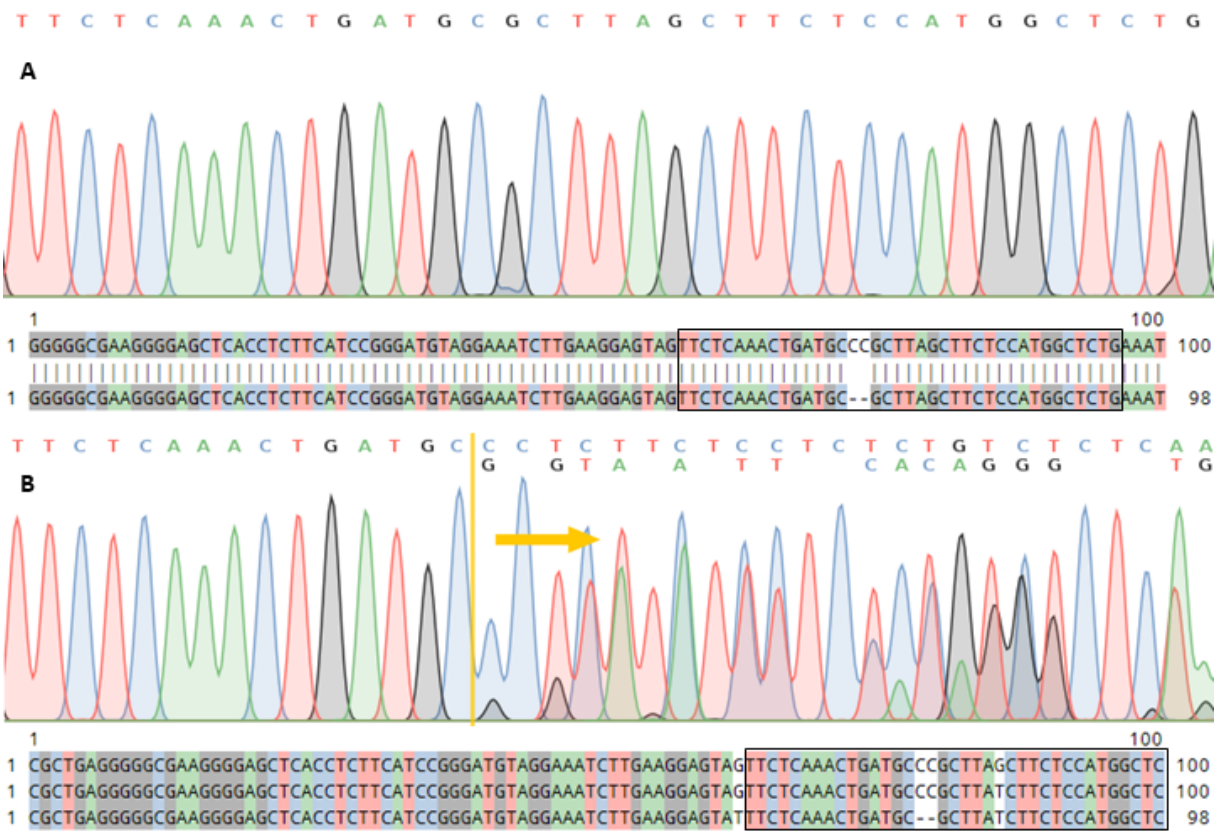

Figure 37| Sanger sequencing of cell clones undergoing CRISPR/Cas9 approach 2 (prime editing). Sequencing chromatograms of HCT116 cell clones showing the biallelic (A, clone 12-1 to 12-3) and monoallelic (B, clone 12-4 and 12-5) GG deletion at the *IGF2BP2* target site. Below the chromatograms related sequence alignments between the wild-type reference (first line) and the mutated alleles are depicted. Black frames in the sequence alignments demonstrate the section shown in the chromatograms above. Yellow arrows highlight the start site of at least two different sequences/alleles in cell clones. Colour code visualises matches in aligned sequences. A: adenine (green), C: cytosine (blue), G: guanine (black), T: thymine (red). -: missing DNA base.

IGF2BP2 gene expression was analysed in selected monoallelic and biallelic edited clones of different cell lines and compared to *IGF2BP2* level in parental cells using qPCR analysis (Figure 38). Contrary to our expectations, gene expression was not completely abolished, but covered a wide range of 30-80% of the parental gene expression. HCT116 clone 47-1 showed no significant reduction of *IGF2BP2* expression. This is in line with findings in a recent report by Smits et al. (2019). They measured the RNA expression levels of 174 mutants, generated by CRISPR/Cas9, and those of their parental cell lines and revealed that many knockout mutants did not show a strongly reduced gene expression, although the presence of PTCs in the genomic sequences of the mutants were confirmed by DNA sequencing (Smits et al., 2019). Normally, as a consequence of PTCs, transcripts are subjected to NMD, making them not accessible for qPCR analysis. This implicates that the *IGF2BP2* transcripts somehow circumvent the degradation by the NMD machinery. Lindeboom et al. (2016) postulated a

broad variation of NMD efficiency depending on, e.g. the proximity of a PTC to the start codon, the length of an exon, where the PTC is located in, the distance from a PTC to the translation termination site, the mRNA half-life, and certain sequence motifs in proximity to a PTC or in the 3'-UTR. As previously described (cf. 1.2.1) alternative splicing represents a well understood compensatory mechanism in cancer cells. During transcription the indel-containing exon can be completely or to some extent excluded to create a new mRNA species, possibly leading to truncated proteins that can remain functional. Tuladhar et al. (2019) revealed foreign mRNAs and proteins in 50% of investigated cell lines undergoing installation of PTCs by frameshift-inducing indels using CRISPR/Cas9. This explanation may also apply here, because for quantitative PCR analysis an amplicon spanning exon 12 of *IGF2BP2* was used, which is far away from the CRISPR-targeted exons 4 and 6, both leading to PTCs in exon 6. Thus, a missing 52 nt long exon 4 fragment or a 273 nt long exon 6 fragment would not be detected with this method and has to be evaluated in further studies. Genomic instability is a hallmark of cancer (Bielski & Taylor, 2021; Hanahan & Weinberg, 2011) and the cancer cell lines used in this study have typically karyotypic abnormalities and exhibit aneuploidy, having to some extent more than two chromosomes (hyperdiploid) and thus more than two alleles per gene. Considering a high genetic variation even within the same cell line across passage numbers or particularly for single-cell derived subclones (Ben-David, et al., 2018), we carefully analysed Sanger sequencing results of the genome-edited cell clones of at least two different cell passages. Nevertheless, we cannot completely exclude a genetic drift during the whole culture time, which may also contribute to variable *IGF2BP2* gene expression of cell clones.

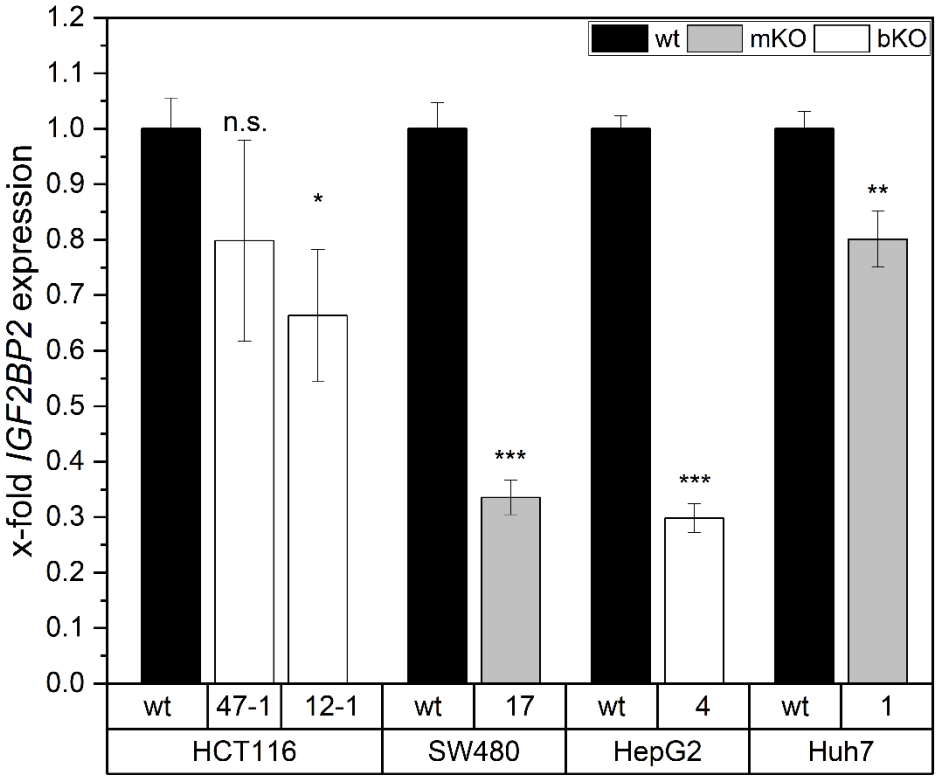

Figure 38| *IGF2BP2* gene expression in edited cell clones of different cell lines. Quantification of *IGF2BP2* expression was analysed *via* qPCR in biallelic edited (bKO) HCT116 clones (47-1, 12-1), monoallelic edited (mKO) SW480 clone 17, biallelic edited HepG2 clone 4, and monoallelic edited Huh7 clone 1, and compared with parental wild-type (wt) cells as controls. Bars represent mean ±SEM. n=3 (triplicates). *: $p<0.05$; **: $p<0.005$; ***: $p<0.001$ (two-sample *t*-test); n.s.: not significant.

5.2.2 Validation of IMP2 knockout on protein level

Biallelic mutations, introduced into *IGF2BP2* gene by different CRISPR/Cas9 approaches, were predicted to create frame shifts with PTCs resulting in NMD of *IGF2BP2* transcripts and thus in knockout of IMP2 protein in mammalian tumour cell lines. We conducted Western blots to proof the consequences of the *IGF2BP2* gene editing on protein level and to quantify both, IMP2 and its splice variant p62.

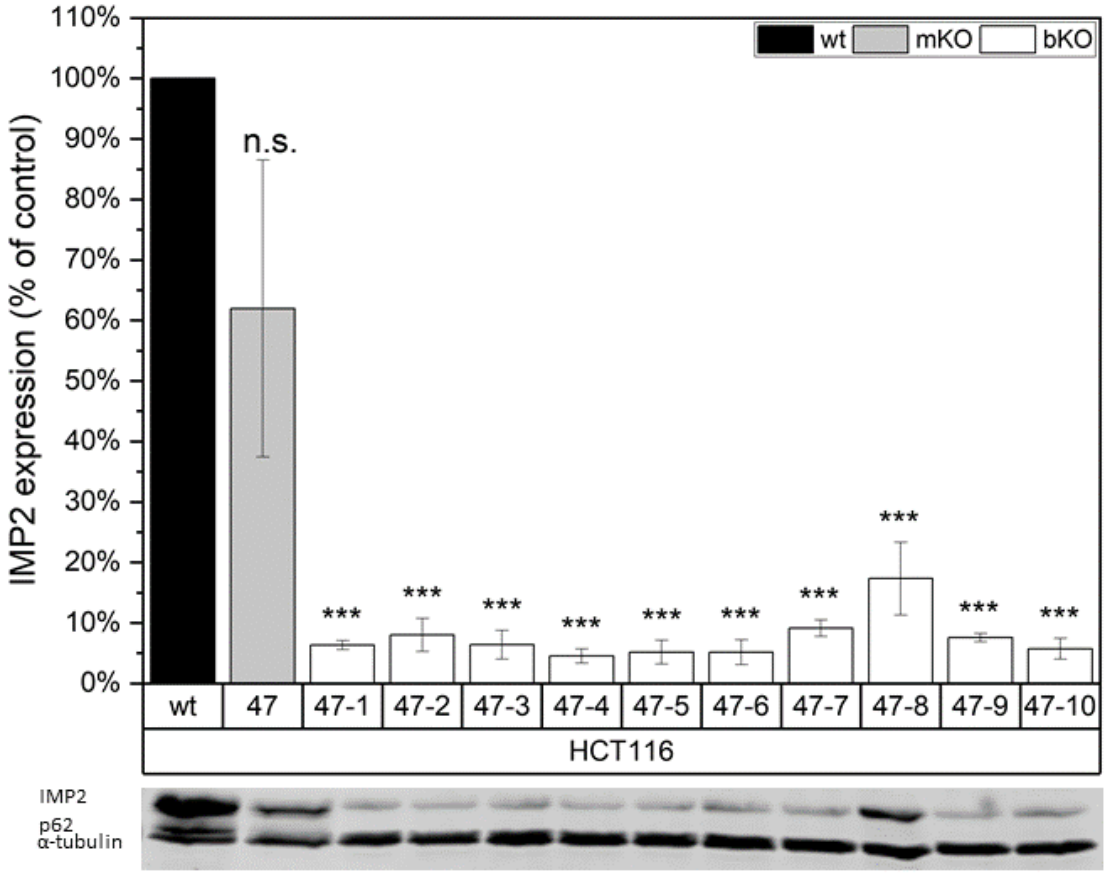

Figure 39| Western blot analyses of HCT116 clones resulting from CRISPR/Cas9 approach 1. Western blot analyses of biallelic edited HCT116 clones (47-1 to 47-10) compared to monoallelic edited clone 47, from which they originated, and wild-type cells (wt) as control. Quantification of the protein levels of IMP2 (66 kDa) and its splice variant p62 (62 kDa) using alpha-tubulin (55 kDa) as internal control/housekeeping protein. Below, a representative Western blot of the analysed cell clones is shown. Bars represent mean ±SEM. n=3. ***: $p<0.001$ (one-way ANOVA); n.s.: not significant.

Western blots of biallelic edited cell clones did not show any band at height of the IMP2 splice variant p62 at 62 kDa (Figure 39, Figure 40A), indicating a complete knockout of p62, and in HCT116 cell clones (Figure 39) only a light, hardly visible band for IMP2 at 66 kDa. The quantification of the protein levels of those HCT116 clones resulted in significantly reduced,

but still 5-10% remaining IMP2 expression as compared to parental HCT116 wild-type cells (Figure 39). One exception was HCT116 clone 47-8 with approximately 17% IMP2 expression left, although harbouring the same biallelic mutation (adenine insertion) in its genetic sequence like other HCT116 clones (Table 9). HCT116 clone 12-1, harbouring a biallelic GG deletion at a different target site, revealed a similar IMP2 expression pattern (Figure 40). Thus, remaining IMP2 expression is not dependant on the target site or kind of mutation. Moreover, clones originating from other colorectal or hepatocellular carcinoma cell lines, also containing biallelic adenine insertions, such as SW480 clone 15 and HepG2 clone 4, displayed a remaining IMP2 expression of 30-50% (Figure 40). Contamination of the cell clones with parental wild-type cells could be excluded due to the use of a cell printer that can proof clonality by taking pictures of the single cell clones when seeded into 96-well plates. Furthermore, edited cell clones from various cell passages were analysed by Sanger sequencing showing identical results, and the sensitive SNuPE method revealed no signs of wild-type cells.

A recent study reported residual protein expression at variable levels in one third of 193 CRISPR-edited HAP1 cell lines (Smits et al., 2019). Furthermore, they found no correlation between remaining mRNA and protein levels of the knockout cell lines, which is why the mRNA levels are not predictive for the protein levels (Smits et al., 2019). Both biallelic edited HCT116 clones, 47-1 and 12-1, showed, compared to other genome edited clones from different cell lines, such as HepG2 clone 4, the highest IMP2 gene expression with approximately 80% and 65% of the parental expression (Figure 38), but the least IMP2 protein levels with 4.52% and 17.38% (Figure 40B). Smits et al. (2019) also identified two underlying mechanisms for this phenomenon, namely translation reinitiation resulting in N-terminally truncated target proteins and skipping of the mutated exon leading to protein isoforms with internal sequence deletions. To the first point: due to the frameshift caused by either biallelic A insertion or GG deletion in different knockout cell lines, new alternative in-frame start codons at amino acid positions 254 or 255 were generated but were also followed downstream by other stop codons. Moreover, there were no signs of N-terminally truncated IMP2 protein on the Western blots visible, which should have been detectable by our antibody against a C-terminal epitope of IMP2 (M. Lu et al., 2001). Related to the second aspect, skipping of the edited exon 4 or exon 6 in IMP2 knockout clones would result in a protein with an internal deletion of 17 aa or 91 aa corresponding to a mass of 1.8 kDa and 10.1 kDa, respectively.

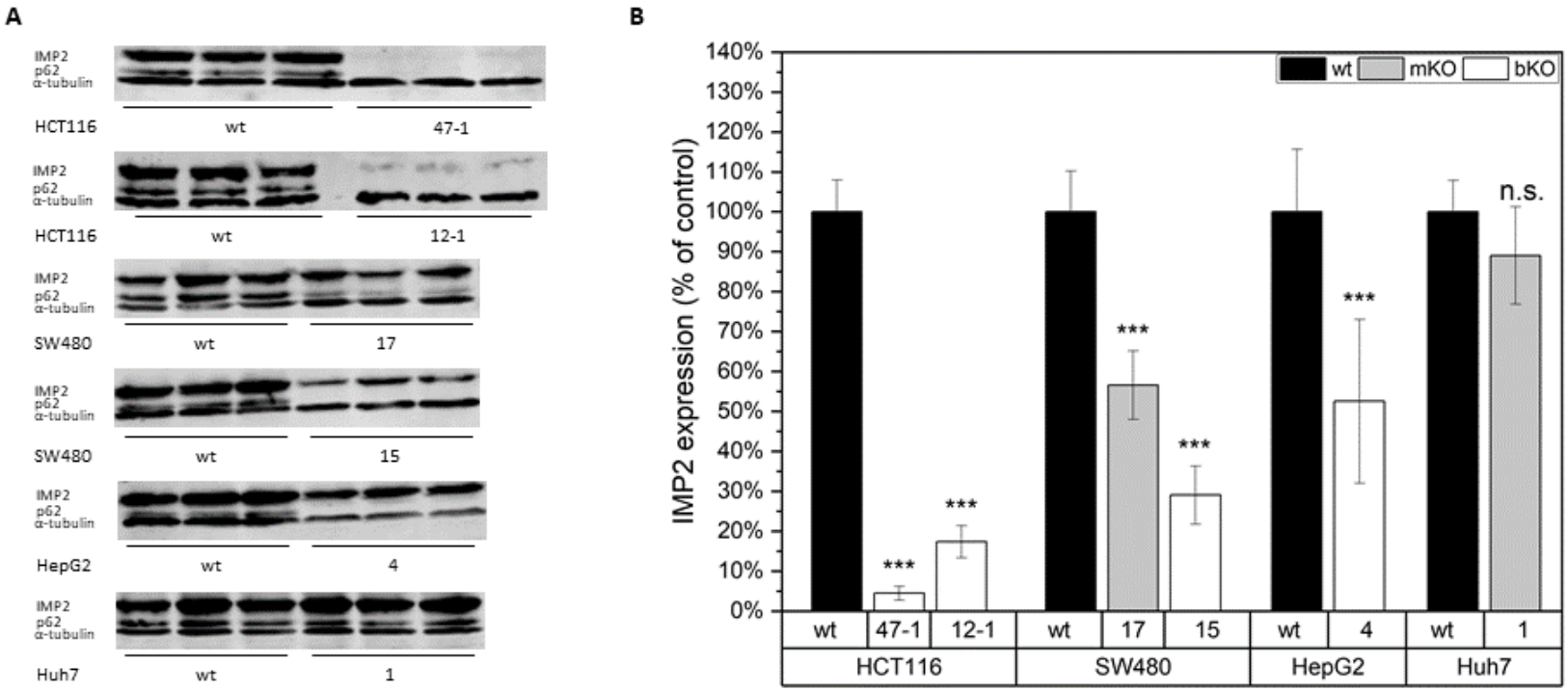

Figure 40| Western blot analyses of edited cell clones of different cell lines resulting from both CRISPR/Cas9 approaches. (A) Western blots of biallelic edited (bKO) HCT116 clones (47-1, 12-1), monoallelic (mKO) and biallelic edited SW480 clones 17 and 15, biallelic edited HepG2 clone 4, and monoallelic edited Huh7 clone 1, all compared to parental wild-type (wt) cells. IMP2 (66 kDa) and its splice variant p62 (62 kDa) was analysed against alpha-tubulin (55 kDa) as housekeeping protein. Representative blots were chosen. (B) Quantification of the protein levels of IMP2 and p62 in the aforementioned cell clones compared to parental wild-type cells as control. Bars represent mean ±SEM. n=3 (triplicates). ***: p<0.001 (two-sample t-test); n.s.: not significant.

A 1.8 kDa difference is hard to discriminate *via* SDS-PAGE and Western blot analysis but could explain the remaining light bands of IMP2 in HCT116 clones (Figure 39), particularly since alternative splicing could not be excluded so far. An IMP2 protein 10.1 kDa smaller in size/mass would mean a band on a Western blot membrane at approximately 56 kDa, which represents the same height as the housekeeping protein α-tubulin (55 kDa) in the used setup. At least in the latter case, truncated versions of IMP2 could be excluded due to immunodetection analysis of IMP2 and α-tubulin at different wave lengths.

5.2.3 IMP2 target validation in vitro and in vivo

Parts of this chapter have been published in:

Dahlem, C., Abuhaliema, A., Kessler, S. M., **Kröhler, Tarek**, Zoller, B., Chanda, S., Wu, Y., Both, S., Müller, F., Lepikhov, K., Kirsch, S. H., Laggai, S., Müller, R., Empting, M., & Kiemer, A. K. (2022). First small-molecule inhibitors targeting the RNA-binding protein IGF2BP2/IMP2 for cancer therapy. *ACS chemical biology*, *17*(2), 361–375. https://doi.org/10.1021/acschembio.1c00833

IMP2 is involved in cancer cell proliferation by stabilising client mRNAs (Dai et al., 2017). Nevertheless, there are inconsistent results regarding the proliferation of cancer cell lines in 2D cultures (Xing et al., 2019) and CRISPR phenotypes in 3D more accurately recapitulate those of *in vivo* tumours (Han et al., 2020). Therefore, we determined the 3D proliferation rate of parental wild-type and various HCT116 IMP2 knockout clones in 3D spheroids using a live-cell analysis system. Clone 47-1 (Figure 41A) and other clones (Supplementary Figure 5), harbouring different gene edits (Table 9 and Table 10), obtained from both CRISPR/Cas knockout approaches, revealed a similar, and compared to parental cells, significantly reduced 3D proliferation rate. Thus, a reduction in 3D proliferation due to clonal artefacts could be excluded. Furthermore, rescue experiments were conducted to confirm the target specificity of IMP2 knockout in HCT116 cells. Therefore, IMP2/p62 was overexpressed in two different IMP2 knockout clones (47-1 and 12-1) resulting in a restored metabolic activity and 2D proliferation rate (Figure 42A-D). Moreover, knockout cells displayed a significantly diminished expression of known IMP2 targets (Figure 42E-F and Supplementary Figure 6), such as the long non-coding RNA (lncRNA) differentiation antagonizing non-protein coding RNA (*DANCR*) and the oncogenes *MYC* and *HMGA1* (Dai et al., 2017; Hu et al., 2020; Y. Wang et al., 2019), which was recovered by IMP2/p62 overexpression (Figure 42G-H).

It has been suggested that IMP2 is linked *via* client mRNAs (LIM zinc finger domain containing 2 [LIMS2], tripartite motif containing 54 [TRIM54]) to cell adhesion and motility (Boudoukha et al., 2010). Jian-Ying Zhang and colleagues demonstrated increased cell migration and reduced cell adhesion in IMP2/p62 transfected breast cancer cell lines (Y. Li et al., 2015) and

liver cancer cells (Xing et al., 2019). Therefore, we employed Electrical Cell–substrate Impedance Sensing allowing us to evaluate the cell adhesion of HCT116 parental and CRISPR/Cas9-mediated IMP2 knockout cells in real time (Stolwijk & Wegener, 2019). Notably, the results were very similar to the 3D growth of the cells (Figure 41B). Moreover, cell migratory ability was assessed in a scratch wound assay resulting in a significant reduction in the IMP2-absent clone 47-1 (Figure 41C).

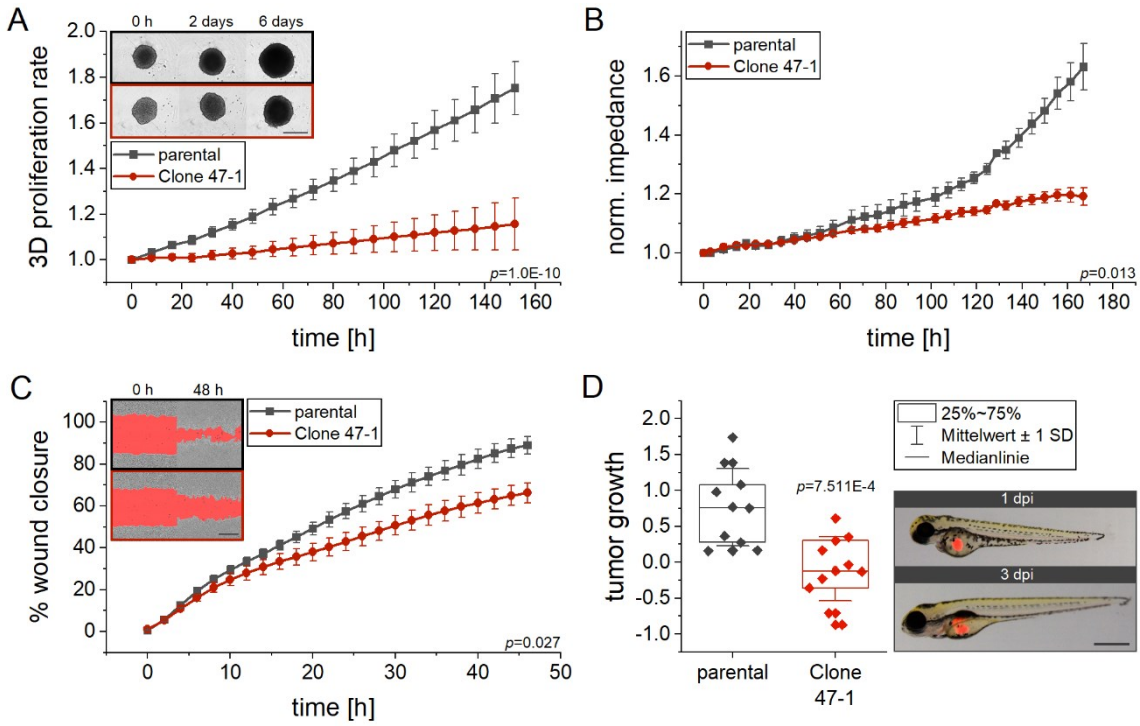

Figure 41| IMP2 target validation in vitro and in vivo. (A) 3D proliferation of spheroids consisting of either HCT116 wild-type (parental) cells or IMP2 knockout clone 47-1. Prior to the monitoring of the spheroid areas by an Incucyte® S3 system for 152 h, spheroid formation was conducted for 3 days. The spheroid areas were normalised to 3-day-old spheroids (0 h). Representative pictures show spheroids at the starting point (0 h), 2 days, and 6 days after initiation of measurement. Scale bar=500 µm; n=2 (quadruplicates). (B) Impact of IMP2 knockout on HCT116 cell impedance was determined in an Electric Cell-substrate Impedance Sensing system. Data are normalised to the starting point (0 h), n=2 (triplicates). (C) Scratch wound assay to determine the migratory activity of clone 47-1 compared to parental HCT116 cells. % wound closure was monitored and evaluated in an Incucyte® S3 system for 48 h. Representative pictures demonstrate the wound area in red at the starting point (0 h) and 48 h after wounding. Scale bar=400 µm; n=3 (quadruplicates). (A-C) *p* values were calculated for the respective last time points acquired. (D) Zebrafish embryo xenograft of HCT116 wild-type and clone 47-1 cells. Fluorescence-labelled cells were injected into the yolk sac 2 days post fertilisation. Embryos were imaged at 1 day post injection (dpi) and 3 dpi. Individual values of tumour growth quantification are presented in a box blot. Representative, merged images of one parental HCT116 xenotransplanted embryo at 1 dpi and 3 dpi, each, are shown. Scale bar=1 mm. This figure and parts of the caption were adopted from "First small-molecule inhibitors targeting the RNA-binding protein IGF2BP2/IMP2 for cancer therapy" by Dahlem, C., Abuhaliema, A., Kessler, S. M., Kröhler, T., Zoller, B., Chanda, S., Wu, Y., Both, S., Müller, F., Lepikhov, K., Kirsch, S. H., Laggai, S., Müller, R., Empting, M., & Kiemer, A. K. (2022),. *ACS Chemical Biology, 17*(2), 361–375 (https://doi.org/10.1021/acschembio.1c00833). With permission, copyright © 2022, American Chemical Society. Also published in similar way in "*In vitro and in vivo characterization of therapeutic approaches for solid tumors: natural compounds and novel targets*" (Doctoral thesis, Saarland University, Saarbrücken, Germany) by Dahlem, C. (2020) (https://doi.org/10.22028/D291-32755).

IMP2 is involved in the maintenance of cancer stem-like features (Janiszewska et al., 2012; Kessler et al., 2015) and inhibition of IMP2 sensitises glioblastoma cancer cells to chemotherapy treatment (Mu et al., 2015). Hence, we investigated the chemosensitivity of HCT116 wild-type and IMP2 knockout cells undergoing treatment with drugs approved for the treatment of colorectal cancer, that is regorafenib (Stivarga®, REGO), oxaliplatin (OHP), and 5-fluorouracil (5FU) (Dhillon, 2018; Ibrahim et al., 2004). Clone 47-1 displayed a significantly increased chemosensitivity towards REGO, particularly in the treatment with the IC_{20} concentration (Supplementary Figure 7A-B), and a tendency for elevated chemosensitivity in OHP-treated knockout cells compared to HCT116 wild-type cells (Supplementary Figure 7E-F). There was no impact of IMP2 knockout on chemosensitivity observed in 5FU treated cells (Supplementary Figure 7C-D).

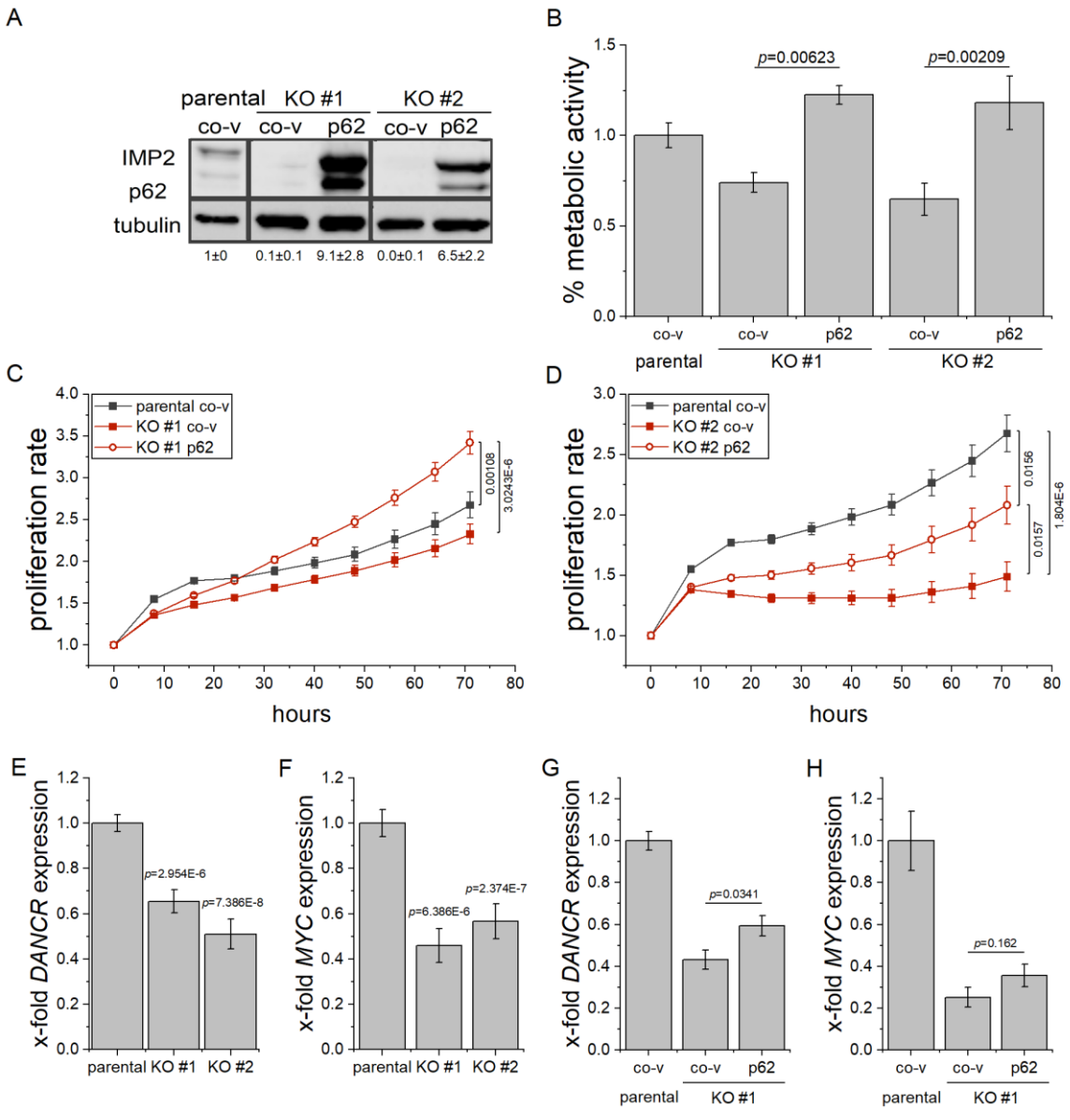

Figure 42| Target specificity of IMP2 knockout in HCT116 cells assessed by IMP2-rescue. (A-D) HCT116 parental and IMP2 knockout HCT116 cells (KO #1: clone 47-1; KO #2: clone 12-1) were transfected with p62/IMP2 or control vector (co-v). (A) Transfection efficiency and p62/IMP2 overexpression was confirmed by Western blot analysis 3 days post transfection. (B) Metabolic activity was measured *via* MTT assay 3 days post transfection. (C, D) Cell confluency was monitored using the Incucyte® S3 system over 3 days. Confluency was normalised to the time point of transfection (0 h). Data are represented as means ±SEM. n=2 (quadruplicates). (E, F) *DANCR*, and *MYC* gene expression was determined in HCT116 IMP2 knockout clones and (G, H) p62/IMP2 overexpressing parental and knockout cells by qPCR. Values were normalised to the housekeeping gene *RNA18SN5*. Data are represented as means ±SEM. n=3 (triplicates). This figure and caption were adopted from "First small-molecule inhibitors targeting the RNA-binding protein IGF2BP2/IMP2 for cancer therapy" by Dahlem, C., Abuhaliema, A., Kessler, S. M., Kröhler, T., Zoller, B., Chanda, S., Wu, Y., Both, S., Müller, F., Lepikhov, K., Kirsch, S. H., Laggai, S., Müller, R., Empting, M., & Kiemer, A. K. (2022),. *ACS Chemical Biology, 17*(2), 361–375 (https://doi.org/10.1021/acschembio.1c00833). With permission, copyright © 2022, American Chemical Society.

Finally, we employed a zebrafish embryo xenograft model to study tumour growth of HCT116 parental and IMP2 knockout cells *in vivo*. According to the 3R rules to avoid animal experiments, zebrafish embryo xenografts represent an outstanding replacement to conduct *in vivo* experiments, since zebrafish embryos do not fall under the animal protection act until 5 days post fertilisation (Strähle et al., 2012). In particular, the usefulness of this model has been proven for studies on colorectal cancer (Fior et al., 2017). IMP2 knockout xenografts displayed a significantly lower tumour growth compared to parental controls (Figure 41D).

The tumour promoter IMP2 is the most abundant paralogue of the IMP family in most cancer entities of different origin (Dai et al., 2017). *In vivo* and *in vitro* data, presented in this chapter as an extract of the publication by Dahlem et al. (2022), as well as published data from our department on IMP2 in HCC (Kessler et al., 2013, 2015; Simon et al., 2014) validate the RBP IMP2 as an interesting target for cancer therapy. Results referring to the growth inhibition by CRISPR/Cas-facilitated IMP2 knockout are in line with data from literature using shRNA in colon cancer cells (S. Lu et al., 2021) or siRNA in pancreas cancer cell lines (X. Xu et al., 2019) for IMP2 knockdown.

Based on these results Ali M. H. Abuhaliema (2020) screened different compound libraries for small-molecule inhibitors of IMP2. Target specificity and biological activity of ten hit compounds were tested in cell culture systems *in vitro*. Thereby, parental HCT116 and HepG2 cells displayed a significantly higher sensitivity toward hit compounds compared to CRISPR-modified cells as assessed by MTT assay after 96 h treatment (Dahlem et al., 2022). Finally, the three most promising compounds were used to study tumour growth inhibition in zebrafish embryo xenografts *in vivo* (Dahlem et al., 2022; Dahlem, 2020).

6 Summary and conclusion

In the year 2020, colorectal cancer and primary liver cancer were among the cancer entities with the highest incidence and mortality rates. In either cancer species, aberrant expression of RBPs, such as IMP2 and TTP, is implicated in tumourigenesis and tumour progression.

We investigated the role of TTP, a suggested tumour suppressor, in HCC by employing various hepatoma cell lines *in vitro* and ls*Ttp*-KO mice in the DEN hepatocarcinogenesis model *in vivo*. Overall, we found a significantly reduced tumour burden and monocyte/macrophage ratio in ls*Ttp*-KO mice compared to wild-type animals. Short-term DEN treatment, mimicking early inflammatory processes in hepatocarcinogenesis, only led to increased saturated and poly-unsaturated hepatic fatty acids in wild-type mice and not in ls*Ttp*-KO mice. Therefore, we suggested an inflammation- and lipid-dependent role of hepatocytic TTP in promoting hepatocarcinogenesis. Contrary, in HCC progression, TTP exerts tumour-suppressing actions by inhibiting proliferation, attenuating migration, and increasing chemosensitivity in hepatoma cells.

Next, we combined two methods to identify new RNA targets of IMP2 for the first time *in vivo* using HGD and the TRIBE method in mice. Preliminary experiments paved the way to assure the transfection of murine hepatocytes with the IMP2-ADAR fusion protein, which enables the discrimination of mRNA targets due to its deaminating action on adenosines. However, RNA sequencing of the transfected liver cells and the subsequent bioinformatic analysis is still pending.

At last, we validated IMP2 as a target for cancer therapy by employing 2D and 3D cell culture models of CRISPR-mediated IMP2 knockout cells *in vitro* as well as zebrafish embryo xenografts *in vivo*. Yet, based on these results, hit compounds in the screening for small molecule inhibitors of IMP2 were tested and can be chemically modified for future pharmacodynamic and pharmacokinetic optimisations.

7 References

Abdelmohsen, K., Srikantan, S., Kuwano, Y., & Gorospe, M. (2008). miR-519 reduces cell proliferation by lowering RNA-binding protein HuR levels. *Proceedings of the National Academy of Sciences of the United States of America, 105*(51), 20297–20302. https://doi.org/10.1073/pnas.0809376106

Abuhaliema, A. (2020). *Discovery of the first small molecules targeting the mRNA binding protein IGF2BP2/IMP2 as potential target in cancer therapy* (Doctoral thesis, Saarland University, Saarbrücken, Germany). https://doi.org/10.22028/D291-32218

Adli M. (2018). The CRISPR tool kit for genome editing and beyond. *Nature Communications, 9*(1), 1911. https://doi.org/10.1038/s41467-018-04252-2

Adriaens, C., Standaert, L., Barra, J., Latil, M., Verfaillie, A., Kalev, P., Boeckx, B., Wijnhoven, P. W., Radaelli, E., Vermi, W., Leucci, E., Lapouge, G., Beck, B., van den Oord, J., Nakagawa, S., Hirose, T., Sablina, A. A., Lambrechts, D., Aerts, S., Blanpain, C., … Marine, J. C. (2016). p53 induces formation of NEAT1 lncRNA-containing paraspeckles that modulate replication stress response and chemosensitivity. *Nature Medicine, 22*(8), 861–868. https://doi.org/10.1038/nm.4135

Al-Haj, L., Blackshear, P. J., & Khabar, K. S. (2012). Regulation of p21/CIP1/WAF-1 mediated cell-cycle arrest by RNase L and tristetraprolin, and involvement of AU-rich elements. *Nucleic Acids Research, 40*(16), 7739–7752. https://doi.org/10.1093/nar/gks545

Al-Souhibani, N., Al-Ahmadi, W., Hesketh, J. E., Blackshear, P. J., & Khabar, K. S. (2010). The RNA-binding zinc-finger protein tristetraprolin regulates AU-rich mRNAs involved in breast cancer-related processes. *Oncogene, 29*(29), 4205–4215. https://doi.org/10.1038/onc.2010.168

Anders, C., Niewoehner, O., Duerst, A., & Jinek, M. (2014). Structural basis of PAM-dependent target DNA recognition by the Cas9 endonuclease. *Nature, 513*(7519), 569–573. https://doi.org/10.1038/nature13579

Anzalone, A. V., Koblan, L. W., & Liu, D. R. (2020). Genome editing with CRISPR-Cas nucleases, base editors, transposases and prime editors. *Nature Biotechnology, 38*(7), 824–844. https://doi.org/10.1038/s41587-020-0561-9

Anzalone, A. V., Randolph, P. B., Davis, J. R., Sousa, A. A., Koblan, L. W., Levy, J. M., Chen, P. J., Wilson, C., Newby, G. A., Raguram, A., & Liu, D. R. (2019). Search-and-replace genome editing without double-strand breaks or donor DNA. *Nature, 576*(7785), 149–157. https://doi.org/10.1038/s41586-019-1711-4

Asencio, C., Chatterjee, A., & Hentze, M. W. (2018). Silica-based solid-phase extraction of cross-linked nucleic acid-bound proteins. *Life Science Alliance, 1*(3), e201800088. https://doi.org/10.26508/lsa.201800088

Babic, I., Jakymiw, A., & Fujita, D. J. (2004). The RNA binding protein Sam68 is acetylated in tumor cell lines, and its acetylation correlates with enhanced RNA binding activity. *Oncogene, 23*(21), 3781–3789. https://doi.org/10.1038/sj.onc.1207484

Balic, M., Lin, H., Young, L., Hawes, D., Giuliano, A., McNamara, G., . . . Cote, R. J. (2006). Most Early Disseminated Cancer Cells Detected in Bone Marrow of Breast Cancer Patients Have a Putative Breast Cancer Stem Cell Phenotype. *Clinical Cancer Research, 12*(19), 5615–5621. doi:10.1158/1078-0432.CCR-06-0169

Baltz, A. G., Munschauer, M., Schwanhäusser, B., Vasile, A., Murakawa, Y., Schueler, M., Youngs, N., Penfold-Brown, D., Drew, K., Milek, M., Wyler, E., Bonneau, R., Selbach, M., Dieterich, C., & Landthaler, M. (2012). The mRNA-bound proteome and its global occupancy profile on protein-coding transcripts. *Molecular cell, 46*(5), 674–690. https://doi.org/10.1016/j.molcel.2012.05.021

Bao, X., Guo, X., Yin, M., Tariq, M., Lai, Y., Kanwal, S., Zhou, J., Li, N., Lv, Y., Pulido-Quetglas, C., Wang, X., Ji, L., Khan, M. J., Zhu, X., Luo, Z., Shao, C., Lim, D. H., Liu, X., Li, N., Wang, W., … Esteban, M. A. (2018). Capturing the interactome of newly transcribed RNA. *Nature Methods, 15*(3), 213–220. https://doi.org/10.1038/nmeth.4595

Barghash, A., Golob-Schwarzl, N., Helms, V., Haybaeck, J., & Kessler, S. M. (2016). Elevated expression of the IGF2 mRNA binding protein 2 (IGF2BP2/IMP2) is linked to short survival and metastasis in esophageal adenocarcinoma. *Oncotarget, 7*(31), 49743–49750. https://doi.org/10.18632/oncotarget.10439

Barghash, A., Helms, V., & Kessler, S. M. (2015). Overexpression of IGF2 mRNA-binding protein 2 (IMP2/p62) as a feature of basal-like breast cancer correlates with short survival. *Scandinavian Journal of Immunology*, *82*(2), 142–143. https://doi.org/10.1111/sji.12307

Barrangou, R., Fremaux, C., Deveau, H., Richards, M., Boyaval, P., Moineau, S., Romero, D. A., & Horvath, P. (2007). CRISPR provides acquired resistance against viruses in prokaryotes. *Science, 315*(5819), 1709–1712. https://doi.org/10.1126/science.1138140

Beckmann, B. M., Castello, A., & Medenbach, J. (2016). The expanding universe of ribonucleoproteins: of novel RNA-binding proteins and unconventional interactions. *Pflügers Archiv : European Journal of Physiology, 468*(6), 1029–1040. https://doi.org/10.1007/s00424-016-1819-4

Beckmann, B. M., Horos, R., Fischer, B., Castello, A., Eichelbaum, K., Alleaume, A. M., Schwarzl, T., Curk, T., Foehr, S., Huber, W., Krijgsveld, J., & Hentze, M. W. (2015). The RNA-binding proteomes from yeast to man harbour conserved enigmRBPs. *Nature Communications, 6*, 10127. https://doi.org/10.1038/ncomms10127

Bell, J. L., Wächter, K., Mühleck, B., Pazaitis, N., Köhn, M., Lederer, M., & Hüttelmaier, S. (2013). Insulin-like growth factor 2 mRNA-binding proteins (IGF2BPs): post-transcriptional drivers of cancer progression?. *Cellular and Molecular Life Sciences : CMLS, 70*(15), 2657–2675. https://doi.org/10.1007/s00018-012-1186-z

Beloribi-Djefaflia, S., Vasseur, S., & Guillaumond, F. (2016). Lipid metabolic reprogramming in cancer cells. *Oncogenesis, 5*(1), e189. https://doi.org/10.1038/oncsis.2015.49

Ben-David, U., Siranosian, B., Ha, G., Tang, H., Oren, Y., Hinohara, K., Strathdee, C. A., Dempster, J., Lyons, N. J., Burns, R., Nag, A., Kugener, G., Cimini, B., Tsvetkov, P., Maruvka, Y. E., O'Rourke, R., Garrity, A., Tubelli, A. A., Bandopadhayay, P., Tsherniak, A., … Golub, T. R. (2018). Genetic and transcriptional evolution alters cancer cell line drug response. *Nature, 560*(7718), 325–330. https://doi.org/10.1038/s41586-018-0409-3

Bereshchenko, O., Migliorati, G., Bruscoli, S., & Riccardi, C. (2019). Glucocorticoid-induced leucine zipper: a novel anti-inflammatory molecule. *Frontiers in Pharmacology, 10*, 308. https://doi.org/10.3389/fphar.2019.00308

Berglund, A. E., Scott, K. E., Li, W., Yang, C., Fernandez, M. R., Schaub, F. X., Cleveland, J. L., & Rounbehler, R. J. (2016). Tristetraprolin disables prostate cancer maintenance by impairing proliferation and metabolic function. *Oncotarget, 7*(50), 83462–83475. https://doi.org/10.18632/oncotarget.13128

Bhadra, M., Howell, P., Dutta, S., Heintz, C., & Mair, W. B. (2020). Alternative splicing in aging and longevity. *Human Genetics, 139*(3), 357–369. https://doi.org/10.1007/s00439-019-02094-6

Bhat, M., Robichaud, N., Hulea, L., Sonenberg, N., Pelletier, J., & Topisirovic, I. (2015). Targeting the translation machinery in cancer. *Nature Reviews. Drug discovery, 14*(4), 261–278. https://doi.org/10.1038/nrd4505

Bielski, C. M., & Taylor, B. S. (2021). Homing in on genomic instability as a therapeutic target in cancer. *Nature Communications, 12*(1), 3663. https://doi.org/10.1038/s41467-021-23965-5B

Biswas, J., Patel, V. L., Bhaskar, V., Chao, J. A., Singer, R. H., & Eliscovich, C. (2019). The structural basis for RNA selectivity by the IMP family of RNA-binding proteins. *Nature Communications, 10*(1), 4440. https://doi.org/10.1038/s41467-019-12193-7

Biswas, J., Rosbash, M., Singer, R. H., & Rahman, R. (2021). Protocol for using TRIBE to study RNA-protein interactions and nuclear organization in mammalian cells. *STAR Protocols, 2*(3), 100634. https://doi.org/10.1016/j.xpro.2021.100634

Blackshear P. J. (2002). Tristetraprolin and other CCCH tandem zinc-finger proteins in the regulation of mRNA turnover. *Biochemical Society Transactions, 30*(Pt 6), 945–952. https://doi.org/10.1042/bst0300945

Blackshear, P. J., Phillips, R. S., Ghosh, S., Ramos, S. B., Richfield, E. K., & Lai, W. S. (2005). Zfp36l3, a rodent X chromosome gene encoding a placenta-specific member of the Tristetraprolin family of CCCH tandem zinc finger proteins. *Biology of Reproduction, 73*(2), 297–307. https://doi.org/10.1095/biolreprod.105.040527

Blériot, C., Dupuis, T., Jouvion, G., Eberl, G., Disson, O., & Lecuit, M. (2015). Liver-resident macrophage necroptosis orchestrates type 1 microbicidal inflammation and type-2-mediated tissue repair during bacterial infection. *Immunity, 42*(1), 145–158. https://doi.org/10.1016/j.immuni.2014.12.020

Bode, H. B., Ring, M. W., Schwär, G., Kroppenstedt, R. M., Kaiser, D., & Müller, R. (2006). 3-Hydroxy-3-methylglutaryl-coenzyme A (CoA) synthase is involved in biosynthesis of isovaleryl-CoA in the myxobacterium Myxococcus xanthus during fruiting body formation. *Journal of Bacteriology, 188*(18), 6524–6528. https://doi.org/10.1128/JB.00825-06

Bonamassa, B., Hai, L., & Liu, D. (2011). Hydrodynamic Gene Delivery and its applications in pharmaceutical research. *Pharmaceutical Research, 28*(4), 694–701. https://doi.org/10.1007/s11095-010-0338-9

Bou-Nader, C., Gordon, J. M., Henderson, F. E., & Zhang, J. (2019). The search for a PKR code-differential regulation of protein kinase R activity by diverse RNA and protein regulators. *RNA, 25*(5), 539–556. https://doi.org/10.1261/rna.070169.118

Boudoukha, S., Cuvellier, S., & Polesskaya, A. (2010). Role of the RNA-binding protein IMP-2 in muscle cell motility. *Molecular and Cellular Biology, 30*(24), 5710–5725. https://doi.org/10.1128/MCB.00665-10

Bray, F., Laversanne, M., Weiderpass, E., & Soerjomataram, I. (2021). The ever-increasing importance of cancer as a leading cause of premature death worldwide. *Cancer, 127*(16), 3029–3030. https://doi.org/10.1002/cncr.33587

Brennan, S. E., Kuwano, Y., Alkharouf, N., Blackshear, P. J., Gorospe, M., & Wilson, G. M. (2009). The mRNA-destabilizing protein tristetraprolin is suppressed in many cancers, altering tumorigenic phenotypes and patient prognosis. *Cancer Research, 69*(12), 5168–5176. https://doi.org/10.1158/0008-5472.CAN-08-4238

Brooks, S. A., & Blackshear, P. J. (2013). Tristetraprolin (TTP): interactions with mRNA and proteins, and current thoughts on mechanisms of action. *Biochimica et Biophysica Acta, 1829*(6-7), 666–679. https://doi.org/10.1016/j.bbagrm.2013.02.003

Bruix, J., Han, K. H., Gores, G., Llovet, J. M., & Mazzaferro, V. (2015). Liver cancer: approaching a personalized care. *Journal of Hepatology, 62*(1 Suppl), S144–S156. https://doi.org/10.1016/j.jhep.2015.02.007

Bui, M., & Liu, Z. (2009). Simple allele-discriminating PCR for cost-effective and rapid genotyping and mapping. *Plant Methods, 5*, 1. https://doi.org/10.1186/1746-4811-5-1

Buratti, E., Romano, M., & Baralle, F. E. (2013). TDP-43 high throughput screening analyses in neurodegeneration: advantages and pitfalls. *Molecular and Cellular Neurosciences, 56*, 465–474. https://doi.org/10.1016/j.mcn.2013.03.001

Burger, K., Mühl, B., Kellner, M., Rohrmoser, M., Gruber-Eber, A., Windhager, L., Friedel, C. C., Dölken, L., & Eick, D. (2013). 4-thiouridine inhibits rRNA synthesis and causes a nucleolar stress response. *RNA Biology, 10*(10), 1623–1630. https://doi.org/10.4161/rna.26214

Calabretta, S., & Richard, S. (2015). Emerging Roles of Disordered Sequences in RNA-Binding Proteins. *Trends in Biochemical Sciences, 40*(11), 662–672. https://doi.org/10.1016/j.tibs.2015.08.012

Cao, J., Mu, Q., & Huang, H. (2018). The roles of insulin-like growth factor 2 mRNA-binding protein 2 in cancer and cancer stem cells. *Stem Cells International, 2018*, 4217259. https://doi.org/10.1155/2018/4217259

Carballo, E., Lai, W. S., & Blackshear, P. J. (1998). Feedback inhibition of macrophage tumor necrosis factor-alpha production by tristetraprolin. *Science, 281*(5379), 1001–1005. https://doi.org/10.1126/science.281.5379.1001

Carrick, D. M., Lai, W. S., & Blackshear, P. J. (2004). The tandem CCCH zinc finger protein tristetraprolin and its relevance to cytokine mRNA turnover and arthritis. *Arthritis Research & Therapy, 6*(6), 248–264. https://doi.org/10.1186/ar1441

Castello, A., Fischer, B., Eichelbaum, K., Horos, R., Beckmann, B. M., Strein, C., Davey, N. E., Humphreys, D. T., Preiss, T., Steinmetz, L. M., Krijgsveld, J., & Hentze, M. W. (2012). Insights into RNA biology from an atlas of mammalian mRNA-binding proteins. *Cell, 149*(6), 1393–1406. https://doi.org/10.1016/j.cell.2012.04.031

Castello, A., Fischer, B., Frese, C. K., Horos, R., Alleaume, A. M., Foehr, S., Curk, T., Krijgsveld, J., & Hentze, M. W. (2016). Comprehensive identification of RNA-binding domains in human cells. *Molecular Cell, 63*(4), 696–710. https://doi.org/10.1016/j.molcel.2016.06.029

Clark, M. B., Johnston, R. L., Inostroza-Ponta, M., Fox, A. H., Fortini, E., Moscato, P., Dinger, M. E., & Mattick, J. S. (2012). Genome-wide analysis of long noncoding RNA stability. *Genome Research, 22*(5), 885–898. https://doi.org/10.1101/gr.131037.111

Cleynen, I., Brants, J. R., Peeters, K., Deckers, R., Debiec-Rychter, M., Sciot, R., Van de Ven, W. J., & Petit, M. M. (2007). HMGA2 regulates transcription of the Imp2 gene via an intronic regulatory element in cooperation with nuclear factor-kappaB. *Molecular Cancer Research : MCR, 5*(4), 363–372. https://doi.org/10.1158/1541-7786.MCR-06-0331

Clingman, C. C., Deveau, L. M., Hay, S. A., Genga, R. M., Shandilya, S. M., Massi, F., & Ryder, S. P. (2014). Allosteric inhibition of a stem cell RNA-binding protein by an intermediary metabolite. *eLife, 3*, e02848. https://doi.org/10.7554/eLife.02848

Coelho, M. A., de Carné Trécesson, S., Rana, S., Zecchin, D., Moore, C., Molina-Arcas, M., East, P., Spencer-Dene, B., Nye, E., Barnouin, K., Snijders, A. P., Lai, W. S., Blackshear, P. J., & Downward, J. (2017). Oncogenic RAS signaling promotes tumor immunoresistance by stabilizing PD-L1 mRNA. *Immunity, 47*(6), 1083–1099.e6. https://doi.org/10.1016/j.immuni.2017.11.016

Coltri, P. P., Dos Santos, M., & da Silva, G. (2019). Splicing and cancer: challenges and opportunities. *Wiley Interdisciplinary Reviews. RNA, 10*(3), e1527. https://doi.org/10.1002/wrna.1527

Cong, L., Ran, F. A., Cox, D., Lin, S., Barretto, R., Habib, N., Hsu, P. D., Wu, X., Jiang, W., Marraffini, L. A., & Zhang, F. (2013). Multiplex genome engineering using CRISPR/Cas systems. *Science, 339*(6121), 819–823. https://doi.org/10.1126/science.1231143

Conway, A. E., Van Nostrand, E. L., Pratt, G. A., Aigner, S., Wilbert, M. L., Sundararaman, B., Freese, P., Lambert, N. J., Sathe, S., Liang, T. Y., Essex, A., Landais, S., Burge, C. B., Jones, D. L., & Yeo, G. W. (2016). Enhanced CLIP uncovers IMP protein-RNA targets in human pluripotent stem cells important for cell adhesion and survival. *Cell Reports, 15*(3), 666–679. https://doi.org/10.1016/j.celrep.2016.03.052

Croce, A. C., Ferrigno, A., Santin, G., Piccolini, V. M., Bottiroli, G., & Vairetti, M. (2014). Autofluorescence of liver tissue and bile: organ functionality monitoring during ischemia and reoxygenation. *Lasers in Surgery and Medicine, 46*(5), 412–421. https://doi.org/10.1002/lsm.22241

Czepukojc, B., Abuhaliema, A., Barghash, A., Tierling, S., Naß, N., Simon, Y., Körbel, C., Cadenas, C., van Hul, N., Sachinidis, A., Hengstler, J. G., Helms, V., Laschke, M. W., Walter, J., Haybaeck, J., Leclercq, I., Kiemer, A. K., & Kessler, S. M. (2019). IGF2 mRNA binding protein 2 transgenic mice are more prone to develop a ductular reaction and to progress toward cirrhosis. *Frontiers in Medicine, 6*, 179. https://doi.org/10.3389/fmed.2019.00179

Dahlem, C. (2020). *In vitro and in vivo characterization of therapeutic approaches for solid tumors: natural compounds and novel targets* (Doctoral thesis, Saarland University, Saarbrücken, Germany). https://doi.org/10.22028/D291-32755

Dahlem, C., Abuhaliema, A., Kessler, S. M., Kröhler, T., Zoller, B., Chanda, S., Wu, Y., Both, S., Müller, F., Lepikhov, K., Kirsch, S. H., Laggai, S., Müller, R., Empting, M., & Kiemer, A. K. (2022). First small-molecule inhibitors targeting the RNA-binding protein IGF2BP2/IMP2 for cancer therapy. *ACS Chemical Biology, 17*(2), 361–375. https://doi.org/10.1021/acschembio.1c00833

Dahlem, C., Siow, W. X., Lopatniuk, M., Tse, W., Kessler, S. M., Kirsch, S. H., Hoppstädter, J., Vollmar, A. M., Müller, R., Luzhetskyy, A., Bartel, K., & Kiemer, A. K. (2020). Thioholgamide A, a new anti-proliferative anti-tumor agent, modulates macrophage polarization and metabolism. *Cancers, 12*(5), 1288. https://doi.org/10.3390/cancers12051288

Dai, N., Ji, F., Wright, J., Minichiello, L., Sadreyev, R., & Avruch, J. (2017). IGF2 mRNA binding protein-2 is a tumor promoter that drives cancer proliferation through its client mRNAs IGF2 and HMGA1. *eLife, 6*, e27155. https://doi.org/10.7554/eLife.27155

Dai, N., Zhao, L., Wrighting, D., Krämer, D., Majithia, A., Wang, Y., Cracan, V., Borges-Rivera, D., Mootha, V. K., Nahrendorf, M., Thorburn, D. R., Minichiello, L., Altshuler, D., & Avruch, J. (2015). IGF2BP2/IMP2-deficient mice resist obesity through enhanced translation of Ucp1 mRNA and other mRNAs encoding mitochondrial proteins. *Cell Metabolism, 21*(4), 609–621. https://doi.org/10.1016/j.cmet.2015.03.006

Dang, H., Takai, A., Forgues, M., Pomyen, Y., Mou, H., Xue, W., Ray, D., Ha, K., Morris, Q. D., Hughes, T. R., & Wang, X. W. (2017). Oncogenic activation of the RNA binding protein NELFE and MYC signaling in hepatocellular carcinoma. *Cancer Cell*, *32*(1), 101–114.e8. https://doi.org/10.1016/j.ccell.2017.06.002

Darnell R. B. (2010). HITS-CLIP: panoramic views of protein-RNA regulation in living cells. *Wiley Interdisciplinary Reviews. RNA, 1*(2), 266–286. https://doi.org/10.1002/wrna.31

Degrauwe, N., Suvà, M. L., Janiszewska, M., Riggi, N., & Stamenkovic, I. (2016). IMPs: an RNA-binding protein family that provides a link between stem cell maintenance in normal development and cancer. *Genes & Development, 30*(22), 2459–2474. https://doi.org/10.1101/gad.287540.116

Deltcheva, E., Chylinski, K., Sharma, C. M., Gonzales, K., Chao, Y., Pirzada, Z. A., Eckert, M. R., Vogel, J., & Charpentier, E. (2011). CRISPR RNA maturation by trans-encoded small RNA and host factor RNase III. *Nature, 471*(7340), 602–607. https://doi.org/10.1038/nature09886

Dembek, A., Laggai, S., Kessler, S. M., Czepukojc, B., Simon, Y., Kiemer, A. K., & Hoppstädter, J. (2017). Hepatic interleukin-6 production is maintained during endotoxin tolerance and facilitates lipid accumulation. *Immunobiology, 222*(6), 786–796. https://doi.org/10.1016/j.imbio.2017.01.003

Deng, X., Jiang, Q., Liu, Z., & Chen, W. (2020). Clinical significance of an m6A reader gene, IGF2BP2, in head and neck squamous cell carcinoma. *Frontiers in Molecular Biosciences, 7*, 68. https://doi.org/10.3389/fmolb.2020.00068

Derry, J. J., Richard, S., Valderrama Carvajal, H., Ye, X., Vasioukhin, V., Cochrane, A. W., Chen, T., & Tyner, A. L. (2000). Sik (BRK) phosphorylates Sam68 in the nucleus and negatively regulates its RNA binding ability. *Molecular and Cellular Biology, 20*(16), 6114–6126. https://doi.org/10.1128/MCB.20.16.6114-6126.2000

Dhanasekaran, R., Kooby, D. A., Staley, C. A., Kauh, J. S., Khanna, V., & Kim, H. S. (2010). Comparison of conventional transarterial chemoembolization (TACE) and chemoembolization with doxorubicin drug eluting beads (DEB) for unresectable hepatocelluar carcinoma (HCC). *Journal of Surgical Oncology, 101*(6), 476–480. https://doi.org/10.1002/jso.21522

Dhillon S. (2018). Regorafenib: a review in metastatic colorectal cancer. *Drugs, 78*(11), 1133–1144. https://doi.org/10.1007/s40265-018-0938-y

Dreyfuss, G., Kim, V. N., & Kataoka, N. (2002). Messenger-RNA-binding proteins and the messages they carry. *Nature Reviews. Molecular Cell Biology, 3*(3), 195–205. https://doi.org/10.1038/nrm760

Durbeej M. (2010). Laminins. *Cell and Tissue Research, 339*(1), 259–268. https://doi.org/10.1007/s00441-009-0838-2

El-Serag H. B. (2012). Surveillance for hepatocellular carcinoma: long way to achieve effectiveness. *Digestive Diseases and Sciences, 57*(12), 3050–3051. https://doi.org/10.1007/s10620-012-2413-z

El-Serag, H. B., & Rudolph, K. L. (2007). Hepatocellular carcinoma: epidemiology and molecular carcinogenesis. *Gastroenterology, 132*(7), 2557–2576. https://doi.org/10.1053/j.gastro.2007.04.061

Eslam, M., Newsome, P. N., Sarin, S. K., Anstee, Q. M., Targher, G., Romero-Gomez, M., Zelber-Sagi, S., Wai-Sun Wong, V., Dufour, J. F., Schattenberg, J. M., Kawaguchi, T., Arrese, M., Valenti, L., Shiha, G., Tiribelli, C., Yki-Järvinen, H., Fan, J. G., Grønbæk, H., Yilmaz, Y., Cortez-Pinto, H., … George, J. (2020). A new definition for metabolic dysfunction-associated fatty liver disease: an international expert consensus statement. *Journal of Hepatology, 73*(1), 202–209. https://doi.org/10.1016/j.jhep.2020.03.039

Essafi-Benkhadir, K., Onesto, C., Stebe, E., Moroni, C., & Pagès, G. (2007). Tristetraprolin inhibits Ras-dependent tumor vascularization by inducing vascular endothelial growth factor mRNA degradation. *Molecular Biology of the Cell, 18*(11), 4648–4658. https://doi.org/10.1091/mbc.e07-06-0570

Fabian, M. R., Frank, F., Rouya, C., Siddiqui, N., Lai, W. S., Karetnikov, A., Blackshear, P. J., Nagar, B., & Sonenberg, N. (2013). Structural basis for the recruitment of the human CCR4-NOT deadenylase complex by tristetraprolin. *Nature Structural & Molecular Biology, 20*(6), 735–739. https://doi.org/10.1038/nsmb.2572

Farazi, P. A., & DePinho, R. A. (2006). Hepatocellular carcinoma pathogenesis: from genes to environment. *Nature Reviews. Cancer, 6*(9), 674–687. https://doi.org/10.1038/nrc1934

Faye, M. D., & Holcik, M. (2015). The role of IRES trans-acting factors in carcinogenesis. *Biochimica et Biophysica Acta, 1849*(7), 887–897. https://doi.org/10.1016/j.bbagrm.2014.09.012

Fechir, M., Linker, K., Pautz, A., Hubrich, T., Förstermann, U., Rodriguez-Pascual, F., & Kleinert, H. (2005). Tristetraprolin regulates the expression of the human inducible nitric-oxide synthase gene. *Molecular Pharmacology, 67*(6), 2148–2161. https://doi.org/10.1124/mol.104.008763

Fenger-Grøn, M., Fillman, C., Norrild, B., & Lykke-Andersen, J. (2005). Multiple processing body factors and the ARE binding protein TTP activate mRNA decapping. *Molecular cell, 20*(6), 905–915. https://doi.org/10.1016/j.molcel.2005.10.031

Fengler, V. H., Macheiner, T., Kessler, S. M., Czepukojc, B., Gemperlein, K., Müller, R., Kiemer, A. K., Magnes, C., Haybaeck, J., Lackner, C., & Sargsyan, K. (2016). Susceptibility of different mouse wild type strains to develop diet-induced NAFLD/AFLD-associated liver disease. *PloS One, 11*(5), e0155163. https://doi.org/10.1371/journal.pone.0155163

Fidler, M. M., Soerjomataram, I., & Bray, F. (2016). A global view on cancer incidence and national levels of the human development index. *International Journal of Cancer, 139*(11), 2436–2446. https://doi.org/10.1002/ijc.30382

Fior, R., Póvoa, V., Mendes, R. V., Carvalho, T., Gomes, A., Figueiredo, N., & Ferreira, M. G. (2017). Single-cell functional and chemosensitive profiling of combinatorial colorectal therapy in zebrafish xenografts. *Proceedings of the National Academy of Sciences of the United States of America, 114*(39), E8234–E8243. https://doi.org/10.1073/pnas.1618389114

Fujii, Y., Kishi, Y., & Gotoh, Y. (2013). IMP2 regulates differentiation potentials of mouse neocortical neural precursor cells. *Genes to Cells : Devoted to Molecular & Cellular Mechanisms, 18*(2), 79–89. https://doi.org/10.1111/gtc.12024

Fujiwara, N., Friedman, S. L., Goossens, N., & Hoshida, Y. (2018). Risk factors and prevention of hepatocellular carcinoma in the era of precision medicine. *Journal of Hepatology, 68*(3), 526–549. https://doi.org/10.1016/j.jhep.2017.09.016

Gaba, A., Grivennikov, S. I., Do, M. V., Stumpo, D. J., Blackshear, P. J., & Karin, M. (2012). Cutting edge: IL-10-mediated tristetraprolin induction is part of a feedback loop that controls macrophage STAT3 activation and cytokine production. *Journal of Immunology, 189*(5), 2089–2093. https://doi.org/10.4049/jimmunol.1201126

Gao, Z., Harwig, A., Berkhout, B., & Herrera-Carrillo, E. (2017). Mutation of nucleotides around the +1 position of type 3 polymerase III promoters: The effect on transcriptional activity and start site usage. *Transcription, 8*(5), 275–287. https://doi.org/10.1080/21541264.2017.1322170

Gasiunas, G., Barrangou, R., Horvath, P., & Siksnys, V. (2012). Cas9-crRNA ribonucleoprotein complex mediates specific DNA cleavage for adaptive immunity in bacteria. *Proceedings of the National Academy of Sciences of the United States of America, 109*(39), E2579–E2586. https://doi.org/10.1073/pnas.1208507109

GBD 2019 Diseases and Injuries Collaborators (2020). Global burden of 369 diseases and injuries in 204 countries and territories, 1990-2019: a systematic analysis for the Global Burden of Disease Study 2019. *Lancet, 396*(10258), 1204–1222. https://doi.org/10.1016/S0140-6736(20)30925-9

Gebauer, F., Schwarzl, T., Valcárcel, J., & Hentze, M. W. (2021). RNA-binding proteins in human genetic disease. *Nature Reviews. Genetics, 22*(3), 185–198. https://doi.org/10.1038/s41576-020-00302-y

Gerstberger, S., Hafner, M., & Tuschl, T. (2014). A census of human RNA-binding proteins. *Nature Reviews. Genetics, 15*(12), 829–845. https://doi.org/10.1038/nrg3813

Ghasemi, R., Ghaffari, S. H., Momeny, M., Pirouzpanah, S., Yousefi, M., Malehmir, M., Alimoghaddam, K., & Ghavamzadeh, A. (2013). Multitargeting and antimetastatic potentials of silibinin in human HepG-2 and PLC/PRF/5 hepatoma cells. *Nutrition and Cancer, 65*(4), 590–599. https://doi.org/10.1080/01635581.2013.770043

Goddio, M. V., Gattelli, A., Slomiansky, V., Lacunza, E., Gingerich, T., Tocci, J. M., Facchinetti, M. M., Curino, A. C., LaMarre, J., Abba, M. C., & Kordon, E. C. (2012). Mammary differentiation induces expression of Tristetraprolin, a tumor suppressor AU-rich mRNA-binding protein. *Breast Cancer Research and Treatment, 135*(3), 749–758. https://doi.org/10.1007/s10549-012-2216-0

Graf, R., Li, X., Chu, V. T., & Rajewsky, K. (2019). sgRNA sequence motifs blocking efficient CRISPR/Cas9-mediated gene editing. *Cell Reports, 26*(5), 1098–1103.e3. https://doi.org/10.1016/j.celrep.2019.01.024

Greenwald, W. W., Chiou, J., Yan, J., Qiu, Y., Dai, N., Wang, A., Nariai, N., Aylward, A., Han, J. Y., Kadakia, N., Regue, L., Okino, M. L., Drees, F., Kramer, D., Vinckier, N., Minichiello, L., Gorkin, D., Avruch, J., Frazer, K. A., Sander, M., … Gaulton, K. J. (2019). Pancreatic islet chromatin accessibility and conformation reveals distal enhancer networks of type 2 diabetes risk. *Nature Communications, 10*(1), 2078. https://doi.org/10.1038/s41467-019-09975-4

Grishin N. V. (2001). KH domain: one motif, two folds. *Nucleic Acids Research, 29*(3), 638–643. https://doi.org/10.1093/nar/29.3.638

Gruber, A. R., Fallmann, J., Kratochvill, F., Kovarik, P., & Hofacker, I. L. (2011). AREsite: a database for the comprehensive investigation of AU-rich elements. *Nucleic Acids Research, 39*(Database issue), D66–D69. https://doi.org/10.1093/nar/gkq990

Gu, W., Katz, Z., Wu, B., Park, H. Y., Li, D., Lin, S., Wells, A. L., & Singer, R. H. (2012). Regulation of local expression of cell adhesion and motility-related mRNAs in breast cancer cells by IMP1/ZBP1. *Journal of Cell Science, 125*(Pt 1), 81–91. https://doi.org/10.1242/jcs.086132

Gu, W., Pan, F., & Singer, R. H. (2009). Blocking beta-catenin binding to the ZBP1 promoter represses ZBP1 expression, leading to increased proliferation and migration of

metastatic breast-cancer cells. *Journal of Cell Science, 122*(Pt 11), 1895–1905. https://doi.org/10.1242/jcs.045278

Guhaniyogi, J., & Brewer, G. (2001). Regulation of mRNA stability in mammalian cells. *Gene, 265*(1-2), 11–23. https://doi.org/10.1016/s0378-1119(01)00350-x

Guo, S., Chen, W., Luo, Y., Ren, F., Zhong, T., Rong, M., Dang, Y., Feng, Z., & Chen, G. (2015). Clinical implication of long non-coding RNA NEAT1 expression in hepatocellular carcinoma patients. *International Journal of Clinical and Experimental Pathology, 8*(5), 5395–5402.

Guo, X., Wu, Y., & Hartley, R. (2009). MicroRNA-125a represses cell growth by targeting HUR in breast cancer. *RNA Biology, 6*(5), 575-583. doi:10.4161/rna.6.5.10079

Gupta, R., Schrooders, Y., Hauser, D., van Herwijnen, M., Albrecht, W., Ter Braak, B., Brecklinghaus, T., Castell, J. V., Elenschneider, L., Escher, S., Guye, P., Hengstler, J. G., Ghallab, A., Hansen, T., Leist, M., Maclennan, R., Moritz, W., Tolosa, L., Tricot, T., Verfaillie, C., … Caiment, F. (2021). Comparing in vitro human liver models to in vivo human liver using RNA-Seq. *Archives of Toxicology, 95*(2), 573–589. https://doi.org/10.1007/s00204-020-02937-6

Gutschner, T., Hämmerle, M., Pazaitis, N., Bley, N., Fiskin, E., Uckelmann, H., Heim, A., Groβ, M., Hofmann, N., Geffers, R., Skawran, B., Longerich, T., Breuhahn, K., Schirmacher, P., Mühleck, B., Hüttelmaier, S., & Diederichs, S. (2014). Insulin-like growth factor 2 mRNA-binding protein 1 (IGF2BP1) is an important protumorigenic factor in hepatocellular carcinoma. *Hepatology, 59*(5), 1900–1911. https://doi.org/10.1002/hep.26997

Habjan, M., & Pichlmair, A. (2015). Cytoplasmic sensing of viral nucleic acids. *Current opinion in virology, 11*, 31–37. https://doi.org/10.1016/j.coviro.2015.01.012

Hafner, M., Landthaler, M., Burger, L., Khorshid, M., Hausser, J., Berninger, P., Rothballer, A., Ascano, M., Jr, Jungkamp, A. C., Munschauer, M., Ulrich, A., Wardle, G. S., Dewell, S., Zavolan, M., & Tuschl, T. (2010). Transcriptome-wide identification of RNA-binding protein and microRNA target sites by PAR-CLIP. *Cell, 141*(1), 129–141. https://doi.org/10.1016/j.cell.2010.03.009

Haghighat, A., & Sonenberg, N. (1997). eIF4G dramatically enhances the binding of eIF4E to the mRNA 5'-cap structure. *The Journal of Biological Chemistry, 272*(35), 21677–21680. https://doi.org/10.1074/jbc.272.35.21677

Hahn, R. T., Hoppstädter, J., Hirschfelder, K., Hachenthal, N., Diesel, B., Kessler, S. M., Huwer, H., & Kiemer, A. K. (2014). Downregulation of the glucocorticoid-induced leucine zipper (GILZ) promotes vascular inflammation. *Atherosclerosis, 234*(2), 391–400. https://doi.org/10.1016/j.atherosclerosis.2014.03.028

Han, K., Pierce, S. E., Li, A., Spees, K., Anderson, G. R., Seoane, J. A., Lo, Y. H., Dubreuil, M., Olivas, M., Kamber, R. A., Wainberg, M., Kostyrko, K., Kelly, M. R., Yousefi, M., Simpkins, S. W., Yao, D., Lee, K., Kuo, C. J., Jackson, P. K., Sweet-Cordero, A., … Bassik, M. C. (2020). CRISPR screens in cancer spheroids identify 3D growth-specific vulnerabilities. *Nature, 580*(7801), 136–141. https://doi.org/10.1038/s41586-020-2099-x

Hanahan D. (2022). Hallmarks of cancer: new dimensions. *Cancer Discovery, 12*(1), 31–46. https://doi.org/10.1158/2159-8290.CD-21-1059

Hanahan, D., & Weinberg, R. A. (2011). Hallmarks of cancer: the next generation. *Cell, 144*(5), 646–674. https://doi.org/10.1016/j.cell.2011.02.013

Hentze, M. W., Castello, A., Schwarzl, T., & Preiss, T. (2018). A brave new world of RNA-binding proteins. *Nature Reviews. Molecular Cell Biology, 19*(5), 327–341. https://doi.org/10.1038/nrm.2017.130

Hitti, E., Bakheet, T., Al-Souhibani, N., Moghrabi, W., Al-Yahya, S., Al-Ghamdi, M., Al-Saif, M., Shoukri, M. M., Lánczky, A., Grépin, R., Győrffy, B., Pagès, G., & Khabar, K. S. (2016). Systematic analysis of AU-rich element expression in cancer reveals common functional clusters regulated by key RNA-binding proteins. *Cancer research, 76*(14), 4068–4080. https://doi.org/10.1158/0008-5472.CAN-15-3110

Hoppstädter, J., Diesel, B., Eifler, L. K., Schmid, T., Brüne, B., & Kiemer, A. K. (2012). Glucocorticoid-induced leucine zipper is downregulated in human alveolar macrophages upon Toll-like receptor activation. *European Journal of Immunology, 42*(5), 1282–1293. https://doi.org/10.1002/eji.201142081

Horie, Y., Suzuki, A., Kataoka, E., Sasaki, T., Hamada, K., Sasaki, J., Mizuno, K., Hasegawa, G., Kishimoto, H., Iizuka, M., Naito, M., Enomoto, K., Watanabe, S., Mak, T. W., & Nakano, T. (2004). Hepatocyte-specific Pten deficiency results in steatohepatitis and hepatocellular carcinomas. *The Journal of Clinical Investigation, 113*(12), 1774–1783. https://doi.org/10.1172/JCI20513

Hosseini, K. (2017). *Pathomechanisms in hepatocellular carcinoma: characterisation of leukocyte recruitment, the role of the mRNA-binding protein tristetraprolin and nuclear paraspeckles* (Doctoral thesis, Saarland University, Saarbrücken, Germany). https://doi.org/10.22028/D291-27154

Hsu, I. C., Tokiwa, T., Bennett, W., Metcalf, R. A., Welsh, J. A., Sun, T., & Harris, C. C. (1993). p53 gene mutation and integrated hepatitis B viral DNA sequences in human liver cancer cell lines. *Carcinogenesis, 14*(5), 987–992. https://doi.org/10.1093/carcin/14.5.987

Hu, X., Peng, W. X., Zhou, H., Jiang, J., Zhou, X., Huang, D., Mo, Y. Y., & Yang, L. (2020). IGF2BP2 regulates DANCR by serving as an N6-methyladenosine reader. *Cell Death and Differentiation, 27*(6), 1782–1794. https://doi.org/10.1038/s41418-019-0461-z

Huang, H., Weng, H., Sun, W., Qin, X., Shi, H., Wu, H., Zhao, B. S., Mesquita, A., Liu, C., Yuan, C. L., Hu, Y. C., Hüttelmaier, S., Skibbe, J. R., Su, R., Deng, X., Dong, L., Sun, M., Li, C., Nachtergaele, S., Wang, Y., … Chen, J. (2018). Recognition of RNA N6-methyladenosine by IGF2BP proteins enhances mRNA stability and translation. *Nature Cell Biology, 20*(3), 285–295. https://doi.org/10.1038/s41556-018-0045-z

Huang, R., Han, M., Meng, L., & Chen, X. (2018). Transcriptome-wide discovery of coding and noncoding RNA-binding proteins. *Proceedings of the National Academy of Sciences of the United States of America, 115*(17), E3879–E3887. https://doi.org/10.1073/pnas.1718406115

Huang, S., Wu, Z., Cheng, Y., Wei, W., & Hao, L. (2019). Insulin-like growth factor 2 mRNA binding protein 2 promotes aerobic glycolysis and cell proliferation in pancreatic ductal adenocarcinoma via stabilizing GLUT1 mRNA. *Acta Biochimica et Biophysica Sinica, 51*(7), 743–752. https://doi.org/10.1093/abbs/gmz048

Hudson, B. P., Martinez-Yamout, M. A., Dyson, H. J., & Wright, P. E. (2004). Recognition of the mRNA AU-rich element by the zinc finger domain of TIS11d. *Nature Structural & Molecular Biology, 11*(3), 257–264. https://doi.org/10.1038/nsmb738

Hüttelmaier, S., Zenklusen, D., Lederer, M., Dictenberg, J., Lorenz, M., Meng, X., Bassell, G. J., Condeelis, J., & Singer, R. H. (2005). Spatial regulation of beta-actin translation by Src-dependent phosphorylation of ZBP1. *Nature, 438*(7067), 512–515. https://doi.org/10.1038/nature04115

Ibrahim, A., Hirschfeld, S., Cohen, M. H., Griebel, D. J., Williams, G. A., & Pazdur, R. (2004). FDA drug approval summaries: oxaliplatin. *The Oncologist, 9*(1), 8–12. https://doi.org/10.1634/theoncologist.9-1-8

Ishino, Y., Shinagawa, H., Makino, K., Amemura, M., & Nakata, A. (1987). Nucleotide sequence of the iap gene, responsible for alkaline phosphatase isozyme conversion in Escherichia coli, and identification of the gene product. *Journal of Bacteriology, 169*(12), 5429–5433. https://doi.org/10.1128/jb.169.12.5429-5433.1987

Jaitin, D. A., Kenigsberg, E., Keren-Shaul, H., Elefant, N., Paul, F., Zaretsky, I., Mildner, A., Cohen, N., Jung, S., Tanay, A., & Amit, I. (2014). Massively parallel single-cell RNA-seq for marker-free decomposition of tissues into cell types. *Science, 343*(6172), 776–779. https://doi.org/10.1126/science.1247651

Janiszewska, M., Suvà, M. L., Riggi, N., Houtkooper, R. H., Auwerx, J., Clément-Schatlo, V., Radovanovic, I., Rheinbay, E., Provero, P., & Stamenkovic, I. (2012). Imp2 controls oxidative phosphorylation and is crucial for preserving glioblastoma cancer stem cells. *Genes & Development, 26*(17), 1926–1944. https://doi.org/10.1101/gad.188292.112

Jansen, R., Embden, J. D., Gaastra, W., & Schouls, L. M. (2002). Identification of genes that are associated with DNA repeats in prokaryotes. *Molecular Microbiology, 43*(6), 1565–1575. https://doi.org/10.1046/j.1365-2958.2002.02839.x

Järvelin, A. I., Noerenberg, M., Davis, I., & Castello, A. (2016). The new (dis)order in RNA regulation. *Cell Communication and Signaling : CCS, 14*, 9. https://doi.org/10.1186/s12964-016-0132-3

Jeng, Y. M., Chang, C. C., Hu, F. C., Chou, H. Y., Kao, H. L., Wang, T. H., & Hsu, H. C. (2008). RNA-binding protein insulin-like growth factor II mRNA-binding protein 3 expression promotes tumor invasion and predicts early recurrence and poor prognosis in hepatocellular carcinoma. *Hepatology, 48*(4), 1118–1127. https://doi.org/10.1002/hep.22459

Jia, M., Gut, H., & Chao, J. A. (2018). Structural basis of IMP3 RRM12 recognition of RNA. R*NA, 24*(12), 1659–1666. https://doi.org/10.1261/rna.065649.118

Jinek, M., Chylinski, K., Fonfara, I., Hauer, M., Doudna, J. A., & Charpentier, E. (2012). A programmable dual-RNA-guided DNA endonuclease in adaptive bacterial immunity. *Science, 337*(6096), 816–821. https://doi.org/10.1126/science.1225829

Jurica, M. S., & Moore, M. J. (2003). Pre-mRNA splicing: awash in a sea of proteins. *Molecular Cell, 12*(1), 5–14. https://doi.org/10.1016/s1097-2765(03)00270-3J

Kanno, S., Kurauchi, K., Tomizawa, A., Yomogida, S., & Ishikawa, M. (2015). Pifithrin-alpha has a p53-independent cytoprotective effect on docosahexaenoic acid-induced cytotoxicity in human hepatocellular carcinoma HepG2 cells. *Toxicology Letters, 232*(2), 393–402. https://doi.org/10.1016/j.toxlet.2014.11.016

Karagozian, R., Derdák, Z., & Baffy, G. (2014). Obesity-associated mechanisms of hepatocarcinogenesis. *Metabolism: Clinical and Experimental, 63*(5), 607–617. https://doi.org/10.1016/j.metabol.2014.01.011

Kasprzak, A., & Adamek, A. (2019). Insulin-like growth factor 2 (IGF2) signaling in colorectal cancer-from basic research to potential clinical applications. *International Journal of Molecular Sciences, 20*(19), 4915. https://doi.org/10.3390/ijms20194915

Kessler, S. M., Hoppstädter, J., Hosseini, K., Laggai, S., Haybaeck, J., & Kiemer, A. K. (2019). Lack of Kupffer cell depletion in diethylnitrosamine-induced hepatic inflammation. *Journal of Hepatology, 70*(4), 813–815. https://doi.org/10.1016/j.jhep.2018.11.018

Kessler, S. M., Hosseini, K., Hussein, U. K., Kim, K. M., List, M., Schultheiß, C. S., Schulz, M. H., Laggai, S., Jang, K. Y., & Kiemer, A. K. (2019). Hepatocellular carcinoma and nuclear paraspeckles: induction in chemoresistance and prediction for poor survival. *Cellular Physiology and Biochemistry : International Journal of Experimental Cellular Physiology, Biochemistry, and Pharmacology, 52*(4), 787–801. https://doi.org/10.33594/000000055

Kessler, S. M., Laggai, S., Barghash, A., Helms, V., & Kiemer, A. K. (2014). Lipid metabolism signatures in NASH-associated HCC—Letter. *Cancer Research, 74*(10), 2903–2904. https://doi.org/10.1158/0008-5472.CAN-13-2852

Kessler, S. M., Laggai, S., Barghash, A., Schultheiss, C. S., Lederer, E., Artl, M., Helms, V., Haybaeck, J., & Kiemer, A. K. (2015). IMP2/p62 induces genomic instability and an aggressive hepatocellular carcinoma phenotype. *Cell Death & Disease, 6*(10), e1894. https://doi.org/10.1038/cddis.2015.241

Kessler, S. M., Lederer, E., Laggai, S., Golob-Schwarzl, N., Hosseini, K., Petzold, J., Schweiger, C., Reihs, R., Keil, M., Hoffmann, J., Mayr, C., Kiesslich, T., Pichler, M., Kim, K. S., Rhee, H., Park, Y. N., Lax, S., Obrist, P., Kiemer, A. K., & Haybaeck, J. (2017). IMP2/IGF2BP2 expression, but not IMP1 and IMP3, predicts poor outcome in patients and high tumor growth rate in xenograft models of gallbladder cancer. *Oncotarget, 8*(52), 89736–89745. https://doi.org/10.18632/oncotarget.21116

Kessler, S. M., Pokorny, J., Zimmer, V., Laggai, S., Lammert, F., Bohle, R. M., & Kiemer, A. K. (2013). IGF2 mRNA binding protein p62/IMP2-2 in hepatocellular carcinoma: antiapoptotic action is independent of IGF2/PI3K signaling. *American Journal of Physiology. Gastrointestinal and Liver Physiology, 304*(4), G328–G336. https://doi.org/10.1152/ajpgi.00005.2012

Kessler, S. M., Simon, Y., Gemperlein, K., Gianmoena, K., Cadenas, C., Zimmer, V., Pokorny, J., Barghash, A., Helms, V., van Rooijen, N., Bohle, R. M., Lammert, F., Hengstler, J. G., Mueller, R., Haybaeck, J., & Kiemer, A. K. (2014). Fatty acid elongation in non-alcoholic steatohepatitis and hepatocellular carcinoma. *International Journal of Molecular Sciences, 15*(4), 5762–5773. https://doi.org/10.3390/ijms15045762

Khabar K. S. (2017). Hallmarks of cancer and AU-rich elements. *Wiley Interdisciplinary Reviews. RNA, 8*(1), e1368. https://doi.org/10.1002/wrna.1368

Kröhler, T., Kessler, S. M., Hosseini, K., List, M., Barghash, A., Patial, S., Laggai, S., Gemperlein, K., Haybaeck, J., Müller, R., Helms, V., Schulz, M. H., Hoppstädter, J., Blackshear, P. J., & Kiemer, A. K. (2019). The mRNA-binding protein TTP/ZFP36 in hepatocarcinogenesis and hepatocellular carcinoma. *Cancers, 11*(11), 1754. https://doi.org/10.3390/cancers11111754

Kucukoglu, O., Sowa, J. P., Mazzolini, G. D., Syn, W. K., & Canbay, A. (2021). Hepatokines and adipokines in NASH-related hepatocellular carcinoma. *Journal of Hepatology, 74*(2), 442–457. https://doi.org/10.1016/j.jhep.2020.10.030

Laggai, S., Kessler, S. M., Boettcher, S., Lebrun, V., Gemperlein, K., Lederer, E., Leclercq, I. A., Mueller, R., Hartmann, R. W., Haybaeck, J., & Kiemer, A. K. (2014). The IGF2 mRNA binding protein p62/IGF2BP2-2 induces fatty acid elongation as a critical feature of steatosis. *Journal of Lipid Research, 55*(6), 1087–1097. https://doi.org/10.1194/jlr.M045500

Lai, W. S., Carballo, E., Strum, J. R., Kennington, E. A., Phillips, R. S., & Blackshear, P. J. (1999). Evidence that tristetraprolin binds to AU-rich elements and promotes the deadenylation and destabilization of tumor necrosis factor alpha mRNA. *Molecular and Cellular Biology, 19*(6), 4311–4323. https://doi.org/10.1128/MCB.19.6.4311

Lai, W. S., Stumpo, D. J., & Blackshear, P. J. (1990). Rapid insulin-stimulated accumulation of an mRNA encoding a proline-rich protein. *The Journal of Biological Chemistry, 265*(27), 16556–16563. https://doi.org/10.1016/S0021-9258(17)46259-4

Lee, F., & Ule, J. (2018). Advances in CLIP technologies for studies of protein-RNA interactions. *Molecular Cell, 69*(3), 354–369. https://doi.org/10.1016/j.molcel.2018.01.005

Lee, H. H., Kim, W. T., Kim, D. H., Park, J. W., Kang, T. H., Chung, J. W., & Leem, S. H. (2013). Tristetraprolin suppresses AHRR expression through mRNA destabilization. *FEBS Letters, 587*(10), 1518–1523. https://doi.org/10.1016/j.febslet.2013.03.031

Lee, H. H., Lee, S. R., & Leem, S. H. (2014). Tristetraprolin regulates prostate cancer cell growth through suppression of E2F1. *Journal of Microbiology and Biotechnology, 24*(2), 287–294. https://doi.org/10.4014/jmb.1309.09070

Lee, H. H., Son, Y. J., Lee, W. H., Park, Y. W., Chae, S. W., Cho, W. J., Kim, Y. M., Choi, H. J., Choi, D. H., Jung, S. W., Min, Y. J., Park, S. E., Lee, B. J., Cha, H. J., & Park, J. W. (2010). Tristetraprolin regulates expression of VEGF and tumorigenesis in human colon cancer. *International Journal of Cancer, 126*(8), 1817–1827. https://doi.org/10.1002/ijc.24847

Lee, H. H., Vo, M. T., Kim, H. J., Lee, U. H., Kim, C. W., Kim, H. K., Ko, M. S., Lee, W. H., Cha, S. J., Min, Y. J., Choi, D. H., Suh, H. S., Lee, B. J., Park, J. W., & Cho, W. J. (2010). Stability of the LATS2 tumor suppressor gene is regulated by tristetraprolin. *The Journal of Biological Chemistry, 285*(23), 17329–17337. https://doi.org/10.1074/jbc.M109.094235

Lee, J. Y., Kim, H. J., Yoon, N. A., Lee, W. H., Min, Y. J., Ko, B. K., Lee, B. J., Lee, A., Cha, H. J., Cho, W. J., & Park, J. W. (2013). Tumor suppressor p53 plays a key role in induction of both tristetraprolin and let-7 in human cancer cells. *Nucleic Acids Research, 41*(11), 5614-5625. https://doi.org/10.1093/nar/gkt222

Lee, S. C., & Abdel-Wahab, O. (2016). Therapeutic targeting of splicing in cancer. *Nature Medicine, 22*(9), 976–986. https://doi.org/10.1038/nm.4165

Li, B., & Dewey, C. N. (2011). RSEM: accurate transcript quantification from RNA-seq data with or without a reference genome. *BMC Bioinformatics, 12*, 323. https://doi.org/10.1186/1471-2105-12-323

Li, F., Tiede, B., Massagué, J., & Kang, Y. (2007). Beyond tumorigenesis: cancer stem cells in metastasis. *Cell Research, 17*(1), 3–14. https://doi.org/10.1038/sj.cr.7310118

Li, L., & Wang, H. (2016). Heterogeneity of liver cancer and personalized therapy. *Cancer Letters, 379*(2), 191–197. https://doi.org/10.1016/j.canlet.2015.07.018

Li, T., Hu, P. S., Zuo, Z., Lin, J. F., Li, X., Wu, Q. N., Chen, Z. H., Zeng, Z. L., Wang, F., Zheng, J., Chen, D., Li, B., Kang, T. B., Xie, D., Lin, D., Ju, H. Q., & Xu, R. H. (2019). METTL3 facilitates tumor progression via an m6A-IGF2BP2-dependent mechanism in colorectal carcinoma. *Molecular cancer, 18*(1), 112. https://doi.org/10.1186/s12943-019-1038-7

Li, T., Li, S., Chen, D., Chen, B., Yu, T., Zhao, F., Wang, Q., Yao, M., Huang, S., Chen, Z., & He, X. (2017). Transcriptomic analyses of RNA-binding proteins reveal eIF3c promotes cell proliferation in hepatocellular carcinoma. *Cancer Science, 108*(5), 877–885. https://doi.org/10.1111/cas.13209

Li, X. M., Tang, Z. Y., Zhou, G., Lui, Y. K., & Ye, S. L. (1998). Significance of vascular endothelial growth factor mRNA expression in invasion and metastasis of hepatocellular carcinoma. *Journal of Experimental & Clinical Cancer Research : CR, 17*(1), 13–17.

Li, Y., Francia, G., & Zhang, J. Y. (2015). p62/IMP2 stimulates cell migration and reduces cell adhesion in breast cancer. *Oncotarget, 6*(32), 32656–32668. https://doi.org/10.18632/oncotarget.5328

Li, Y., Pang, Y., Xiang, X., Du, J., Mai, K., & Ai, Q. (2019). Molecular cloning, characterization, and nutritional regulation of Elovl6 in large yellow Croaker (Larimichthys crocea). *International Journal of Molecular Sciences, 20*(7), 1801. https://doi.org/10.3390/ijms20071801

Liang, X., Potter, J., Kumar, S., Zou, Y., Quintanilla, R., Sridharan, M., Carte, J., Chen, W., Roark, N., Ranganathan, S., Ravinder, N., & Chesnut, J. D. (2015). Rapid and highly efficient mammalian cell engineering via Cas9 protein transfection. *Journal of Biotechnology, 208*, 44–53. https://doi.org/10.1016/j.jbiotec.2015.04.024

Lindeboom, R. G., Supek, F., & Lehner, B. (2016). The rules and impact of nonsense-mediated mRNA decay in human cancers. *Nature Genetics, 48*(10), 1112–1118. https://doi.org/10.1038/ng.3664

Liu, H. B., Muhammad, T., Guo, Y., Li, M. J., Sha, Q. Q., Zhang, C. X., Liu, H., Zhao, S. G., Zhao, H., Zhang, H., Du, Y. Z., Sun, K., Liu, K., Lu, G., Guo, X. J., Sha, J., Fan, H. Y., Gao, F., & Chen, Z. J. (2019). RNA-binding protein IGF2BP2/IMP2 is a critical maternal activator in early zygotic genome activation. *Advanced Science, 6*(15), 1900295. https://doi.org/10.1002/advs.201900295

Liu, W., Li, Z., Xu, W., Wang, Q., & Yang, S. (2013). Humoral autoimmune response to IGF2 mRNA-binding protein (IMP2/p62) and its tissue-specific expression in colon cancer. *Scandinavian journal of immunology, 77*(4), 255–260. https://doi.org/10.1111/sji.12032

Lourou, N., Gavriilidis, M., & Kontoyiannis, D. L. (2019). Lessons from studying the AU-rich elements in chronic inflammation and autoimmunity. *Journal of Autoimmunity, 104*, 102334. https://doi.org/10.1016/j.jaut.2019.102334

Lu, M., Nakamura, R. M., Dent, E. D., Zhang, J. Y., Nielsen, F. C., Christiansen, J., Chan, E. K., & Tan, E. M. (2001). Aberrant expression of fetal RNA-binding protein p62 in liver cancer and liver cirrhosis. *The American Journal of Pathology, 159*(3), 945–953. https://doi.org/10.1016/S0002-9440(10)61770-1

Lu, S., Han, L., Hu, X., Sun, T., Xu, D., Li, Y., Chen, Q., Yao, W., He, M., Wang, Z., Wu, H., & Wei, M. (2021). N6-methyladenosine reader IMP2 stabilizes the ZFAS1/OLA1 axis and activates the Warburg effect: implication in colorectal cancer. *Journal of Hematology & Oncology, 14*(1), 188. https://doi.org/10.1186/s13045-021-01204-0

Lu, Y., Xue, J., Deng, T., Zhou, X., Yu, K., Deng, L., Huang, M., Yi, X., Liang, M., Wang, Y., Shen, H., Tong, R., Wang, W., Li, L., Song, J., Li, J., Su, X., Ding, Z., Gong, Y., Zhu, J., … Mok, T. (2020). Safety and feasibility of CRISPR-edited T cells in patients with refractory non-small-cell lung cancer. *Nature Medicine, 26*(5), 732–740. https://doi.org/10.1038/s41591-020-0840-5

Lukong, K. E., Chang, K. W., Khandjian, E. W., & Richard, S. (2008). RNA-binding proteins in human genetic disease. *Trends in Genetics : TIG, 24*(8), 416–425. https://doi.org/10.1016/j.tig.2008.05.004

Lunde, B. M., Moore, C., & Varani, G. (2007). RNA-binding proteins: modular design for efficient function. *Nature Reviews. Molecular Cell Biology, 8*(6), 479–490. https://doi.org/10.1038/nrm2178

Lykke-Andersen, J., & Wagner, E. (2005). Recruitment and activation of mRNA decay enzymes by two ARE-mediated decay activation domains in the proteins TTP and BRF-1. *Genes & Development, 19*(3), 351–361. https://doi.org/10.1101/gad.1282305

Ma, H., Wu, Y., Dang, Y., Choi, J. G., Zhang, J., & Wu, H. (2014). Pol III promoters to express small RNAs: delineation of transcription initiation. *Molecular Therapy - Nucleic Acids, 3*(5), e161. https://doi.org/10.1038/mtna.2014.12

Maeder, M. L., Stefanidakis, M., Wilson, C. J., Baral, R., Barrera, L. A., Bounoutas, G. S., Bumcrot, D., Chao, H., Ciulla, D. M., DaSilva, J. A., Dass, A., Dhanapal, V., Fennell, T. J., Friedland, A. E., Giannoukos, G., Gloskowski, S. W., Glucksmann, A., Gotta, G. M., Jayaram, H., Haskett, S. J., … Jiang, H. (2019). Development of a gene-editing approach to restore vision loss in Leber congenital amaurosis type 10. *Nature Medicine, 25*(2), 229-233. https://doi.org/10.1038/s41591-018-0327-9

Makarova, K. S., Wolf, Y. I., Alkhnbashi, O. S., Costa, F., Shah, S. A., Saunders, S. J., Barrangou, R., Brouns, S. J., Charpentier, E., Haft, D. H., Horvath, P., Moineau, S., Mojica, F. J., Terns, R. M., Terns, M. P., White, M. F., Yakunin, A. F., Garrett, R. A., van der Oost, J., Backofen, R., … Koonin, E. V. (2015). An updated evolutionary classification of CRISPR-Cas systems. *Nature Reviews. Microbiology, 13*(11), 722–736. https://doi.org/10.1038/nrmicro3569

Makarova, K. S., Wolf, Y. I., Iranzo, J., Shmakov, S. A., Alkhnbashi, O. S., Brouns, S., Charpentier, E., Cheng, D., Haft, D. H., Horvath, P., Moineau, S., Mojica, F., Scott, D., Shah, S. A., Siksnys, V., Terns, M. P., Venclovas, Č., White, M. F., Yakunin, A. F., Yan, W., … Koonin, E. V. (2020). Evolutionary classification of CRISPR-Cas systems: a burst of class 2 and derived variants. *Nature Reviews. Microbiology, 18*(2), 67–83. https://doi.org/10.1038/s41579-019-0299-x

Mali, P., Yang, L., Esvelt, K. M., Aach, J., Guell, M., DiCarlo, J. E., Norville, J. E., & Church, G. M. (2013). RNA-guided human genome engineering via Cas9. *Science, 339*(6121), 823-826. https://doi.org/10.1126/science.1232033

Mansoori, B., Mohammadi, A., Ditzel, H. J., Duijf, P., Khaze, V., Gjerstorff, M. F., & Baradaran, B. (2021). HMGA2 as a critical regulator in cancer development. *Genes, 12*(2), 269. https://doi.org/10.3390/genes12020269

Matsui, A., Uchida, S., Ishii, T., Itaka, K., & Kataoka, K. (2015). Messenger RNA-based therapeutics for the treatment of apoptosis-associated diseases. *Scientific Reports, 5*, 15810. https://doi.org/10.1038/srep15810

Matsuzaka, T., Atsumi, A., Matsumori, R., Nie, T., Shinozaki, H., Suzuki-Kemuriyama, N., Kuba, M., Nakagawa, Y., Ishii, K., Shimada, M., Kobayashi, K., Yatoh, S., Takahashi, A., Takekoshi, K., Sone, H., Yahagi, N., Suzuki, H., Murata, S., Nakamuta, M., Yamada, N., … Shimano, H. (2012). Elovl6 promotes nonalcoholic steatohepatitis. *Hepatology, 56*(6), 2199–2208. https://doi.org/10.1002/hep.25932

Mayr, C., & Bartel, D. P. (2009). Widespread shortening of 3'UTRs by alternative cleavage and polyadenylation activates oncogenes in cancer cells. *Cell, 138*(4), 673–684. https://doi.org/10.1016/j.cell.2009.06.016

McMahon, A. C., Rahman, R., Jin, H., Shen, J. L., Fieldsend, A., Luo, W., & Rosbash, M. (2016). TRIBE: Hijacking an RNA-editing enzyme to identify cell-specific targets of RNA-binding proteins. *Cell, 165*(3), 742–753. https://doi.org/10.1016/j.cell.2016.03.007

Milke, L., Schulz, K., Weigert, A., Sha, W., Schmid, T., & Brüne, B. (2013). Depletion of tristetraprolin in breast cancer cells increases interleukin-16 expression and promotes tumor infiltration with monocytes/macrophages. *Carcinogenesis, 34*(4), 850–857. https://doi.org/10.1093/carcin/bgs387

Mínguez, B., Hoshida, Y., Villanueva, A., Toffanin, S., Cabellos, L., Thung, S., Mandeli, J., Sia, D., April, C., Fan, J. B., Lachenmayer, A., Savic, R., Roayaie, S., Mazzaferro, V., Bruix, J., Schwartz, M., Friedman, S. L., & Llovet, J. M. (2011). Gene-expression signature of vascular invasion in hepatocellular carcinoma. *Journal of Hepatology, 55*(6), 1325–1331. https://doi.org/10.1016/j.jhep.2011.02.034

Mitchell, S. F., & Parker, R. (2014). Principles and properties of eukaryotic mRNPs. *Molecular cell, 54*(4), 547–558. https://doi.org/10.1016/j.molcel.2014.04.033

Mohibi, S., Chen, X., & Zhang, J. (2019). Cancer the'RBP'eutics-RNA-binding proteins as therapeutic targets for cancer. *Pharmacology & Therapeutics, 203*, 107390. https://doi.org/10.1016/j.pharmthera.2019.07.001

Mojica, F. J., Díez-Villaseñor, C., García-Martínez, J., & Soria, E. (2005). Intervening sequences of regularly spaced prokaryotic repeats derive from foreign genetic elements. *Journal of Molecular Evolution, 60*(2), 174–182. https://doi.org/10.1007/s00239-004-0046-3

Mojica, F. J., Díez-Villaseñor, C., Soria, E., & Juez, G. (2000). Biological significance of a family of regularly spaced repeats in the genomes of Archaea, Bacteria and mitochondria. *Molecular Microbiology, 36*(1), 244–246. https://doi.org/10.1046/j.1365-2958.2000.01838.x

Montorsi, L., Guizzetti, F., Alecci, C., Caporali, A., Martello, A., Atene, C. G., Parenti, S., Pizzini, S., Zanovello, P., Bortoluzzi, S., Ferrari, S., Grande, A., & Zanocco-Marani, T. (2016). Loss of ZFP36 expression in colorectal cancer correlates to wnt/ß-catenin activity and enhances epithelial-to-mesenchymal transition through upregulation of ZEB1, SOX9 and MACC1. *Oncotarget, 7*(37), 59144–59157. https://doi.org/10.18632/oncotarget.10828

Mu, Q., Wang, L., Yu, F., Gao, H., Lei, T., Li, P., Liu, P., Zheng, X., Hu, X., Chen, Y., Jiang, Z., Sayari, A. J., Shen, J., & Huang, H. (2015). Imp2 regulates GBM progression by activating IGF2/PI3K/Akt pathway. *Cancer Biology & Therapy, 16*(4), 623–633. https://doi.org/10.1080/15384047.2015.1019185

Mucci, L. A., Kuper, H. E., Tamimi, R., Lagiou, P., Spanos, E., & Trichopoulos, D. (2001). Age at menarche and age at menopause in relation to hepatocellular carcinoma in women. *BJOG : An International Journal of Obstetrics and Gynaecology, 108*(3), 291–294. https://doi.org/10.1111/j.1471-0528.2001.00032.x

Mukherjee, N., Jacobs, N. C., Hafner, M., Kennington, E. A., Nusbaum, J. D., Tuschl, T., Blackshear, P. J., & Ohler, U. (2014). Global target mRNA specification and regulation by the RNA-binding protein ZFP36. *Genome Biology, 15*(1), R12. https://doi.org/10.1186/gb-2014-15-1-r12

Naugler, W. E., Sakurai, T., Kim, S., Maeda, S., Kim, K., Elsharkawy, A. M., & Karin, M. (2007). Gender disparity in liver cancer due to sex differences in MyD88-dependent IL-6 production. *Science, 317*(5834), 121–124. https://doi.org/10.1126/science.1140485

Neelamraju, Y., Gonzalez-Perez, A., Bhat-Nakshatri, P., Nakshatri, H., & Janga, S. C. (2018). Mutational landscape of RNA-binding proteins in human cancers. *RNA Biology, 15*(1), 115–129. https://doi.org/10.1080/15476286.2017.1391436

Nidhi, S., Anand, U., Oleksak, P., Tripathi, P., Lal, J. A., Thomas, G., Kuca, K., & Tripathi, V. (2021). Novel CRISPR-Cas systems: an updated review of the current achievements, applications, and future research perspectives. *International Journal of Molecular Sciences, 22*(7), 3327. https://doi.org/10.3390/ijms22073327

Nielsen, J., Adolph, S. K., Rajpert-De Meyts, E., Lykke-Andersen, J., Koch, G., Christiansen, J., & Nielsen, F. C. (2003). Nuclear transit of human zipcode-binding protein IMP1. *The Biochemical Journal, 376*(Pt 2), 383–391. https://doi.org/10.1042/BJ20030943

Nielsen, J., Christiansen, J., Lykke-Andersen, J., Johnsen, A. H., Wewer, U. M., & Nielsen, F. C. (1999). A family of insulin-like growth factor II mRNA-binding proteins represses translation in late development. *Molecular and Cellular Biology, 19*(2), 1262–1270. https://doi.org/10.1128/MCB.19.2.1262

Nuñez, J. K., Harrington, L. B., Kranzusch, P. J., Engelman, A. N., & Doudna, J. A. (2015). Foreign DNA capture during CRISPR-Cas adaptive immunity. *Nature, 527*(7579), 535-538. https://doi.org/10.1038/nature15760

Otsuka, H., Fukao, A., Funakami, Y., Duncan, K. E., & Fujiwara, T. (2019). Emerging evidence of translational control by AU-rich element-binding proteins. *Frontiers in Genetics, 10*, 332. https://doi.org/10.3389/fgene.2019.00332

Park, J. M., Lee, T. H., & Kang, T. H. (2018). Roles of tristetraprolin in tumorigenesis. *International Journal of Molecular Sciences, 19*(11), 3384. https://doi.org/10.3390/ijms19113384

Park, S. B., Lee, J. H., Jeong, W. W., Kim, Y. H., Cha, H. J., Joe, Y., Chung, H. T., Cho, W. J., Do, J. W., Lee, B. J., Park, J. W., & Ko, B. K. (2015). TTP mediates cisplatin-induced apoptosis of head and neck cancer cells by down-regulating the expression of Bcl-2. *Journal of Chemotherapy, 27*(3), 174–180. https://doi.org/10.1179/1973947814Y.0000000234

Patial, S., & Blackshear, P. J. (2016). Tristetraprolin as a therapeutic target in inflammatory disease. *Trends in Pharmacological Sciences, 37*(10), 811–821. https://doi.org/10.1016/j.tips.2016.07.002P

Perez-Perri, J. I., Noerenberg, M., Kamel, W., Lenz, C. E., Mohammed, S., Hentze, M. W., & Castello, A. (2021). Global analysis of RNA-binding protein dynamics by comparative and enhanced RNA interactome capture. *Nature Protocols, 16*(1), 27–60. https://doi.org/10.1038/s41596-020-00404-1

Piqué, L., Martinez de Paz, A., Piñeyro, D., Martínez-Cardús, A., Castro de Moura, M., Llinàs-Arias, P., Setien, F., Gomez-Miragaya, J., Gonzalez-Suarez, E., Sigurdsson, S., Jonasson, J. G., Villanueva, A., Vidal, A., Davalos, V., & Esteller, M. (2019). Epigenetic inactivation of the splicing RNA-binding protein CELF2 in human breast cancer. *Oncogene, 38*(45), 7106–7112. https://doi.org/10.1038/s41388-019-0936-x

Probert, L., Akassoglou, K., Alexopoulou, L., Douni, E., Haralambous, S., Hill, S., Kassiotis, G., Kontoyiannis, D., Pasparakis, M., Plows, D., & Kollias, G. (1996). Dissection of the pathologies induced by transmembrane and wild-type tumor necrosis factor in transgenic mice. *Journal of Leukocyte Biology, 59*(4), 518–525. https://doi.org/10.1002/jlb.59.4.518

Qiu, L. Q., Stumpo, D. J., & Blackshear, P. J. (2012). Myeloid-specific tristetraprolin deficiency in mice results in extreme lipopolysaccharide sensitivity in an otherwise minimal phenotype. *Journal of Immunology, 188*(10), 5150–5159. https://doi.org/10.4049/jimmunol.1103700

Queiroz, R., Smith, T., Villanueva, E., Marti-Solano, M., Monti, M., Pizzinga, M., Mirea, D. M., Ramakrishna, M., Harvey, R. F., Dezi, V., Thomas, G. H., Willis, A. E., & Lilley, K. S. (2019). Comprehensive identification of RNA-protein interactions in any organism using orthogonal organic phase separation (OOPS). *Nature Biotechnology, 37*(2), 169–178. https://doi.org/10.1038/s41587-018-0001-2

Ramachandran, P., Pellicoro, A., Vernon, M. A., Boulter, L., Aucott, R. L., Ali, A., Hartland, S. N., Snowdon, V. K., Cappon, A., Gordon-Walker, T. T., Williams, M. J., Dunbar, D. R., Manning, J. R., van Rooijen, N., Fallowfield, J. A., Forbes, S. J., & Iredale, J. P. (2012). Differential Ly-6C expression identifies the recruited macrophage phenotype, which orchestrates the regression of murine liver fibrosis. *Proceedings of the National Academy of Sciences of the United States of America, 109*(46), E3186–E3195. https://doi.org/10.1073/pnas.1119964109

Ramanathan, M., Porter, D. F., & Khavari, P. A. (2019). Methods to study RNA-protein interactions. *Nature methods, 16*(3), 225–234. https://doi.org/10.1038/s41592-019-0330-1

Reeves, H. L., Zaki, M. Y., & Day, C. P. (2016). Hepatocellular carcinoma in obesity, type 2 diabetes, and NAFLD. *Digestive Diseases and Sciences, 61*(5), 1234–1245. https://doi.org/10.1007/s10620-016-4085-6R

Rehwinkel J. (2013). RNA sensing: the more RIG-I the merrier?. *EMBO Reports, 14*(9), 751–752. https://doi.org/10.1038/embor.2013.120

Rho, J., Choi, S., Jung, C. R., & Im, D. S. (2007). Arginine methylation of Sam68 and SLM proteins negatively regulates their poly(U) RNA binding activity. *Archives of Biochemistry and Biophysics, 466*(1), 49–57. https://doi.org/10.1016/j.abb.2007.07.017

Rino, J., & Carmo-Fonseca, M. (2009). The spliceosome: a self-organized macromolecular machine in the nucleus?. *Trends in Cell Biology, 19*(8), 375–384. https://doi.org/10.1016/j.tcb.2009.05.004

Roessler, S., Jia, H. L., Budhu, A., Forgues, M., Ye, Q. H., Lee, J. S., Thorgeirsson, S. S., Sun, Z., Tang, Z. Y., Qin, L. X., & Wang, X. W. (2010). A unique metastasis gene signature enables prediction of tumor relapse in early-stage hepatocellular carcinoma patients. *Cancer Research, 70*(24), 10202–10212. https://doi.org/10.1158/0008-5472.CAN-10-2607

Ruggero D. (2013). Translational control in cancer etiology. *Cold Spring Harbor Perspectives in Biology, 5*(2), a012336. https://doi.org/10.1101/cshperspect.a012336

Sanduja, S., Blanco, F. F., Young, L. E., Kaza, V., & Dixon, D. A. (2012). The role of tristetraprolin in cancer and inflammation. *Frontiers in Bioscience (Landmark edition), 17*(1), 174–188. https://doi.org/10.2741/3920

Sanduja, S., Kaza, V., & Dixon, D. A. (2009). The mRNA decay factor tristetraprolin (TTP) induces senescence in human papillomavirus-transformed cervical cancer cells by targeting E6-AP ubiquitin ligase. *Aging, 1*(9), 803–817. https://doi.org/10.18632/aging.100086

Sapranauskas, R., Gasiunas, G., Fremaux, C., Barrangou, R., Horvath, P., & Siksnys, V. (2011). The Streptococcus thermophilus CRISPR/Cas system provides immunity in Escherichia coli. *Nucleic Acids Research, 39*(21), 9275–9282. https://doi.org/10.1093/nar/gkr606

Sawicki, K. T., Chang, H. C., Shapiro, J. S., Bayeva, M., De Jesus, A., Finck, B. N., Wertheim, J. A., Blackshear, P. J., & Ardehali, H. (2018). Hepatic tristetraprolin promotes insulin resistance through RNA destabilization of FGF21. *JCI Insight, 3*(13), e95948. https://doi.org/10.1172/jci.insight.95948

Saxena, R., Voight, B. F., Lyssenko, V., Burtt, N. P., de Bakker, P. I., Chen, H., Roix, J. J., Kathiresan, S., Hirschhorn, J. N., Daly, M. J., Hughes, T. E., Groop, L., Altshuler, D., Almgren, P., Florez, J. C., Meyer, J., Ardlie, K., Bengtsson Boström, K., Isomaa, B., … Purcell, S. (2007). Genome-wide association analysis identifies loci for type 2 diabetes and triglyceride levels. *Science, 316*(5829), 1331–1336. https://doi.org/10.1126/science.1142358

Schaeffer, V., Hansen, K. M., Morris, D. R., LeBoeuf, R. C., & Abrass, C. K. (2012). RNA-binding protein IGF2BP2/IMP2 is required for laminin-β2 mRNA translation and is modulated by glucose concentration. *American Journal of Physiology. Renal Physiology, 303*(1), F75-F82. https://doi.org/10.1152/ajprenal.00185.2012

Scholefield, J., & Harrison, P. T. (2021). Prime editing - an update on the field. *Gene Therapy, 28*(7-8), 396–401. https://doi.org/10.1038/s41434-021-00263-9

Schultheiss, C. S., Laggai, S., Czepukojc, B., Hussein, U. K., List, M., Barghash, A., Tierling, S., Hosseini, K., Golob-Schwarzl, N., Pokorny, J., Hachenthal, N., Schulz, M., Helms, V., Walter, J., Zimmer, V., Lammert, F., Bohle, R. M., Dandolo, L., Haybaeck, J., Kiemer, A. K., … Kessler, S. M. (2017). The long non-coding RNA H19 suppresses carcinogenesis and chemoresistance in hepatocellular carcinoma. *Cell Stress, 1*(1), 37–54. https://doi.org/10.15698/cst2017.10.105

Schwarz, J. M., Cooper, D. N., Schuelke, M., & Seelow, D. (2014). MutationTaster2: mutation prediction for the deep-sequencing age. *Nature Methods, 11*(4), 361–362. https://doi.org/10.1038/nmeth.2890

Scott, L. J., Mohlke, K. L., Bonnycastle, L. L., Willer, C. J., Li, Y., Duren, W. L., Erdos, M. R., Stringham, H. M., Chines, P. S., Jackson, A. U., Prokunina-Olsson, L., Ding, C. J., Swift, A. J., Narisu, N., Hu, T., Pruim, R., Xiao, R., Li, X. Y., Conneely, K. N., Riebow, N. L., … Boehnke, M. (2007). A genome-wide association study of type 2 diabetes in Finns detects multiple susceptibility variants. *Science, 316*(5829), 1341–1345. https://doi.org/10.1126/science.1142382

Sebestyén, E., Singh, B., Miñana, B., Pagès, A., Mateo, F., Pujana, M. A., Valcárcel, J., & Eyras, E. (2016). Large-scale analysis of genome and transcriptome alterations in multiple tumors unveils novel cancer-relevant splicing networks. *Genome Research, 26*(6), 732–744. https://doi.org/10.1101/gr.199935.115

Selmi, T., Alecci, C., dell' Aquila, M., Montorsi, L., Martello, A., Guizzetti, F., Volpi, N., Parenti, S., Ferrari, S., Salomoni, P., Grande, A., & Zanocco-Marani, T. (2015). ZFP36 stabilizes RIP1 via degradation of XIAP and cIAP2 thereby promoting ripoptosome assembly. *BMC Cancer, 15*, 357. https://doi.org/10.1186/s12885-015-1388-5

Shchepachev, V., Bresson, S., Spanos, C., Petfalski, E., Fischer, L., Rappsilber, J., & Tollervey, D. (2019). Defining the RNA interactome by total RNA-associated protein purification. *Molecular Systems Biology, 15*(4), e8689. https://doi.org/10.15252/msb.20188689

Simon, Y., Kessler, S. M., Bohle, R. M., Haybaeck, J., & Kiemer, A. K. (2014). The insulin-like growth factor 2 (IGF2) mRNA-binding protein p62/IGF2BP2-2 as a promoter of NAFLD and HCC?. *Gut, 63*(5), 861–863. https://doi.org/10.1136/gutjnl-2013-305736

Simon, Y., Kessler, S. M., Gemperlein, K., Bohle, R. M., Müller, R., Haybaeck, J., & Kiemer, A. K. (2014). Elevated free cholesterol in a p62 overexpression model of non-alcoholic steatohepatitis. *World Journal of Gastroenterology, 20*(47), 17839–17850. https://doi.org/10.3748/wjg.v20.i47.17839

Singh, G., Pratt, G., Yeo, G. W., & Moore, M. J. (2015). The Clothes Make the mRNA: Past and Present Trends in mRNP Fashion. *Annual Review of Biochemistry, 84*, 325–354. https://doi.org/10.1146/annurev-biochem-080111-092106

Smith, T., Villanueva, E., Queiroz, R., Dawson, C. S., Elzek, M., Urdaneta, E. C., Willis, A. E., Beckmann, B. M., Krijgsveld, J., & Lilley, K. S. (2020). Organic phase separation opens up new opportunities to interrogate the RNA-binding proteome. *Current Opinion in Chemical Biology, 54*, 70–75. https://doi.org/10.1016/j.cbpa.2020.01.009

Smits, A. H., Ziebell, F., Joberty, G., Zinn, N., Mueller, W. F., Clauder-Münster, S., Eberhard, D., Fälth Savitski, M., Grandi, P., Jakob, P., Michon, A. M., Sun, H., Tessmer, K., Bürckstümmer, T., Bantscheff, M., Steinmetz, L. M., Drewes, G., & Huber, W. (2019). Biological plasticity rescues target activity in CRISPR knock outs. *Nature Methods, 16*(11), 1087–1093. https://doi.org/10.1038/s41592-019-0614-5

Sohn, B. H., Park, I. Y., Lee, J. J., Yang, S. J., Jang, Y. J., Park, K. C., Kim, D. J., Lee, D. C., Sohn, H. A., Kim, T. W., Yoo, H. S., Choi, J. Y., Bae, Y. S., & Yeom, Y. I. (2010). Functional switching of TGF-beta1 signaling in liver cancer via epigenetic modulation of a single CpG site in TTP promoter. *Gastroenterology, 138*(5), 1898–1908. https://doi.org/10.1053/j.gastro.2009.12.044

Stadtmauer, E. A., Fraietta, J. A., Davis, M. M., Cohen, A. D., Weber, K. L., Lancaster, E., Mangan, P. A., Kulikovskaya, I., Gupta, M., Chen, F., Tian, L., Gonzalez, V. E., Xu, J., Jung, I. Y., Melenhorst, J. J., Plesa, G., Shea, J., Matlawski, T., Cervini, A., Gaymon, A. L., … June, C. H. (2020). CRISPR-engineered T cells in patients with refractory cancer. *Science, 367*(6481), eaba7365. https://doi.org/10.1126/science.aba7365

Stolwijk, J. A., & Wegener, J. (2019). Impedance-based assays along the life span of adherent mammalian cells in vitro: from initial adhesion to cell death. In: Wegener, J.(Ed.), *Label-Free Monitoring of Cells in Vitro* (pp. 1-75). Cham: Springer International Publishing. https://doi.org/10.1007/11663_2019_7

Strähle, U., Scholz, S., Geisler, R., Greiner, P., Hollert, H., Rastegar, S., Schumacher, A., Selderslaghs, I., Weiss, C., Witters, H., & Braunbeck, T. (2012). Zebrafish embryos as an alternative to animal experiments--a commentary on the definition of the onset of protected life stages in animal welfare regulations. *Reproductive Toxicology, 33*(2), 128-132. https://doi.org/10.1016/j.reprotox.2011.06.121

Suda, T., Gao, X., Stolz, D. B., & Liu, D. (2007). Structural impact of hydrodynamic injection on mouse liver. *Gene Therapy, 14*(2), 129–137. https://doi.org/10.1038/sj.gt.3302865

Sung, H., Ferlay, J., Siegel, R. L., Laversanne, M., Soerjomataram, I., Jemal, A., & Bray, F. (2021). Global Cancer Statistics 2020: GLOBOCAN estimates of incidence and mortality worldwide for 36 cancers in 185 countries. *CA: A Cancer Journal for Clinicians, 71*(3), 209-249. https://doi.org/10.3322/caac.21660

Swarts, D. C., van der Oost, J., & Jinek, M. (2017). Structural basis for guide RNA processing and seed-dependent DNA targeting by CRISPR-Cas12a. *Molecular Cell, 66*(2), 221-233.e4. https://doi.org/10.1016/j.molcel.2017.03.016

Tang, A., Hallouch, O., Chernyak, V., Kamaya, A., & Sirlin, C. B. (2018). Epidemiology of hepatocellular carcinoma: target population for surveillance and diagnosis. *Abdominal Radiology, 43*(1), 13–25. https://doi.org/10.1007/s00261-017-1209-1

Taylor, G. A., Carballo, E., Lee, D. M., Lai, W. S., Thompson, M. J., Patel, D. D., Schenkman, D. I., Gilkeson, G. S., Broxmeyer, H. E., Haynes, B. F., & Blackshear, P. J. (1996). A pathogenetic role for TNF alpha in the syndrome of cachexia, arthritis, and autoimmunity resulting from tristetraprolin (TTP) deficiency. *Immunity, 4*(5), 445–454. https://doi.org/10.1016/s1074-7613(00)80411-2

Trendel, J., Schwarzl, T., Horos, R., Prakash, A., Bateman, A., Hentze, M. W., & Krijgsveld, J. (2019). The human RNA-binding proteome and its dynamics during translational Arrest. *Cell, 176*(1-2), 391–403.e19. https://doi.org/10.1016/j.cell.2018.11.004

Tuladhar, R., Yeu, Y., Tyler Piazza, J., Tan, Z., Rene Clemenceau, J., Wu, X., Barrett, Q., Herbert, J., Mathews, D. H., Kim, J., Hyun Hwang, T., & Lum, L. (2019). CRISPR-Cas9-based mutagenesis frequently provokes on-target mRNA misregulation. *Nature Communications, 10*(1), 4056. https://doi.org/10.1038/s41467-019-12028-5

Tung, E. K., Mak, C. K., Fatima, S., Lo, R. C., Zhao, H., Zhang, C., Dai, H., Poon, R. T., Yuen, M. F., Lai, C. L., Li, J. J., Luk, J. M., & Ng, I. O. (2011). Clinicopathological and prognostic significance of serum and tissue Dickkopf-1 levels in human hepatocellular carcinoma. *Liver International : Official Journal of the International Association for the Study of the Liver, 31*(10), 1494–1504. https://doi.org/10.1111/j.1478-3231.2011.02597.x

Tybl, E., Shi, F. D., Kessler, S. M., Tierling, S., Walter, J., Bohle, R. M., Wieland, S., Zhang, J., Tan, E. M., & Kiemer, A. K. (2011). Overexpression of the IGF2-mRNA binding protein p62 in transgenic mice induces a steatotic phenotype. *Journal of Hepatology, 54*(5), 994-1001. https://doi.org/10.1016/j.jhep.2010.08.034

Urdaneta, E. C., Vieira-Vieira, C. H., Hick, T., Wessels, H. H., Figini, D., Moschall, R., Medenbach, J., Ohler, U., Granneman, S., Selbach, M., & Beckmann, B. M. (2019). Purification of cross-linked RNA-protein complexes by phenol-toluol extraction. *Nature Communications, 10*(1), 990. https://doi.org/10.1038/s41467-019-08942-3

Van Tubergen, E. A., Vander Broek, R., Lee, J., Wolf, G., Carey, T., Bradford, C., Prince, M., Kirkwood, K. L., & D'Silva, N. J. (2011). Tristetraprolin regulates interleukin-6, which is correlated with tumor progression in patients with head and neck squamous cell carcinoma. *Cancer, 117*(12), 2677–2689. https://doi.org/10.1002/cncr.25859

Van Tubergen, E. A., Banerjee, R., Liu, M., Vander Broek, R., Light, E., Kuo, S., Feinberg, S. E., Willis, A. L., Wolf, G., Carey, T., Bradford, C., Prince, M., Worden, F. P., Kirkwood, K. L., & D'Silva, N. J. (2013). Inactivation or loss of TTP promotes invasion in head and neck cancer via transcript stabilization and secretion of MMP9, MMP2, and IL-6. *Clinical Cancer Research : An Official Journal of the American Association for Cancer Research, 19*(5), 1169–1179. https://doi.org/10.1158/1078-0432.CCR-12-2927

Vesselinovitch, S. (1990). Perinatal mouse liver carcinogenesis as a sensitive carcinogenesis model and the role of the sex hormonal environment in tumor development. *Progress in Clinical and Biological Research*(331), 53-68.

Vicente-Manzanares, M., & Horwitz, A. R. (2011). Cell migration: an overview. *Methods in Molecular Biology, 769*, 1–24. https://doi.org/10.1007/978-1-61779-207-6_1

Vivian, J., Rao, A. A., Nothaft, F. A., Ketchum, C., Armstrong, J., Novak, A., Pfeil, J., Narkizian, J., Deran, A. D., Musselman-Brown, A., Schmidt, H., Amstutz, P., Craft, B., Goldman, M., Rosenbloom, K., Cline, M., O'Connor, B., Hanna, M., Birger, C., Kent, W. J., … Paten, B. (2017). Toil enables reproducible, open source, big biomedical data analyses. *Nature biotechnology, 35*(4), 314–316. https://doi.org/10.1038/nbt.3772

Vo, D. T., Abdelmohsen, K., Martindale, J. L., Qiao, M., Tominaga, K., Burton, T. L., Gelfond, J. A., Brenner, A. J., Patel, V., Trageser, D., Scheffler, B., Gorospe, M., & Penalva, L. O. (2012). The oncogenic RNA-binding protein Musashi1 is regulated by HuR via mRNA translation and stability in glioblastoma cells. *Molecular Cancer Research : MCR, 10*(1), 143–155. https://doi.org/10.1158/1541-7786.MCR-11-0208

Wang, E., & Aifantis, I. (2020). RNA splicing and cancer. *Trends in Cancer, 6*(8), 631–644. https://doi.org/10.1016/j.trecan.2020.04.011

Wang, H., Ding, N., Guo, J., Xia, J., & Ruan, Y. (2016). Dysregulation of TTP and HuR plays an important role in cancers. *Tumour Biology : The Journal of the International Society for Oncodevelopmental Biology and Medicine, 37*(11), 14451–14461. https://doi.org/10.1007/s13277-016-5397-z

Wang, J., Chen, L., & Qiang, P. (2021). The role of IGF2BP2, an m6A reader gene, in human metabolic diseases and cancers. *Cancer Cell International, 21*(1), 99. https://doi.org/10.1186/s12935-021-01799-x

Wang, J. Y., Pausch, P., & Doudna, J. A. (2022). Structural biology of CRISPR-Cas immunity and genome editing enzymes. *Nature Reviews. Microbiology*. https://doi.org/10.1038/s41579-022-00739-4

Wang, N., Strugnell, R., Wijburg, O., & Brodnicki, T. (2011). Measuring bacterial load and immune responses in mice infected with Listeria monocytogenes. *Journal of Visualized Experiments : JoVE*, (54), 3076. https://doi.org/10.3791/3076

Wang, S., Lv, W., Li, T., Zhang, S., Wang, H., Li, X., Wang, L., Ma, D., Zang, Y., Shen, J., Xu, Y., & Wei, W. (2022). Dynamic regulation and functions of mRNA m6A modification. *Cancer Cell International, 22*(1), 48. https://doi.org/10.1186/s12935-022-02452-x

Wang, Y., Lu, J. H., Wu, Q. N., Jin, Y., Wang, D. S., Chen, Y. X., Liu, J., Luo, X. J., Meng, Q., Pu, H. Y., Wang, Y. N., Hu, P. S., Liu, Z. X., Zeng, Z. L., Zhao, Q., Deng, R., Zhu, X. F., Ju, H. Q., & Xu, R. H. (2019). LncRNA LINRIS stabilizes IGF2BP2 and promotes the aerobic glycolysis in colorectal cancer. *Molecular Cancer, 18*(1), 174. https://doi.org/10.1186/s12943-019-1105-0

Wei, Z. R., Liang, C., Feng, D., Cheng, Y. J., Wang, W. M., Yang, D. J., Wang, Y. X., & Cai, Q. P. (2016). Low tristetraprolin expression promotes cell proliferation and predicts poor patients outcome in pancreatic cancer. *Oncotarget, 7*(14), 17737–17750. https://doi.org/10.18632/oncotarget.7397

Weitz, J., Koch, M., Debus, J., Höhler, T., Galle, P. R., & Büchler, M. W. (2005). Colorectal cancer. *Lancet, 365*(9454), 153–165. https://doi.org/10.1016/S0140-6736(05)17706-X

World Health Organization. Global health estimates 2020: deaths by cause, age, sex, by country and by region, 2000-2019. World Health Organization; 2020.

Wong, N., Liu, W., & Wang, X. (2015). WU-CRISPR: characteristics of functional guide RNAs for the CRISPR/Cas9 system. *Genome Biology, 16*, 218. https://doi.org/10.1186/s13059-015-0784-0

Wörns, M. A., Weinmann, A., Schuchmann, M., & Galle, P. R. (2009). Systemic therapies in hepatocellular carcinoma. *Digestive Diseases, 27*(2), 175–188. https://doi.org/10.1159/000218351

Wu, H., Ding, X., Hu, X., Zhao, Q., Chen, Q., Sun, T., Li, Y., Guo, H., Li, M., Gao, Z., Yao, W., Zhao, L., Li, K., & Wei, M. (2022). LINC01021 maintains tumorigenicity by enhancing N6-methyladenosine reader IMP2 dependent stabilization of MSX1 and JARID2: implication in colorectal cancer. *Oncogene, 41*(13), 1959–1973. https://doi.org/10.1038/s41388-022-02189-x

Xiang, J. F., Yang, Q., Liu, C. X., Wu, M., Chen, L. L., & Yang, L. (2018). N6-Methyladenosines Modulate A-to-I RNA Editing. *Molecular Cell, 69*(1), 126–135.e6. https://doi.org/10.1016/j.molcel.2017.12.006

Xiao, Y., Luo, M., Dolan, A. E., Liao, M., & Ke, A. (2018). Structure basis for RNA-guided DNA degradation by Cascade and Cas3. *Science, 361*(6397), eaat0839. https://doi.org/10.1126/science.aat0839

Xing, M., Li, P., Wang, X., Li, J., Shi, J., Qin, J., Zhang, X., Ma, Y., Francia, G., & Zhang, J. Y. (2019). Overexpression of p62/IMP2 can promote cell migration in hepatocellular carcinoma via activation of the wnt/β-catenin pathway. *Cancers, 12*(1), 7. https://doi.org/10.3390/cancers12010007

Xu, L., Ning, H., Gu, L., Wang, Q., Lu, W., Peng, H., Cui, W., Ying, B., Ross, C. R., Wilson, G. M., Wei, L., Wold, W. S., & Liu, J. (2015). Tristetraprolin induces cell cycle arrest in breast tumor cells through targeting AP-1/c-Jun and NF-κB pathway. *Oncotarget, 6*(39), 41679–41691. https://doi.org/10.18632/oncotarget.6149

Xu, X., Yu, Y., Zong, K., Lv, P., & Gu, Y. (2019). Up-regulation of IGF2BP2 by multiple mechanisms in pancreatic cancer promotes cancer proliferation by activating the PI3K/Akt signaling pathway. *Journal of Experimental & Clinical Cancer Research : CR, 38*(1), 497. https://doi.org/10.1186/s13046-019-1470-y

Ye, S., Song, W., Xu, X., Zhao, X., & Yang, L. (2016). IGF2BP2 promotes colorectal cancer cell proliferation and survival through interfering with RAF-1 degradation by miR-195. *FEBS Letters, 590*(11), 1641–1650. https://doi.org/10.1002/1873-3468.12205

Yoon, N. A., Jo, H. G., Lee, U. H., Park, J. H., Yoon, J. E., Ryu, J., Kang, S. S., Min, Y. J., Ju, S. A., Seo, E. H., Huh, I. Y., Lee, B. J., Park, J. W., & Cho, W. J. (2016). Tristetraprolin suppresses the EMT through the down-regulation of Twist1 and Snail1 in cancer cells. *Oncotarget, 7*(8), 8931–8943. https://doi.org/10.18632/oncotarget.7094

Yu, M. W., Cheng, S. W., Lin, M. W., Yang, S. Y., Liaw, Y. F., Chang, H. C., Hsiao, T. J., Lin, S. M., Lee, S. D., Chen, P. J., Liu, C. J., & Chen, C. J. (2000). Androgen-receptor gene CAG repeats, plasma testosterone levels, and risk of hepatitis B-related hepatocellular carcinoma. *Journal of the National Cancer Institute, 92*(24), 2023–2028. https://doi.org/10.1093/jnci/92.24.2023

Zeggini, E., Weedon, M. N., Lindgren, C. M., Frayling, T. M., Elliott, K. S., Lango, H., Timpson, N. J., Perry, J. R., Rayner, N. W., Freathy, R. M., Barrett, J. C., Shields, B., Morris, A. P., Ellard, S., Groves, C. J., Harries, L. W., Marchini, J. L., Owen, K. R., Knight, B., Cardon, L. R., … Hattersley, A. T. (2007). Replication of genome-wide association signals in UK samples reveals risk loci for type 2 diabetes. *Science, 316*(5829), 1336–1341. https://doi.org/10.1126/science.1142364

Zhang, G., Gao, X., Song, Y. K., Vollmer, R., Stolz, D. B., Gasiorowski, J. Z., Dean, D. A., & Liu, D. (2004). Hydroporation as the mechanism of hydrodynamic delivery. *Gene Therapy, 11*(8), 675–682. https://doi.org/10.1038/sj.gt.3302210

Zhang, J. Y., Chan, E. K., Peng, X. X., & Tan, E. M. (1999). A novel cytoplasmic protein with RNA-binding motifs is an autoantigen in human hepatocellular carcinoma. *The Journal of Experimental Medicine, 189*(7), 1101–1110. https://doi.org/10.1084/jem.189.7.1101

Zhang, Z., Liu, T., Dong, H., Li, J., Sun, H., Qian, X., & Qin, W. (2021). An RNA tagging approach for system-wide RNA-binding proteome profiling and dynamics investigation upon transcription inhibition. *Nucleic Acids Research, 49*(11), e65. https://doi.org/10.1093/nar/gkab156

Zhanmu, O., Zhao, P., Yang, Y., Yang, X., Gong, H., & Li, X. (2019). Maintenance of fluorescence during paraffin embedding of fluorescent protein-labeled specimens. *Frontiers in Neuroscience, 13*, 752. https://doi.org/10.3389/fnins.2019.00752

8 Appendix

8.1 Abbreviations

7-AAD	7-amino-actinomycin D
3′-UTR	3′-untranslated region
5′-UTR	5′-untranslated region
5FU	5-Fluoruracil
aa	Amino acids
ACTB	Actin beta
AHRR	Aryl-hydrocarbon receptor repressor
ANOVA	Analysis of variance
APA	Alternative polyadenylation
APC	Allophycocyanin
ARE	AU-rich elements
Arp2/3	Actin-related protein 2/3
AU-rich	Adenosine-uridine-rich
bp	Base pairs
BCL2	B-cell lymphoma 2, BCL2 apoptosis regulator
BSA	Bovine serum albumine
cAMP	Cyclic adenosine monophosphate
Cas9	CRISPR associated (protein) 9
CD	Cluster of differentiation
cDNA	Complementary DNA
CDKN1A	Cyclin-dependant kinase inhibitor 1A
CELF2	CUGBP Elav-like family member 2
c-NHEJ	Classical non-homologous end joining
CRC	Colorectal cancer
CREB	cAMP responsive element binding
CRISPR/Cas	Clustered regularly interspaced short palindromic repeats
crRNA	CRISPR RNA
DANCR	Differentiation antagonizing non-protein coding RNA
ddGTP	Dideoxyguanine triphosphate
ddTTP	Dideoxythymine triphosphate
DEN	Diethylnitrosamine
DMEM	Dulbecco's modified Eagle’s medium
DMSO	Dimethyl sulfoxide
DNA	Deoxyribonucleic acid
E2F1	E2F transcription factor 1
eIF	Eukaryotic translation initiation factor
ELAVL1	ELAV-like RNA-binding protein 1
ELOVL6	Elongation of very long chain fatty acids protein 6
EMT	Epithelial-mesenchymal-transition
FA	Fatty acid

FACS	Fluorescence-activated cell sorting
FCS	Fetal calf serum
FITC	Fluorescein isothiocyanate
FSC	Forward scatter
GC-MS	Gas chromatography-mass spectrometry
GFP	Green fluorescent protein
GILZ	Glucocorticoid-induced leucine zipper
GRCh	Genome reference consortium human
HBV	Hepatitis B virus
HCV	Hepatitis C virus
HCC	Hepatocellular carcinoma
HDI	Human development index
HDR	Homology directed repair (HDR)
HGD	Hydrodynamic gene delivery
HMGA1, HMGA2	High mobility group AT-hook 1 or 2
KH domain	Heterogeneous nuclear ribonucleoprotein (hnRNP)-K homology (KH) domain
IGF	Insulin-like growth factor
IGF2BP1/IMP1/VICKZ1/ ZBP1	Insulin-like growth factor 2 mRNA-binding protein 1
IGF2BP2/IMP2/VICKZ2	Insulin-like growth factor 2 mRNA-binding protein 2
IL	Interleukin
Indel	Insertion and/or deletion
IP/RP-HPLC	Ion-pair reversed-phase high-performance liquid chromatography
IRES	Internal ribosome entry sites
Jun	Jun proto-oncogene, AP-1 transcription factor subunit
LATS2	Large tumour suppressor kinase 2
LB	Lysogeny broth
LIMS2	LIM zinc finger domain containing 2
Lin28A	Lin-28-homolog A
lncRNA	Long non-coding RNA
ls*Ttp*-KO	Liver-specific *Ttp* knockout
m6A	N6-methyladenosine
m^7G	7-methylguanylate
MACC1	MET transcriptional regulator MACC1 (metastasis-associated in colon cancer 1)
mRNA	messenger-RNA
miRNA	micro-RNA
MMP	Matrix metalloproteinase
MSI1	Musashi RNA binding protein 1
MYC	c-MYC, MYC proto-oncogene, bHLH transcription factor
NF-κB	Nuclear factor kappa B
nt	Nucleotide
OHP	Oxaliplatin
OD_{600}	Optical density measured at a wavelength of λ=600 nm

PAM	Protospacer adjacent motif
PBS	Primer-binding site
PBS (1×)	Phosphate-buffered saline
PE	Phycoerythrin
pegRNA	Prime editing guide RNA
PIK3CA	Phosphatidylinositol-4,5-bisphosphate 3-kinase catalytic subunit-α
PKR	Protein kinase R
PTC	Premature termination codon
PTEN	Phosphatase and tensin homologue
qPCR	Quantitative polymerase chain reaction
RBB	Rockland blocking buffer
RBD	RNA-binding domain
RBP	(m)RNA-binding protein
REGO	Regorafenib
RIGI	Retinoic acid-inducible gene I protein
RNA	Ribonucleic acid
RNP	Ribonucleoprotein
RPMI	Roswell Park Memorial Institute
RRM	RNA recognition motif
RT	Reverse transcriptase
Sam68	Src-associated protein in mitosis of 68 kDa
SDS-PAGE	Sodium dodecyl sulfate-polyacrylamide gel electrophoresis
(s)gRNA	(Single) guide RNA
SH	Src-homology
shRNA	Short hairpin RNA
siRNA	Small interfering RNA
Snail1	Zinc finger protein snail 1
SNP	Single nucleotide polymorphism
SNuPE	Single nucleotide primer extension
SOX9	SRY-box transcription factor 9
SSC	Side scatter
T2DM	Diabetes mellitus type 2
TALEN	Transcription activator-like effector nuclease
TDP-43/TARDBP	TAR DNA-binding protein
TEAA	Triethylammonium acetate
TIS11	TPA-inducible sequence 11
TNF	Tumour necrosis factor
TP53	Tumour protein p53
TPA	Tetradecanoylphorbol acetate
TRIBE	Targets of RNA-binding proteins identified by editing
TRIM54	Tripartite motif containing 54
Twist1	twist-related protein 1
VEGF	Vascular endothelial growth factor
XIAP	X-linked inhibitor of apoptosis

XRN1	5′-3′ exoribonuclease 1
ZEB1	Zinc finger E-box binding homeobox 1
ZFN	Zinc finger nuclease

8.2 Supporting information

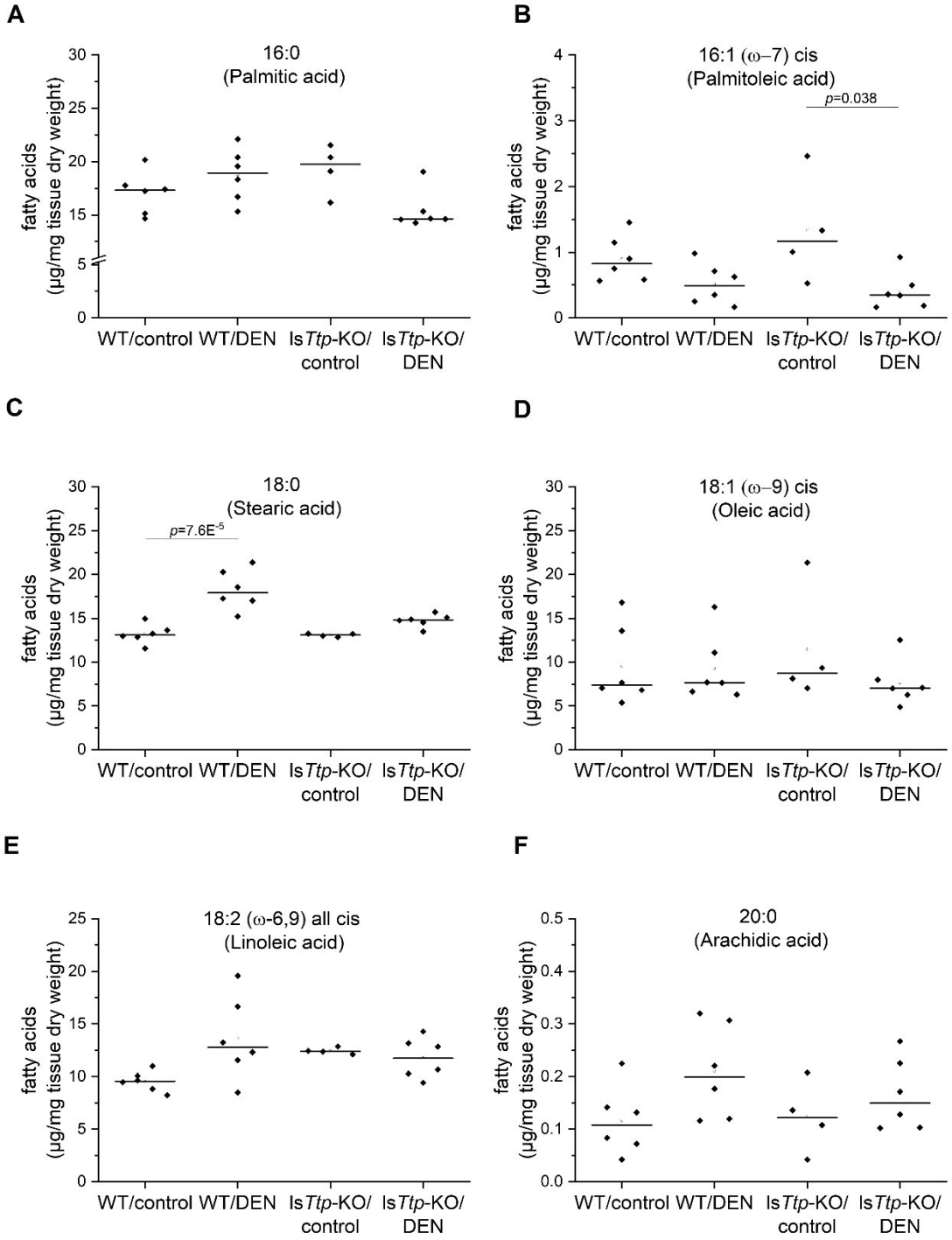

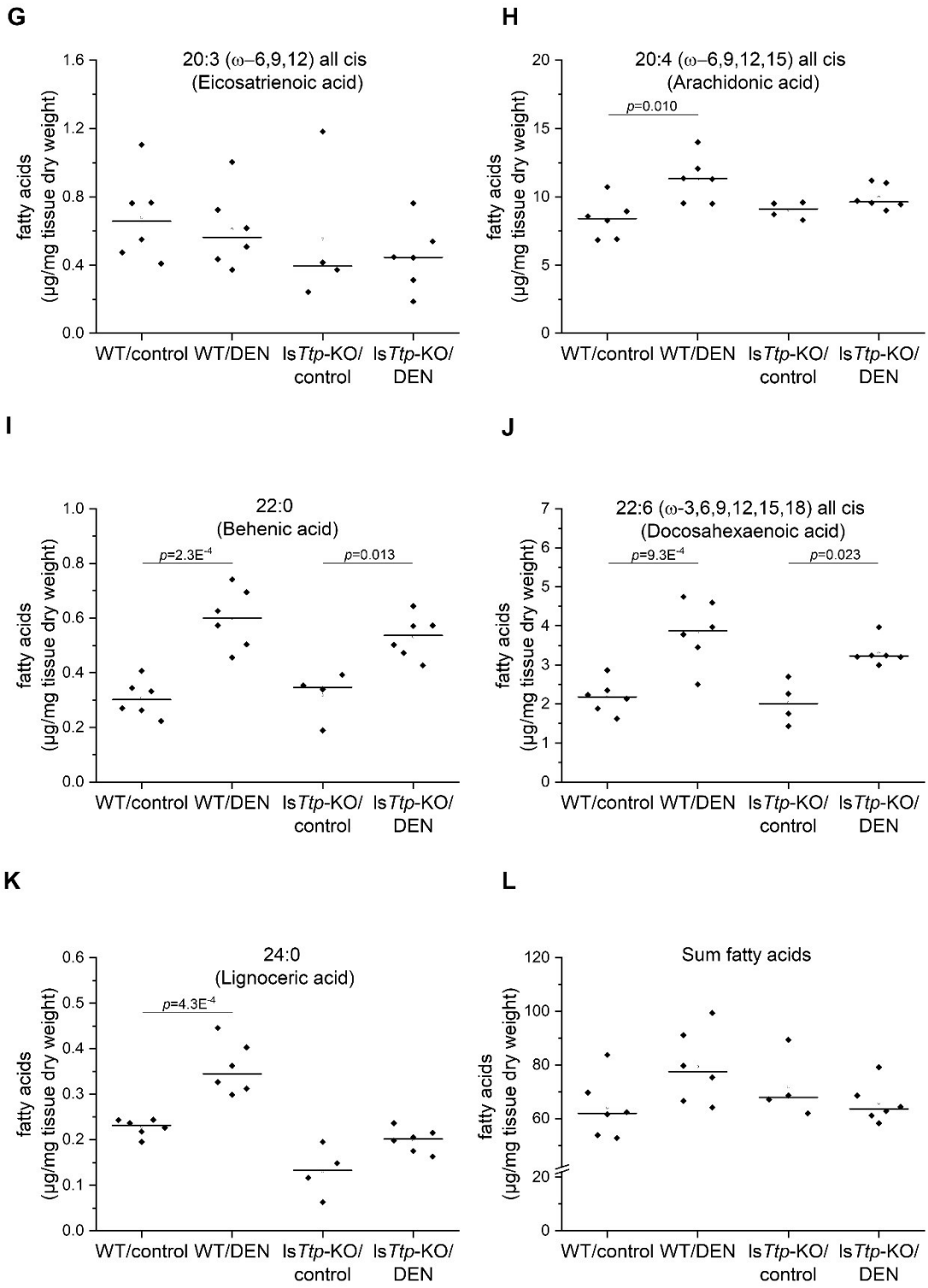

Supplementary Figure 1| Hepatic fatty acids in short-term sham- (control) or DEN-treated WT and ls*Ttp*-KO mice. n=6 (WT/control), n=6 (WT/DEN), n=4 (ls*Ttp*-KO/control), n=6 (ls*Ttp*-KO/DEN). Rhombi illustrate single data points, horizontal black lines illustrate median and white rectangles illustrate means. Significant *p* values (α<0.05) are shown. From "The mRNA-binding protein TTP/ZFP36 in hepatocarcinogenesis and hepatocellular carcinoma" by Kröhler, T., Kessler, S. M., Hosseini, K., List, M., Barghash, A., Patial, S., Laggai, S., Gemperlein, K., Haybaeck, J., Müller, R., Helms, V., Schulz, M. H., Hoppstädter, J., Blackshear, P. J., & Kiemer, A. K. (2019), *Cancers, 11*(11), 1754 (https://doi.org/10.3390/cancers11111754). Licensed under CC BY 4.0.

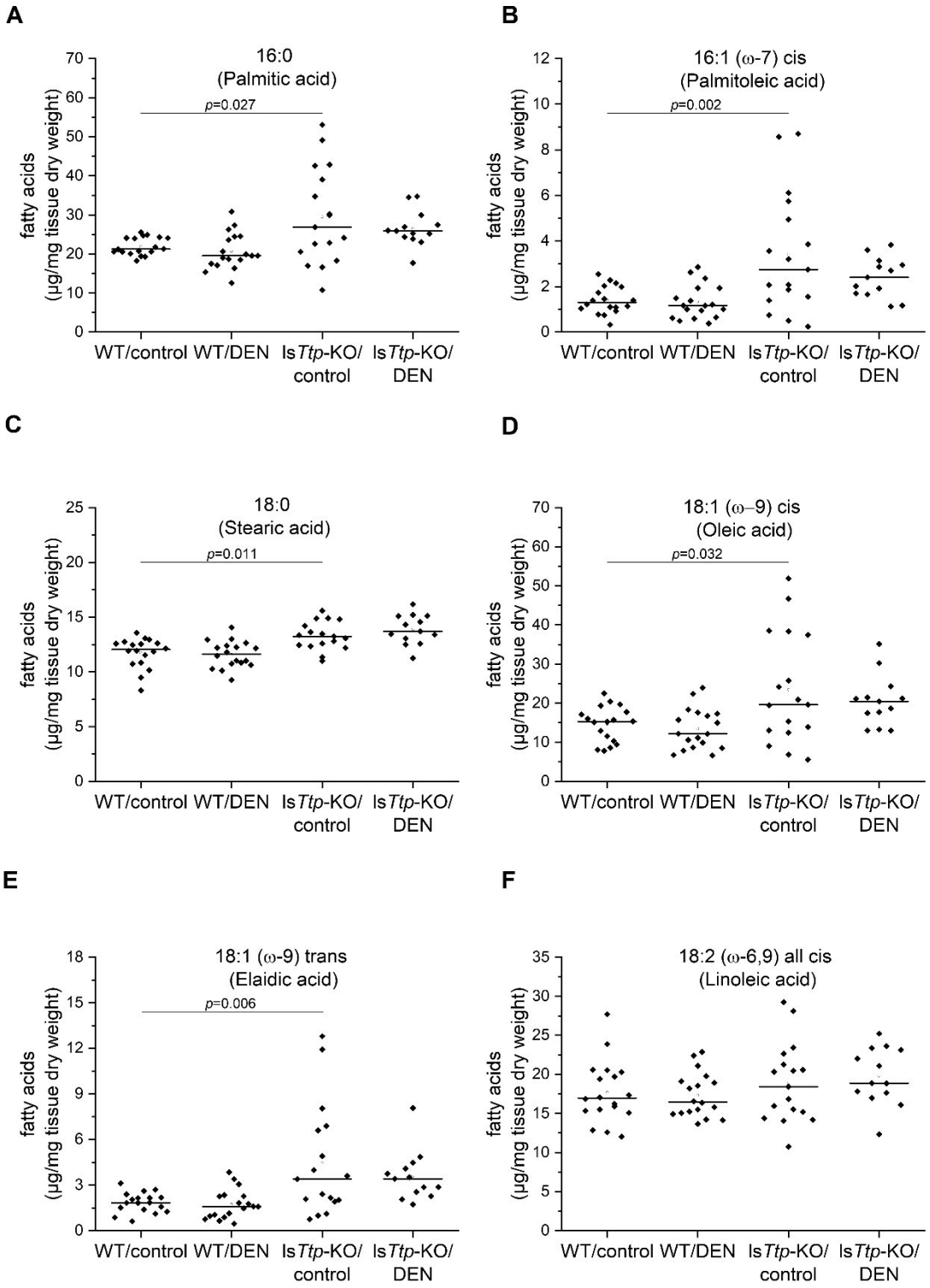
A
16:0
(Palmitic acid)
p=0.027
fatty acids
(µg/mg tissue dry weight)
WT/control
WT/DEN
IsTtp-KO/ control
IsTtp-KO/ DEN
B
16:1 (ω-7) cis
(Palmitoleic acid)
p=0.002
C
18:0
(Stearic acid)
p=0.011
D
18:1 (ω–9) cis
(Oleic acid)
p=0.032
E
18:1 (ω-9) trans
(Elaidic acid)
p=0.006
F
18:2 (ω-6,9) all cis
(Linoleic acid)

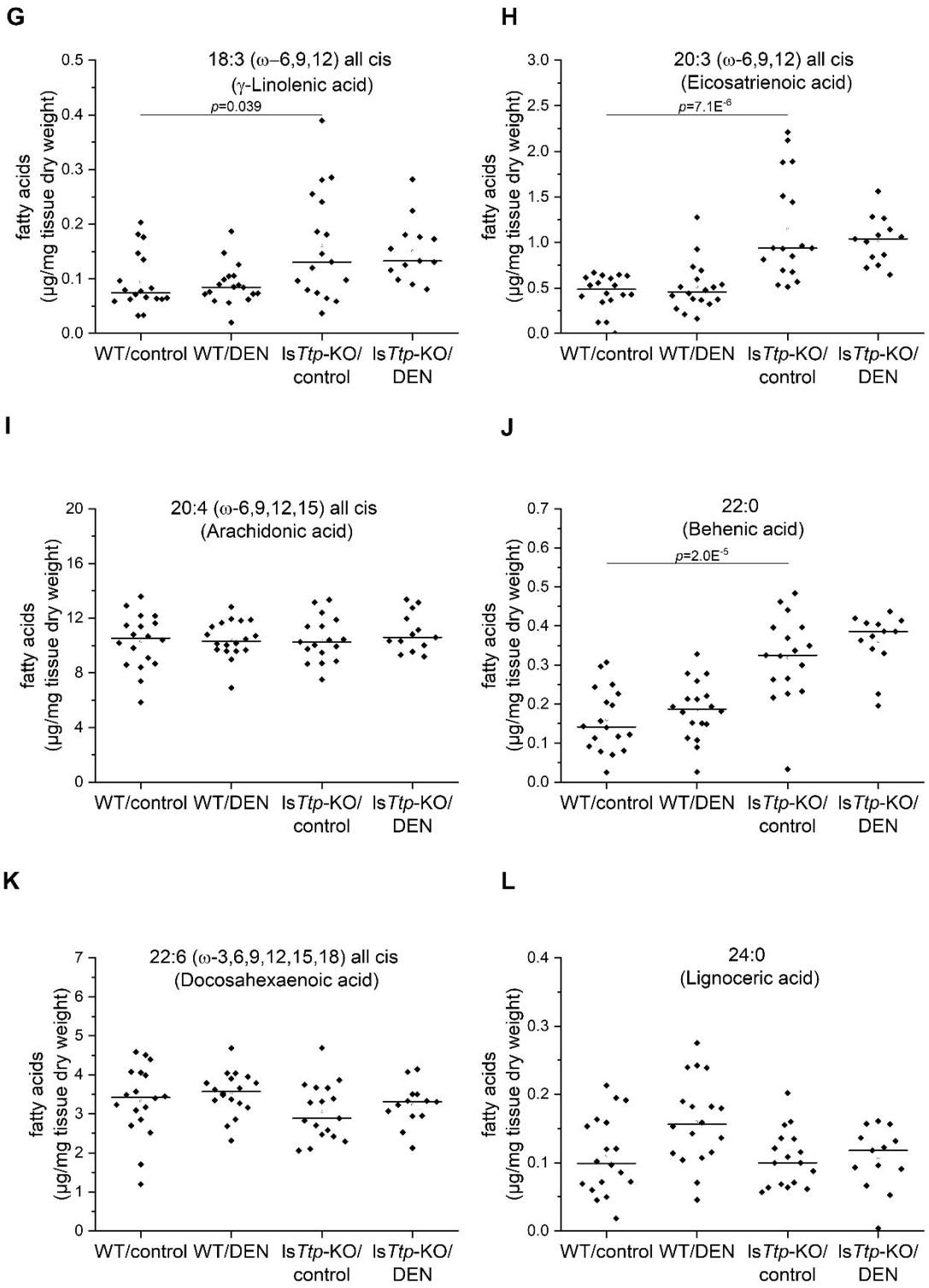
G
18:3 (ω–6,9,12) all cis
(γ-Linolenic acid)
p=0.039
fatty acids
(µg/mg tissue dry weight)
WT/control
WT/DEN
IsTtp-KO/ control
IsTtp-KO/ DEN
H
20:3 (ω-6,9,12) all cis
(Eicosatrienoic acid)
p=7.1E-6
I
20:4 (ω-6,9,12,15) all cis
(Arachidonic acid)
J
22:0
(Behenic acid)
p=2.0E-5
K
22:6 (ω-3,6,9,12,15,18) all cis
(Docosahexaenoic acid)
L
24:0
(Lignoceric acid)

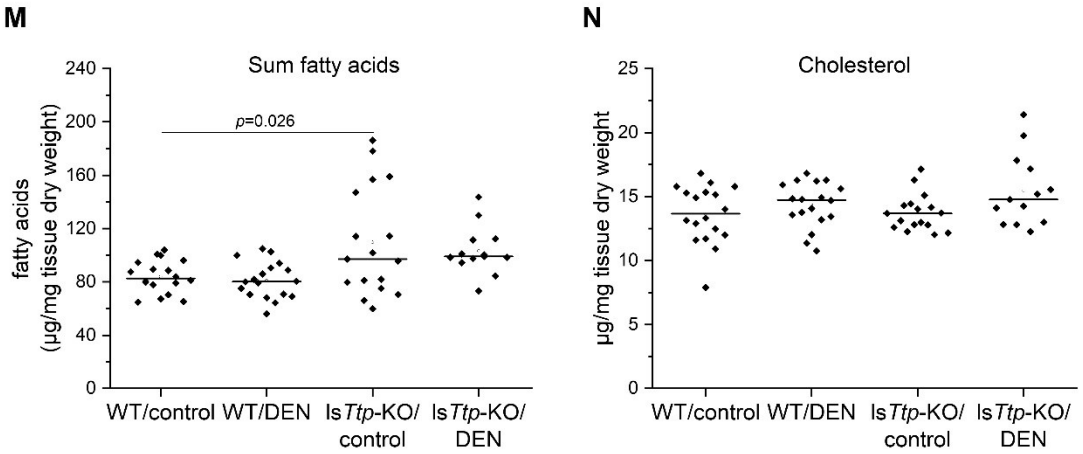

Supplementary Figure 2| Hepatic fatty acids in long-term sham- (control) or DEN-treated WT and ls*Ttp*-KO mice. n=18 (WT/control), n=18 (WT/DEN), n=17 (ls*Ttp*-KO/control), n=13 (ls*Ttp*-KO/DEN). Rhombi illustrate single data points, horizontal black lines illustrate median and white rectangles illustrate means. Significant *p* values (α<0.05) are shown. From "The mRNA-binding protein TTP/ZFP36 in hepatocarcinogenesis and hepatocellular carcinoma" by Kröhler, T., Kessler, S. M., Hosseini, K., List, M., Barghash, A., Patial, S., Laggai, S., Gemperlein, K., Haybaeck, J., Müller, R., Helms, V., Schulz, M. H., Hoppstädter, J., Blackshear, P. J., & Kiemer, A. K. (2019), *Cancers, 11*(11), 1754 (https://doi.org/10.3390/cancers11111754). Licensed under CC BY 4.0.

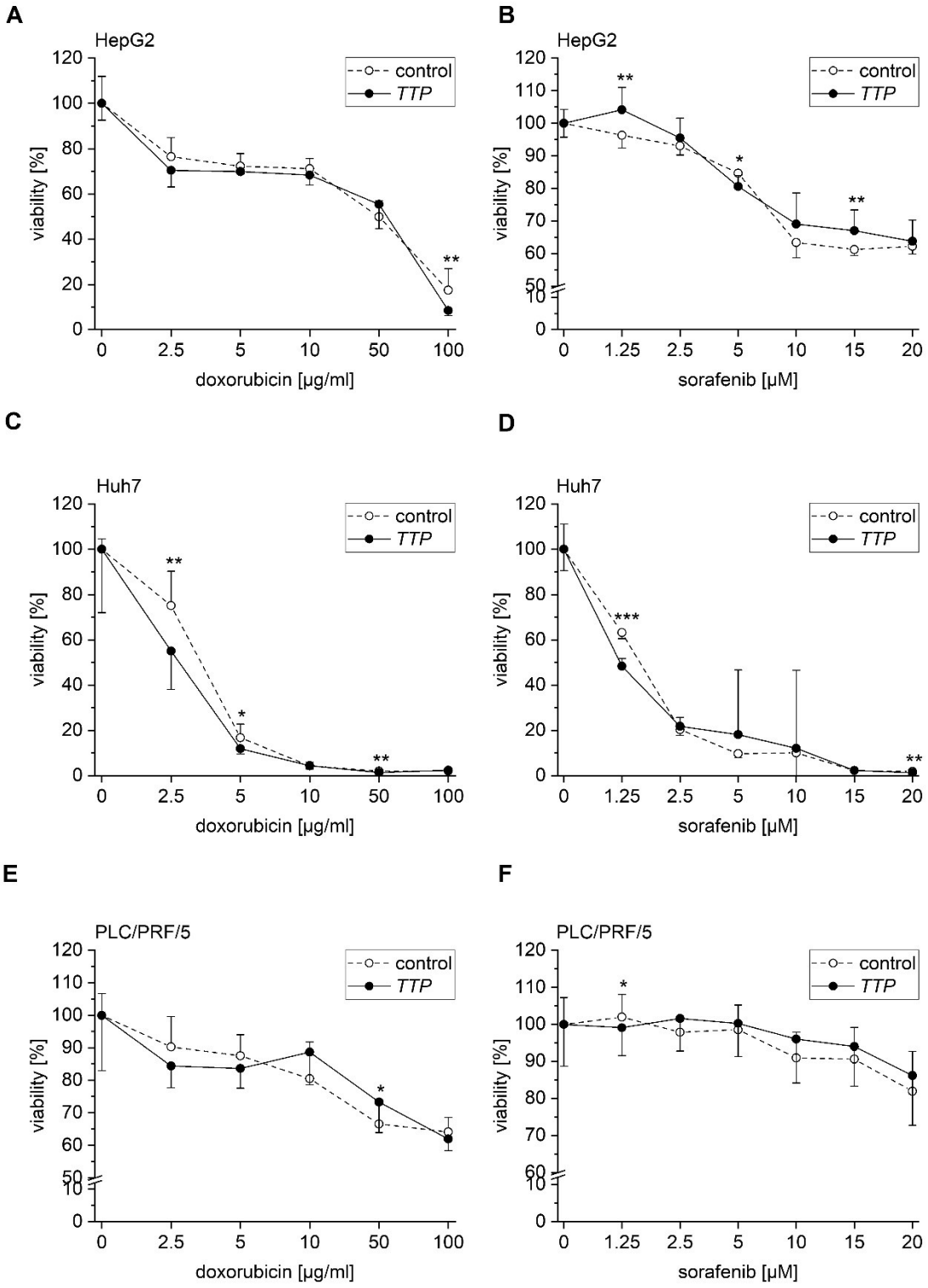
A
HepG2
control
TTP
viability [%]
doxorubicin [µg/ml]
B
HepG2
control
TTP
viability [%]
sorafenib [µM]
C
Huh7
control
TTP
viability [%]
doxorubicin [µg/ml]
D
Huh7
control
TTP
viability [%]
sorafenib [µM]
E
PLC/PRF/5
control
TTP
viability [%]
doxorubicin [µg/ml]
F
PLC/PRF/5
control
TTP
viability [%]
sorafenib [µM]

Supplementary Figure 3| Effects of TTP overexpression on chemoresistance in hepatoma cells. Cells were transfected with either TTP or a control vector. Twenty-four hours after transfection, cells were treated with different concentrations of doxorubicin or sorafenib for 24 h. Cell viability was determined via MTT assay. Both groups (TTP and control vector) are normalised to the viability of the control vector transfected cells without addition of doxorubicin or sorafenib (=100%). (A): HepG2 cells treated with doxorubicin. (B): HepG2 cells treated with sorafenib. (C): Huh7 cells treated with doxorubicin. (D): Huh7 cells treated with sorafenib. (E): PLC/PRF/5 cells treated with doxorubicin. (F): PLC/PRF/5 cells treated with sorafenib. n=3 (quadruplicates). Statistical difference: *: $p<0.05$; **: $p<0.01$; ***: $p<0.001$. From "The mRNA-binding protein TTP/ZFP36 in hepatocarcinogenesis and hepatocellular carcinoma" by Kröhler, T., Kessler, S. M., Hosseini, K., List, M., Barghash, A., Patial, S., Laggai, S., Gemperlein, K., Haybaeck, J., Müller, R., Helms, V., Schulz, M. H., Hoppstädter, J., Blackshear, P. J., & Kiemer, A. K. (2019), *Cancers, 11*(11), 1754 (https://doi.org/10.3390/cancers11111754). Licensed under CC BY 4.0. Also published in similar way in "Pathomechanisms in hepatocellular carcinoma: characterisation of leukocyte recruitment, the role of the mRNA-binding protein tristetraprolin and nuclear paraspeckles" (Doctoral thesis, Saarland University, Saarbrücken, Germany) by Hosseini, K. (2017) (https://doi.org/10.22028/D291-27154).

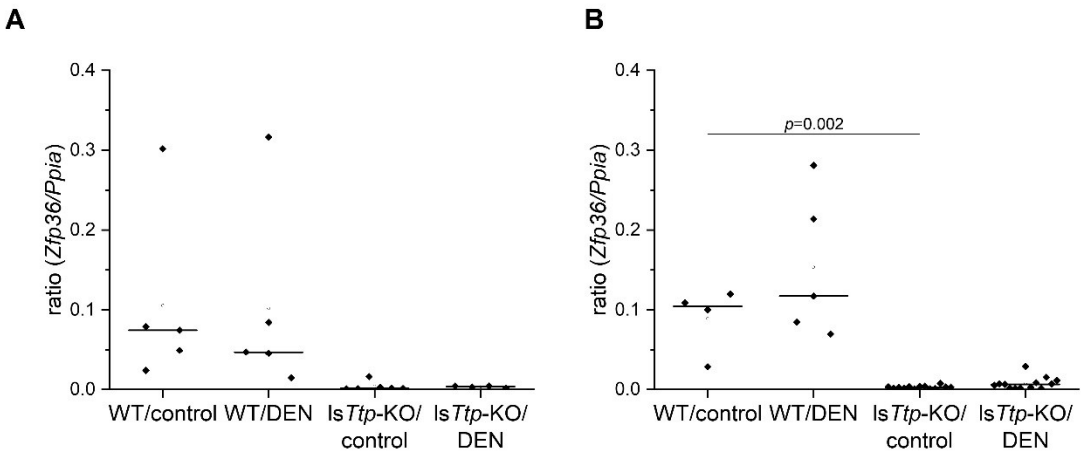

Supplementary Figure 4| *Zfp36* mRNA levels in liver-specific *Ttp*-KO and wild-type animals. *Zfp36*/*Ppia* mRNA ratio in wild-type (WT) and ls*Ttp*-KO animals injected with either 0.9% NaCl as sham-treatment or DEN following the short-term (A) or long-term (B) protocol. From "The mRNA-binding protein TTP/ZFP36 in hepatocarcinogenesis and hepatocellular carcinoma" by Kröhler, T., Kessler, S. M., Hosseini, K., List, M., Barghash, A., Patial, S., Laggai, S., Gemperlein, K., Haybaeck, J., Müller, R., Helms, V., Schulz, M. H., Hoppstädter, J., Blackshear, P. J., & Kiemer, A. K. (2019), *Cancers, 11*(11), 1754 (https://doi.org/10.3390/cancers11111754). Licensed under CC BY 4.0.

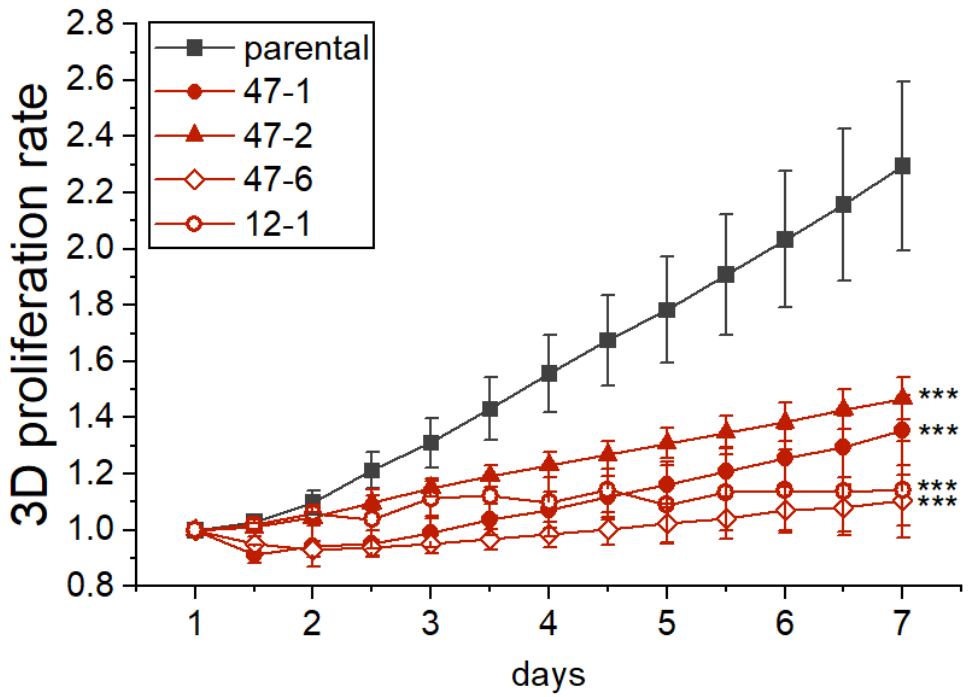

Supplementary Figure 5| Comparison of the 3D proliferation rate of various HCT116 IMP2 knockout clones. 3D proliferation of spheroids consisting of either HCT116 wild-type (parental) cells or IMP2 knockout clones, harbouring different gene edits, was monitored by automated live-cell microscopy, starting after spheroid formation for 24 h. Spheroid area was analysed using the Incucyte® S3 system and was normalised to 1-day old spheroids. Data are represented as means ±SEM. n=3 (quadruplicates). Statistical analysis was performed for the last acquired time point (7 days). Asterisks represent *p* values for the comparisons between the growth of parental and respective knockout cells. ***: $p<0.001$. This figure and parts of the caption were adopted from "First small-molecule inhibitors targeting the RNA-binding protein IGF2BP2/IMP2 for cancer therapy" by Dahlem, C., Abuhaliema, A., Kessler, S. M., Kröhler, T., Zoller, B., Chanda, S., Wu, Y., Both, S., Müller, F., Lepikhov, K., Kirsch, S. H., Laggai, S., Müller, R., Empting, M., & Kiemer, A. K. (2022),. *ACS Chemical Biology, 17*(2), 361–375 (https://doi.org/10.1021/acschembio.1c00833). With permission, copyright © 2022, American Chemical Society.

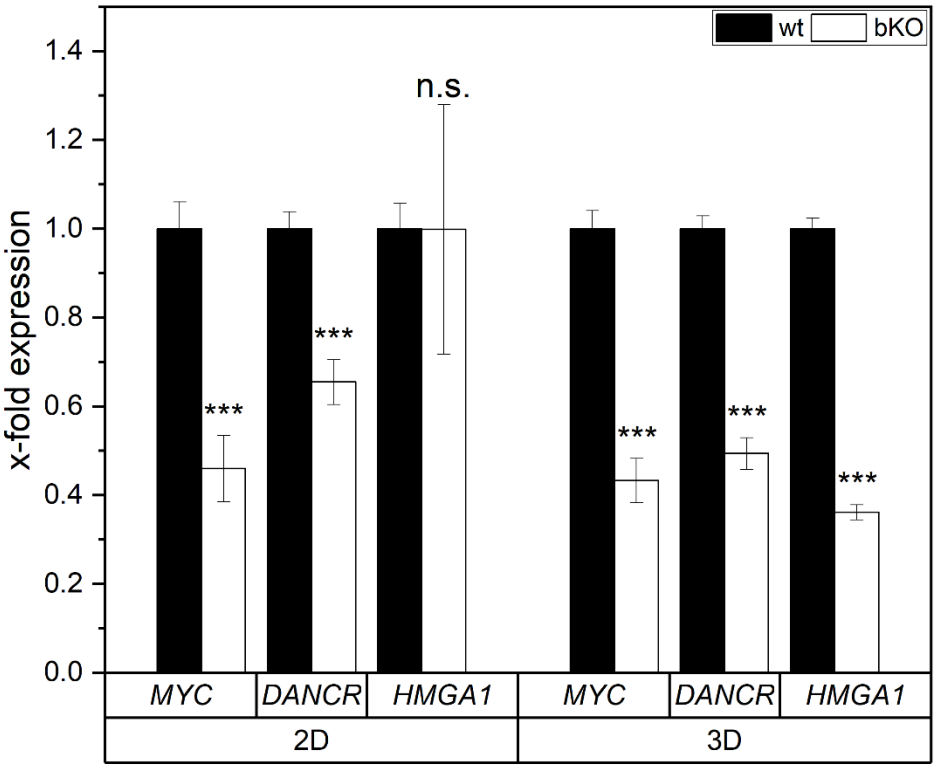

Supplementary Figure 6| Expression of IMP2 target genes. Comparison of *MYC*, *DANCR*, and *HMGA1* gene expression in HCT116 parental wild-type (wt) and IMP2 knockout cells (clone 47-1, bKO) evaluated in 2D cell culture and 3D spheroids. Values were normalised to the housekeeping gene *RNA18SN5*. Data are represented as means ±SEM. n=3 (triplicates). ***: $p<0.001$ (two-sample *t*-test); n.s.: not significant.

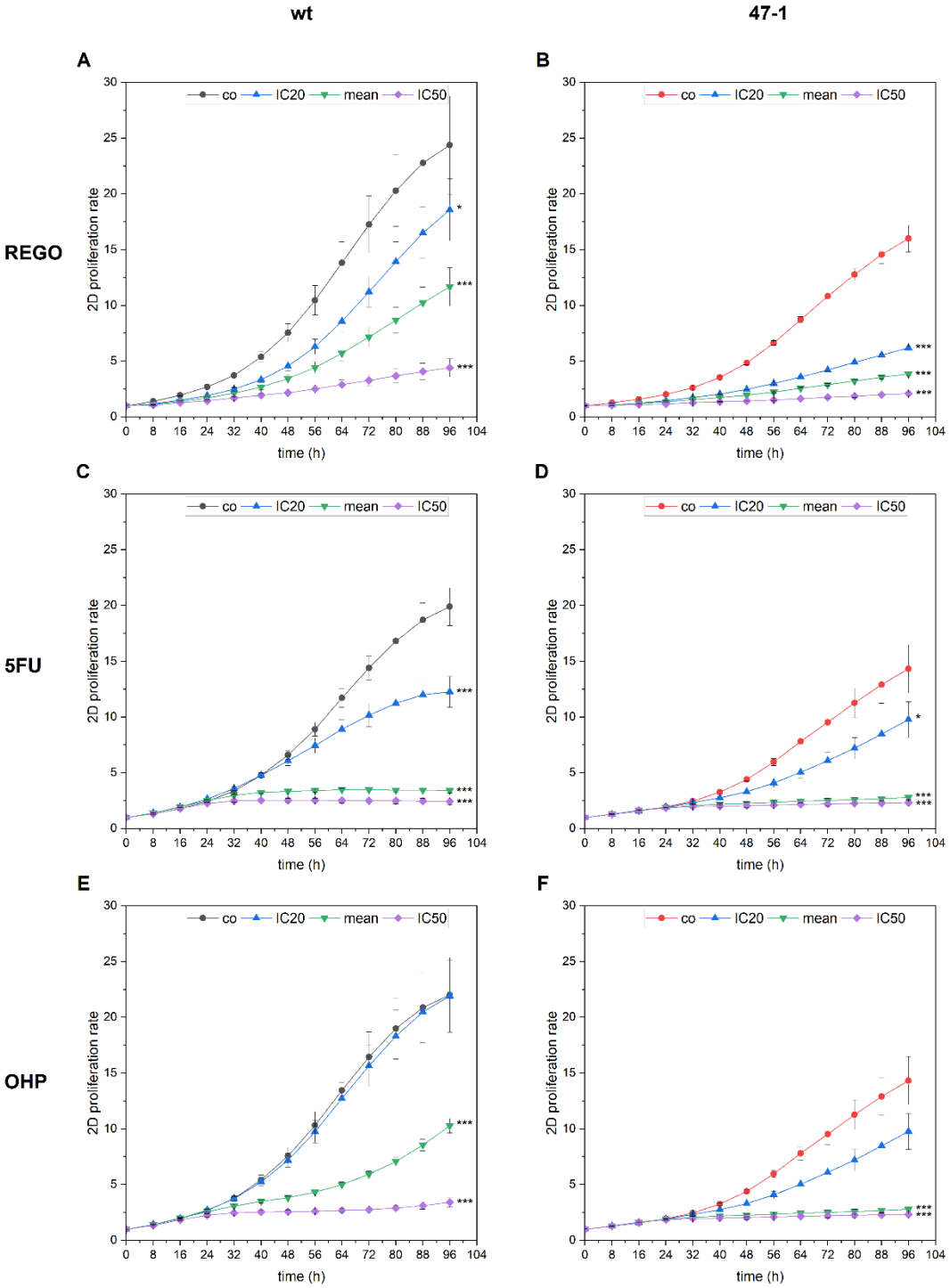

Supplementary Figure 7| Impact of IMP2 knockout on chemosensitivity of HCT116 cells. 2D proliferation rate of HCT116 wild-type (wt) cells (A, C, E) and IMP2 knockout clone 47-1 (B, D, F) undergoing treatment of the chemotherapeutics regorafenib (REGO), 5-fluoruracil (5FU), and oxaliplatin (OHP). The cells were monitored for 96 h and cell's confluency was analysed by an Incucyte® S3 system. Data were normalised to t=0 h and are represented as means ±SEM. n=3 (sextuplicates). co: solvent control; IC20: 20% inhibitory concentration of the respective compound; IC50: 50% inhibitory concentration of the respective compound; mean: mean of the 20% and 50% inhibitory concentration of the respective compound; *: $p<0.05$; ***: $p<0.001$ (two-way ANOVA).

8.3 Plasmid maps

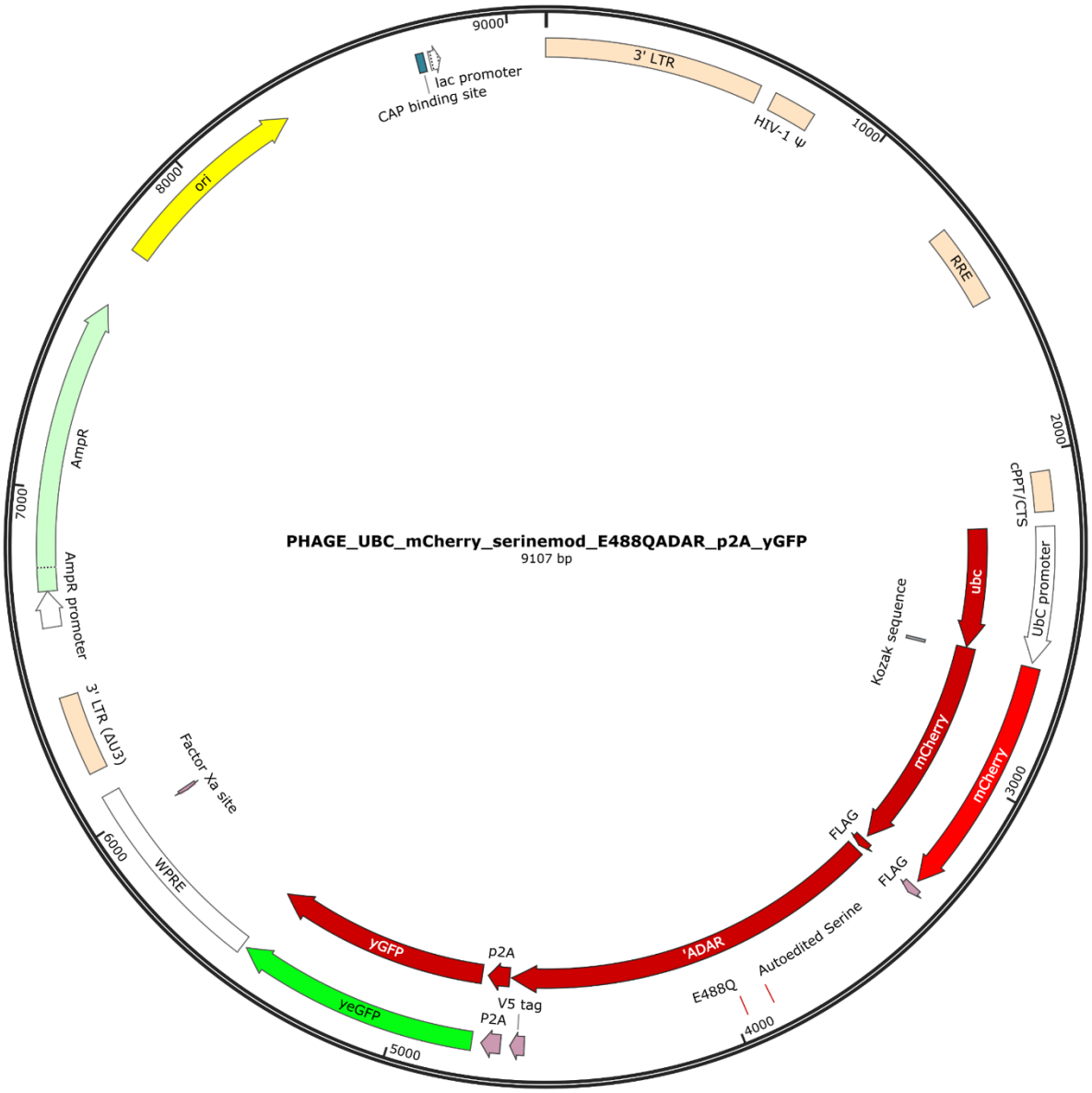

Supplementary Figure 8| PHAGE_UBC_mCherry_serinemod_E488QADAR_p2A_yGFP. Control plasmid "mCherry-ADAR" for the "TRIBE" experiments in chapter II. It harbours an ubiquitin C promoter (UbC), followed by the sequence of a fusion protein composed of the dye mCherry with a FLAG-tag and the ADAR enzyme, the self-cleaving peptide P2A and a modified GFP (yGFP). This plasmid was kindly provided by Jeetayu Biswas and Robert H. Singer (Albert Einstein College of Medicine, Jack and Pearl Resnick Campus, New York, USA). Created with SnapGene®.

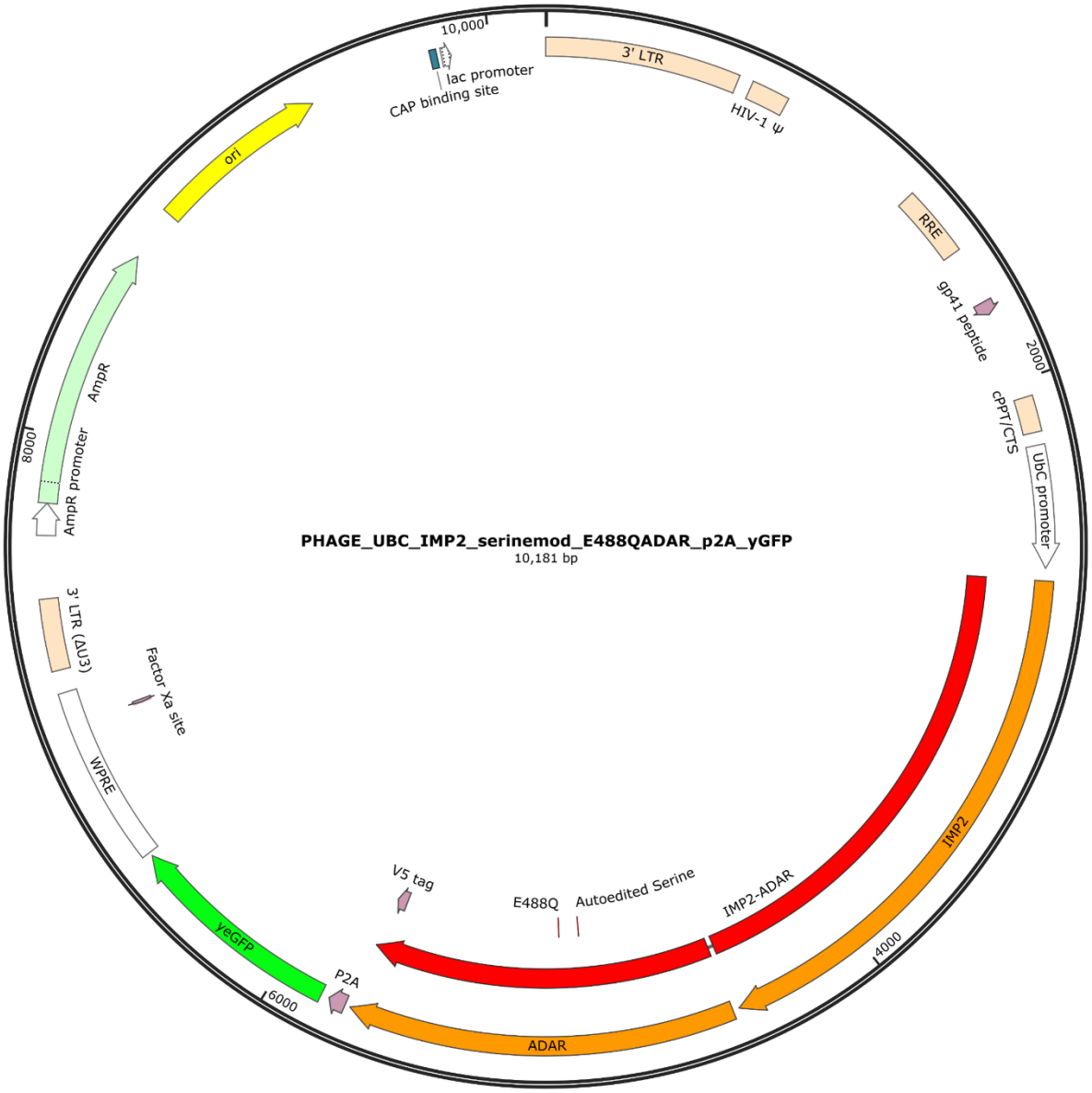

Supplementary Figure 9| PHAGE_UBC_IMP2_serinemod_E488QADAR_p2A_yGFP. Experimental plasmid "IMP2-ADAR" for the "TRIBE" experiments in chapter II. It harbours an ubiquitin C promoter (UbC), followed by the sequence of a fusion protein composed of IMP2 and the ADAR enzyme, the self-cleaving peptide P2A and a modified GFP (yGFP). This plasmid was kindly provided by Jeetayu Biswas and Robert H. Singer (Albert Einstein College of Medicine, Jack and Pearl Resnick Campus, New York, USA). Created with SnapGene®.

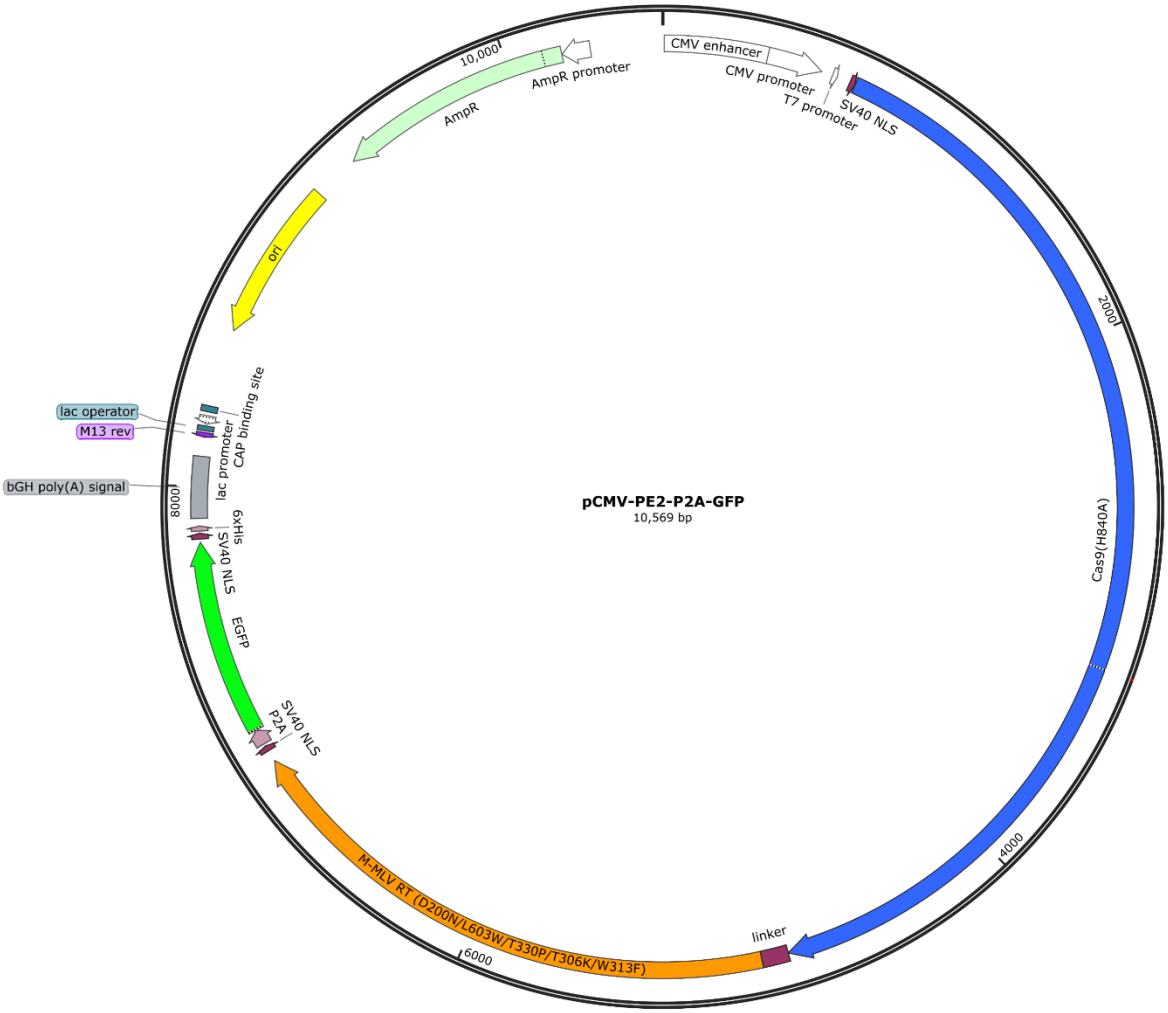

Supplementary Figure 10| pCMV-PE2-PE2A-GFP (plasmid #132776, Addgene). Prime editing plasmid harbouring the sequence of the prime editor 2, that is the fusion protein composed of Cas9-H840A nickase and the pentamutant Moloney murine leukaemia virus reverse transcriptase (M-MLV RT), the self-cleaving peptide P2A and a modified GFP (EGFP) as selection marker. Created with SnapGene®.

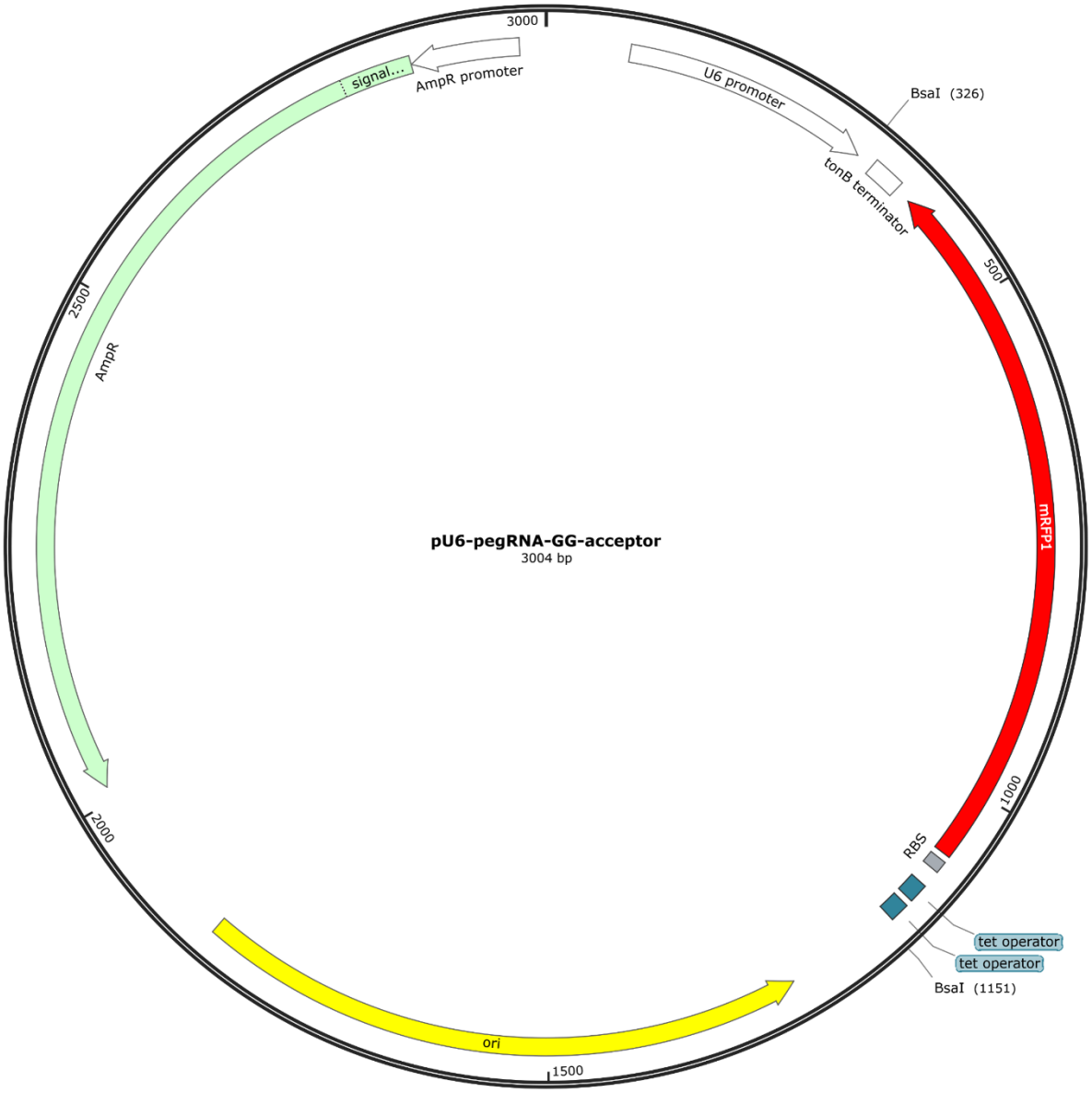

Supplementary Figure 11| pU6-pegRNA-GG-acceptor (plasmid #132777, Addgene). Prime editing plasmid with red fluorescent protein (mRFP1) dropout cassette as placeholder for cloning of pegRNAs. After successful cloning and transformation, bacterial colonies do not appear red anymore on agar plates. Created with SnapGene®.

8.4 List of figures and supplementary figures

8.5 List of tables

8.6 Publications

Original publications

Tarek Kröhler, Sonja M. Kessler, Kevan Hosseini, Markus List, Ahmad Barghash, Sonika Patial, Stephan Laggai, Katja Gemperlein, Johannes Haybaeck, Rolf Müller, Volkhard Helms, Marcel H. Schulz, Jessica Hoppstädter, Perry J. Blackshear and Alexandra K. Kiemer. 2019. "The mRNA-binding Protein TTP/*ZFP36* in Hepatocarcinogenesis and Hepatocellular Carcinoma." *Cancers*, *11*, 1754; https://doi.org/10.3390/cancers11111754.

Charlotte Dahlem, Ali Abuhaliema, Sonja M. Kessler, **Tarek Kröhler**, Ben G. E. Zoller, Shilpee Chanda, Yingwen Wu, Simon Both, Fabian Müller, Konstantin Lepikhov, Susanne H. Kirsch, Stephan Laggai, Rolf Müller, Martin Empting, and Alexandra K. Kiemer. 2022. "First Small-Molecule Inhibitors Targeting the RNA-Binding Protein IGF2BP2/IMP2 for Cancer Therapy." *ACS Chemical Biology*, *17*, 2, 361-375; https://doi.org/10.1021/acschembio.1c00833

Nikolai Köhler, Marcus Höring, Beate Czepukojc, Tim Daniel Rose, Christa Buechler, **Tarek Kröhler**, Johannes Haybaeck, Gerhard Liebisch, Josch K. Pauling, Sonja M. Kessler, Alexandra K. Kiemer. 2022. "Kupffer cells are protective in alcoholic steatosis." *Biochimica et Biophysica Acta (BBA) – Molecular Basis of Disease*, *1868*, 6, 166398; https://doi.org/10.1016/j.bbadis.2022.166398

Conference contributions

Ali Abuhaliema, Sonja M. Kessler, **Tarek Kröhler**, Martin Empting, Alexandra K. Kiemer. "Discovery of the first small molecules targeting the mRNA binding protein IGF2BP2/IMP2 as potential target in cancer therapy." *Helmholtz-Institut für Pharmazeutische Forschung (HIPS) Symposium on Pharmaceutical Sciences Devoted to Infection Research*, Saarbrücken, 2019

Sonja M. Kessler, Kevan Hosseini, **Tarek Kröhler**, Ahmad Barghash, Sonika Patial, Jessica Hoppstädter, Katja Gemperlein, Johannes Haybäck, Markus List, Rolf Müller, Volkhard Helms, Marcel H. Schulz, Stephan Laggai, Perry J. Blackshear, Alexandra K. Kiemer. "THU-470-The mRNA-binding protein tristetraprolin promotes hepatocarcinogenesis but inhibits tumour progression in liver cancer." *The International Liver Congress (ILC)*, Wien, 2019

Tarek Kröhler, Ali Abuhaliema, Charlotte Dahlem, Kevan Hosseini, Konstantin Lepikhov, Martin Empting, Markus List, Ahmad Barghash, Sonika Patial, Stephan Laggai, Katja Gemperlein, Johannes Haybaeck, Rolf Müller, Volkhard Helms, Marcel H. Schulz, Jessica Hoppstädter, Perry J. Blackshear, Sonja M. Kessler and Alexandra K. Kiemer. "Characterisation of mRNA binding proteins as potential therapeutic targets: models and tools." *International PhD Students/Postdoc Meeting of the German Pharmaceutical Society (DPhG)*, remote, 2021.

Sandra Kendzia, Susanne Franke, **Tarek Kröhler**, Nicole Golob-Schwarzl, Caroline Schweiger, Anna M. Toeglhofer, Christina Skofler, Helmut Bergler, Brigitte Pertschy, Stefan Uranitsch, Magdalena Holte, Amin El-Heliebi, Julia Fuchs, Andreas Punschart, Philipp Stiegler, Marlen Keil, Jens Hoffmann, David Henderson, Hans Lehrach, Marie-Laure Yaspo, Christoph Reinhard, Ulrich Keilholz, Christian Regenbrecht, Rudolf Schicho, Peter Fickert, Sigurd Lax, Frank Erdmann, Marcel H. Schulz, Alexandra K. Kiemer, Johannes Haybaeck, Sonja M. Kessler. "IGF2BP2 in colorectal cancer chemoresistance: an integrated approach employing clinical data, patient-derived organoids and xenografts, 2D and 3D cell culture models, and bioinformatics." *Cancer Metabolism Meeting of the European Association for Cancer Research (EACR)*, Bilbao, 2022.

8.7 Danksagung

Meinen besonderen Dank gilt Frau Prof. Dr. Alexandra K. Kiemer für die Möglichkeit in ihrer Arbeitsgruppe promovieren zu dürfen, für ihr Vertrauen und ihre Unterstützung in den vergangenen Jahren.

Herrn Prof. Dr. Jörn Walter möchte ich für die Übernahme der Rolle des wissenschaftlichen Begleiters danken und für sein stehts kritisches und konstruktives Feedback bei vielen Kooperationen mit seiner Arbeitsgruppe. Besonders hervorheben möchte ich hierbei die hilfreichen Diskussionen sowie die tatkräftige Unterstützung von Dr. Sascha Tierling und Dr. Konstantin Lepikhov zur Generierung und Analyse meiner knockout Klone. Dr. Gilles Gasparoni danke ich für sein umfassendes Wissen bezüglich RNA sequencing und der dazu notwendigen Probenvorbereitung. Für die Hilfe bei den praktischen Vorbereitungen für die SNuPE- und RRBS-Analysen möchte ich mich bei Beate Schmitt bedanken. Eva Dilly danke ich herzlich für ihre Unterstützung und ihre Tipps rund um das Thema Mäuse und deren Handling.

Darüber hinaus bedanke ich mich bei allen Kooperationspartnern, die an der Erhebung und Analyse der Lipidom-Daten beteiligt waren und zu einem glücklichen Ausgang verholfen haben, insbesondere Nikolai Köhler und Dr. Josch K. Pauling von der Nachwuchsgruppe LipiTUM der Technischen Universität München, Dr. Gerhard Liebisch und Dr. Marcus Höring vom Lipidomics Lab Regensburg und Prof. Dr. Christa Büchler vom Universitätsklinikum Regensburg.

Ein herzliches Dankeschön gilt Dr. Eileen Schulz (Helmholtz Institut für Pharmazeutische Forschung Saarland) und Silke Kiefer (Leibniz-Institut für Neue Materialien), die mich in verschiedene Techniken zur Isolation extrazellulärer Vesikel eingeführt haben.

Weiterhin bedanken möchte ich mich bei Prof. Dr. Uli Müller für seinen wissenschaftlichen Input zur Analyse von Fluoreszenzfarbstoffen in tierischen Geweben und Marion Schwarz für die Herstellung der Kryo-Schnitte und deren Analyse via Fluoreszenzmikroskopie.

Herrn Prof. Dr. Johannes Haybäck und seinen tatkräftigen Helfern im Hintergrund danke ich für immunohistochemische Analyse zahlreicher Gewebeproben.

Sandra Kendzia danke ich für die Zusammenarbeit im Rahmen der Testung der Chemosensitivität der KO-Klone.

Mein persönlicher Dank gilt den fleißigen Helfern Theo Ranßweiler, Matti Müller, Lisa Flöck, Tiffany-Maria Peters und Herr Schneider, die mich bei der praktischen Umsetzung zahlreicher verschiedener Projekte unterstützt haben, die sonst nicht möglich gewesen wären. Hierbei möchte ich besonders Theo für seine menschliche Art und sein jederzeit offenes Ohr hervorheben. Bedanken möchte ich mich auch bei Astrid Decker für das Bewältigen organisatorischer und bürokratischer Angelegenheiten im Hintergrund, sowie Herrn Dr. Zapp für seine stets freundliche und aufheiternde Art.

Außerdem danke ich Dr. Jessica Hoppstädter für die Hilfe beim Troubleshooting vieler wissenschaftlicher Probleme und die Einführung in die Durchflusszytometrie.

Ein herzlicher Dank gilt Prof. Dr. Sonja Keßler, die mich als Betreuerin in viele praktische Tätigkeiten eingeführt hat, bereit war, mich jederzeit mit Rat und Tat zu unterstützen und dafür, dass ich anfangs nicht die einzige jecke Person im Arbeitskreis war.

An dieser Stelle möchte ich allen Tischnachbarn des „coolen Büros“ für die gleichzeitig produktive, aber auch angenehme und witzige Atmosphäre danken (Thierry Maxime Legroux, Dr. Jenny Vanessa Valbuena Perez, Rebecca Linnenberger), sowie allen anderen Arbeitskollegen, die zu damaligem Zeitpunkt ihre Reise gerade erst begonnen haben (Muriel Charlotte Hans, Hanna Schymik, Arefeh Kardani) oder schon abgeschlossen haben (Dr. Beate Czepukojc, Dr. Anna Dembek). Shilpee Chanda danke ich für die herzlichen Gespräche und Diskussionen rund um das CRISPRn. Dr. Charlotte Dahlem möchte ich besonders danken für ihre herzliche Aufnahme und Einführung in das Saarland.

Schließlich möchte ich mich bei allen neuen Bekanntschaften, die ich machen durfte und die mir die Zeit im Saarland versüßt haben, bedanken. Vor allem aber bin ich dankbar, dass alte Freundschaften bestand hielten und teilweise während meiner Zeit in Saarbrücken wieder aufgeblüht sind.

Meiner Freundin Verena möchte ich ganz besonders danken, nicht nur für ihre Hilfe bei grafischen Umsetzungen wissenschaftlicher Illustrationen, sondern auch für ihre Geduld mit mir beim Verfassen dieser Arbeit und einfach dafür, dass wir uns gefunden haben.

Meiner Familie, die mich bisher auf all meinen Wegen unterstützt hat, gebührt der größte Dank. Eure Hilfe ist beneidenswert und unbezahlbar!